

SILESIA UNIVERSITY OF TECHNOLOGY
FACULTY OF CIVIL ENGINEERING



DOCTORAL THESIS

Analysis of early-age thermal–shrinkage stresses in reinforced concrete walls

Author:
MSc Eng. Agnieszka
Knoppik-Wróbel

Supervisor:
DSc PhD Eng. Barbara
Klemczak, SUT Prof.

January 2015

Acknowledgements

I am using this opportunity to express my gratitude to everyone who supported me throughout this thesis. I am thankful for your aspiring guidance, invaluable constructive criticism and friendly advice during the work. I am sincerely grateful to you for sharing your truthful and illuminating views on issues related to the thesis.

I would like to express my deepest gratitude to my supervisor, Barbara Klemczak – you have been a tremendous mentor for me. I would like to thank you for encouraging my research and for allowing me to grow as a research scientist. Your advice on both research as well as on my career have been priceless.

I would like to express special appreciation to my beloved husband Michał Wróbel who spent sleepless nights by my side and was always my support in the moments when there was no one to answer my queries. I would like to thank you not only for your innumerable sacrifices and yet encouragement, but also for insightful comments and hard questions. I could not have wished for a better life companion.

I would also like to thank my external guide, Farid Benboudjema from the Laboratoire de Mécanique et Technologie (LMT-Cachan, France) who has shown the attitude and the substance of a genius. You continually and persuasively conveyed a spirit of adventure in regard to research and an excitement in regard to teaching. Without your supervision and constant help this thesis would not have been possible.

I am very thankful to all the people who have helped me realise this thesis, especially Anders Hösthagen from the Luleå University of Technology (LTU, Sweden). I also express my warm thanks to the reviewers of my papers throughout the whole research. For your brilliant comments and suggestions – thank you.

I thank my colleagues at the Department of Structural Engineering for the stimulating discussions, sleepless nights we were working together before deadlines and for all the fun we have had in the last four years. Special thanks to Grzegorz Wandzik, Rafał Krzywoń, Marcin Górski, Szymon Dawczyński, Gosia Pająk and Marcin Kozłowski.

Special thanks go also to my family. Words cannot express how grateful I am to my mother Małgosia and father Artur as well as my grandma Stasia and grandpa Włodek for your endless love and support. Your belief in me was what sustained me thus far. I would also like to thank all of my friends who supported me in writing and encouraged me to strive towards my goal, especially Kasia Niechoj who has supported me throughout the entire process, both by keeping me harmonious and helping me putting pieces together. I would also like to thank Kasia Zielińska, Ania Kopyto, Jasiu Pizoń and Natalia Paszek. I will be grateful forever for your love.

I gratefully acknowledge financial support from the following institutions: Polish National Science Centre for funding the research project no. N N506 043440 “Numerical prediction of cracking risk and methods of its reduction in massive and medium-thick concrete structures” which was the basis of this research project (2011–2014), Erasmus+ program and LMT-Cachan (France) for funding my internship at the Laboratoire de Mécanique et Technologie (2014), and the Silesian University of Technology. I would also like to acknowledge that while realising

the research project presented in this thesis I was a scholar under the programs “SWIFT (Scholarships Supporting Innovative Technological Forum) POKL.08.02.01-24-005/10” (2012–2013) and “DoktoRIS – Scholarship program for innovative Silesia” (2013–2015) co-funded by the European Union under the European Social Fund.

SILESIAIAN UNIVERSITY OF TECHNOLOGY
Faculty of Civil Engineering
Department of Structural Engineering

Doctoral Thesis

Abstract

Analysis of early-age thermal–shrinkage stresses in reinforced concrete walls

by MSc Eng. Agnieszka Knoppik-Wróbel

The character of early-age stresses is well-recognised in massive concrete elements such as slabs, blocks or water dams. In such elements stresses are induced mainly by significant temperature differences developing between the interior and the surface of the element. However, the impact of the early-age thermal–shrinkage effects is usually underestimated in elements with thinner sections but in which the ability of free deformation is limited. These externally-restrained elements are subjected to restraint stresses caused by potential contraction limited by the restraint along one or more edges of the element; if not restrained, they would not be subjected to such stresses.

There is a very wide range of externally-restrained reinforced concrete elements, such as walls, with different massivity and restraint conditions in which similar character of cracking is observed. The aim of the research presented in this thesis was to analyse the character and magnitude of early-age stresses occurring in reinforced concrete walls due to thermal–shrinkage effects and to investigate the influence of various factors on these stresses, especially the influence of restraint conditions including the founding subsoil. Because of a large scale of the elements in question the analysis was performed in a “virtual laboratory” with use the of computational models.

Firstly, the simplified analytic models were reviewed and evaluated. The stress analysis in these approached is based on the *compensation plane method*. The method takes into account the fact that the early-age stresses in externally-restrained elements result from a coupled action of the internal and external restraints. The external restraint acts against axial deformation and flexural deformation. The concept of the restraint factor is used to represent the degree of restraint of the element by the restraining body. In the most complete form the restraint factor takes into account the geometry of the early-age element and the restraining body, the relative stiffness of the restraining body and the influence of cracking on the change of restraint.

Then, the thermo–physical and mechanical phenomena which govern the early-age behaviour of reinforced concrete walls were defined. A thorough review was made of the proposals for phenomenological description of the thermo–physical and mechanical behaviour of early-age concrete and soil. Based on this review a mathematical model was formulated for simulation of the behaviour of early-age reinforced concrete walls including structure–subsoil interaction. A FEM-based numerical model was developed which was implemented in a form of modular software. The main modules were TEMWIL for thermal–moisture analysis and MAFEM for stress and damage analysis. The main goal of the model was to estimate the thermal–shrinkage stresses in early-age concrete elements without the necessity to perform a series of experimental tests to determine the values of the subsequent parameters. The model was verified on a real

benchmark wall (NPP wall for CEOS.fr benchmark); this aim was successfully achieved. The model was used for a series of analyses of early-age walls. Three-dimensional numerical analysis allowed to explain the important phenomena observed in early-age elements, impossible to explain with the use of simplified models. The numerical approach allowed to describe the time evolution of various phenomena as concrete maturity developed. The results of the analyses confirmed a typical, two-phase character of stresses in the wall. The spatial analysis showed the influence of the self-induced stresses which are responsible for the variation of the total stresses in the cross-section of the wall. Taking into account the subsoil the real temperature distribution in the concrete element was obtained and real values of the degree of restraint were obtained.

Both analytic and numerical models were used for the analysis of the influence of the restraint conditions on the early-age stresses in walls. It was shown that the restraint stresses play predominant role and the effect of the external restraint can be well described by the restraint factor. The value of the restraint factor varies throughout the volume of the wall and is the greatest at the joint between the wall and the restraining body decreasing towards the free edges. The value of the restraint factor depends on the degree of translational restraint (length and height of the wall and their ratio and relative stiffness of the restraining body), rotational restraint, possibility of slip at the joint as well as the properties of the founding soil (friction, cohesion and stiffness); all these characteristics must be taken into account for proper determination of the degree of restraint.

Finally, a discussion was made on the influence of other factors on the magnitude and character of stresses in early-age walls. The factors which influence the early-age stresses relate to the concrete composition, environmental and technological conditions during casting and curing of the element. The most common way of mitigation of the early-age effects is optimum concrete mix design, however, special attention must be paid in externally-restrained elements to the relationship between the hydration heat development rate and the mechanical properties development rate. Development of the early-age stresses is highly dependent on the environmental conditions during curing of concrete. It is advised to realise concreting in moderate ambient temperature with additional pre-cooling of the concrete mix. Appropriate curing technology can be applied when curing is realised in unfavourable conditions. To mitigate early-age cracking in walls insulation should be applied and the moment of the formwork removal should be delayed; at that moment it must be assured that the tensile strength of the concrete element able to withstand the cooling tensile stresses.

Contents

Acknowledgements	iii
Abstract	v
Contents	vii
List of Figures	ix
List of Tables	xiii
List of Symbols	xv
1 Aim and range of thesis	1
1.1 Aim of thesis	1
1.2 Background of the thesis	2
1.3 Range of thesis	2
2 Early-age behaviour of reinforced concrete walls	5
2.1 Problem overview	5
2.2 Characteristics of early-age concrete	6
2.3 Early-age thermal–shrinkage stresses	10
2.4 Externally restrained concrete elements subject to early-age cracking	12
2.4.1 Tank walls	12
2.4.2 Elements of bridge structures	17
2.4.3 Nuclear containment walls	22
2.4.4 Tunnel walls	25
3 Analytic models for early-age reinforced concrete walls	27
3.1 Temperature and shrinkage	28
3.1.1 Temperature-induced strains	28
3.1.2 Shrinkage-induced strains	32
3.2 Thermal–shrinkage stresses	35
3.2.1 Stresses in uncracked walls	35
3.2.2 Stresses in cracked walls	45
3.3 Creep and ageing	46

4	Modelling of early-age reinforced concrete walls behaviour	49
4.1	Early-age concrete	50
4.1.1	Cement hydration	51
4.1.2	Thermal and shrinkage strain	57
4.1.3	Thermo-physical properties of concrete	60
4.1.4	Creep and ageing	65
4.1.5	Damage analysis	72
4.2	Subsoil	75
4.2.1	Heat and moisture transport	75
4.2.2	Material model and failure criterion	80
4.3	Reinforcement	81
4.3.1	Modelling of reinforcement	81
4.3.2	Heat transport	82
4.3.3	Material model and failure criterion	82
4.4	Summary	82
5	Analysis of early-age stresses in reinforced concrete walls	85
5.1	Models for analysis of early-age reinforced concrete walls	85
5.1.1	Numerical model	85
5.1.2	Analytic model	96
5.2	Character of early-age stresses in reinforced concrete walls	98
5.2.1	Nuclear containment wall	98
5.2.2	Tunnel wall	105
5.3	Influence of geometry and restraint conditions on early-age stresses in walls	113
5.3.1	Dimensions of the wall	113
5.3.2	Support conditions	122
5.4	Influence of other factors on early-age stresses in walls	126
5.4.1	Concrete mix composition	127
5.4.2	Environmental conditions	129
5.4.3	Technological conditions	130
6	Summary and conclusions	135
6.1	Final conclusions	135
6.2	Future work	138
	Bibliography	139

List of Figures

2.1	Temperature, moisture content, thermal and shrinkage stress development in time in an externally-restrained concrete wall.	6
2.2	Typical cracking patterns in early-age reinforced concrete walls.	7
2.3	Cracking pattern in an externally-restrained reinforced concrete element [88]. . .	7
2.4	Concrete behaviour during progressing hydration of cement after SCHINDLER [200].	8
2.5	Development of early-age thermal–shrinkage stresses in time in an externally-restrained element.	10
2.6	Distribution of early-age thermal–shrinkage stresses in a cross-section of a wall. .	11
2.7	Cylindrical industrial sewage tank, Poland [206].	13
2.8	Cracking pattern in segment 1 of a cylindrical sewage tank (external view) [206].	13
2.9	Rectangular tank at a sewage treatment facility, Poland [236].	14
2.10	Cracking pattern in a wall of a sewage tank (external view), Poland [206].	15
2.11	Sludge chamber in a sewage treatment facility, Poland [147].	16
2.12	Cylindrical industrial sewage tank, Poland [96].	16
2.13	Cracking pattern in chosen segments of an industrial sewage tank, Poland [96]. .	16
2.14	Cross-section of a highway bridge abutment, Poland [223].	18
2.15	Cracking pattern in highway bridge abutments, Poland [223].	18
2.16	Cross-section of road and river bridge abutments, Poland [224, 225].	19
2.17	Cracking pattern in road bridge abutments, Poland [225].	20
2.18	Longitudinal section of a highway frame bridge, Poland [87].	20
2.19	Cracking pattern in walls of a highway frame bridge, Poland [87].	21
2.20	Reactor building structures, France (private collection of Francis Barré).	23
2.21	Disposal structure for interim storage of radioactive waste, Germany [167].	24
2.22	X-ray shielding bunker, Near East [150].	25
2.23	Cracking in a wall of an X-ray shielding bunker (external view), Near East [150].	25
2.24	Tunnel, Sweden [108].	26
2.25	Cracking pattern in chosen segments of a tunnel, Sweden [108].	26
2.26	Tunnel, France (private collection of Farid Benboudjema).	26
3.1	Graphical interpretation of 3 rd type boundary condition for heat equation solution after FLAGA [82].	31
3.2	Differential strain in a new part of a concrete structure after FLAGA [83].	35
3.3	Distribution of stresses at the height of the wall after FLAGA [83].	36
3.4	Models of the wall applied in analytic approaches.	36
3.5	Determination of stresses in a concrete element caused by the internal restraint according to compensation plane method after JSCE STANDARD [116].	37
3.6	Determination of stresses in a concrete element caused by the external restraint according to compensation plane method after JSCE STANDARD [116].	38

3.7	External restraint factors according to JSCE STANDARD [116].	38
3.8	Axial restraint factor R_N in restrained elements according to EUROCODE 2 [184].	39
3.9	Structural shape restraint factor K_R at the centre section according to ACI 207.2 [5].	40
3.10	Factors accounting for high-walls effect in determination of the restraint factor according to NILSSON [177].	42
4.1	Models of the wall applied in numerical approaches with FEA.	50
4.2	Thermal–moisture analysis: modelling paths.	83
4.3	Stress and damage analysis: modelling paths.	83
5.1	Model for analysis of early-age walls with the use of the numerical approach. . . .	86
5.2	Boundary surface acc. to the modified 3-parameter Willam–Warnke (MWW3) failure criterion.	93
5.3	Development of the boundary surface in time with the maturing process.	93
5.4	Graphical interpretation of the damage intensity factor.	95
5.5	Scheme of the software architecture.	96
5.6	Model for analysis of early-age walls with the use of the analytic approach.	97
5.7	Geometry of the CEOS.fr benchmark wall.	99
5.8	Temperature development in the CEOS.fr benchmark wall.	99
5.9	Model and FE mesh of the CEOS.fr benchmark wall.	100
5.10	Results of thermal analysis of the CEOS.fr benchmark wall.	101
5.11	Damage intensity in lift 1 of the CEOS.fr benchmark wall at $t = 672$ hrs (age of lift 336 hrs).	103
5.12	Cracking pattern in lift 1 of the CEOS.fr benchmark wall.	103
5.13	Distribution of σ_{xx} stresses in lift 1 of the CEOS.fr benchmark wall: heating phase, $t = 348$ hrs (age of lift 12 hrs), MPa.	103
5.14	Distribution of σ_{xx} stresses in lift 1 of the CEOS.fr benchmark wall: cooling phase before initiation of cracking, $t = 516$ hrs (age of lift 180 hrs), MPa.	104
5.15	Time-development of stresses and damage intensity in lift 1 of the CEOS.fr benchmark wall.	104
5.16	Models and FE mesh of the tunnel benchmark wall.	106
5.17	Temperature development and moisture loss in time in the tunnel benchmark wall.	108
5.18	Temperature distribution and moisture concentration in the tunnel benchmark wall.	109
5.19	Damage intensity in the C07 model of the tunnel benchmark wall.	110
5.20	Damage intensity in the C08 model of the tunnel benchmark wall.	110
5.21	Cracking pattern in segments of the tunnel benchmark wall.	111
5.22	σ_{xx} stress development in time in the tunnel benchmark wall.	112
5.23	σ_{xx} stress distribution in the C07 model of the tunnel benchmark wall, MPa. . .	112
5.24	σ_{xx} stress distribution in the C08 model of the tunnel benchmark wall, MPa. . .	112
5.25	Model and FE mesh of an exemplary wall used in the parametric study.	115
5.26	Temperature and shrinkage development in time in an exemplary wall.	116
5.27	Relative thermal strain in an exemplary wall.	117
5.28	Relative stiffness development in time in an exemplary wall.	117
5.29	Degree of restraint distribution along the centreline of the walls.	119
5.30	Degree of restraint for the walls with equal lengths and different L/H ratios. . . .	120
5.31	Degree of restraint for the walls with equal L/H ratios and different lengths. . . .	121
5.32	Modification factor M_1 for the walls with equal lengths and different L/H ratios.	122

5.33	Modification factor M_2 for the walls with equal L/H ratios and different lengths.	122
5.34	Models and FE mesh of the walls with real support conditions (founding soil).	124
5.35	Degree of restraint in the walls with different support conditions.	125
5.36	Deformation (scale 500:1) and σ_{xx} stresses, MPa, in the walls with different support conditions.	125
5.37	Damage intensity in the walls made of concretes with different cements [148].	129
5.38	Influence of the initial and ambient temperature on the cracking risk of walls [139].	132
5.39	Influence of formwork conditions during curing on the cracking risk of walls [139].	133

List of Tables

2.1	Concrete mixes used for bridge construction.	21
2.2	Concrete mixes used for nuclear containments construction.	23
3.1	Coefficients α_{ca} , α_{ds1} and α_{ds2} for calculation of shrinkage strain acc. to MODEL CODE 2010 [50].	34
4.1	Thermal properties of concrete components.	61
4.2	Thermal properties of concretes with different aggregates.	62
4.3	Thermal properties of soil components [80].	77
4.4	Parameters for liquid diffusivity of soils acc. to CLAPP AND HORNBERGER [55].	80
5.1	Liquid diffusivities of fully-saturated soils after CLAPP AND HORNBERGER [55].	88
5.2	Time discretisation used in the analysis of the CEOS.fr benchmark wall.	100
5.3	Thermo-physical parameters used in the analysis of the CEOS.fr benchmark wall.	100
5.4	Mechanical parameters used in the analysis of the CEOS.fr benchmark wall.	102
5.5	Time discretisation used in the analysis of the tunnel benchmark wall.	105
5.6	Thermo-physical parameters used in the analysis of the tunnel benchmark wall.	107
5.7	Mechanical parameters used in the analysis of the tunnel benchmark wall.	110
5.8	Geometrical data for the analysed walls.	114
5.9	Mineral composition of cement used in the parametric study.	114
5.10	Thermo-physical parameters used in the parametric study.	114
5.11	Mechanical parameters used in the parametric study.	115
5.12	Time discretisation used in the parametric study.	115
5.13	Polynomial coefficients for calculation of δ_{res} acc. to LULEÅ method used in the parametric study.	118
5.14	Slip factor δ_{slip} acc. to LULEÅ method used in the parametric study.	118
5.15	Thermo-physical parameters of soil used in parametric study.	123
5.16	Mechanical parameters of soil used in parametric study.	123
5.17	Concrete mix compositions used in the parametric study of the influence of the concrete mix composition of the cracking risk of walls [148].	129

List of Symbols

ROMAN LOWER-CASE LETTERS

$a, b, c,$	constants	-
c	moisture content by mass (humidity)	kg/kg
c_a	humidity of the ambient air	kg/kg
c_{int}	humidity in the interior of the element	kg/kg
c_{sur}	humidity at the surface of the element	kg/kg
c_s	cohesion of soil	kPa
c_b	specific heat	kJ/(kg K)
c_v	heat capacity	kJ/(m ³ K)
d_{damp}	damping depth of soil	m
d_{eq}	equivalent thickness of the concrete element	m
d_i	thickness of the layer	m
e	emissivity	-
e_{lim}	viscoelasticity limit	-
f	yield surface	-
$f(r_H)$	heat production rate function	-
f_c	uniaxial compressive strength of concrete	MPa
f_{cc}	biaxial compressive strength of concrete	MPa
f_{ccc}	triaxial compressive strength of concrete	MPa
f_{cd}	design compressive strength of concrete	MPa
f_{ck}	characteristic compressive strength of concrete	MPa
f_{cm}	mean compressive strength of concrete	MPa
f_t	uniaxial tensile strength of concrete	MPa
f_{tt}	biaxial tensile strength of concrete	MPa
f_{ttt}	triaxial tensile strength of concrete	MPa
f_{ctd}	design tensile strength of concrete	MPa
f_{ctk}	characteristic tensile strength of concrete	MPa
f_{ctm}	mean tensile strength of concrete	MPa

f_y	yield strength of steel	MPa
f_{yd}	design yield strength of steel	MPa
f_A	correction factor for age (for α_T)	-
f_M	correction factor for moisture content (for α_T)	-
f_T	correction factor for temperature (for α_T)	-
$g(T)$	temperature function	-
h_0	notional size of the element	m
h_{cr}	height of the crack	m
k, m, n	material constants	-
k_i	volume fraction	-
l_{cr}	distance between cracks	m
m	massiveness, surface modulus	m^{-1}
m_{cc}	ratio between biaxial and uniaxial compressive strength	-
m_t	ratio between tensile and compressive strength	-
m_H	quantity of hydrated cementitious material	g
$m_{H,i}$	initial quantity of cementitious material	g
n	porosity	MPa
p_a	atmospheric pressure	-
p_i	weight fraction	-
q	unit rate of the hydration heat development	W/g
q_{\max}	maximum unit rate of the hydration heat development	W/g
q_v	total rate of the hydration heat development	W/m ³
\tilde{q}	heat flux	W/m ²
r_c	compressive radius of deviatoric section (failure surface)	-
r_f	material parameter (for shear modulus of soil)	-
r_t	tensile radius of deviatoric section (failure surface)	-
r_H	degree of reaction	-
s	cement-dependent material constant	-
s_l	damage intensity factor	-
t	time	s, h or d
t_a	concrete age when reaching the ambient temperature	s, h or d
t_{cr}	time of crack appearance	s, h or d
t_s	setting time of concrete	s, h or d
t_e	equivalent age of concrete	s, h or d
t_d	concrete age at the beginning of drying	s, h or d
t_0	concrete age at the beginning of loading	s, h or d

$t_{0,adj}$	concrete age at the beginning of loading adjusted for the effects of temperature	s, h or d
$t_{0,e}$	equivalent concrete age of concrete at the beginning of loading	s, h or d
u	perimeter of the element in contact with atmosphere	m
v	wind speed	m/s
w_k	width of crack	mm
w_i	weight (in weighted average)	-
w_H	amount of water bound in the hydration process	l/m ³
w/c	water-to-cement ratio	-
w/cm	water-to-cementitious material (binder) ratio	-
$w_{H,tot}$	amount of water needed for complete hydration	l/m ³
x, y, z	coordinates	m
x_{cen}, y_{cen}	coordinates of the center of gravity	m

ROMAN UPPER-CASE LETTERS

$A(T)$	affinity ratio with respect to reference temperature	-
A_c	cross-section area of the early-age concrete element	m ²
A_F	cross-section area of the restraining concrete element	m ²
$\tilde{A}(t)$	normalised affinity	-
B	width	m
B_c	thickness of the early-age concrete element	m
B_F	width of the restraining concrete element	m
$B_{F,eff}$	effective width of the restraining concrete element	m
$Blaine$	specific surface area of cement	m ² /kg
C_c	amount of cement in concrete mix	kg/m ³
C_{SCM}	amount of supplementary cementitious material in concrete mix	kg/m ³
$C(t, t_0)$	compliance function (for creep)	-
D	damage	-
D_v	thermal vapour diffusivity of water	m ² /(s K)
D_{WT}	thermal liquid diffusivity of soil	m ² /(s K)
D_{WW}	isothermal liquid diffusivity of soil	m ² /s
E_c	modulus of elasticity of concrete	GPa
$E_{c,eff}$	effective modulus of elasticity of concrete	GPa
E_{cm}	mean modulus of elasticity of concrete	GPa
E_F	modulus of elasticity of restraining element	GPa
E_K	activation energy	J/mol

$E_{K,\text{ref}}$	material constant (for activation energy)	-
F	boundary surface	-
F_1, F_2	compressive and tensile bond force at the joint	kN
G	shear modulus of soil	GPa
G_o	material constant (for shear modulus of soil)	-
H	height	m
H_{bas}	basic height of the early-age element	m
H_c	height of the early-age concrete element	m
H_F	depth of the restraining concrete element	m
I_c	moment of inertia of early-age concrete element	m ⁴
I_{cr}	cracking index	-
$J(t, t_0)$	creep function	-
K	bulk modulus of soil	GPa
K_1	coefficient to account for the effect of sustained loading and creep	-
K_2	restraint reduction factor during cracking	-
K_e	Kersten number	-
K_h	hydraulic conductivity	m/s
$K_{h,\text{sat}}$	saturated hydraulic conductivity	m/s
K_o	material constant (for bulk modulus of soil)	-
K_F	degree of foundation restraint	-
K_H	water-to-cement proportionality coefficient	m ³ /J
K_R	degree of structural geometry restraint	-
L	length	m
L_{bas}	basic length of the early-age element	m
L_c	length of the early-age concrete element	m
L_e	elastic length of the early-age concrete element	m
L_v	latent heat of vaporisation of water	J/m ³
L_z	bond length	m
L_F	length of the restraining concrete element	m
M	maturity of concrete	-
M_1	modification factor to account for the influence of the wall's height on the degree of restraint	-
M_2	modification factor to account for the influence of the wall's length on the degree of restraint	-
M_c	massivity of the concrete element	-
M_R	bending moment due to the restrained strain	kNm
N_R	axial force due to the restrained strain	kN

Q	hydration heat	J/g
Q_{\max}	total amount of hydration heat corresponding to the end of the test	J/g
Q_{tot}	total amount of hydration heat	J/g
P	period of temperature oscillation at the soil surface	h or d
$P(t)$	value of the material property of ageing concrete	Pa
R	universal gas constant = 8.314	J/(mol K)
R_a	restraint factor after crack formation	-
R_b	restraint factor before crack formation	-
R_i	restraint factor for the self-induced stress	-
R_N	translational restraint factor	-
R_M	rotational restraint factor	-
RH	relative humidity of the ambient air	%
ΔR	change in restraint after cracking	-
S	saturation	-
S_e	effective saturation	-
T	temperature	°C or K
T_0	threshold temperature for hardening of concrete	°C or K
T_a	ambient temperature	°C or K
T_{ad}	adiabatic temperature rise of concrete	°C or K
T_{env}	temperature change due to environmental conditions	°C or K
T_f	final stable temperature of concrete	°C or K
T_i	initial temperature	°C or K
T_{int}	internal temperature	°C or K
T_m	mean temperature	°C or K
T_{\max}	maximum (peak) temperature of concrete	°C or K
T_{ref}	reference temperature	°C or K
T_{sur}	surface temperature	°C or K
ΔT	temperature change during cooling	°C or K
ΔT_{allow}	allowable temperature change during cooling	°C or K
$\Delta T'_{\text{allow}}$	allowable temperature difference in cross-section	°C or K
ΔT_W	shrinkage strain equivalent temperature change	°C or K
ΔT_{diff}	difference of temperature between the early-age element and the restraining body	°C or K
W	moisture content by volume	m ³ /m ³
W_a	moisture content in the ambient air	m ³ /m ³
W_c	bending index of the early-age concrete element	m ³

W_i	initial moisture content	m^3/m^3
W_r	residual moisture content	m^3/m^3
$Y(\kappa)$	hardening function	-

GREEK LOWER-CASE LETTERS

α	reinforcement inclination angle	$^\circ$
α_0	percolation threshold	-
α_c	moisture dilation coefficient	kg/kg
α_{ca}	coefficient for determination of autogenous shrinkage	-
$\alpha_{ds1}, \alpha_{ds1}$	coefficients for determination of drying shrinkage	-
α_h	coefficient representing the lower bound of diffusivity	-
α_p	free-convection heat exchange coefficient	$\text{W}/(\text{m}^2 \text{K})$
α_{pv}	forced-convection heat exchange coefficient	$\text{W}/(\text{m}^2 \text{K})$
α_{pr}	convection–radiation heat exchange coefficient	$\text{W}/(\text{m}^2 \text{K})$
$\alpha_{p,\text{eq}}$	equivalent heat exchange coefficient of a covered surface	$\text{W}/(\text{m}^2 \text{K})$
α_r	radiation heat exchange coefficient	$\text{W}/(\text{m}^2 \text{K})$
α_E	material coefficient (for modulus of elasticity)	-
α_H	degree of hydration	-
α_{Hu}	ultimate degree of hydration	-
α_T	thermal dilation coefficient	$1/^\circ\text{C}$
α_{TT}	coefficient of thermal diffusion	m^2/s
α_{TW}	coefficient representing the influence of moisture transport on heat transfer	$(\text{m}^2 \text{K})/\text{s}$
α_W	moisture dilation coefficient	m^3/m^3
α_{WT}	coefficient representing the influence of heat transfer on moisture transport	$\text{m}^2/(\text{s K})$
α_{WW}	coefficient of moisture diffusion	m^2/s
$\alpha_{WW,0}$	coefficient of moisture diffusion in dry concrete	m^2/s
$\alpha_{WW,1}$	coefficient of moisture diffusion in saturated concrete	m^2/s
$\bar{\alpha}(t)$	function of degree of hydration	-
$\dot{\alpha}_H$	rate of degree of hydration development	-
β	hydration shape parameter	-
$\beta(t, t_0)$	ageing coefficient (time-development of creep)	-
$\beta(t_0)$	function of time for the concrete age at loading (for creep)	-
$\beta(f_{cm})$	coefficient dependent on the class of concrete (for creep)	-
$\beta_{as}(t)$	function of autogenous shrinkage time-development	-
$\beta_{bc}(t, t_0)$	function of basic creep time-development	-

$\beta_c(t)$	function of material properties time-development	-
$\beta_{dc}(t, t_0)$	function of drying creep time-development	-
$\beta_{ds}(t, t_d)$	function of drying shrinkage time-development	-
β_{dT}	coefficient expressing the effect of the increased temperature on the rate of drying shrinkage strain development	-
β_h	diffusivity increment coefficient	-
β_{sT}	coefficient expressing the effect of the increased temperature on the magnitude of drying shrinkage strain	-
β_p	humidity exchange coefficient	m/s
$\beta_{p,eq}$	equivalent humidity exchange coefficient of covered surface	m/s
β_H	coefficient describing the kinetics of creep process	-
β_{HT}	coefficient describing the kinetics of creep process adjusted for the effect of temperature	-
β_{RH}	coefficient taking into account the effect of the ambient relative humidity on drying shrinkage	-
β_T	temperature correction factor (for creep)	-
γ	temperature difference reduction coefficient	-
$\gamma(t_0)$	coefficient of creep development	-
γ_a	correction factor (for equivalent the thickness of the element)	-
γ_h	coefficient characterising the humidity level at which the diffusivity begins to increase	-
γ_R	restraint factor	-
γ_R^0	plane-section restraint factor	-
$\gamma_R^{rx}, \gamma_R^{ry}$	rotational restraint factors	-
γ_R^t	translational restraint factor	-
γ_T	relative change of surface tension with respect to temperature	1/°C
δ_{res}	resilience factor	-
δ_{res}^0	basic resilience factor	-
δ_{trans}^0	translational correction factor (for γ_R)	-
δ_{rot}^0	rotational correction factor (for γ_R)	-
δ_{slip}	slip factor	-
ε	strain	m/m
ε_0	strain (in strain distribution)	m/m
ε_{ca}	autogenous shrinkage strain	m/m
$\varepsilon_{ca,0}$	notional autogenous shrinkage strain	m/m
ε_{cc}	creep strain	m/m
ε_{cd}	drying shrinkage strain	m/m
$\varepsilon_{cd,0}$	notional drying shrinkage strain	m/m

$\varepsilon_{\text{comp}}$	strain at compensation plane	m/m
ε_{ctu}	strain capacity of concrete in tension	m/m
ε_e	elastic strain	m/m
ε_n	strain independent of the applied load	m/m
ε_σ	strain due to the applied load	m/m
ε_{tot}	total strain	m/m
ε_T	thermal strain	m/m
ε_W	shrinkage strain	m/m
$\varepsilon_{W,\text{diff}}$	difference of shrinkage strain between the early-age element and the restraining body	m/m
$\bar{\varepsilon}$	free axial strain	m/m
$\hat{\varepsilon}$	equivalent tensile strain	m/m
ζ_H	wall height ratio	-
ζ_L	wall length ratio	-
$\tilde{\eta}$	moisture flux	m ² /s
θ	Lode angle	°
κ	hardening/softening parameter	-
κ_0	tensile strain threshold	m/m
κ_s	shape factor (for elastic length L_e)	-
κ_H	function of mechanical parameters development	-
λ	thermal conductivity	W/(m K)
λ_{dry}	thermal conductivity in dry state	W/(m K)
λ_{sat}	thermal conductivity in saturated state	W/(m K)
$\bar{\lambda}$	instantaneous thermal conductivity of soil	W/(m K)
$\dot{\lambda}$	consistent parameter (for viscoelastic model)	-
μ	coefficient of joint surface roughness	-
ν	Poisson ratio	-
ρ	volume density	kg/m ³
ρ_r	degree of vertical reinforcement in the joint	-
ρ_s	volume density of soil	kg/m ³
ρ_w	volume density of water	kg/m ³
σ	stress	MPa
σ_{ext}	stress due to the external restraint	MPa
σ_{fix}	stress at total restraint	MPa
σ_{int}	stress due to the internal restraint	MPa
σ_m	mean stress	MPa

σ_n	stress normal to the joint	MPa
σ_{res}	restraint stress	MPa
$\sigma_{\text{s-ind}}$	self-induced stress	MPa
σ_t	tensile stress	MPa
σ_{tot}	total stress	MPa
$\bar{\sigma}$	stress intensity	MPa
$\hat{\sigma}$	effective stress (in damage analysis)	MPa
τ	hydration time parameter	-
τ	shear stress	MPa
τ_{oct}	octahedral stress	MPa
$\bar{\tau}$	shear strength	MPa
$\phi(t, t_0)$	creep coefficient	-
$\phi(RH)$	coefficient dependent on the relative humidity of the ambient air (for creep)	-
$\phi_T(t, t_0)$	creep coefficient adjusted for the effect of temperature	-
ϕ_T	temperature correction factor (for creep)	-
φ	internal friction angle of soil	°
$\bar{\varphi}$	increment in curvature	-
χ	adiabatic temperature rise reduction coefficient	-
ψ	matric potential	m
ψ_a	air-entry tension	m
ω	location factor (for γ_R)	-

MATRICES AND VECTORS

\mathbf{n}	vector normal to the boundary surface
$\boldsymbol{\varepsilon}$	strain matrix
$\boldsymbol{\varepsilon}_n$	imposed thermal-shrinkage strain matrix
$\boldsymbol{\varepsilon}_p$	plastic strain matrix
$\boldsymbol{\varepsilon}_{vp}$	viscoplastic strain matrix
$\boldsymbol{\sigma}$	stress matrix
\mathbf{D}	matrix of the Poisson's ratio, $\mathbf{D} = \frac{1}{E(t)}\mathbf{D}_e(t)$
\mathbf{D}_e	elasticity matrix
\mathbf{D}_{ep}	elasto-plasticity matrix
\mathbf{D}_p	plasticity matrix
\mathbf{D}_{ve}	viscoelasticity matrix

Chapter 1

Aim and range of thesis

1.1 Aim of thesis

Concrete elements are subjected to early-age volume changes due to temperature and moisture variations which characterise the process of concrete hardening. The variations of concrete temperature during curing are caused by exothermic character of the chemical reaction between cement and water. In thick sections internal temperature can increase significantly and due to poor thermal conductivity of concrete high temperature gradients may occur between the interior and the surface of the elements. During hardening the water is bound within the concrete element and also transported out of the element due to drying in conditions of variable temperature, which results in shrinkage. The volume changes due to temperature and moisture variations have consequences in stresses arising in concrete elements.

The character of the early-age stresses is well-recognised in massive concrete elements such as slabs, blocks or water dams. In such elements the temperature and moisture concentration during the hydration process are different in each point of the structure. The stresses are induced mainly by significant temperature differences developing between the interior and the surface of the element. However, the impact of the early-age thermal-shrinkage effects is usually underestimated in elements with thinner sections but in which the ability of free deformation is limited. These elements are referred to as externally-restrained elements because they are predominantly subjected to the restraint stresses caused by potential contraction limited by the restraint along one or more edges of the element; if not restrained, these elements would not be subjected to such high levels of stresses. The restraint is exerted by the bond between the new concrete of the element and the older concrete of the foundation or a previous lift.

There is a very wide range of reinforced concrete wall structures with different massivity and restraint conditions in which similar character of cracking is observed. The aim of the research presented in this thesis was **to analyse the character and magnitude of early-age stresses which lead to cracking in reinforced concrete walls due to thermal-shrinkage effects and to investigate the influence of various factors on these stresses, especially the influence of restraint conditions including the founding subsoil**. Because of a large scale of the elements in question the analysis was performed in a “virtual laboratory” with use of computational models.

1.2 Background of the thesis

This thesis is the effect of research work performed between 2011 and 2014, based on an extensive work of the author on this topic which results were continually published. The numerical model used as a main tool in this thesis was based on a model developed by KLEMCZAK [134] for massive concrete structures, adjusted for analysis of reinforced concrete walls and presented in its early form by KLEMCZAK AND KNOPPIK-WRÓBEL [141]. The characteristics of early-age stresses in reinforced concrete walls were described by KLEMCZAK AND KNOPPIK-WRÓBEL [138]. This characterisation was elaborated by KNOPPIK-WRÓBEL [149] and KLEMCZAK AND KNOPPIK-WRÓBEL [145]. The parametric study was performed pointing out the factors which influence the early-age stresses in walls: initial considerations on the effect of geometry and dimensions [140], curing conditions [139] and concrete mix composition [148] were presented. The findings of this detailed, spatial analysis of reinforced concrete walls were evaluated based on the current knowledge in the field. Emphasis was put on the simplified approaches proposed in the literature of the subject: an overview with comparative analysis of currently used simplified methods for analysis of early-age walls was presented by KLEMCZAK AND KNOPPIK-WRÓBEL [142, 144]. The models, both numerical and simplified engineering models, were verified on the real-scale benchmarks [84, 136, 146, 150].

This research allowed to understand the behaviour of early-age reinforced concrete walls and phenomena that govern this behaviour. Because of a large number and complexity of relevant factors there was a need to summarise the findings of the research and elaborate on the major phenomena that characterise the behaviour of the walls. The main focus was put on the structural behaviour of walls and the influence of restraint conditions on this behaviour, which included the geometry of the walls and stiffness of the restraining body.

1.3 Range of thesis

KLAAS VAN BREUGEL [215] wrote that *it is [...] a classical dilemma that people always run the risk to lose the balance between [...] the model and reality. Indeed, aware of the fact that models may be no more than a shadow of reality, it is believed that models can be of great help, both for doing research and for serving engineering purposes.* However, recent studies on volume changes of concrete at early ages have revealed the complexity of the phenomenon rather than solving the problem. Thus, for the purpose of this thesis firstly the phenomena which govern the early-age behaviour of reinforced concrete walls were characterised and constitutive equations for their description were proposed. Then, the model was formulated, it was shown that the model can properly reproduce the real behaviour of the analysed structures, and it was used to perform a study of the early-age stresses on different types of reinforced concrete walls. Finally, a discussion was made about the factors which influence the character and magnitude of early-age stresses in walls and what are their effects.

The detailed range of the thesis is as follows:

1. Characterisation of early-age cracking observed in various reinforced concrete walls. Discussion of similarities and differences related to their geometry, dimensions, materials, construction sequence, technological and environmental conditions during execution and curing, etc.
2. Definition of thermo–physical and mechanical phenomena which govern the early-age behaviour of reinforced concrete walls: hydration heat, autogenous and drying shrinkage, maturity development, creep.
3. Review and preliminary assessment of proposals for phenomenological description of thermo–physical and mechanical behaviour of early-age concrete and soil.
4. Review and preliminary assessment of simplified engineering methods for description of the structural behaviour of early-age concrete walls.
5. Formulation of a mathematical model for simulation of the behaviour of early-age reinforced concrete walls including structure–subsoil interaction. Formulation of a numerical model based on Finite Element Method and its computer implementation. Verification of the model on a real benchmark wall.
6. Study of the character and magnitude of stresses on a wide range of typical early-age reinforced concrete walls with the use of the computer implementation of the mathematical model, investigating the effect of:
 - dimensions of the wall on the degree of restraint and resulting restraint stresses;
 - stiffness of the restraining body (foundation, subsoil) on the degree of restraint and the resulting stresses;
 - restraint conditions on the character of stresses.
7. Formulation of a simplified engineering model for the structural behaviour of early-age reinforced concrete walls. Evaluation of the model by comparison with the results obtained with the use of the computer implementation.
8. Discussion of the influence of various factors on the magnitude and character of stresses in early-age walls.
9. Formulation of final conclusions.
10. Definition of limitations of the presented analysis and proposals for the future work.

Chapter 2

Early-age behaviour of reinforced concrete walls

2.1 Problem overview

During the concrete hardening process two main phases can be distinguished in a concrete element behaviour according to the temperature change in time (Fig. 2.1a): a phase of the concrete temperature increase (self-heating) and a phase of cooling of the element down to the temperature of the ambient air. The restrained wall extends in the first phase, opposed by the foundation, which results in formation of compressive stresses (Fig. 2.1c, $t < t_2$). As soon as the maximum temperature is reached, the wall starts to cool down, restrained by a cooled foundation. This leads to development of tensile stresses in the wall (Fig. 2.1c, $t > t_2$). During the whole process water is being removed from or consumed within the element (Fig. 2.1b) which leads to shrinkage of the element and, consequently, adds to the tensile stresses (Fig. 2.1d). Development of stresses begins a few hours after casting of concrete, at the setting time, t_s , when concrete starts to gain stiffness. The graphs in Fig. 2.1 present generalised illustration of the discussed phenomena. The values of the temperature and humidity are different in each point of the wall so the values of the generated stresses vary within the wall due to different thermal and shrinkage strains as well as due to different degree of the restraint. Nevertheless, their character presented in Fig. 2.1 is valid in most areas of the wall. Total tensile stresses in cooling phase concentrate near the joint and reach a significant height of the wall. These stresses may lead to cracking of the element.

A typical pattern of cracking due to the edge restraint of a wall is shown in Fig. 2.2a, assuming that the base is rigid. Without a restraint the section would contract along the line of the base, and so with the restraint a horizontal force develops along the construction joint. The occurring cracks are vertical in the central part of the wall and splay towards the ends of the element where a vertical tensile force is required to balance the tendency of the horizontal force to warp the wall. A horizontal crack may occur at the construction joint at the ends of the walls due to this warping restraint. Fig. 2.2b presents the cracking of the wall with end restraint. The external restraint might be a combination of base and side restraint (Fig. 2.2c, Fig. 2.2d). Usually the first crack occurs at the construction joint as the strength of the bond between the new and mature concrete is less than the tensile strength of the element. Such a crack is therefore less likely to be

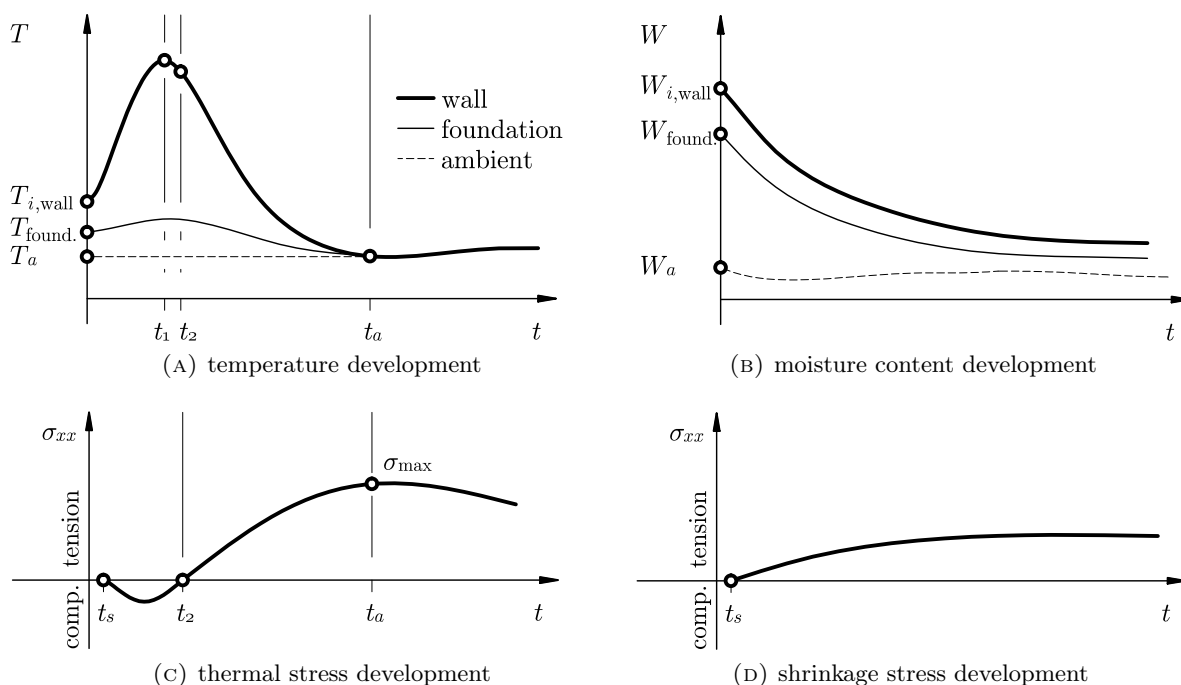


FIGURE 2.1: Temperature, moisture content, thermal and shrinkage stress development in time in an externally-restrained concrete wall.

fully developed. If the overall contraction of the wall can be satisfied by fully developed cracks at one or both construction joints then the intermediate cracks shown in Fig. 2.2c and Fig. 2.2d may not occur. This explains why the worst cracks are usually seen at construction joints or at changes of section where stresses concentrate. The occurring cracks have vertical alignment and may reach a significant height (Fig. 2.3). The greatest height of the crack is observed in the middle of the wall and it declines towards the side edges of the wall or towards the expansion joints. The maximum width of the crack, $w_{k,max}$, occurs at some level above the joint: the cracks start at the wall–foundation joint, widen up to the $w_{k,max}$ value and then decrease in width [88, 177]. Cracking pattern does not depend on the amount of reinforcement applied. When sufficient reinforcement is provided the widths of the primary cracks are controlled but secondary cracks may be induced. Thus, the extent and size of cracking depends on the amount and distribution of the applied reinforcement [3, 171, 196, 197].

2.2 Characteristics of early-age concrete

Physical and mechanical properties of concrete undergo continuous changes from the moment of mixing of the concrete constituents up to the moment of achieving their final values in the mature concrete. Development of these properties is connected with the progressing process of cement hydration and its advancement depends directly on the degree of hydration [66] (Fig. 2.4). The degree of hydration, α_H , is a measure of the extent of the reactions between cementitious materials with water and is defined as the ratio between the quantity of hydrated, $m_H(t)$, and the initial quantity, $m_{H,i}$, of the cementitious material [65, 154, 202], which is expressed as a ratio between the water bound in the process of cement hydration, $w_H(t)$, to the total amount

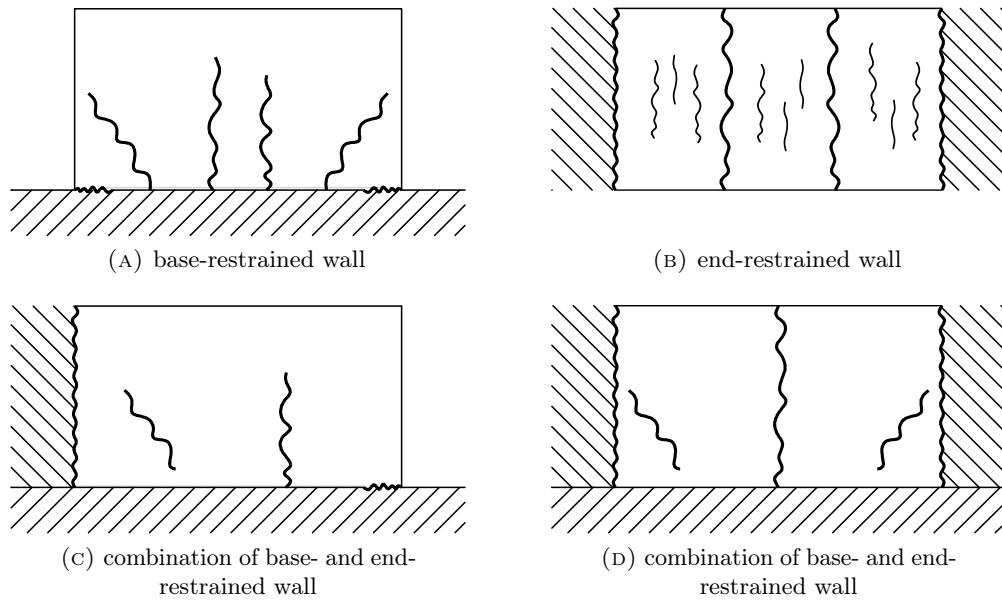


FIGURE 2.2: Typical cracking patterns in early-age reinforced concrete walls.

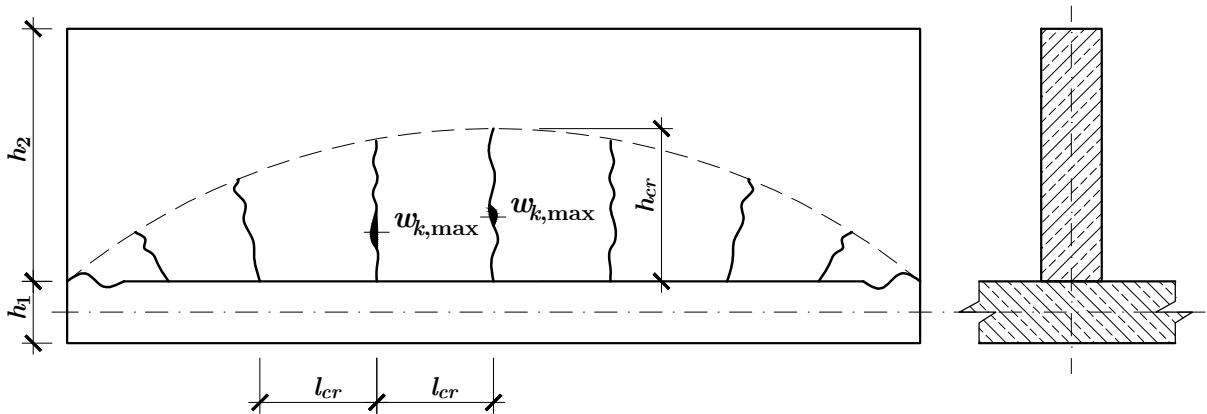


FIGURE 2.3: Cracking pattern in an externally-restrained reinforced concrete element [88].

of water needed for complete hydration, $w_{H,\text{tot}}$. Assuming that the quantity of the hydrated products is proportional to the relative heat of hydration, degree of hydration can be expressed as a ratio between the cumulative heat, $Q(t)$, released up to a certain time, t , and the total heat, Q_{tot} , expected at the completion of the cement hydration reaction [214]:

$$\alpha_H(t) = \frac{m_H(t)}{m_{H,i}} = \frac{w_H(t)}{w_{H,\text{tot}}} = \frac{Q(t)}{Q_{\text{tot}}}. \quad (2.1)$$

The degree of hydration is a function of time and increases from 0% at the beginning of hydration to 100% when hydration is fully completed. In reality not whole cementitious material hydrates and 100% degree of hydration may never be reached [202].

Three main characteristic phases in concrete life can be distinguished: fresh concrete, early-age concrete (transient phase) and mature concrete [130]. Fresh concrete is a multi-component material, composed of aggregate, cement and water, characterised by properties of a plastic

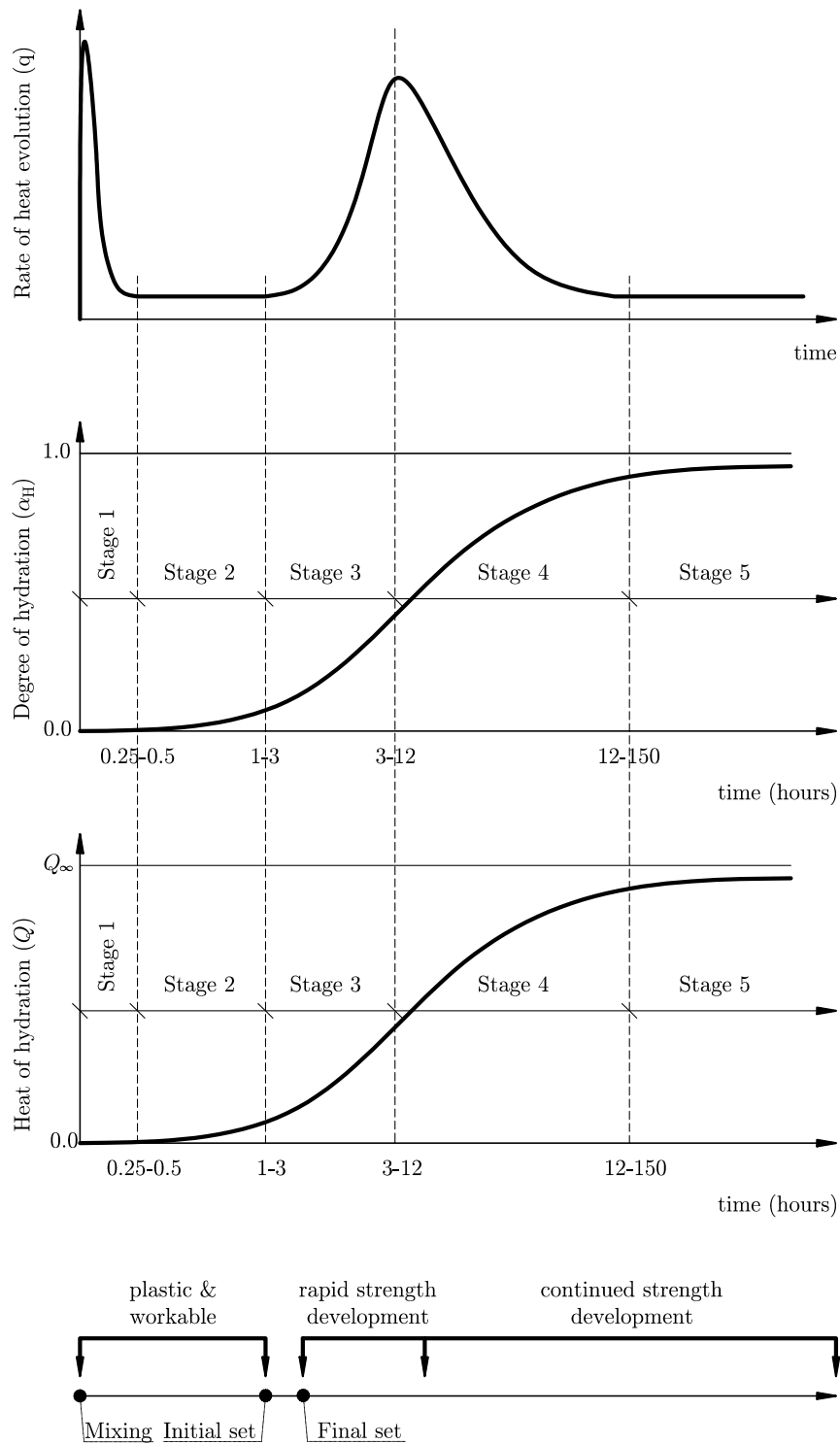


FIGURE 2.4: Concrete behaviour during progressing hydration of cement after SCHINDLER [200].

material and liquid. This phase of concrete is workable and allows for transportation and casting until the setting process begins. According to the development of hydration heat, in the first stage after mixing (stage 1) a rapid increase of heat production is observed, which is connected with wetting of cement grains. Then, the rate of heat production decelerates almost completely (stage 2); this phase is called a dormant period [175]. Fresh concrete generally does not have strength. Due to capillary pressure and friction between the concrete mix constituents it is possible to determine the instantaneous strength of fresh concrete but it is an apparent strength.

Setting of concrete initiates a few (1 to 3) hours after mixing. When setting begins, the rate of hydration heat development increases (stage 3), but with a slower rate than in the stage 1; C-S-H gel is produced in that phase. As soon as the setting of the concrete mix is terminated, concrete can be regarded as a solid material, characterised by elastic, plastic and also strong viscous properties. This phase is called early-age concrete. Progressing cement hydration leads to strength development in concrete. An increased rate of strength development is observed in the very early ages of concrete hardening connected with an increase in the rate of hydration heat development (stage 3). Then, the hydration process decelerates again (stage 4) and so does the rate of strength development. In some types of cements second peak in the rate of hydration heat development might be observed [175].

Theoretically, the strength gain proceeds until the hydration of cement is completed (stage 5). Then the concrete strength reaches its final, steady value. Practically, the hydration process is never completed and strength gain continues in mature concrete. However, for practical reasons, it is assumed that hardening of concrete terminates after 28 days, the concrete at that moment is considered as mature and its strength as final. Nevertheless, it was observed that in concrete mixes made of blended cements hydration rate is slower and significant gain in material properties occurs way beyond 28th day [130].

Due to the exothermic character of cement hydration temperature development is observed in concrete elements. The process of concrete hardening is also accompanied with moisture migration which leads to reduction of concrete volume and consequent shrinkage of a concrete element. Water is transported within and out of the concrete element due to various phenomena. The loss of water through desiccation and evaporation at the surface of the element is called external drying shrinkage. Desiccation of water is driven by concentration gradients within the elements caused by humidity difference between the element and the ambient surrounding. Water is transported by vapour transfer and capillary transfer [2]. The internal drying is associated with self-desiccation of concrete (lowering of the internal relative humidity). Self-desiccation is commonly attributed to autogenous shrinkage, however, it must be emphasised that autogenous shrinkage is governed by both self-desiccation and chemical shrinkage, with the influence of the latter one more pronounced in the very early ages [104]. Chemical shrinkage results from the reduction in the material's volume as water is consumed by hydration: when water and cement react the volume of the products of this reaction is 7 to 10% less than that of cement and water [234]. The autogenous shrinkage is considered proportional to the degree of hydration [215].

The early-age concrete is characterised by very strong viscous behaviour due to high rates of creep [209]. Creep is also proportional to the degree of hydration. The phenomenon of creep has an influence on the cracking risk in early-age concrete because it reduces the magnitude of stress, and thus reduces cracking intensity or extends the period until cracking occurs.

2.3 Early-age thermal–shrinkage stresses

Thermal–shrinkage stresses in externally-restrained elements result from a coupled action of self-induced and restraint stresses with a predominant role of the latter ones [145, 149]. The influence of the self-induced stresses is much smaller. This results from the fact that temperature and humidity gradients (volumetric strains) are relatively small in comparison to the linear strains caused by contraction of the element along the line of the restraint joint.

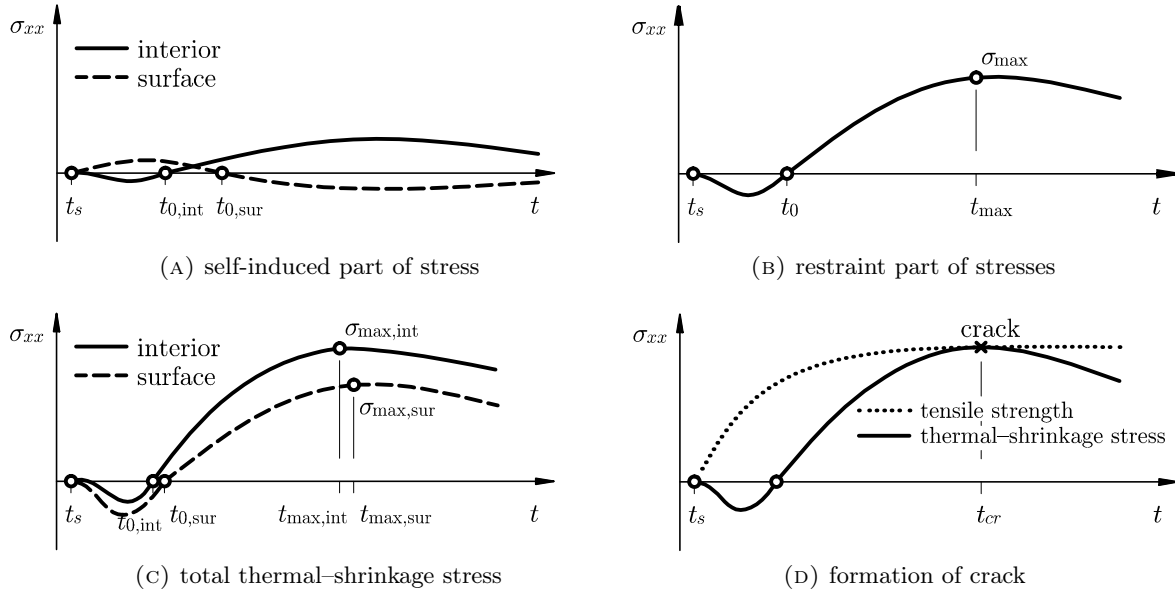


FIGURE 2.5: Development of early-age thermal–shrinkage stresses in time in an externally-restrained element.

Self-induced stresses originate from the material itself due to the internal restraint caused by the temperature and humidity gradients. In an internally-restrained element time-development of stresses is characterised by formation of compressive stresses in the interior and tensile stresses on the surface of the element in the heating phase while in the cooling phase stress inversion might be observed (Fig. 2.5a). Their magnitude depends on a number of material and technological parameters determining the values of generated temperatures and the rate of cooling, with a major influence of the thickness of the element.

Restraint stresses result from the external limitation of deformation, usually caused by previously cast layers. Continuous restraint exists along the contact surface of concrete and any material against which concrete has been cast, e.g. between the concrete structure and its foundation. In a concrete wall cast against a mature layer of concrete tensile stresses result from restraining potential contraction caused by the length changes associated with decreasing temperature within the wall. Their magnitude depends on a degree of restraint induced by an older part against a newer part of the structure. The degree of restraint can be expressed in a form of the restraint factor, γ_R , which in any point of the element is defined as a ratio between the actual stress generated in the element, σ , to the stress at total restraint, σ^{fix} , [5, 116, 177, 184, 232]:

$$\gamma_R = \frac{\sigma}{\sigma^{fix}}, \quad (2.2)$$

and may take values between 0 at no restraint to 1 at total restraint. It varies throughout the element with the maximum value at the joint between the wall and the restraining element and decreasing towards free edges of the element. The degree of restraint of the element depends on its length-to-height ratio, L/H , and on the ratio of the stiffness of the element and the restraining body. Restraint stresses have different character than self-induced stresses: in the heating phase almost the whole volume of the element is subjected to compression while in the cooling phase tensile stresses occur (Fig. 2.5b).

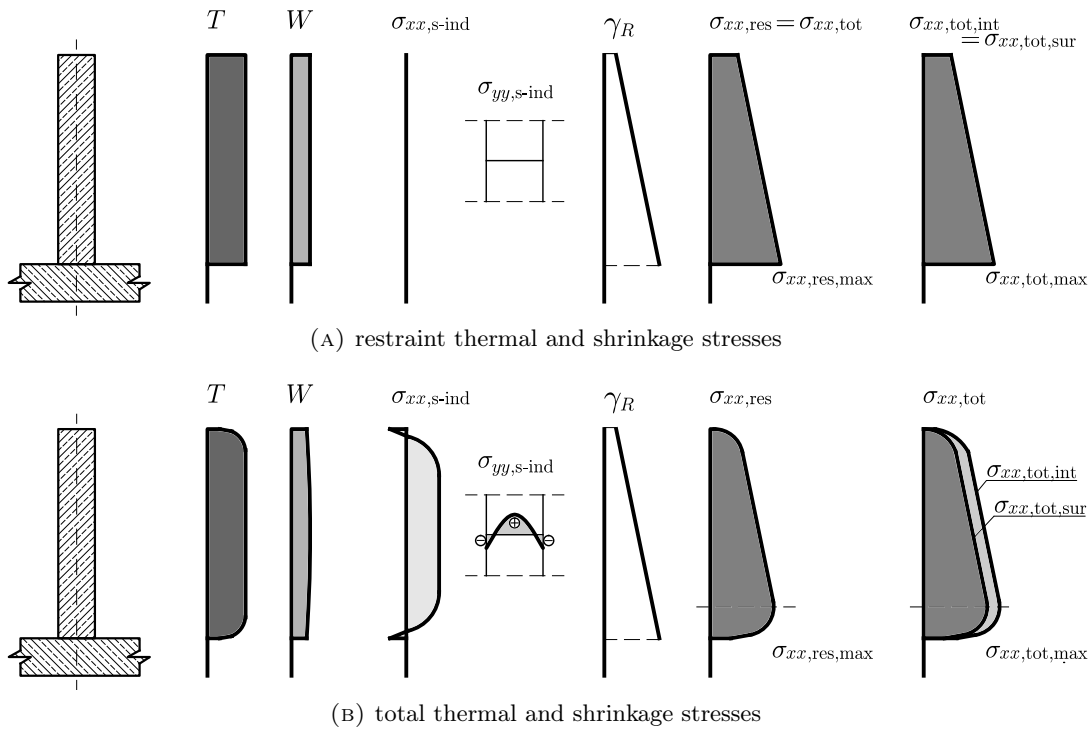


FIGURE 2.6: Distribution of early-age thermal–shrinkage stresses in a cross-section of a wall.

Figure 2.6 presents distribution of stresses in the cross-section of a wall. Stresses generated by the external restraint (σ_{res}) have a major influence on the values and character of the total stresses (σ_{tot}). If there were no temperature and humidity gradients within the element, the stress distribution would be proportional to the degree of restraint as shown in Fig. 2.6a (there would be no self-induced stresses, σ_{s-ind}). The maximum value of the stress would be then observed at the joint between the wall and the restraining body. Such a situation occurs when the thickness of the element is relatively small or when curing technology (e.g. formwork with insulation) reduces the rate of heat and mass exchange. Nevertheless, in most of the cases the maximum stress appears above the joint. This results from the temperature and humidity gradients at the height of the wall which generate the self-induced stresses. The distribution of the total thermal–shrinkage stresses at the height of the wall looks like in Fig. 2.6b with the maximum value of the stress above the joint. The temperature and humidity gradients at the thickness of the wall also cause self-induced stresses, which are the reason why the values of the total thermal–shrinkage stresses differ in magnitude between the interior and the surface of the wall (Fig. 2.5c, Fig. 2.6b).

If the value of tensile stress in any location of the element exceeds the actual tensile strength of concrete in that location, a crack is formed (Fig. 2.5d). The diagram of stress distribution in

the cross-section of the wall in Fig. 2.6b explains why the greatest width of the crack appears above the joint between the restrained element and the restraining body. If the stress state in cooling phase looks like in Fig. 2.6b, which happens when the wall is kept in formwork during the whole process of concrete hardening, development of cracks initiates from the interior of the wall (internal stresses reach higher value than surface stresses). Nevertheless, more often formwork is removed from the wall in cooling phase, and then first cracks appear on the surface of the element. The internal stress can also become of considerable magnitude and consequently through cracks may develop.

2.4 Externally restrained concrete elements subject to early-age cracking

There are multiple examples of externally restrained concrete elements, e.g.: structural elements of bridges, such as bridge decks, especially with box sections, and bridge abutments; tank walls, walls of nuclear containments, retaining walls and tunnel walls cast against hardened foundation of cast in stages. These elements are susceptible to cracking in early ages of concrete curing. In responsible structures such as liquid tanks and nuclear containments cracking, especially deep and through cracking, impairs tightness and promotes leakage of aggressive liquids or radioactive elements. Such cracking is a limit state failure which can lead to environmental catastrophe. Formation of surface cracking leads to exposure of reinforcement and promotes intrusion of water and aggressive chemicals (chlorides, sulfates) which then causes corrosion of reinforcement and spalling of concrete cover. Such cracking is a durability issue. In all cases cracking of concrete elements impairs their functionality and aesthetics. Repair works are then required.

2.4.1 Tank walls

Tanks are engineering structures which geometry results from technological requirements [95]. They are usually built on a plan of a circle (cylindrical or conical shells and domes) or a rectangle (prismatic tanks). The walls of the tanks are usually supported on a base slab; sometimes sealing tape is introduced between the walls and the slab but most often the joint between the foundation and the walls is monolithic. The circular tanks are usually realised as pre-stressed concrete structures; rectangular tanks, because of their geometry, are made of reinforced concrete.

The tanks serve to collect water, sewage, liquid gas and oil, biogas and industrial liquids. They can also serve as cooling water tanks, reservoirs and swimming pools. Hence, the main condition to satisfy is their tightness. The requirements of tightness in tanks are very harsh – ultimate limit state of cracking is a decisive design limit state. EUROCODE 2 in Part 3 [184] provides the classification of reinforced concrete tanks according to their tightness. Four tightness classes, from 0 to 3, are distinguished. Class 2 or 3 is mostly used in design which means that either minimal or no leakage is allowed in such structures; through cracks are unacceptable.

Tank walls are perfect examples of externally-restrained structures. Tanks are usually realised in stages; if the height of the tank is moderate, the walls are divided into segments of the final tank height. First, every second segment is constructed and then the remaining segments are

cast. If the height of the wall is too big to construct the segment at once, there are also breaks at the height. Each segment is therefore realised in different ambient conditions, the age of each segment is diverse, so developing thermal and shrinkage strains are on different levels. Moreover, the segments differ also by restraint conditions due to a difference in a number of restrained edges. For construction of tanks concrete based on Type III cement is usually used to limit hydration temperatures in the elements. The required concrete class is either C30/37 or C25/30 and it is achieved by appropriate class of cement: for higher strengths class 42.5 is applied, otherwise class 32.5 is used.

Early-age cracking is frequent in monolithic concrete tank walls. The notion of that problem is emphasised worldwide so the efforts are made to prevent that cracking even at the design phase [155, 168, 176]. However, only recently several failures of tanks due to early-age cracking were recorded solely in Poland. Early-age cracking with cracks width reaching even up to 0.5 mm has been commonly observed in tank walls constructed after 1995 because since then such realisations begun to be performed by unexperienced design and construction teams not aware of the specific nature of externally-restrained concrete structures [206].

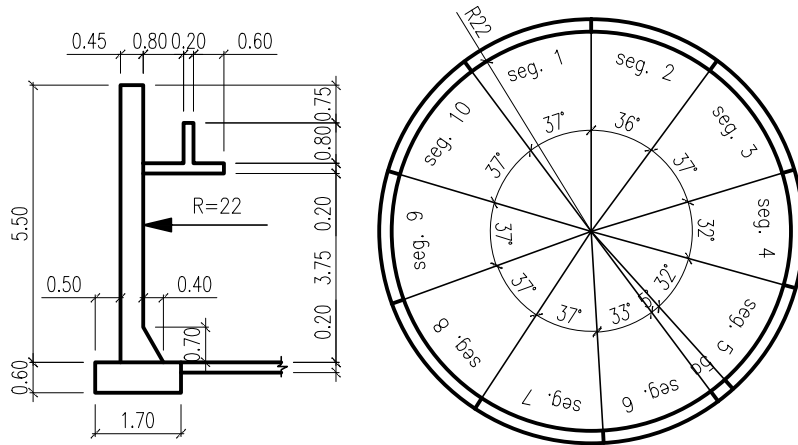


FIGURE 2.7: Cylindrical industrial sewage tank, Poland [206].

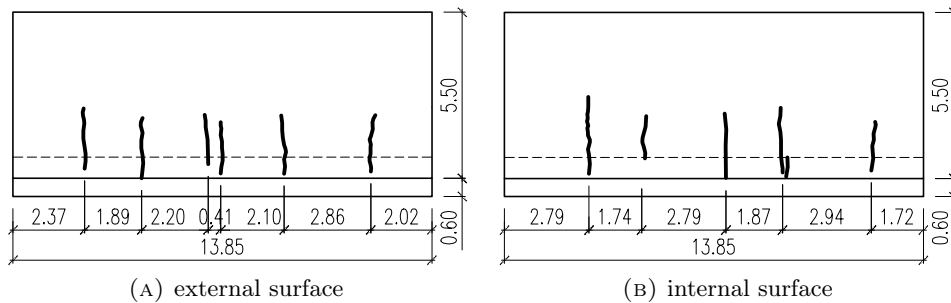


FIGURE 2.8: Cracking pattern in segment 1 of a cylindrical sewage tank (external view) [206].

The first example comes from the observations of a group of cylindrical reinforced concrete tanks [206, 235]. 10 identical tanks were built for the purposes of sewage treatment facility. The tanks had capacity of 8300 m³ and internal radius of 22.45 m. The walls with thickness of 45 cm and height of 5.5 m were cast in segments of 13.8 m length ($L/H = 2.51$, $m = 4.44 \text{ m}^{-1}$). Geometry of a typical tank is shown in Fig. 2.7. First the odd segments were cast and then the even ones. For vertical reinforcement $\varnothing 12$ bars, every 125 mm were applied. Horizontal (peripheral)

reinforcement was diverse: near internal surface these were $\varnothing 16$ bars up to 2.80 m above the foundation ring and then $\varnothing 12$ bars every 125 mm; near external surface these were $\varnothing 20$ bars up to 1.20 m, then $\varnothing 16$ bars up to 2.50 m, $\varnothing 12$ bars up to 4.50 m and again $\varnothing 16$ bars, all spaced every 1 m. Concrete class C30/37 was used with either cement CEM III/A or CEM II/B-S. Concrete of the walls was cured for 7 days by water pouring. In each of the tanks early-age cracking occurred, detected during tightness test. Detailed cracking inventory was done in one of the tanks. Only one segment was uncracked; this segment was cast as a segment restrained along one edge only. The lightest cracking was observed in the segment restrained along 3 edges but kept in formwork for 10 days (in contrary to 2 – 3 days as in other segments): only 2 splayed surface cracks of 0.1 mm thickness appeared. In other segments mostly through cracks were formed with width up to 0.2 to 0.3 mm reaching on average 1/2 of the wall height. The greatest width of the crack was always formed at ca. 1.1 m above the slab. Fig. 2.8 shows cracking pattern in the most severely cracked segment.

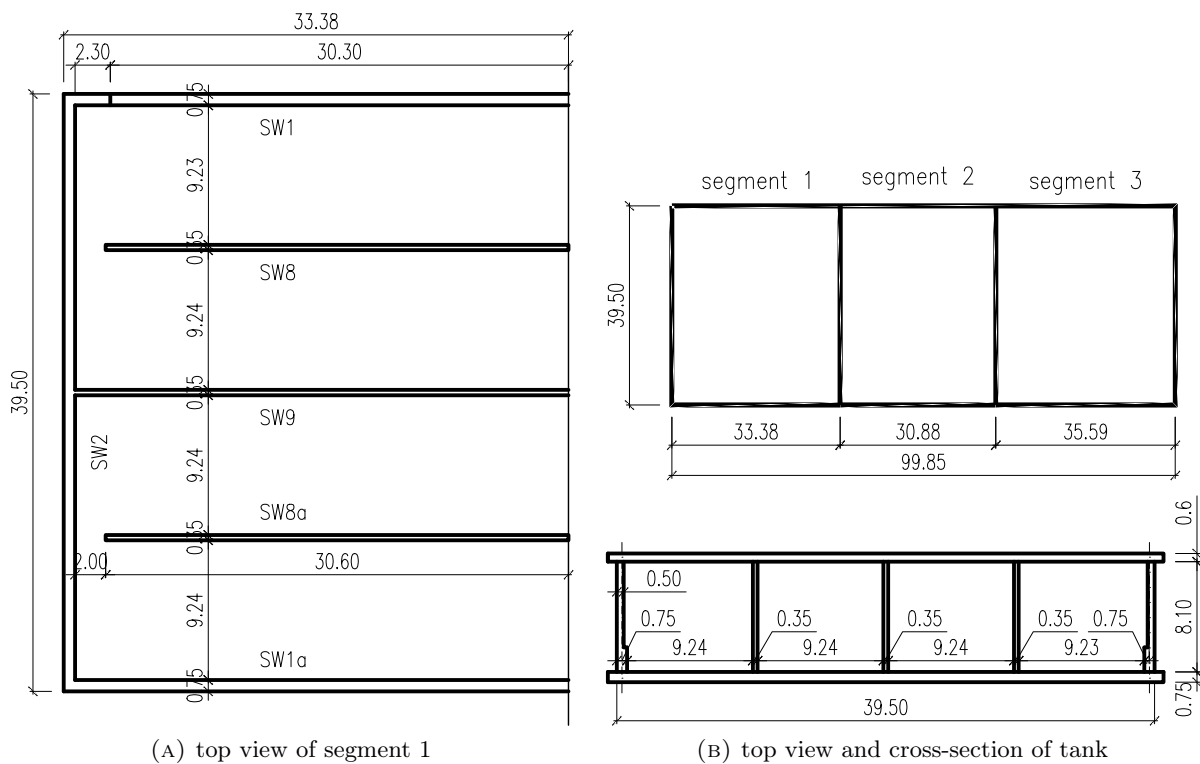


FIGURE 2.9: Rectangular tank at a sewage treatment facility, Poland [236].

Together with the construction of cylindrical tanks, a rectangular tank with capacity of 30,000 m³ was built at the sewage treatment facility [236]. The tank had plan dimensions of 98.35 m \times 38.00 m. The walls of the tank had height of 8.1 m and thickness of 0.75 m at the bottom part and 0.5 m at the top part. One of the external walls was investigated in detail. Geometry of the tank with emphasis on the analysed segment is shown in Fig. 2.9. The wall of interest was constructed in 6 stages. In the first stage the slab was constructed, then the bottom part of the wall with height of 1.8 m and thickness of 0.75 m ($L/H = 16.83$, $m = 2.67 \text{ m}^{-1}$), and finally the upper part of the wall with thickness of 0.5 m was executed in 4 stages: first two stages covered additional 3 m of height with two segments of 15.0 m and 15.3 m length ($L/H \simeq 5.00$, $m = 4.00 \text{ m}^{-1}$) and the remaining two stages completed the wall. Concrete class was C25/30. First three segments were made of cement CEM III/A 42.5, the fourth segment was made of cement CEM II/B-S

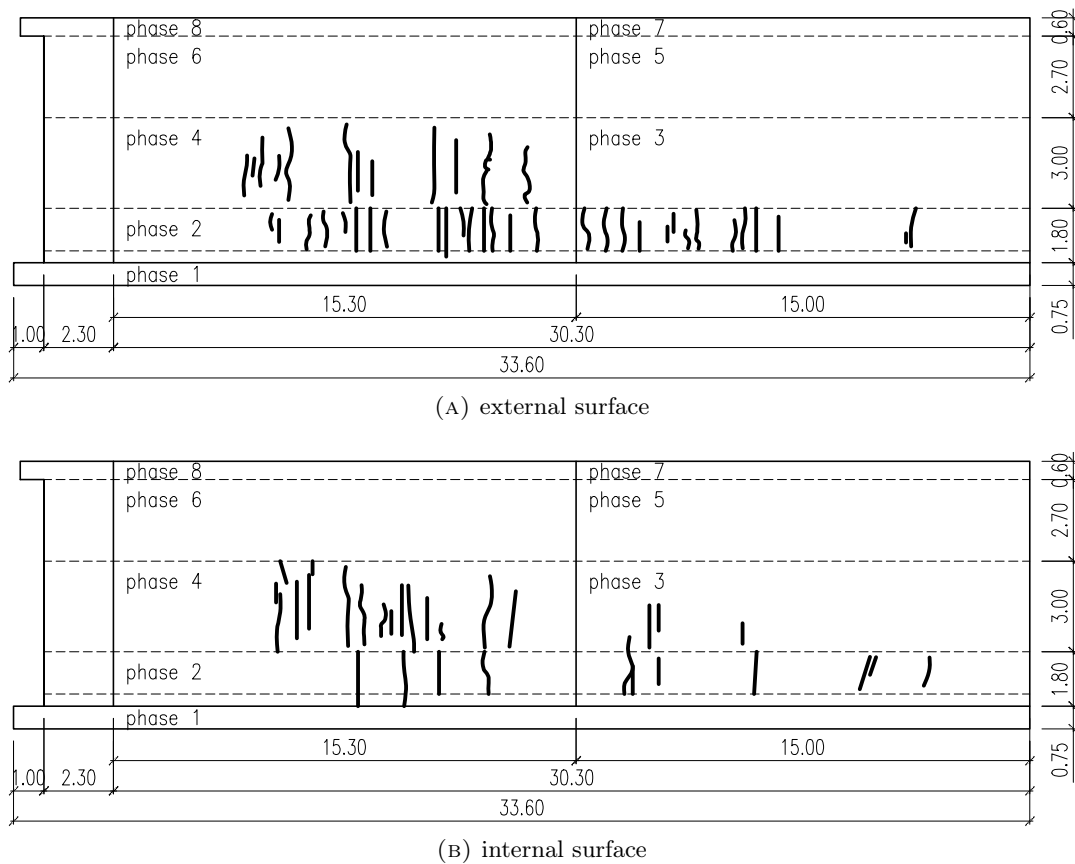


FIGURE 2.10: Cracking pattern in a wall of a sewage tank (external view), Poland [206].

32.5R. $\varnothing 20$ bars were used for reinforcement. In vertical direction bars were spaced every 150 mm. In horizontal direction in the bottom part of the wall bars were spaced every 100 mm on the external side and 150 mm on the internal side. In the upper part that spacing was continued at 1.2 m, then equal spacing of 150 mm was applied on both sides. Intensive cracking was observed in the segments of the first four stages. Geometry of the wall, construction stages and resultant cracking are presented in Fig. 2.10. Concrete of stage 2 was severely cracked at the whole height of the segment due to a very high degree of restraint. In the upper part, some cracking appeared on the third segment while the fourth segment was also intensively cracked – cracks reached $3/4$ of the segments height and some cracks appeared even on the whole height of the segment. Such severe cracking was caused mainly by the restraint of the wall along two edges.

Another example is a set of cylindrical water tanks in another sewage treatment facility [147]. The set was composed of two biological blocks with the outer diameter of 23.2 m and sludge chamber of 11.7 m diameter. The latter one was executed as a monolithic structure with walls joint with the foundation slab; in biological blocks sealing tape was introduced in that joint. Severe cracking was observed in the walls of the tanks before putting the tank into operation. The most severe cracking occurred in a sludge chamber. Fig. 2.11 shows the geometry of the chamber. The walls of the sludge chamber had thickness of 35 cm with a trapezoidal ring with thickness up to 135 cm. Concrete class C25/30 was used. The walls as well as the ring were reinforced with $\varnothing 16$ bars spaced every 200 mm in both vertical and horizontal direction. The walls were cast two months after the slab. The cracks started at the joint between the walls and the base slab and appeared at the whole height of the joint ring (up to 1.75 m), their width reached up

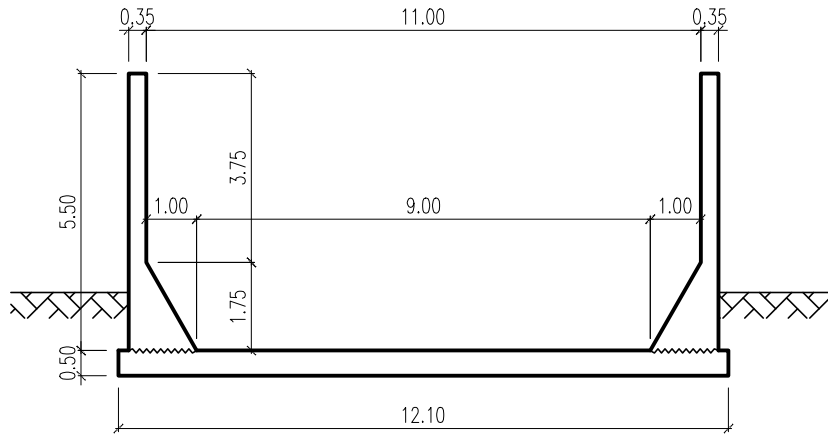


FIGURE 2.11: Sludge chamber in a sewage treatment facility, Poland [147].

to 0.5 mm and they were spaced on average every 100 cm. The cracks appeared because of the underestimated reinforcement in the ring, mainly horizontal reinforcement. That is because the structure was characterised by a high degree of restraint – the base slab was already mature and at the moment of execution of the walls thermal and shrinkage strains no longer developed in the slab, moreover, the walls were cast in long segments (however, the exact length of the segment cannot be determined) so L/H was high.

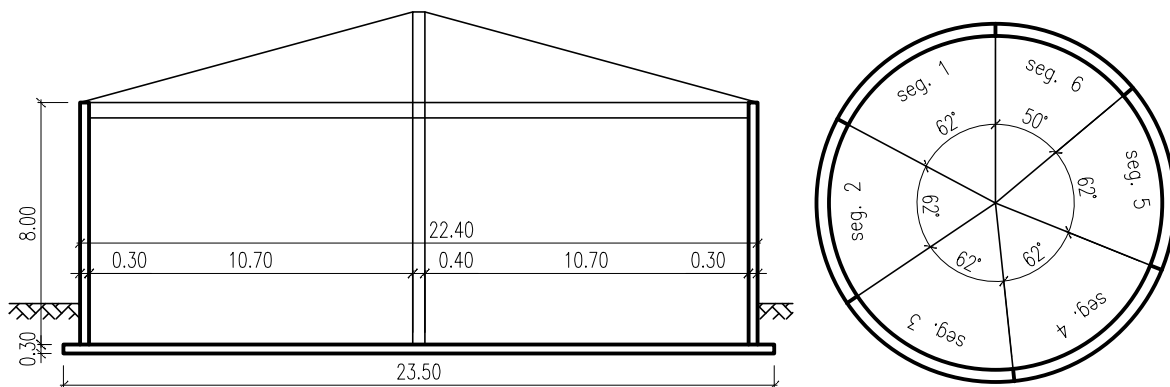


FIGURE 2.12: Cylindrical industrial sewage tank, Poland [96].

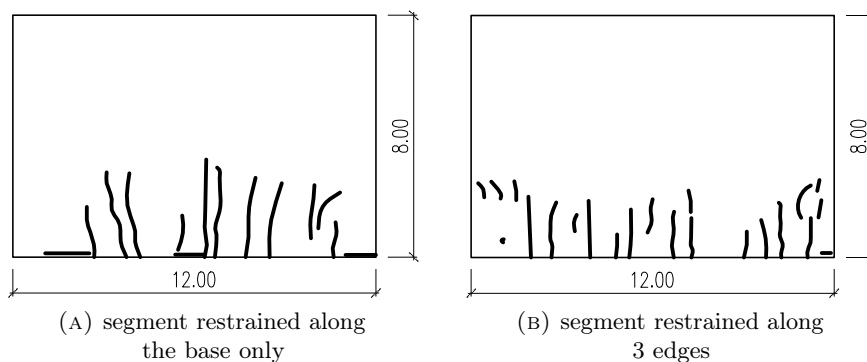


FIGURE 2.13: Cracking pattern in chosen segments of an industrial sewage tank, Poland [96].

Similar problem occurred in a reinforced concrete cylindrical industrial sewage tank [96]. The walls had 8 m height and 30 cm thickness and were supported on a 30 cm thick slab. Geometry

of the tank is shown in Fig. 2.12. The connection between the walls and the slab was a hinged connection ($\varnothing 12$ bars spaced by 200 mm in the axis of the wall). The tank walls were constructed in segments. Each segment had length of about 12 m and the final height of the tank ($L/H = 1.50$, $m = 6.67 \text{ m}^{-1}$). Firstly, every second segment was cast, the formwork was removed after 3 days and the gaps were filled with the remaining segments, so half of the segments were restrained along one edge, and the other half along three edges. Reinforcement near the external surface was made with $\varnothing 16$ bars, spaced every 95 mm for vertical reinforcement and from 95 mm at the bottom to 55 mm at the top for horizontal reinforcement. Reinforcement near the internal surface was made with $\varnothing 10$ bars, spaced every 150 mm for vertical reinforcement and 80 mm for horizontal reinforcement. The tightness test showed the existence of numerous through cracks. The cracks were vertical in the center of the segment and splayed towards the edges of the segments; they reached 1/3 of the wall height. The cracks were formed also at the joint between the walls and the slab, mainly due to the slip at the corners. Fig. 2.13 shows the cracking pattern in exemplary odd and even segments.

2.4.2 Elements of bridge structures

In a majority of cases construction of a bridge structure begins with casting of a foundation, shallow or deep but with cooperating cap, after 2 to 3 months proceeded with concreting of the rest of the supporting structure in a form of a stem wall or walls of a frame system. All of these elements in bridge structures are usually massive elements. They are characterised by the surface modulus $m \simeq 2.0 \text{ m}^{-1}$ or less, which signifies that in the interior of such elements almost adiabatic curing conditions are formed. In a design of concrete mix used for bridge engineering applications specifications limit the use of materials forcing application of Type I (Portland) cement and crushed granite/basalt as coarse aggregate [30, 190]. Although such a composition of concrete mix ensures desired strength, durability and quality of concrete, other properties may be impaired. High amount of hydration heat generated by Portland cement leads to generation of high temperatures in the early-age concrete elements; in the interior of bridge abutments the temperature increase of up to 40°C can be observed. The temperature in such elements increases during the first 2 to 3 days and then it starts to decrease slowly until after about 2 weeks it reaches the ambient temperature.

The coupled action of self-induced and restraint stresses is observed in bridge abutments. Self-induced stresses result from considerable temperature gradients formed during cooling of concrete if it is characterised by low value of thermal conductivity coefficient, λ , and high specific heat, c_b ; the values of λ and c_b depend on the concrete mix composition, mainly the type and amount of aggregate. The restraint stresses depend mainly on the degree of restraint and are proportional to the temperature difference between the maximum (peak) hydration temperature and the ambient temperature according to the thermal expansion coefficient, α_T . The values of thermal expansion coefficients for typical aggregates differ in wide range from about 5 to $13 \cdot 10^{-6}/^\circ\text{C}$ [175]. The generated tensile stresses can reach significant levels and cracking in an early-age stem wall may occur. The observed cracks are formed mostly on the surface, exposing reinforcement, but they might be also through cracks reaching a considerable height (up to 0.6 of the height of the stem and even the whole height of the walls in frame systems). Such cracking endangers tightness of the structure exposing it to the action of aggressive environment. Once their durability is

structures intensive cracking was observed. The observed cracks were vertical in orientation, started at the wall–foundation joint and reached 1/2 to 3/4 of the wall height; the highest cracks appeared in the middle of the wall. The cracks width ranged from 0.1 to 0.4 mm and near the joint the cracks were through. Fig. 2.14 show a cross-section of one of the motorway bridge abutments. The segments of the abutment had length of 14.35 to 22.24 m and a stem of 1.5 m thickness and height of 7.05 to 7.78 m, without a back wall ($L/H = 1.84$ to 3.15 , $m = 1.63 \text{ m}^{-1}$). Reinforcement in a form of $\varnothing 16$ bars every 100 mm was used. The stem of the abutment was cast 15 days after the foundation. Cracking was observed in all segments of the abutment (Fig. 2.15). Cracks of width between 0.2 to 0.4 mm reached 1/3 of the stem height.

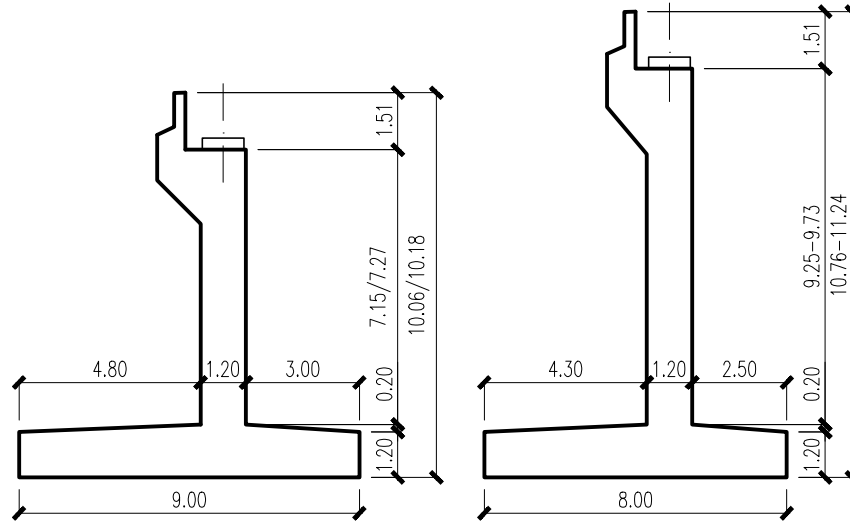


FIGURE 2.16: Cross-section of road and river bridge abutments, Poland [224, 225].

A similar problem was observed in the abutments of a road bridge and a river bridge along the express road [224, 225]. Geometry of the abutments is shown in Fig. 2.16. The abutments of the road bridge were composed of two segments of 16.32 m and 17.33 m length. The stem wall had 1.20 m thickness and 7.27/7.15 m height ($L/H = 2.24$ and 2.42 , $m = 1.67 \text{ m}^{-1}$). The abutments of the river bridge were composed of two segments of 20.24 m each. The stem wall had 1.20 m thickness and height from 9.40 m to 9.73 m and from 9.25 m to 9.57 m in each axis, respectively ($L/H = 2.08$ to 2.19 , $m = 1.67 \text{ m}^{-1}$). The stem walls were reinforced with $\varnothing 16$ bars spaced every 100 mm. Here also vertical cracks appeared, starting at the joint and diminishing towards the top edge of the wall. In road bridge abutment the cracks reached up to ~ 100 cm height and the cracks width was from 0.1 to 0.3 mm with some through cracks in the bottom parts. The geometry and cracking pattern in the road bridge abutment is shown in Fig. 2.17. In the river bridge the cracking was less intensive: cracks reached at most up to 1/5 of the wall height and their width did not exceed 0.2 mm.

Another example is cracking observed in 15 bridge structures along highway [87]. Only one of the examined segments was uncracked. In the remaining ones the crack widths ranged from 0.1 to 0.5 mm. The cracks were spaced usually 1.35 to 2.70 m and reached on average 70% of the wall height; some of the cracks appeared at the whole height of the walls. In the vicinity of the wall–foundation joint through cracks were formed. The bridge structures had a form of single-span frame systems composed of two segments for each carriageway of the A4 motorway. The frame system consisted of two walls with thickness of 0.75 to 0.80 m and a deck of thickness

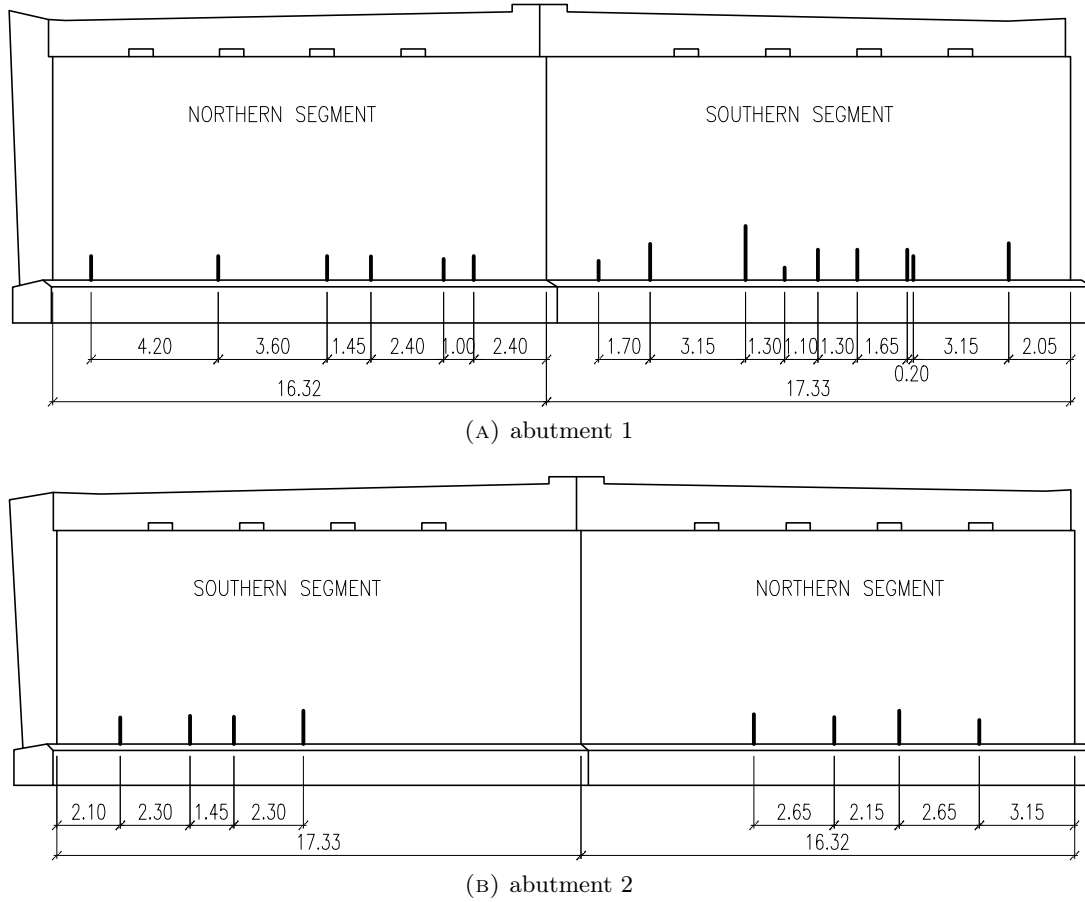


FIGURE 2.17: Cracking pattern in road bridge abutments, Poland [225].

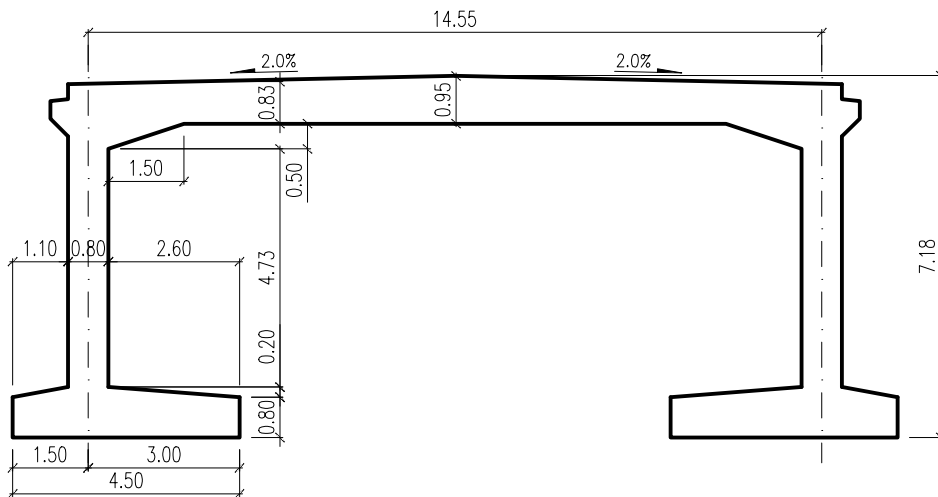


FIGURE 2.18: Longitudinal section of a highway frame bridge, Poland [87].

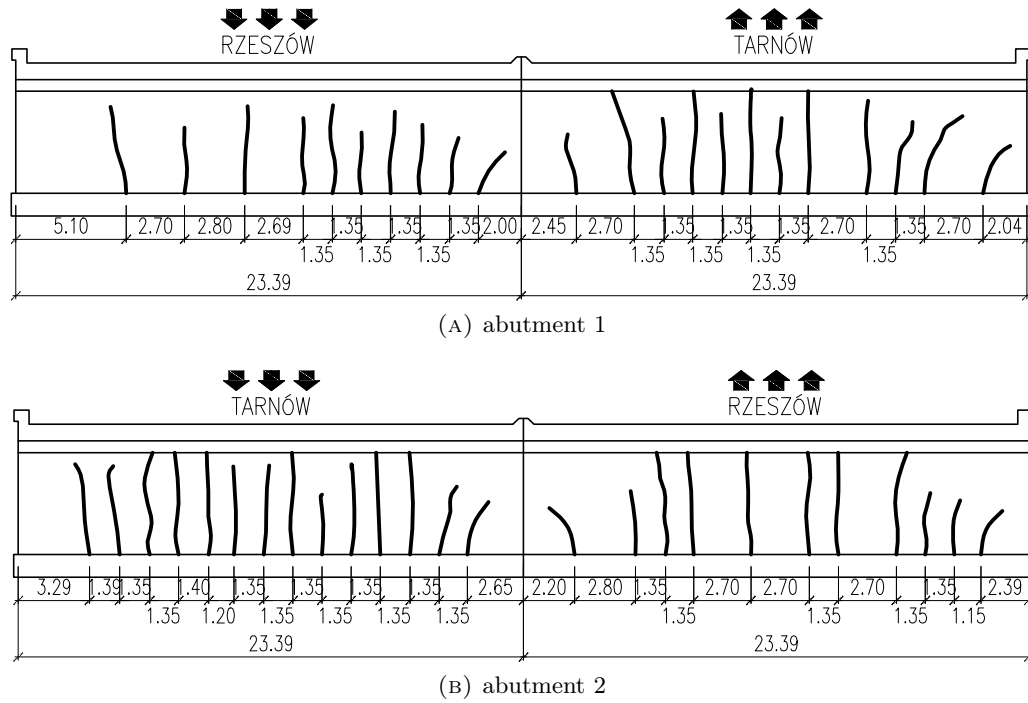


FIGURE 2.19: Cracking pattern in walls of a highway frame bridge, Poland [87].

0.90 to 0.95 m. The walls were monolithically connected with slab foundations (executed 3 to 4 months before the walls). A typical bridge cross-section is presented in Fig. 2.18. The walls of the bridge had thickness of 0.80 m, span of 23.39 m and clear height of 4.75 m. The deck had thickness of 0.95 m and span of 15.3 m. Hence, the elements were characterised by surface moduli of 2.50 m^{-1} for the walls and 2.25 m^{-1} for the deck. Reinforcement in a form of $\varnothing 16$ bars every 100 mm was used. Vertical cracks were observed along the entire span of the walls spaced every 1.35 to 2.70 m. The cracks reached on average as much as 0.8 height of the wall and almost 1/3 of all cracks reached the whole height of the wall. The width of the cracks was between 0.1 and 0.3 mm but 20% of all cracks exceeded the allowable cracks width $w_{k,\text{lim}} = 0.2 \text{ mm}$. Fig. 2.19 shows the observed cracking pattern in the walls.

OBJECT	BRIDGE [85]	BRIDGE [224, 225]	BRIDGE [87]
concrete class	C30/37	C30/37	C35/45
water, kg/m^3	161	151	153
cement type	CEM I 42.5N	CEM I 42.5N	CEM I 52.5N
cement amount, kg/m^3	365	350	380
fine aggregate (sand), kg/m^3	641	633	650
coarse aggregate type	crushed basalt	crushed granite	crushed granite
coarse aggregate amount, kg/m^3	1289	1176	1155
additives & admixtures, kg/m^3	6	6	2
density, kg/m^3	2462	2316	2340

TABLE 2.1: Concrete mixes used for bridge construction.

The presented bridge abutments were made of typical concrete for bridge applications. Tab. 2.1 presents the detailed composition of the applied concretes. For construction of abutments concrete class C30/37 was used; frame systems were made of a higher class, C35/45. Composition and

proportions of concrete were similar; cement Type I was always used and higher class of concrete was achieved by application of higher class of cement (52.5 instead of 42.5).

2.4.3 Nuclear containment walls

Building structures required for operation of nuclear power plants and other radiological facilities have to meet particular safety-related requirements. The buildings which primary aim is shielding the radiation are nuclear containments. They are used in nuclear power plants, health care facilities conducting radiation therapy, nuclear research facilities and storage/transport casks for radioactive waste. The walls of nuclear containments are usually massive concrete elements threatened by the risk of early-age thermal-shrinkage cracking unacceptable in the view of tightness and durability conditions to be satisfied for appropriate radiological protection.

The materials used for shielding have to satisfy a series of requirements of durability and effective radiation protection, mainly gamma ray shielding and neutron shielding. Concrete is one of the most popular materials used for that purpose [36, 48, 167]. Nuclear containments are usually made of normal concrete with Portland cement of higher class, C30/37 or C35/45 [48, 167]. The size of aggregate has to be limited to assure tightness of hardened concrete [48]. To provide appropriate radiation shielding properties, high-density aggregates are used to attenuate gamma rays and light atomic weight aggregates are used to absorb neutrons. Appropriate gamma-ray protection requires application of aggregates characterised by high bulk density [167]. Most commonly applied aggregates are natural heavy aggregates produced of iron or barite ores (haematite, ilmenite, magnetite or barite) and artificial aggregates (slag and other blast furnace wastes) [36, 157, 164, 211]. These concretes are though characterised by higher thermal expansion, greater shrinkage and worse thermal conductivity than normal concretes [77, 211]. Neutron shielding properties depend on the type of chemical elements contained in the aggregate; hydrogen and boron are especially effective in capturing fast neutrons. Aggregates that contain bound water (produced from ores of hydrous iron, serpentine or bauxite) and aggregates that contain boron (produced from borate ores) are used [157, 164, 167].

High-performance concretes gain popularity in nuclear containment construction. In their production Portland cement is partially replaced with supplementary materials such as lime filler, silica fume or fly ash, which allow to reduce the hydration heat and creep [27, 59]. However, lower density of such concretes impairs their shielding properties. Moreover, its robustness is questionable – due to very high strength (class C55/67) and lower ductility the cracks develop through aggregates which affects the integrity of the structure [167]. Normal concrete is also replaced with self-compacting concrete to simplify the casting process. In case of self-compacting concrete, however, more severe early-age effects are observed [57]. Exemplary concrete mixes used in construction of nuclear containments are collectively shown in Tab. 2.2.

The walls of nuclear containments have significant thickness (1 to 2 m). Because a considerable amount of concrete has to be cast, the walls are constructed in stages: concrete lifts are about 3 m high and the duration between lifts is about 2 weeks [27]. During this time the concrete of previous phase hardens and gains significant stiffness. The difference in stiffness between the old part of the wall and the new part limits the thermal strains in the new part and restraint stresses occur. These stresses can lead to cracking. The cracks can be later closed due to relaxation

CONCRETE TYPE	NC [27]	HPC [27]	HPC [234]	HWC [211]	SCC [57]
Concrete mix composition, kg/m ³					
water	195	161	141	140	175
cement type	CEM II 52.5	CEM II 52.5	CEM I 52.5	CEM III 42.5	CEM I 42.5
cement amount	350	266	420	350	350
SCM type	none	limestone filler & silica fume	none	N/A	limestone filler
SCM amount	0	114 + 40	0	N/A	100
fine aggregate type	sand	sand	sand		limestone
fine aggregate amount	772	759	780	barite 2876	840
coarse aggregate type	N/A	N/A	N/A		limestone
coarse aggregate amount	1099	1100	1073		886
plasticisers	1	8	6	0	14
density	2417	2448	2420	3346	2233

TABLE 2.2: Concrete mixes used for nuclear containments construction.

or pre-stressing, however, in case of an accident they may reopen and promote the leakage of radioactive material. This is why early-age effects are thoroughly considered in the design and controlled during construction [27, 57, 187].

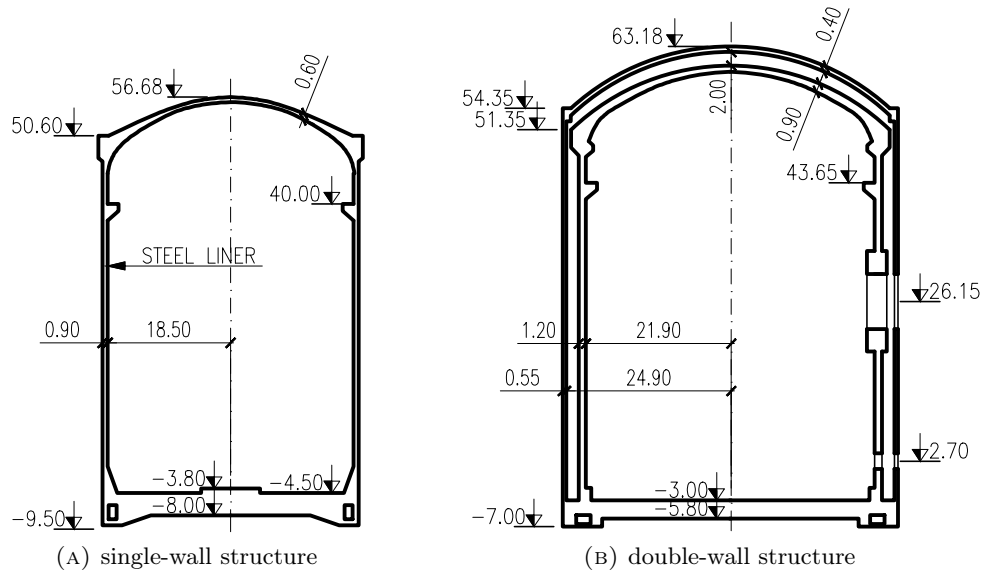


FIGURE 2.20: Reactor building structures, France (private collection of Francis Barré).

Geometry and dimensions of the walls in nuclear containments depend on their destination. In nuclear power plants containment is an element of a power plant safety system. The containment is a main structural element. In the safety system, according to the rule of the *defense in depth*, it is the fourth and the last safety barrier for radioactive material to leak to the environment in case on an accident. Most of the containments are cylindrical shell structures made of reinforced concrete or pre-stressed concrete. Their dimensions differ between different types of nuclear power plants. Currently, the most popular industrial power plants use pressurised water reactors, PWRs (ca. 60%), and boiling water reactors, BWRs (ca. 20%) [109]. The type of the applied reactor determines the geometry of the containment [48, 167]. PWR containments are prestressed concrete cylinders with domes or shells with internal diameter of ca. 40 m, settled on a reinforced concrete slab. For BWR containments are usually rectangular, rarely cylindrical, with internal diameter of ca. 30 m. The containments are covered with a slab or a dome. In the construction of reactor containments either single-wall or double-wall concept is used [48, 167]. In a single-wall

concept the containment wall is a single reinforced or pre-stressed concrete wall with steel lining which ensures tightness in case of leakage. 6 mm thick lining is used for pre-stressed concrete walls and 10 mm thick for non-pre-stressed concrete walls (pre-stressing is not used to reduce time-dependent deformations in steel elements) [167]. In a double-wall concept the containment wall is composed of two concentric walls, spaced 1 to 2 m, with steel lining. Outer wall is usually made of reinforced concrete and inner wall of pre-stressed concrete [167]. Double-wall concept provides independent protection of the reactor for internal and external accidents. Fig. 2.20 presents the examples of reactor buildings: the older single-wall concept (Fig. 2.20a) and currently more popular double-wall concept (Fig. 2.20b).

Disposal structures are used for storage of radioactive waste coming from decommissioning and operating nuclear power plants, medical applications, nuclear industry, nuclear research centres and the army. Before the cooled and low-radioactive waste is finally stored in designated deep geological formations interim storage facilities must be provided. This is especially important for storage of used fuel. Different designs are proposed, among the others the German hall structures [167] or Belgian cylindrical supercontainer [57]. An exemplary disposal structure is presented in Fig. 2.21; it presents a STEAG single-aisle hall design [167].

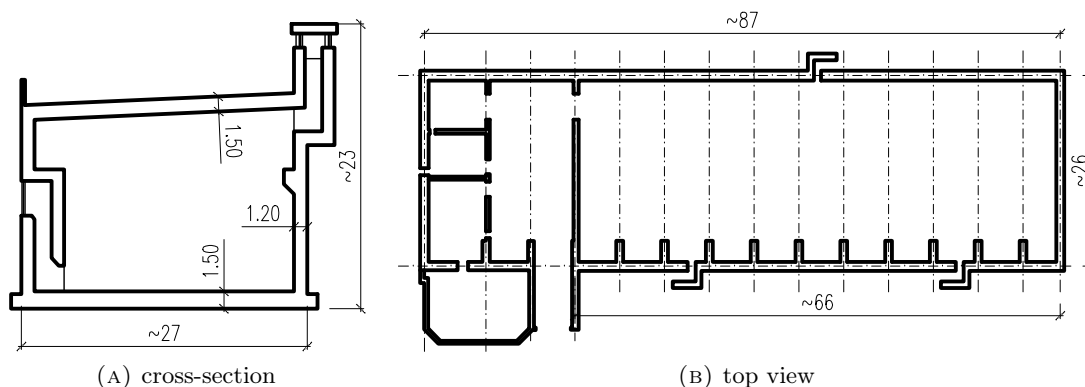


FIGURE 2.21: Disposal structure for interim storage of radioactive waste, Germany [167].

Another type of nuclear containments are shielding bunkers. Although – because of the safety reasons – no cracking is being reported in containment structures, some examples of cracking in shielding bunkers can be referred. One of them is an X-ray radiation shielding building [150]. The structure of the building consisted of a steel shade roof supported by two reinforced concrete walls and foundations. The first RC wall was 0.5 m thick, with total height of 6.4 m and total length of 47.9 m ($L/H = 9.04$ and $m = 4.00 \text{ m}^{-1}$). The second RC wall was 0.85 m thick, with total height of 6.3 m and total length of 40.0 m ($L/H = 7.69$ and $m = 2.35 \text{ m}^{-1}$). Both walls were reinforced with 2 layers of 16 mm steel bars in both directions. Geometry of one of the walls is presented in Fig. 2.22. The walls were made of normal-weight concrete with design strength of 35 MPa (C35/45), however, the actual concrete strength ranged from 43 MPa to 55 MPa. 400 kg of Type I cement was used with a water-to-cement ratio of 0.44. Both walls were cast in two stages. Wall in stage one was cast from the top of foundation up to the ground level (1.1 m height), and in the stage two was cast from ground level up to 5.3 m from the ground. The structure was built in a hot, dry desert climate. After removing the formworks, the concrete wall was moist-cured for 7 days. When curing has completed, cracks were observed on each side of the

walls (Fig. 2.23). The cracks reached up to 3.5 m of the wall's height. The cracks width ranged from 0.1 mm to 0.2 mm. Location of the cracks suggests that the cracks might be through cracks.

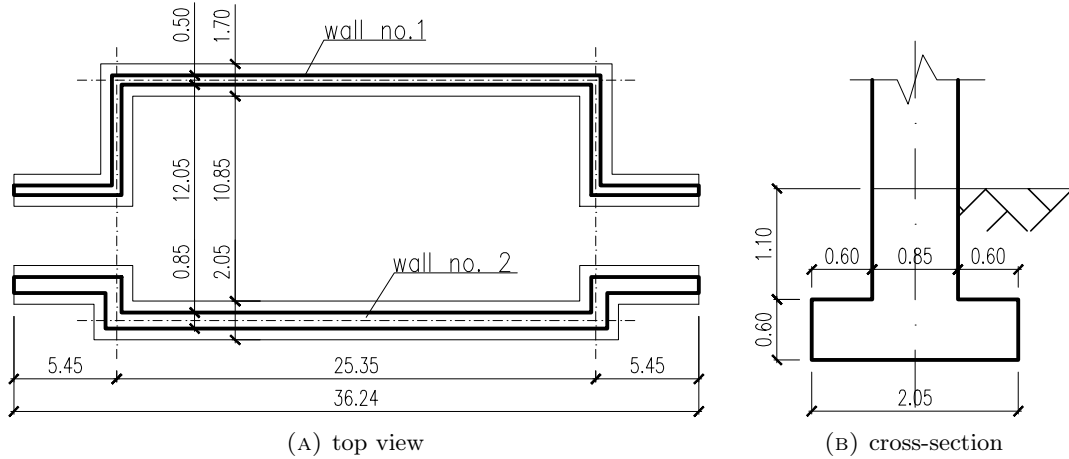


FIGURE 2.22: X-ray shielding bunker, Near East [150].

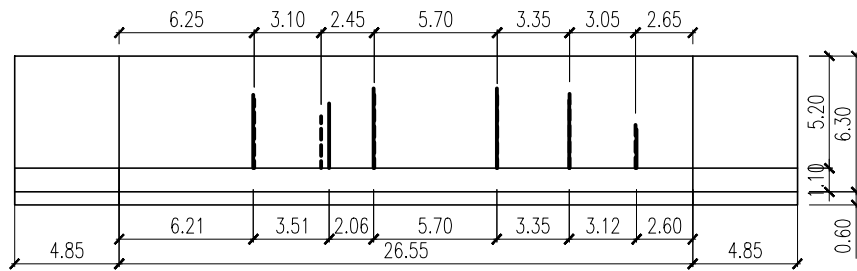


FIGURE 2.23: Cracking in a wall as an X-ray shielding bunker (external view), Near East [150].

2.4.4 Tunnel walls

Externally restrained walls appear also in tunnel structures. The problem of early-age cracking was observed in a tunnel in Sweden [108]. The tunnel with a rectangular cross-section was constructed in stages with wall and roof slab panels. Various restraint conditions were formed in different segments. A typical internal wall segment had 8.50 m height, 17.50 m length and 1.20 m thickness ($L/H = 2.06$, $m = 1.67 \text{ m}^{-1}$) and was supported on a 3.50 m wide and 1.20 m deep strip foundation. Fig. 2.24 presents the geometry of the tunnel. The concrete of C35/45 class was applied with 430 kg/m^3 of cement. Concreting was realised in the ambient temperature of 0°C while the concrete mix had temperature of 15°C . Formwork was removed 14 days after concrete casting. Cracking was observed in a majority of wall and roof segments; some of the cracks were through cracks. Cracking pattern depended on the restraint conditions. Fig. 2.25 shows cracking in exemplary tunnel segments.

Cracking was also observed in the segments of a tunnel in France. The walls of the tunnel were constructed in segments, subsequently cast along the length of the tunnel; two symmetrical segments formed the cross-section. The thickness of the segment was varying from 0.45 m to 0.50 m, height (in plan view) was ~ 10 m and its length was 7.5 m ($L/H = 0.75$, $m = 4.00 \div 4.44 \text{ m}^{-1}$). Exemplary cross-section geometry is shown in Fig. 2.26a. In a number of segments intensive

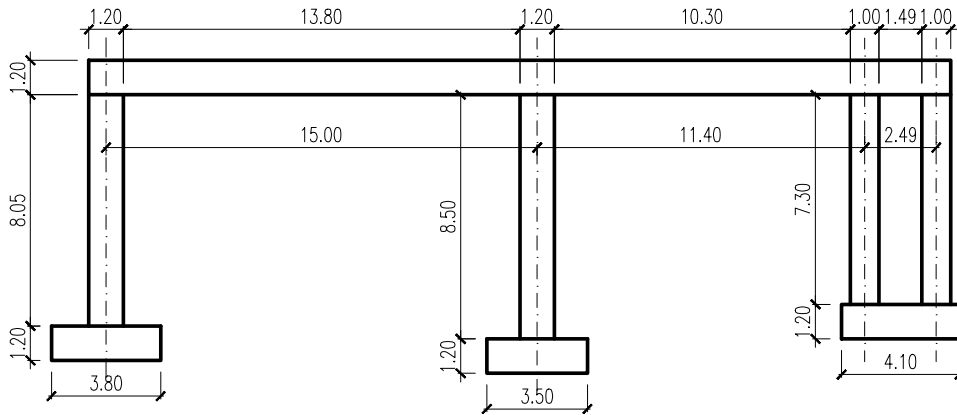


FIGURE 2.24: Tunnel, Sweden [108].

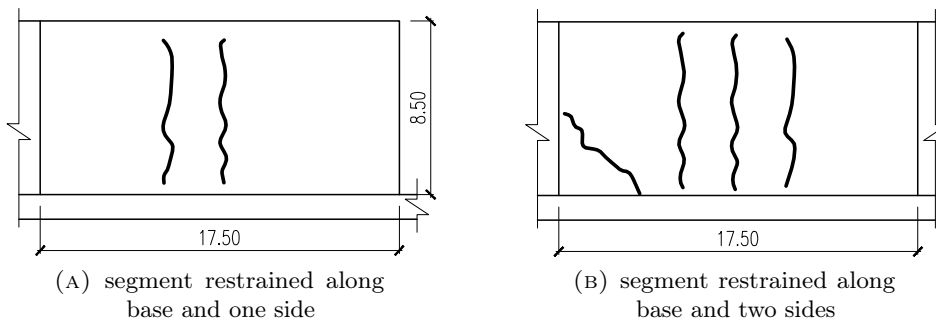


FIGURE 2.25: Cracking pattern in chosen segments of a tunnel, Sweden [108].

cracking was observed with a lot of through cracks through which the water infiltrated from the soil. An exemplary cracking pattern in an internal plan view of the segment is shown in Fig. 2.26b. Apart from the vertical cracks horizontal and splayed cracks were also formed in the segments. This was caused by complicated restraint conditions as the segment was also restraint along the edges by the neighbouring segments and on its entire surface by the soil.

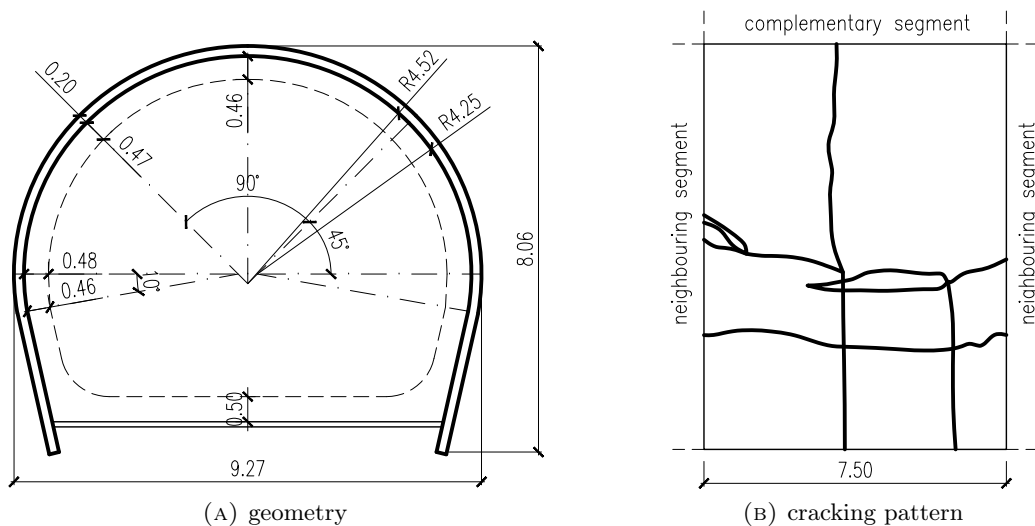


FIGURE 2.26: Tunnel, France (private collection of Farid Benboudjema).

Chapter 3

Analytic models for early-age reinforced concrete walls

Analysis of early-age concrete elements is a difficult task because of complex nature of the material and loading. However, determination of the early-age stresses and consequent cracking risk in concrete elements is crucial for their functionality and durability. Thus, methods have been developed to predict these stresses in concrete elements. The works on modelling of early-age concrete began in 1930s. when first dams were constructed in the U.S. [190]. Since then multiple models for description of physical and mechanical phenomena in early-age concrete were developed. Initially, analytic formulations were introduced and simplified solutions allowing for manual calculations were developed. Later on, when computer-aided calculations became possible, computer implementations of these models were used which enabled faster and more accurate simulation of the phenomena in question. Because of the possibilities provided by fast computers, numerical approaches gain more and more popularity but they are used mostly in research activities or design of responsible structures. For typical engineering design analytic methods are used. This section presents some of the currently used simplified approaches for the analysis of externally-restrained reinforced concrete elements.

In the analysis two main steps can be distinguished: the first step is determination of thermal and shrinkage strains and the second step is calculation of stresses. Computation of thermal strain relates to determination of the peak temperature due to development of the hydration heat; the methods for temperature determination are recommended by, among the others, ACI COMMITTEE 207 [5], JCI GUIDELINE FOR CONCRETE [110] and CIRIA C660 [21]. Methods for evaluation of shrinkage strains are proposed by standards, e.g. MODEL CODE 2010 [50], EUROCODE 2 [183], JCI GUIDELINE FOR CONCRETE [110] and JSCE GUIDELINE FOR CONCRETE [116], but other proposals are also being published, e.g. by LARSON [155]. The stress analysis of early-age concrete walls is based on the *compensation plane method* (CPM). The approach was introduced into the JSCE GUIDELINE FOR CONCRETE [116], and also into EUROCODE 2 - PART 3 [184], CIRIA C660 [21], by ACI COMMITTEE 207 [5], by NILSSON [177] and by FLAGA [83]. These approaches are based on the assumption of linear behaviour of concrete (uncracked sections). The method for analysis of stresses based on the restraint factor in cracked walls was introduced by KHEDER ET AL. [9, 128, 129].

3.1 Temperature and shrinkage

The total strain, $\varepsilon_{\text{tot}}(t)$, results from thermal strain, $\varepsilon_T(t)$, and shrinkage strain, $\varepsilon_W(t)$:

$$\varepsilon_{\text{tot}}(t) = \varepsilon_T(t) + \varepsilon_W(t). \quad (3.1)$$

The strains developing during early-ages of concrete hardening should be determined taking into account the expected conditions during the early life of the element: the mix design, the nature of the formwork, the ambient conditions and the boundary conditions.

3.1.1 Temperature-induced strains

Thermal strain induced by a temperature change, ΔT , can be calculated as:

$$\varepsilon_T = \alpha_T \Delta T, \quad (3.2)$$

where:

- α_T – coefficient of thermal dilation, $1/^\circ\text{C}$. The value of thermal expansion coefficient depends on the type of aggregate and moisture content in concrete mix; the values of α_T can be found in the literature, e.g. were given by NEVILLE [175];
- ΔT – temperature change, $^\circ\text{C}$.

The maximum temperature change depends on the placing temperature, the temperature rise of concrete due to hydration and temperature difference between the element and the ambient surrounding. The volume change that leads to thermal cracking results from the temperature difference between the peak temperature of concrete reached during early hydration and the minimum temperature to which the element will be subject under service conditions [5]:

$$\Delta T = T_{\text{max}} - T_f = T_i + T_{\text{ad}} + T_{\text{env}} - T_f. \quad (3.3)$$

where:

- T_i – initial placing temperature of concrete, $^\circ\text{C}$;
- T_{ad} – adiabatic temperature rise of concrete, $^\circ\text{C}$;
- T_{env} – temperature change from the heat added or removed from the concrete due to environmental conditions, $^\circ\text{C}$;
- T_f – final stable temperature of concrete, $^\circ\text{C}$.

Concrete of the initial temperature, T_i , heats up to the maximum temperature, T_{max} , [86]:

$$T_{\text{max}} = T_i + \chi T_{\text{ad}}. \quad (3.4)$$

χ is equal to 1 for perfectly adiabatic conditions. Because the heat dissipates from the element and the rise of the internal temperature is smaller than the adiabatic rise, $\chi < 1$ ($\chi T_{\text{ad}} = T_{\text{ad}} + T_{\text{env}}$).

When the data about the hydration heat are known the adiabatic temperature rise due to cement hydration can be calculated from the equation:

$$T_{\text{ad}} = \frac{C_c Q_{\text{tot}}}{c_v}, \quad (3.5)$$

where:

- C_c – amount of cement in 1 m³ of concrete mix, kg/m³;
- Q_{tot} – total amount of hydration heat, kJ/kg;
- c_v – heat capacity of concrete, kJ/(m³ K); $c_v = c_b \rho$;
- c_b – specific heat of concrete, kJ/(kg K);
- ρ – density of concrete, kg/m³.

The amount of heat generated in the hydration process and its development in time can be obtained in laboratory tests or data provided by the producers can be used. For typical cements such data are collected in the literature and were given by e.g. KIERNOŻYCKI [130].

THE PORTLAND CEMENT ASSOCIATION [151] gives a quick method for estimation of the adiabatic temperature development in massive concrete elements. The maximum concrete rise above the concrete placement temperature is defined to be 12°C for every 100 kg of cement. This is limited to the concretes in which the Type I cement was used in the amount between 300 and 600 kg/m³ and in the elements in which the least dimension is at least 1.8 m. To account for the partial replacement of Portland cement with supplementary cementitious materials (SCMs) the maximum temperature rise can be calculated as:

$$T_{\text{max}} = T_i + 12 \frac{C_c}{100} + 6 \frac{C_{\text{SCM}}}{100}, \quad (3.6)$$

where:

- C_c – cement content, kg/m³;
- C_{SCM} – content of supplementary cementitious materials, kg/m³.

This method of concrete temperature prediction provides no information on the time when the maximum temperature is reached and criteria for using this method are very narrow – most of medium-thick elements do not satisfy the assumptions of the method. The formula was improved by BAMFORTH AND PRICE [22] who created diagrams to correct the formula for elements with the least dimension less than 2 m and to account for fly ash and slag content.

To determine the maximum temperature in massive concrete element accounting for the heat exchange ACI REPORT 207.2 [5] provides charts for given conditions: the element size, cement type, placement temperature as well as the exposure conditions. However, the research performed by RIDING ET AL. [190] has shown that the results obtained with this graphical method do not compare well with the recorded concrete temperatures, mostly because the data about the cements are outdated and do not correspond with the properties of cements used nowadays. More actual diagrams are provided in CIRIA C660 [21] and JCI GUIDELINES [110].

FLAGA suggests the values of the temperature rise in elements according to their massiveness (ratio of the area of surfaces to the volume), m , based on the experience [82]. In massive elements, characterised by the massiveness $m < 2 \text{ m}^{-1}$, the expected temperature rise is $\Delta T = 20$ to 50°C . In medium-thick elements, with $2 \text{ m}^{-1} \leq m \leq 15 \text{ m}^{-1}$, $\Delta T = 3$ to 20°C . Finally, in thin elements, $m \geq 15 \text{ m}^{-1}$, the expected temperature increase is $\Delta T = 1$ to 3°C .

To determine the temperature gradients and the time of the maximum temperature occurrence, the heat equation must be solved. This equation describes the variation in temperature in a given region over time. In the most general three-dimensional form the equation has a form:

$$c_v \frac{\partial T}{\partial t} = \lambda \nabla^2 T + q_v(t), \quad (3.7)$$

where:

- T – temperature in the point of (x, y, z) coordinates, K;
- t – duration time of the process, s;
- λ – thermal conductivity, W/(m K);
- c_v – heat capacity of concrete, kJ/(m³ K);
- ∇^2 – Laplace operator, $\nabla^2 = \left(\frac{\partial^2}{\partial x^2}, \frac{\partial^2}{\partial y^2}, \frac{\partial^2}{\partial z^2} \right)$;
- $q_v(t)$ – rate of hydration heat generation, W/m³.

To solve the equation the initial condition and the boundary condition have to be known. For the initial condition uniform initial temperature distribution in the element is assumed:

$$T(x, y, z, t = 0) = T_i. \quad (3.8)$$

There are three types of boundary conditions used for solution of the heat equation:

1. 1st type boundary condition which assumes that the temperature at the surface of the element (at the boundary), T_{sur} , is equal to the temperature of the surrounding air, T_a :

$$T_{\text{sur}} = T_a; \quad (3.9)$$

2. 2nd type boundary condition in which the heat flux at the boundary, \tilde{q} , is defined. For thermal gradient at the thickness of the element the condition has a form:

$$\left. \frac{dT}{dx} \right|_p = -\frac{\tilde{q}}{\lambda}; \quad (3.10)$$

3. 3rd type boundary condition in which the heat flux relates the ambient temperature, T_a , temperature at the surface of the element, T_{sur} , thermal transfer coefficient, α_p , and the surface gradient of thermal fields:

$$\left. \frac{dT}{dx} \right|_p = -\frac{\alpha_p}{\lambda} (T_{\text{sur}} - T_a). \quad (3.11)$$

This formulation has a simple graphical interpretation [82]: a line tangent to the temperature field in concrete at the surface p crosses the point at the line depicting the level of the ambient temperature, T_a , at the distance λ/α_p from the surface (Fig. 3.1).

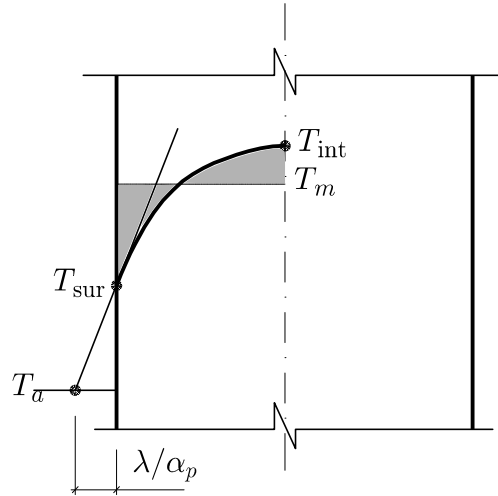


FIGURE 3.1: Graphical interpretation of 3rd type boundary condition for heat equation solution after FLAGA [82].

1st type boundary condition is the easiest to use for manual calculations but it is also the least accurate. When using the higher type boundary conditions, however, the surface thermal gradient has to be known. Schmidt Method is recommended by ACI COMMITTEE 207 [5] for the solution of the heat equation if the temperature gradients need to be known. It is a simplified finite difference method in which the temperatures are calculated for discrete nodes as the element is divided into equal slices of Δx thickness at discrete time steps Δt . The time step is calculated as:

$$\Delta t = \frac{(\Delta x)^2}{2\alpha_{TT}}, \quad (3.12)$$

where α_{TT} is thermal diffusivity of concrete (see Eq. 4.39). If the body under question is considered to be divided into a number of equal elements, the temperature for a given increment at the end of an interval of time is the average of the temperature of the two neighbouring elements at the beginning of that time interval. The averaging results from the solution of the heat equation assuming one-directional heat transfer and neglecting the internal heat source. If $T_{n-1}(t)$, $T_n(t)$, and $T_{n+1}(t)$ are the temperatures of three successive elements at time t , then:

$$T_n(t + \Delta t) = \frac{T_{n-1}(t) + T_{n+1}(t)}{2}. \quad (3.13)$$

The increase in temperature due to the internal heat source (hydration heat) is taken into account by adding the expected adiabatic temperature increase in a given time step. The calculation in each time step requires a two-phase procedure: the first phase averages the adjacent temperatures and the second phase increases the temperature by adding the adiabatic temperature rise of concrete in a given time step. The Schmidt Method can be extended to cases of two-dimensional and three-dimensional heat flow. RIDING ET AL. [190] conclude that the Schmidt Method proves to adequately model conductive heat transfer when real boundary conditions comply with the

assumptions of the method and given that the heat generation component is taken from the measured adiabatic temperature development curves.

For further calculations, the mean temperature has to be known. This is the temperature which produces only the longitudinal strain. The mean temperature can be determined precisely if the surface temperature gradient is known. It can also be approximated based on the known internal and surface temperature according to FLAGA [86] as:

$$T_m = T_{\text{int}} - \frac{1}{3}(T_{\text{int}} - T_{\text{sur}}). \quad (3.14)$$

To account for the difference in thermal strain between the new part undergoing hydration and the old, heated part, the temperature change should be corrected [86]:

$$\Delta T_{\text{diff}} = \gamma(T_m - T_a), \quad (3.15)$$

where coefficient γ accounts for the fact that the foundation slab is also being heated by the wall. The value γ was proposed to be taken as 0.9 by FLAGA [86], $0.6 \div 0.8$ by FLAGA ET AL. [84] and 0.6 by BARRÉ.

3.1.2 Shrinkage-induced strains

Total shrinkage strain, $\varepsilon_W(t)$, is a sum of drying shrinkage strain, ε_{cd} , and autogenous shrinkage strain, ε_{ca} :

$$\varepsilon_W(t) = \varepsilon_{cd}(t) + \varepsilon_{ca}(t). \quad (3.16)$$

There are multiple proposals for description of shrinkage strain; here the most recent approach proposed in MODEL CODE 2010 [50] is presented. The drying shrinkage strain is expressed as:

$$\varepsilon_{cd}(t) = \beta_{ds}(t, t_d) \varepsilon_{cd,0}, \quad (3.17)$$

where:

- t – concrete age, days;
- t_d – concrete age at the beginning of drying, days;
- $\beta_{ds}(t, t_d)$ – function describing the time-development of drying shrinkage strain;
- $\varepsilon_{cd,0}$ – notional drying shrinkage strain.

The time-development function, $\beta_{ds}(t, t_d)$, is given as:

$$\beta_{ds}(t, t_d) = \sqrt{\frac{t - t_d}{(t - t_d) + 0.035 h_0^2 \beta_{dT}}}, \quad (3.18)$$

where:

- h_0 – notional size of the element, mm; $h_0 = \frac{2A_c}{u}$; A_c is the cross-section, mm², and u is the perimeter of the element in contact with atmosphere, mm;

β_{dT} – coefficient expressing the effect of the increased temperature on the rate of drying shrinkage strain development;

while the notional drying shrinkage strain, $\varepsilon_{cd,0}$, is given by the empirical formula:

$$\varepsilon_{cd,0} = \left[(220 + 110 \alpha_{ds1}) e^{-\alpha_{ds2} f_{cm,28}} \right] \beta_{RH} \cdot 10^{-6}, \quad (3.19)$$

with:

$$\beta_{RH} = -1.55 \left[1 - \left(\frac{RH}{100} \right)^3 \right] \beta_{sT}, \quad (3.20)$$

where:

- $f_{cm,28}$ – mean compressive strength of concrete at the age of 28 days, MPa.
- β_{RH} – coefficient taking into account the effect of the ambient relative humidity;
- RH – relative humidity of the ambient atmosphere, %;
- $\alpha_{ds1}, \alpha_{ds2}$ – coefficients dependent on the type of cement acc. to Tab. 3.1;
- β_{sT} – coefficient expressing the effect of the increased temperature on the magnitude of drying shrinkage strain.

The effect of the increased temperature of concrete, T [°C], on drying shrinkage strain can be accounted by two coefficients: β_{dT} and β_{sT} . The coefficient β_{dT} expresses the effect of the increased temperature on the rate of drying shrinkage strain development and is defined as:

$$\beta_{dT} = e^{-0.06(T-20)}, \quad (3.21)$$

while coefficient β_{sT} expresses the effect of the increased temperature on the magnitude of drying shrinkage strain and is defined as:

$$\beta_{sT} = 1 + \left(\frac{4}{103 - RH} \right) \left(\frac{T - 20}{40} \right). \quad (3.22)$$

To neglect the effect of temperature both coefficients should be taken as equal to 1.

Autogenous shrinkage strain is expressed as:

$$\varepsilon_{ca} = \beta_{as}(t) \varepsilon_{ca,0}, \quad (3.23)$$

where:

- $\beta_{as}(t)$ – function describing the time-development of autogenous shrinkage strain;
- $\varepsilon_{ca,0}$ – notional autogenous shrinkage strain.

The time-development function, $\beta_{as}(t)$, is given as:

$$\beta_{as}(t) = 1 - e^{-0.2\sqrt{t_e}}, \quad (3.24)$$

while the notional autogenous shrinkage strain, $\varepsilon_{ca,0}$, is given also with an empirical formula:

$$\varepsilon_{ca,0} = -\alpha_{ca} \left(\frac{0.1 f_{cm,28}}{6 + 0.1 f_{cm,28}} \right)^{2.5} \cdot 10^{-6}, \quad (3.25)$$

where:

- $f_{ck,28}$ – characteristic compressive strength of concrete at the age of 28 days, MPa;
- α_{ca} – coefficient dependent on the type of cement acc. to Tab. 3.1.

cement strength class	α_{ca}	α_{ds1}	α_{ds2}
32.5 N	800	3	0.013
32.5 R, 42.5 N	700	4	0.012
42.5 R, 52.5 N, 52.5 R	600	6	0.012

TABLE 3.1: Coefficients α_{ca} , α_{ds1} and α_{ds2} for calculation of shrinkage strain acc. to MODEL CODE 2010 [50].

Equivalent age of concrete, t_e , expresses the effect of the increased temperature on the rate of development of autogenous shrinkage strain. When the effect of temperature is neglected, the real time should be used instead.

ABBASNIA ET AL. [2] concluded that although the presented model is currently the most developed it is still unreliable because it shows significant difference between the observed and calculated results and does not enable prediction of strain distribution. Ability to predict the strain distribution is not an issue for modelling the autogenous shrinkage which develops almost uniformly throughout the section. However, it becomes a problem for drying shrinkage because drying of concrete is a slow diffusion process and considerable moisture gradients may form in the cross-section of the element. Tensile stresses generated in the near-surface regions as a result of these gradients cause the commonly-observed surface cracking [49].

Determination of the total shrinkage strain in a hardened part of the structure (e.g. foundation) and an early-age part of the structure (a wall) allows to determine a strain difference resulting from different times of concrete casting of these parts, $\varepsilon_{W,\text{diff}}$. According to the proposal of FLAGA [83] the strain difference is equal to (Fig. 3.2):

$$\varepsilon_{W,\text{diff}} = \varepsilon_{W,\text{II}}(t_{\text{II}}) - [\varepsilon_{W,\text{I}}(t_{\text{I}} + t_{\text{II}}) - \varepsilon_{W,\text{I}}(t_{\text{I}})], \quad (3.26)$$

where:

- t_{I} – time of execution of the new part (wall) = age of the old part (foundation) at that moment, days;
- t_{II} – age of the new part (wall) at the moment of analysis, days;
- $t_{\text{I}} + t_{\text{II}}$ – age of the old part (foundation) at the moment of analysis, days;
- $\varepsilon_{W,\text{I}}$ – shrinkage strain of the old part (foundation);
- $\varepsilon_{W,\text{II}}$ – shrinkage strain of the new part (wall).

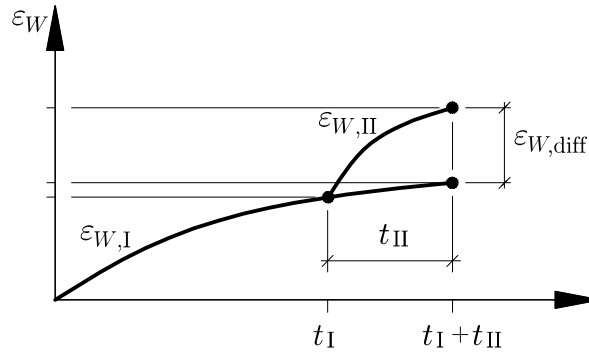


FIGURE 3.2: Differential strain in a new part of a concrete structure after FLAGA [83].

Whenever it is convenient, shrinkage can be expressed in terms of an equivalent change in concrete temperature, ΔT_W , as uniform cooling of the early-age element:

$$\Delta T_W = \frac{\varepsilon_{W,diff}}{\alpha_T}. \quad (3.27)$$

3.2 Thermal–shrinkage stresses

3.2.1 Stresses in uncracked walls

Stresses in the wall are caused by bond forces generated in the joint between the wall and the restraining body (e.g. a foundation). The main cause of the bond force generation are unbalanced thermal–shrinkage strains in the wall and the foundation if the two are executed separately one after another. At the moment of execution of the wall the foundation is cooled down and has more or less the temperature of the surrounding air. The wall is in turn subjected to intensive self-heating during the process of cement hydration. At this phase it has a tendency to expand (with respect to the cooler foundation). This process is accompanied with generation of small compressive forces in the concrete of the wall and tensile forces in the foundation (Fig. 3.3a). As soon as the total bond stresses develop at the joint as a result of the bond between the old concrete and the new concrete, the concrete of the wall starts to cool down. This process leads to contraction of the wall. The contracting wall is restrained by the cooled foundation, which leads to formation of compressive force in the foundation and tensile force in the joint. The bond forces developing in the joint act on the whole cross-section of the wall, subjecting it to the eccentric load with respect to the neutral axis of the element (Fig. 3.3b).

For simplicity of calculations both the thermal–moisture fields and stresses are assumed to be uniform at the thickness of the wall. For more detailed analysis temperature gradient at the thickness can be calculated. As the stresses in early-age wall arise mainly due to an external restraint, modelling of the foundation is also of great importance. In the most simplified way it is assumed that the wall is settled on an undeformable foundation of infinite stiffness, as presented in Fig. 3.4a [83, 116, 184]. In other approaches the real stiffness of the foundation and the resulting restraint is considered as in Fig. 3.4b [5, 177].

Analytic approaches neglect the heating phase as the initial temperature rise produces little stress in concrete – at early age the modulus of elasticity of concrete is so small that compressive stresses

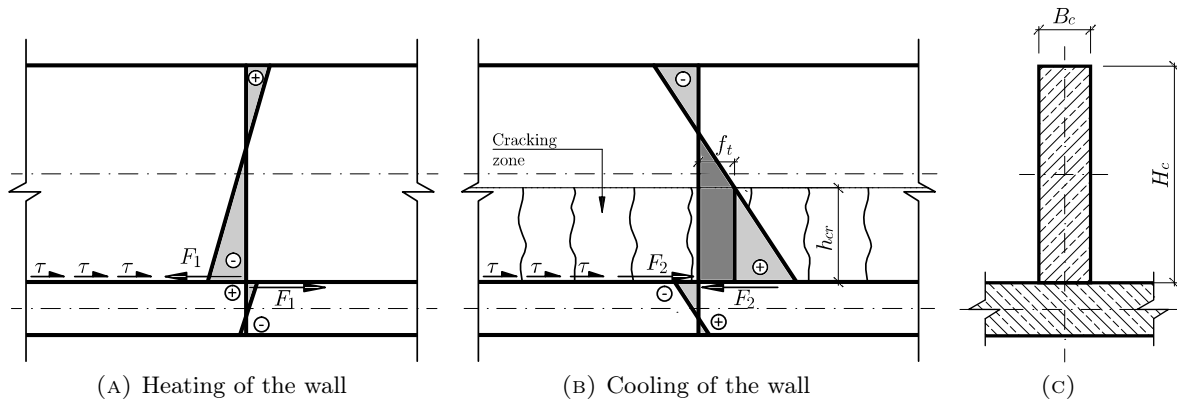


FIGURE 3.3: Distribution of stresses at the height of the wall after FLAGA [83].

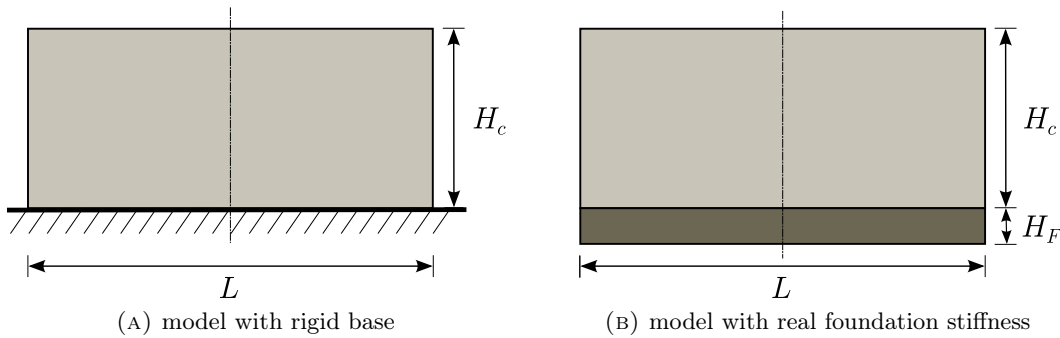


FIGURE 3.4: Models of the wall applied in analytic approaches.

induced by the rise in temperature are insignificant even in zones of full restraint and additionally are relaxed by a high rate of creep [5, 21]. The analysis is focused on the cooling phase when tensile stresses are due to occur. Elastic behaviour of early-age concrete is assumed: the stress in any point in an uncracked concrete element is proportional to the strain in concrete. Simplified viscoelastic material model is used which applies the effective value of the modulus of elasticity reduced to account for creep effects [5, 82, 83, 176, 183]. Analytic methods for determination of stress state in early-age concrete walls base on the compensation plane method (CPM) [8]. The most known analytic approaches based on this method were developed by JAPAN SOCIETY OF CIVIL ENGINEERS and published in JSCE STANDARD SPECIFICATION FOR CONCRETE STRUCTURES [116], AMERICAN CONCRETE INSTITUTE published in ACI REPORT 207 [5], in EUROCODE 2 – PART 3 [184] and enhanced in CIRIA C660 [21], by NILSSON introduced in his Licentiate thesis [177] and developed in further research [176], and by FLAGA [83].

Compensation plane method was introduced by Japan Society of Civil Engineers in STANDARD SPECIFICATIONS FOR CONCRETE STRUCTURES [116]. The method takes into account the fact that the early-age stresses in externally-restrained elements result from a coupled action of internal and external restraints. The external restraint acts against axial deformation and flexural deformation. A free deformation of the concrete element can be separated into deformation in an axial direction (expansion or contraction) and flexural deformation in a vertical direction. The total stress consists then of three components: due to the internal restraint, due to the external restraint against axial deformation and due to the external restraint against flexural deformation.

The stress exerted due to the internal restraint is caused by a differential strain in the cross section resulting from the temperature and moisture concentration gradients. The increment of stress due to the internal restraint can be determined from the difference between the strain value at a point of the compensation line, $\varepsilon_{\text{comp}}$, and the thermal–shrinkage strain distribution curve, ε_0 , (Fig. 3.5) by the equation:

$$\sigma_{\text{int}} = E_c(\varepsilon_0 - \varepsilon_{\text{comp}}). \quad (3.28)$$

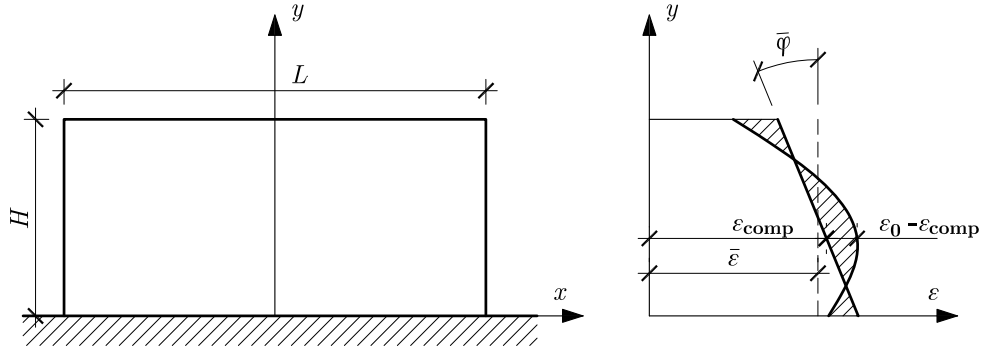


FIGURE 3.5: Determination of stresses in a concrete element caused by the internal restraint according to compensation plane method after JSCE STANDARD [116].

This approach allows to obtain the increment of free axial strain, $\bar{\varepsilon}$, and the increment of curvature, $\bar{\varphi}$ (Fig. 3.5). The internal forces are generated in the element trying to return the plane after deformation to the original restrained position – axial force N_R and bending moment M_R . The restraint stresses are then caused by the coupled action of the axial force and bending moment, as presented in Fig. 3.6, according to the equations:

$$\sigma_{\text{ext}} = \frac{N_R}{A_c} + \frac{M_R}{I_c}(y - y_{\text{cen}}), \quad (3.29)$$

where:

- A_c , – area of the concrete element's cross-section, m^2 ;
- I_c – moment of inertia of the concrete element's cross-section; m^4 ;
- $(y - y_{\text{cen}})$ – distance from the center of gravity of the concrete element's cross-section, m.

The internal forces can be defined as follows:

$$N_R = R_N E_c A_c \bar{\varepsilon}, \quad (3.30a)$$

$$M_R = R_M E_c I_c \bar{\varphi} \quad (3.30b)$$

where the external restraining coefficients, R_N and R_M , are introduced to represent the degree of restraint of the element by the restraining body. The Eq. 3.29 gets a form:

$$\sigma_{\text{ext}} = R_N E_c \bar{\varepsilon} + R_M E_c \bar{\varphi} (y - y_{\text{cen}}), \quad (3.31)$$

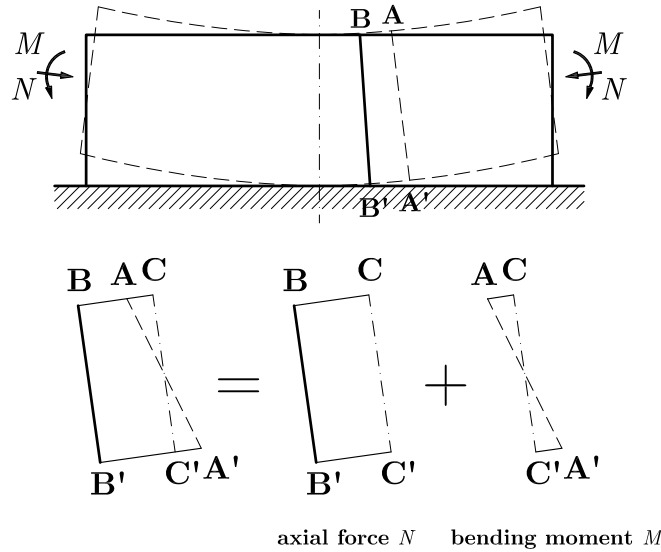


FIGURE 3.6: Determination of stresses in a concrete element caused by the external restraint according to compensation plane method after JSCE STANDARD [116].

and the total thermal–shrinkage stress at any position (x, y) can be calculated as:

$$\sigma_{\text{tot}}(x, y) = E_c(x, y) [(\varepsilon_0(x, y) - \bar{\varepsilon} - \bar{\varphi}(y - y_{\text{cen}})) + R_N \bar{\varepsilon} + R_M \bar{\varphi}(y - y_{\text{cen}})]. \quad (3.32)$$

The values of the restraining coefficients vary within the element according to the degree of restraint. They depend on the difference in stiffness between the restraining body and the early-age concrete element as well as the ratio of the length to the height of the element (L/H). For very low L/H ratios the assumption of plane sections is no longer valid. For that purpose the functions of the restraining factors need to be defined. JSCE GUIDELINE FOR CONCRETE [116] proposes the diagrams of restraining factors, determined with 3D numerical calculations. The diagrams are presented in Fig. 3.7 accounting for a single lift.

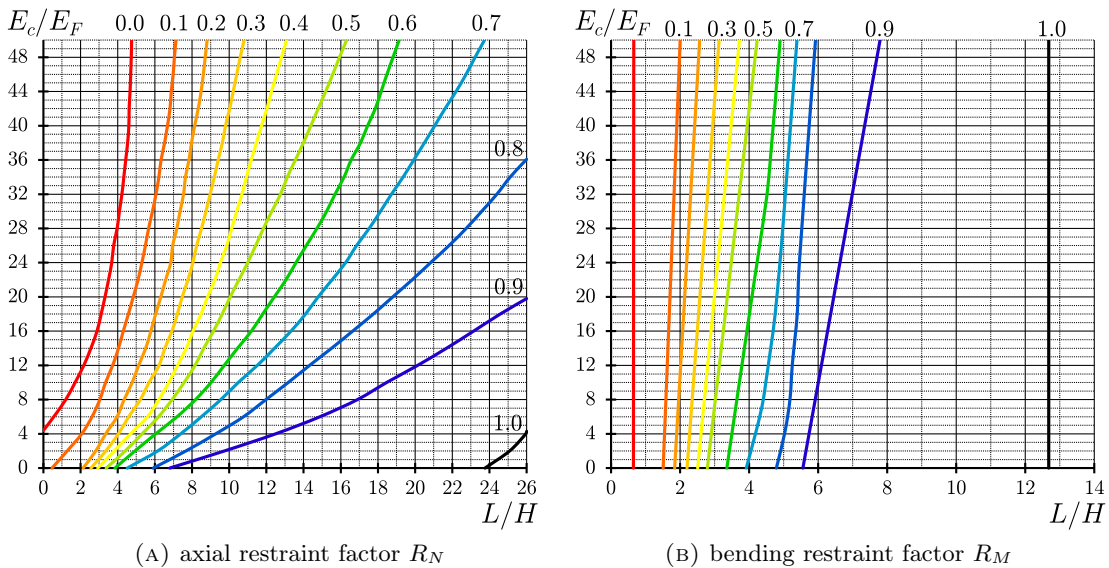


FIGURE 3.7: External restraint factors according to JSCE STANDARD [116].

The CPM was implemented into numerous standards worldwide. EUROCODE 2 – PART 3 [184] states that the stress at any level y in an uncracked section due to translational and rotational restraint of the element can be calculated based on the known imposed strain from the equation:

$$\sigma(y) = E_{c,\text{eff}}(\varepsilon_i(y) - \varepsilon_a(y)), \quad (3.33)$$

in which the actual strain at level y , $\varepsilon_a(y)$, is given by:

$$\varepsilon_a(y) = (1 - R_N)\bar{\varepsilon} + (1 + R_M)\bar{\varphi}(y - y_{\text{cen}}), \quad (3.34)$$

where:

- R_N – factor defining the degree of the external axial restraint; practical axial restraint factors for common situations may be taken from Fig. 3.8;
- R_M – factor defining the degree of the moment restraint; it can be taken as 1.0;
- $E_{c,\text{eff}}$ – effective modulus of elasticity of concrete allowing for creep, GPa;
- $\bar{\varepsilon}$ – average imposed strain in the element (the average free strain);
- $\varepsilon_a(y)$ – actual strain at level y ;
- $\varepsilon_i(y)$ – imposed strain at level y ;
- $(y - y_{\text{cen}})$ – distance to the section centroid, m;
- $\bar{\varphi}$ – curvature of the joint plane.

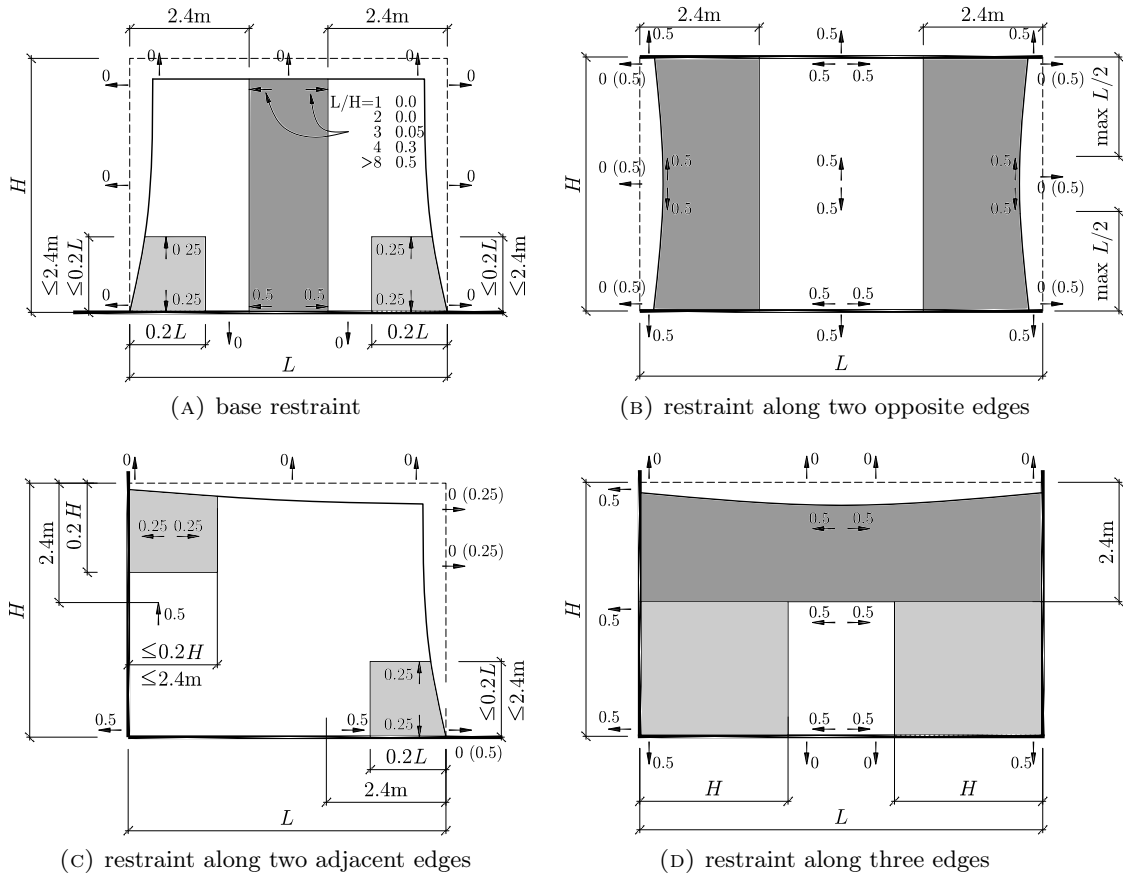


FIGURE 3.8: Axial restraint factor R_N in restrained elements according to EUROCODE 2 [184].

It must be strongly emphasised that the values of the restraint factors given by EUROCODE 2 presented in Fig. 3.8 include reduction of restraint due to creep. The coefficient of reduction to account for creep is estimated to be at the level of 0.65 which means that the actual expected degree of restraint due to the geometry of the wall is equal to $R = R_N/0.65$, which e.g. at the joint with the restraining body would give $R = 0.5/0.65 = 0.8$.

ACI COMMITTEE 207 ACI REPORT 207.2R [5] proposed a simplified approach, allowing for determination of stresses at the centerline of the element, assuming pure translation (no flexure) of the element. Two restraint factors were defined: the structural shape restraint factor, K_R , and the foundation restraint factor, K_F . The tensile stress at any point on the centreline due to a decrease in length, $\bar{\epsilon}$, can be calculated from the equation:

$$\sigma = K_R K_F \bar{\epsilon} E_{c,\text{eff}}, \quad (3.35)$$

where:

- K_R – degree of structural geometry restraint;
- K_F – degree of foundation restraint;
- $\bar{\epsilon}$ – free strain;
- $E_{c,\text{eff}}$ – effective modulus of elasticity of concrete at the time when $\bar{\epsilon}$ occurred, GPa.

The structural shape restraint factor, K_R , describes the variation of the restraint with the L/H of the element. The following approximation of K_R distribution is proposed:

$$K_R = \begin{cases} \left(\frac{L_c/H_c - 2}{L_c/H_c + 1} \right)^{y/H_c} & \text{if } L_c/H_c \geq 2.5 \\ \left(\frac{L_c/H_c - 1}{L_c/H_c + 10} \right)^{y/H_c} & \text{if } L_c/H_c < 2.5 \end{cases} \quad (3.36)$$

where y signifies the location above the construction joint. The tensile restraint distribution at the centre section is shown in Fig. 3.9.

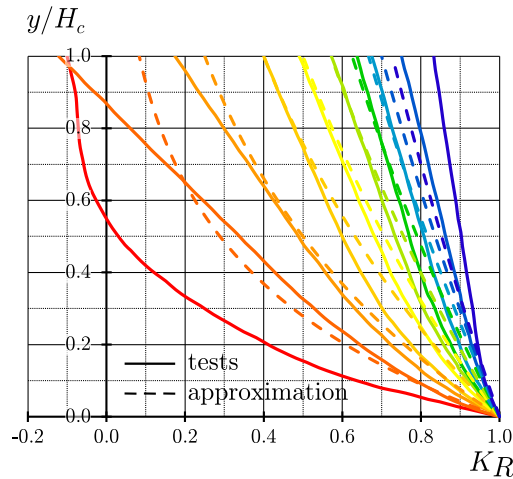


FIGURE 3.9: Structural shape restraint factor K_R at the centre section according to ACI 207.2 [5].

The restraint stresses decrease in direct proportion to the decrease in stiffness of the restraining foundation material. The foundation restraint factor, K_F , was introduced to account for the influence of the foundation stiffness on the restraint of the concrete element:

$$K_F = \frac{1}{1 + \frac{A_c E_c}{A_F E_F}}, \quad (3.37)$$

where:

- A_c – cross-section of the concrete element, m²;
- A_F – area of the foundation or other element restraining shortening of the element, m²;
- E_c – modulus of elasticity of concrete, GPa;
- E_F – modulus of elasticity of concrete of the restraining element, GPa.

For the restraint by the rock, ACI REPORT 207.2 suggests to take $A_F = 2.5 A_c$. CIRIA C660 states that the K_F multiplier can be also used to account for the influence of the actual stiffness of the restraining element on the degree of restraint, R_N .

When the stresses generated at the joint exceed the bond strength, a horizontal crack at the joint occurs and bond between the two is limited – a slip of the element is observed. This has an influence on further development of stresses in the element. This effect was taken into consideration by NILSSON [176, 177]. The approach based on CPM introduces a restraint factor, γ_R , to determine the restraint stress, σ , based on the stress at the total restraint, σ^{fix} :

$$\sigma = \gamma_R (\gamma_R^0, \delta_{\text{res}}, \delta_{\text{slip}}) \sigma^{\text{fix}}, \quad (3.38)$$

where:

- γ_R^0 – plane-section restraint coefficient, which depends on the geometry of the structure as well as the rotational, γ_R^{rx} , γ_R^{ry} , and translational, γ_R^t , boundary restraints;
- δ_{res} – resilience factor considering the non-linear effects;
- δ_{slip} – slip factor which depicts a restraint stresses reduction as a result of slip failure.

The value of δ_{res} changes at the height of the wall and depends on the boundary restraint. It is a product of the basic resilience factor and translational and rotational correction factors, $\delta_{\text{res}} = \delta_{\text{res}} (\delta_{\text{res}}^0, \delta_{\text{trans}}^0, \delta_{\text{rot}}^0)$. To simplify, the resilience factor is taken as equivalent to the basic resilience factor, $\delta_{\text{res}} = \delta_{\text{res}}^0$, and the correction to account for the translational and rotational boundary influence is included by introduction of the effective width of the restraining body, $B_{F,\text{eff}}$, instead of the real width, B_F , (see Eq. 3.44). The resilience factor is analogical to the structural shape restraint factor, K_R , given by ACI REPORT 207.2 [5]. The values of δ_{res}^0 are given in diagrams in Fig. 3.10a or can be approximated with a polynomial function [176]:

$$\delta_{\text{res}}^0 = \sum_{i=1}^n a_i \left(\frac{y}{H_c} \right)^i, \quad (3.39)$$

where:

- a_i – coefficients of a polynomial function describing resilience factor distribution;
- y/H_c – relative location of the analysed point above the joint.

The slip coefficient depends on the free length, the width and the height of the casting section. It can be determined experimentally or numerically. The values of δ_{slip} proposed by NILSSON [177] are given in diagrams in Fig. 3.10b.

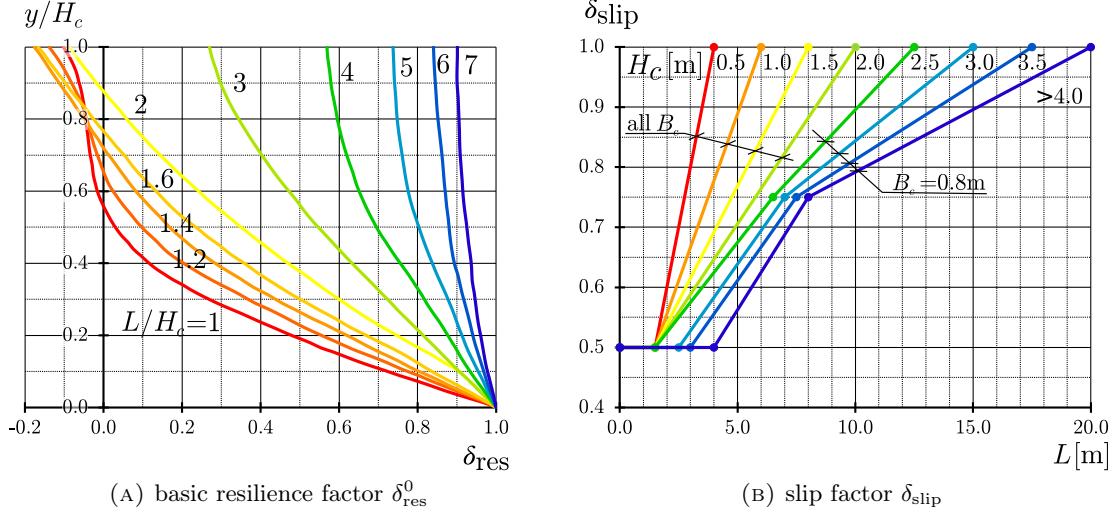


FIGURE 3.10: Factors accounting for high-walls effect in determination of the restraint factor according to NILSSON [177].

The decisive restraint coefficient distribution at height y in the central section of a wall can be calculated according to the following equation:

$$\gamma_R = \delta_{\text{res}} \delta_{\text{slip}} - \gamma_R^0 = \delta_{\text{res}} \delta_{\text{slip}} - \gamma_R^t - \gamma_R^{rx} - \gamma_R^{ry}. \quad (3.40)$$

When the plane-section hypothesis applies, no slip occurs (for the walls with $L/H > 5$), no volume change in the restraining body occurs and there are no translational or rotational boundaries, the restraint factor can be expressed with an analytic expression [176]:

$$\gamma_R(y) = 1 - \gamma_R^0 = 1 - (\gamma_R^t(y) + \gamma_R^{ry}(y) + \gamma_R^{rx}(y)), \quad (3.41)$$

where $\gamma_R^t(y)$, $\gamma_R^{ry}(y)$ and γ_R^{rx} are given as follows:

$$\gamma_R^t(y) = \frac{1}{1 + \frac{E_F H_F B_{F,\text{eff}}}{E_c H_c B_c}}, \quad (3.42a)$$

$$\gamma_R^{ry}(y) = \frac{(y_{\text{cen}} - y)(y_{\text{cen}} - 0.5H_c)}{\frac{H_c^2}{12} + \left(y_{\text{cen}} - \frac{H_c}{2}\right)^2 + \frac{E_F H_F B_{F,\text{eff}}}{E_c H_c B_c} \left(\frac{H_F^2}{12} + \left(y_{\text{cen}} + \frac{H_F}{2}\right)^2\right)}, \quad (3.42b)$$

$$\gamma_R^{rx} = \frac{(x_{\text{cen}} - \omega 0.5(B_{F,\text{eff}} - B_c))^2}{\frac{B_c^2}{12} + \left(x_{\text{cen}} - \omega \frac{B_{F,\text{eff}} - B_c}{2}\right)^2 + \frac{E_F}{E_c} \frac{H_F B_{F,\text{eff}}}{H_c B_c} \left(\frac{B_{F,\text{eff}}^2}{12} + x_{\text{cen}}^2\right)}, \quad (3.42c)$$

where:

- x, y – coordinates of the analysed point, m;
- $x_{\text{cen}}, y_{\text{cen}}$ – coordinates of the centre of gravity of a transformed section (considering old and new part of the element), m;
- H_c, B_c – height and thickness of the wall, m;
- $H_F, B_{F,\text{eff}}$ – depth and effective width of the foundation, m; the effective width of the foundation is determined to comply with the curvature obtained in FE-analysis;
- E_c, E_F – elasticity moduli of the wall and the foundation at the moment of analysis, GPa;
- ω – location factor (defines relative location of the wall with respect to the central axis of foundation).

When slip failure in the joint is possible and if the sections do not remain plane under deformation (high-walls effect), the restraint in the wall is defined as:

$$\gamma_R(y) = \delta_{\text{slip}} \cdot (\delta_{\text{res}}(y) - (\gamma_R^t(y) + \gamma_R^{ry}(y) + \gamma_R^{rx}(y))) \quad (3.43)$$

and then $\gamma_R^t(y)$, $\gamma_R^{ry}(y)$ and γ_R^{rx} are given as follows:

$$\gamma_R^t(y) = \frac{\sum_{i=1}^n \frac{a_i}{i+1}}{1 + \frac{E_F}{E_c} \frac{H_F B_{F,\text{eff}}}{H_c B_c}}, \quad (3.44a)$$

$$\gamma_R^{ry}(y) = \frac{(y_{\text{cen}} - y) \left(y_{\text{cen}} \sum_{i=1}^n \frac{a_i}{i+1} - H_c \sum_{i=1}^n \frac{a_i}{i+2} \right)}{\frac{H_c^2}{12} + \left(y_{\text{cen}} - \frac{H_c}{2} \right)^2 + \frac{E_F}{E_c} \frac{H_F B_{F,\text{eff}}}{H_c B_c} \left(\frac{H_F^2}{12} + \left(y_{\text{cen}} + \frac{H_F}{2} \right)^2 \right)}, \quad (3.44b)$$

$$\gamma_R^{rx}(y) = \frac{(x_{\text{cen}} - \omega 0.5(B_{F,\text{eff}} - B_c))^2}{\frac{B_c^2}{12} + \left(x_{\text{cen}} - \omega \frac{B_{F,\text{eff}} - B_c}{2} \right)^2 + \frac{E_F}{E_c} \frac{H_F B_{F,\text{eff}}}{H_c B_c} \left(\frac{B_{F,\text{eff}}^2}{12} + x_{\text{cen}}^2 \right)}. \quad (3.44c)$$

The influence of subsoil on the values of the restraint factor were thoroughly analysed by NILSSON [177]. He concluded that a low-friction and non-cohesive foundation material will pose almost zero translational restraint (restraint against contraction) and the restraint will increase with the increased frictional and cohesive properties of the restraining body material. Analogically, the stiffness of the foundation material will influence the possibility of bending of the concrete element and as such will influence the rotational restraint to this element. The restraint will increase with the increasing stiffness of the restraining body material and the length of the element. NILSSON does not propose the approach to account for the foundation material in determination of the translational boundary restraint. To determine the rotational restraint accounting for the stiffness of the foundation material, the material is treated as elastic and

so-called elastic length of the structural element, L_e , is determined [177]:

$$L_e = \sqrt[4]{\frac{2EI(t) \kappa_s}{K}}, \quad (3.45)$$

where:

- $EI(t)$ – bending stiffness of the structure at the time of analysis t , Nm^2 ;
- κ_s – shape factor depending on the width-to-length ratio of the element in contact with the ground, B_F/L_F ;
- K – bulk modulus of the founding ground material, N/m^2 .

NILSSON presents the approach to control if lifting of the elements ends occur and how to account for that fact in determination of the rotational restraint. The procedure of the rotational restraint calculation is presented in [177]. For practical applications it is assumed that torsion of the structure does not occur, so only the rotation in x direction is considered ($\gamma_R^{xy} = 0$).

The possibility of slip failure in high walls was also taken into consideration by FLAGA [83, 84]. The approach assumes that the foundation is undeformable and that bond forces result from the bond strength of concrete. The bond stresses appear along the contact layer between the wall and the foundation and can be calculated by the equation:

$$\tau(t) = \frac{A_c \bar{\varepsilon} E_{c,\text{eff}}(t)}{0.5 L_z B_c}, \quad (3.46)$$

where:

- $\tau(t)$ – bond stress, MPa ;
- A_c – cross-section area of the wall, m^2 ;
- $E_{c,\text{eff}}(t)$ – effective modulus of elasticity of concrete at time t , GPa ;
- ε_0 – thermal-shrinkage strain;
- L_z – bond length; at the beginning it is assumed that the bond forces occur at the whole length of the wall, so $L_z = 0.5 L_c$, m ;
- B_c – thickness of the wall, m .

The bond stresses predicted with Eq. 3.46 cannot exceed the maximum value of the bond strength. The bond strength is recommended by FLAGA [83] to be determined with the Mörsh formula:

$$\bar{\tau}(t) = 0.5 \sqrt{f_c(t) f_t(t)}. \quad (3.47)$$

According to EUROCODE 2 [183] the bond strength between two concretes of different age depends also on normal stresses and reinforcement at the joint, and should be calculated as:

$$\bar{\tau}(t) = c f_{ctd}(t) + \mu \sigma_n + \rho_r f_{yd}(\mu \sin \alpha + \cos \alpha). \quad (3.48)$$

where:

- $\bar{\tau}(t)$ – bond strength, MPa ;

- c, μ – coefficients dependent on the roughness of joint surface;
 f_{ctd} – design tensile strength of the concrete, MPa;
 σ_n – stress per unit area caused by the minimum external normal force across the interface that can act simultaneously with the shear force, MPa;
 ρ_r – degree of vertical reinforcement in the joint;
 α – reinforcement inclination angle, $\alpha = 90^\circ$.

During cooling of the wall tensile stress normal to the joint is formed at the ends of the wall as the wall is being rotated due to vertical restraint (see e.g. Fig. 3.8). This stress can be accounted as σ_n . Because σ_n is tensile, the component $c f_{ctd}(t)$ should be omitted (taken as equal to 0).

The case in which $\tau > \bar{\tau}$ signifies a break of the bond forces between the wall and the foundation at the beginning and end of the joint. In such a case the length at which bond forces still exist must be determined as $L_z = (\bar{\tau} \cdot 0.5 L) / \tau$ and it must be assumed for further calculations that $\tau = \bar{\tau}$.

The axial bond force at the joint can be determined as:

$$N_R = 0.5 \tau L_z B_c. \quad (3.49)$$

The values of stresses at the joint and at the top of the wall are then equal to:

$$\sigma|_{y=0} = \frac{N_R}{A_c} + \frac{N_R y_{cen}}{W_{c,b}}, \quad (3.50a)$$

$$\sigma|_{y=H_c} = \frac{N_R}{A_c} - \frac{N_R y_{cen}}{W_{c,t}}, \quad (3.50b)$$

where:

- y_{cen} – location of the centre of gravity of the section above the joint, m;
 $W_{c,b}, W_{c,t}$ – bending indices of the section with respect to bottom ($y = 0$) and top ($h = H_c$) fibres of the wall, respectively, m³.

Linear distribution of stresses at the height of the wall is assumed which means that variations in the degree of restraint are neglected ($R_N = R_M = 1.0$).

3.2.2 Stresses in cracked walls

The stresses occurring in externally-restrained elements vary according to the degree of restraint, which depends on the L/H ratio, dimensions of the wall and the restraining body, and the roughness of the contact surface between the two, including the vertical reinforcement. The methods of analysis of externally-restrained elements presented so far are based on the assumption that the analysed element is uncracked and that both the material of the wall and the restraining body exhibit linear elastic behaviour.

Nevertheless, it must be remembered that crack occurrence has an influence on distribution of stresses. To define the crack occurrence two approaches are proposed: either the strength criterion or the strain criterion. According to the strength criterion the stress in the early-age wall, $\sigma(t)$, calculated under the assumption of uncracked sections, is compared with the tensile strength of concrete [83]; design tensile strength, $f_{ctd}(t)$, is recommended for new structures and mean tensile strength, $f_{ctm}(t)$, for existing ones. When $\sigma > f_t$, crack is formed. In the strain criterion the expected strain in the early-age wall accounting for the restraint, $\varepsilon_{tot}/\gamma_R$, is compared with the strain capacity of concrete, ε_{ctu} , calculated as the ratio between the mean tensile strength and the effective modulus of elasticity, $f_{ctm}(t)/E_{cm,eff}(t)$ [21].

The influence of horizontal cracks at the joint formed due to the slip of the wall on the restraint was accounted by NILSSON [177] – he proposed the slip reduction factor, $\delta_{slip} \leq 1$, which represents the decrease in restraint when slip occurs, and by FLAGA [83]. Nevertheless, in externally-restrained elements the degree of restraint would change also due to cracks in the wall itself – the degree of restraint would decrease at crack. KHEDER ET AL. [9, 128, 129] developed the *change of restraint theory* accounting for stress redistribution due to a change of restraint at crack in cracked elements. This method also introduces the restraint factor, which in this case was experimentally determined for the walls with different L/H ratio and for the given crack width.

The change of restraint theory defines that the change in restraint during cracking, ΔR , equals to the difference between the degrees of restraint before, R_b , and after, R_a , crack formation [9]. The effect of slip is expressed by introduction of the reduction factor, K_2 [129]:

$$\Delta R = R_b - K_2 R_a. \quad (3.51)$$

It was proposed to take $K_2 = 0.8$, however, it must be remembered that the actual magnitude of the influence of slip on the restraint depends on the geometry of the wall [177]. The change of restraint factors were presented by KHEDER [128] in a form of diagrams. As the residual restraint was observed to depend on the L/H ratio [9], the diagrams of the change of restraint factor were prepared in dependence of L/H ratio of the walls.

3.3 Creep and ageing

The material model of early-age concrete should account for ageing of concrete and its effect on material properties development, for the effect of elevated temperature and for creep. Development of material properties of early-age concrete is connected with development of its maturity. The most popular and simple approach to describe the development of material properties in time in increased temperature is the equivalent age method. This approach is presented in Sec. 4.1.4.2.

Direct approaches are used to account for creep which allow for calculation of creep effects in a single time step [23]. The most popular method is the effective modulus method in which the effective modulus of elasticity, $E_{c,eff}$ is used. According to this approach the effect of creep is taken into account by reduction of the modulus of elasticity [49]:

$$E_{c,eff}(t, T) = K_1 E_c(t, T) = \frac{E_c(t, T)}{1 + \beta(t, t_0)\phi(t, t_0)}, \quad (3.52)$$

where:

- $E_c(t, T)$ – modulus of elasticity at time t accounting for the effect of temperature (equivalent age method can be used), GPa;
- $\beta(t, t_0)$ – ageing coefficient;
- $\phi(t, t_0)$ – creep coefficient.

The ageing coefficient varies within narrow range of $0.5 \leq \beta(t, t_0) \leq 1.0$ and can be assumed constant at $\beta = 0.8$ for many practical problems [49]. The creep coefficient can be calculated with any desired method. Methods for calculation of the creep coefficient are presented in Sec. 4.1.4.1. KIERNOŻYCKI [130] suggests to take $\phi = 0.60$, which gives the value of $K_1 = 0.68$. CIRIA C660 [21] suggests the value of $K_1 = 0.65$.

The JSCE STANDARD [116] proposes to reduce the modulus of elasticity as calculated with Eq. 4.80 with a coefficient which accounts for creep, ϕ , which should be taken as $\phi(3 \text{ days}) \leq 0.73$ and $\phi(5 \text{ days}) \geq 1.0$, and from 3 to 5 days linear interpolation can be used. Analogically, the JCI GUIDELINE [110] suggests the value of $\phi = 0.42$ should be taken at the age of concrete up to reaching the maximum temperature and $\phi = 0.65$ at the age one day after reaching that temperature; between the linear interpolation can be used. Parameters K_1 and ϕ in the European and Japanese approach can be related, however, according to the JSCE STANDARD proposal $\phi \gg K_1$ while the JCI GUIDELINE is in the agreement with CIRIA C660 which suggests the value of $K_1 = \phi = 0.65$ for cooling phase.

Chapter 4

Modelling of early-age reinforced concrete walls behaviour

Modelling of early-age concrete structures behaviour becomes an increasingly challenging task. More is known about the early-age concrete as a material, which extends the material model. At the same time focus is put on the behaviour of early-age structures as elements of complex structural systems, including cooperation with the founding subsoil. Thus, the analysis of early-age concrete structures requires appropriate constitutive equations to be defined not only for the early-age concrete, but also the subsoil, reinforcing steel and interaction between these materials. These issues will be discussed in the following sections. This leads to a situation in which a complete model of even a relatively simple reinforced concrete wall becomes impossible to be solved manually. As a consequence, computer implementations of the models are used in which numerical methods are applied for the solution of the governing equations.

In the numerical approaches the Finite Element Method is applied in a majority of cases. The structure is divided into a discrete number of elements and the desired values are determined in each point of the structure. The simplest approach is to reduce the wall into 2 dimensions and assume undeformable foundation (Fig. 4.1a); this approach is used for analysis of early-age walls with general-purpose software [95, 96, 147, 223]. In the detailed analysis usually a 3D model of both the wall and the foundation is used. The foundation may be settled firmly on the subsoil – total restraint of the foundation is then assumed as shown in Fig. 4.1b. Alternatively, interaction between the foundation and the subsoil may be taken into account (Fig. 4.1c). In the latter case appropriate dimensions of the soil block must be chosen and parameters of the soil must be provided in the analysis. This approach is used rarely and most often it is limited to thermal analysis [152, 218]. Few examples of full cooperation can be referred [136, 146]. An interesting hybrid approach was proposed at the Luleå University of Technology. According to this approach the wall is analysed in 2D, but the cross-section instead of longitudinal section is analysed (as the right scheme in Fig. 4.1c). The total stress is calculated by introduction of the restraint factor, γ_R , analogically as in the analytic approach proposed by NILSSON [177]. The restraint factor is, however, calculated numerically with the general-purpose software according to either of two methods: Linear Restraint Method (LRM) [155, 176] or Equivalent Restraint Method (EQM) [8, 108].

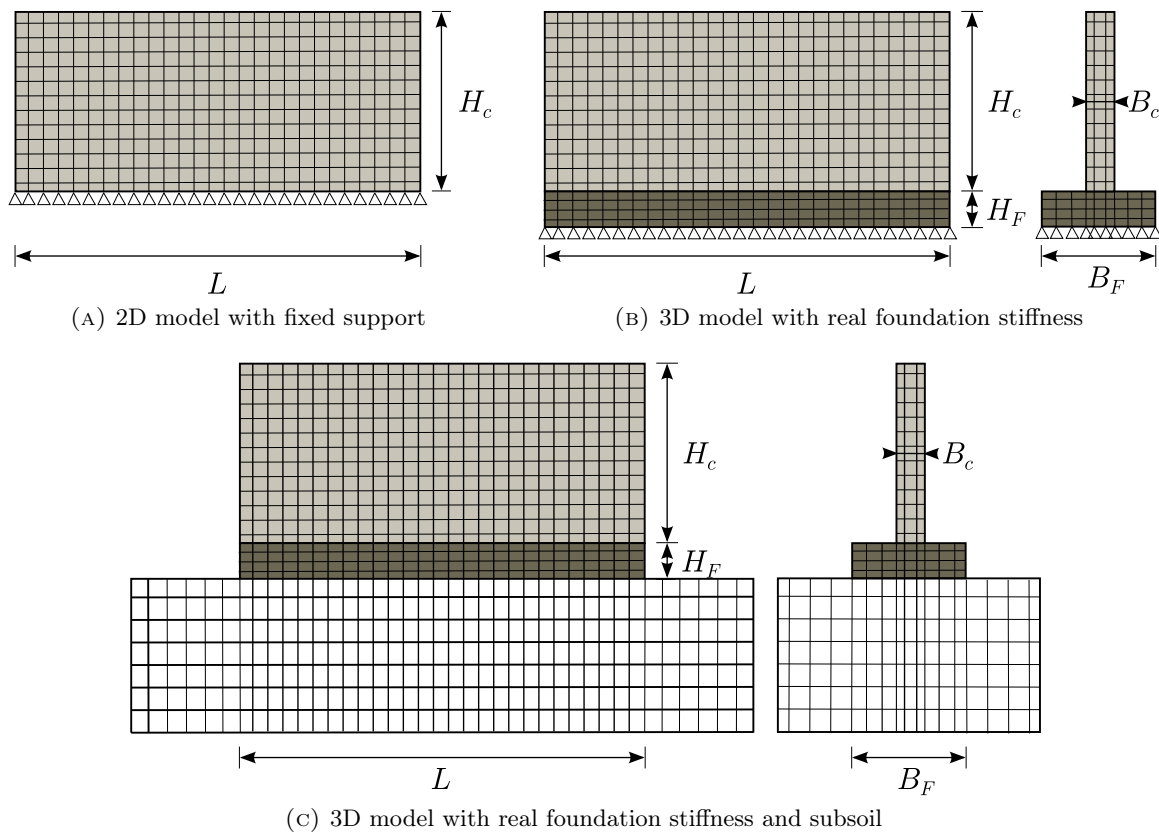


FIGURE 4.1: Models of the wall applied in numerical approaches with FEA.

4.1 Early-age concrete

Early-age concrete is undoubtedly one of the most difficult structural materials for modelling. The difficulties arise from a complex concrete structure which is additionally subjected to transformations as a result of cement hydration. Initially it is a mixture of liquids and solids of varying diameters and shapes. Such a medium is characterised by strong viscous and plastic properties. With progressing cement hydration concrete becomes a solid, with elastic, viscous and plastic characteristics, where the mutual proportions of these features depend on the progress of the concrete hardening process.

Taking into account the concrete structure and its changes during hardening two possibilities to model early-age concrete appear. The first approach is related to multi-phase models, in which a precise analysis of the physical phenomena and the influence of the material's internal structure on these phenomena is made. Appropriate constitutive equations are defined for the solid, liquid and gaseous phase of the medium and then averaged for a multi-phase medium. Several works in which the multi-phase models of early-age concrete were developed can be referred [72, 73, 90, 91, 204, 217, 230, 233]. The main drawback of multi-phase models is their computational complexity.

The second approach is related to phenomenological models, where concrete is treated as a continuous medium. A detailed analysis of physical processes related to phase transitions and chemical processes occurring in hardening concrete is neglected in these models and a macroscopic

description of the thermal–moisture–mechanical phenomena is used. Phenomenological models are used more often and many examples of their applications can be referred [27, 69, 71, 79, 99, 120, 153, 159, 232]. The main advantage of phenomenological models is their simplicity (with respect to multi-phase models). Because the main purpose of the structural analysis of concrete elements is to evaluate the stress state, the use of phenomenological models seems a more appropriate choice in thermal–moisture analysis.

In an early-age concrete element the total strain includes the thermal and shrinkage strain and the effect of creep expressed in a form a delayed part of strain [103]:

$$\varepsilon(t) = \varepsilon_{\sigma}(t) + \varepsilon_n(t) = \varepsilon_e(t) + \varepsilon_{cc}(t) + \varepsilon_W(t) + \varepsilon_T(t), \quad (4.1)$$

where:

- $\varepsilon_{\sigma}(t)$ – strain due to the applied load;
- $\varepsilon_n(t)$ – strain independent of the applied load;
- $\varepsilon_e(t)$ – load-dependent initial strain (elastic strain) at the time of load application;
- $\varepsilon_{cc}(t)$ – creep strain at a concrete age t ;
- $\varepsilon_W(t)$ – shrinkage strain at time t ;
- $\varepsilon_T(t)$ – thermal strain at time t .

The methods used for determination of the constitutive strains and resulting stresses in early-age concrete are presented in detail in the following sections.

4.1.1 Cement hydration

The process of cement hydration is a driving force for all phenomena occurring in early-age concrete. Cement hydration is responsible for strength and stiffness gain of hardening concrete and the exothermic character of this process is responsible for the increase of temperature as well as transport of moisture in the conditions of variable temperature. That is why it is crucial to characterise the time-development of this process prior to definition of any constitutive equations for early-age concrete. Development of the properties of early-age concrete can be expressed as a function of time or degree of hydration. The influence of the temperature history on the maturity of concrete can be described by various temperature functions.

4.1.1.1 Time development and maturity

To express the effect of temperature on time-development of early-age concrete properties described as a function of time, the concept of maturity was introduced by SAUL [199]; according to his maturity method samples of given concrete acquire the same strength when equal maturities are reached, irrespective of their temperature histories. The maturity of concrete is a time-accumulated surplus of current temperature, $T(t)$, above a threshold temperature, T_0 , below

which hardening would not occur:

$$M = \int_0^t (T(t) - T_0) dt. \quad (4.2)$$

The concept of the equivalent age as an alternative to the maturity was introduced by RASTRUP [188]. The equivalent age was defined as the time during which the concrete would have to be cured at a constant reference temperature, T_{ref} , to achieve the same maturity as the concrete undergoing the actual curing history:

$$t_e = \int_0^t A(T) dt, \quad (4.3)$$

where $A(T)$ is the affinity ratio with respect to the reference temperature. The linear dependence proposed by SAUL used in definition of the equivalent age:

$$t_e = \int_0^t \frac{T(t) - T_0}{T_{\text{ref}} - T_0} dt, \quad (4.4)$$

did not comply with real observations so HANSEN AND PEDERSEN [98] proposed to apply the Arrhenius law to define the affinity ratio. The equivalent age was given by the function:

$$t_e(t, T) = \int_0^t e^{-\frac{E_K}{R} \left(\frac{1}{T} - \frac{1}{T_{\text{ref}}} \right)} dt. \quad (4.5)$$

where:

- E_K – activation energy, J/mol;
- R – universal gas constant, $R = 8.314 \text{ J}/(\text{mol K})$;
- T – actual temperature at time t , K;
- T_{ref} – reference temperature, $T_{\text{ref}} = 293.15 \text{ K}$.

There were also proposals of other functions to define the temperature dependence in the equivalent age, e.g. a parabolic expression given by WEAVER AND SADGROVE [222]. However, it has been proven by many authors, e.g. CHENGJU [54] or BALLIM AND GRAHAM [20], that the formulation governing the Arrhenius law gives the most accurate results.

4.1.1.2 Degree of hydration

According to the degree of hydration method time-development of the material properties of early-age concrete can be expressed as a function of the degree of hydration which relates the amount of heat released to a certain point, $Q(t)$, to the total amount of hydration heat expected

upon the completion of the hydration, Q_{tot} , [214]:

$$\alpha_H(t) = \frac{Q(t)}{Q_{\text{tot}}}. \quad (4.6)$$

For blended cements with an addition of supplementary cementitious materials (fly ash or slag) the degree of hydration was proposed to be replaced with the degree of reaction, $r_H(t)$ [64]:

$$r_H(t) = \frac{Q(t)}{Q_{\text{max}}}, \quad (4.7)$$

where Q_{max} is the total hydration heat corresponding to the end of the hydration tests. The degree of hydration and the degree of reaction are then in the following relationship [64]:

$$\alpha_H(t) = r_H(t) \frac{Q_{\text{max}}}{Q_{\text{tot}}}. \quad (4.8)$$

The degree of reaction is practical when the hydration development is determined experimentally while the degree of hydration is more practical for civil engineering applications when the total hydration heat is determined from the cement composition [159]. The total heat Q_{max} can be calculated from the chemical composition of cement as proposed by BOGUE [32]:

$$Q_{\text{max}} = 500 p_{\text{C}_3\text{S}} + 260 p_{\text{C}_2\text{S}} + 866 p_{\text{C}_3\text{A}} + 420 p_{\text{C}_4\text{AF}} + 642 p_{\text{SO}_3} + 1186 p_{\text{FreeCaO}} + 850 p_{\text{MgO}}, \quad (4.9)$$

while the total heat Q_{tot} , accounting for supplementary cementitious materials in blended cements, was proposed by SCHINDLER AND FOLLARD [202] to be calculated as follows:

$$Q_{\text{tot}} = Q_{\text{max}} + 1800 p_{\text{FA,CaO}} + 461 p_{\text{Slag}}, \quad (4.10)$$

where p_i is a weight ratio of an i -th compound of the binder with respect to the total binder content. It should be noted that the values of the hydration heat of the subsequent compounds obtained by other authors differ slightly from the results of BOGUE. Moreover, the BOGUE formulation is the most complete and includes all the compounds of cement while it can be observed that because of their amount C_3S , C_2S , C_3A and C_4AF have a decisive influence on the total hydration heat of cement.

The heat development, $Q(t)$, can be calculated by time integration of the heat development rate, $q(t)$. Such formulation was proposed by REINHARDT ET AL. [189]; in this formulation the effect of temperature was expressed with a temperature function:

$$q(t, T) = q_{\text{max}} f(r_H(t)) g(T), \quad (4.11)$$

where:

- q_{max} – the maximum heat production rate determined at reference temperature, J/s;
- $f(r_H(t))$ – heat-production rate function;
- $g(T)$ – temperature function.

The degree of reaction was used here because no equivalent for the BOGUE formulation was known

for blended cements. The hydration rate was defined as superposition of the rates determined for Portland cement and supplementary materials [64]. However, if the degree of hydration is calculated for the total hydration heat according to e.g. SCHINDLER AND FOLLARD formulation, the degree of hydration can be used instead of the degree of reaction.

The component $f(\alpha_H(t))g(T)$ represents the rate of the degree of hydration development, $\dot{\alpha}_H$, [79]. For the function describing the influence of temperature on the hydration heat rate, $g(T)$, Arrhenius function is applied. The function of the heat production rate is usually determined experimentally but some proposals of analytic description were given. DE SCHUTTER AND TAERWE [64] proposed an exponentially-decaying sine-powered function of the heat production rate and an Arrhenius-based temperature-dependence function:

$$\dot{\alpha}_H = f(\alpha_H(t))g(T) = c [\sin(\alpha_H(t)\pi)]^a e^{-b\alpha_H(t)} e^{\frac{E_K}{R}\left(\frac{1}{T_{\text{ref}}} - \frac{1}{T}\right)}, \quad (4.12)$$

where a , b and c are material constants. ULM AND COUSSY [212] and CERVERA ET AL. [52] used the rate of degree of hydration development with normalised affinity, $\tilde{A}(\alpha_H)$:

$$\dot{\alpha}_H = \tilde{A}(\alpha_H)g(T) = \tilde{A}(\alpha_H)e^{-\frac{E_K}{RT}}. \quad (4.13)$$

Polynomial function of the hydration degree was proposed by BENBOUDJEMA AND TORRENTI [27]:

$$\tilde{A}(\alpha_H) = (a_0 + a_1\alpha_H + a_2\alpha_H^2 + a_3\alpha_H^3 + a_4\alpha_H^4 + a_5\alpha_H^5 + a_6\alpha_H^6)^2, \quad (4.14)$$

and exponentially decaying parabolic function was proposed by CERVERA ET AL. [52] and refined by GAWIN ET AL. [90] for description of the normalised affinity:

$$\tilde{A}(\alpha_H) = a_1 \left(\frac{a_2}{\alpha_u} + \alpha_u \alpha_H(t) \right) (1 - \alpha_H(t)) e^{-a\alpha_H(t)}, \quad (4.15)$$

where a_1 , a_2 and a are material coefficients.

In a way similar to REINHARDT ET AL. the heat production rate was proposed by SCHINDLER AND FOLLARD [202]:

$$q(t, T) = Q_{\text{tot}} \left(\frac{\tau}{t_e} \right)^\beta \left(\frac{\beta}{t_e} \right) \alpha_H(t_e) e^{\frac{E_K}{R}\left(\frac{1}{T_{\text{ref}}} - \frac{1}{T}\right)}, \quad (4.16)$$

where:

- Q_{tot} – total heat of hydration, J/g;
- $\alpha_H(t_e)$ – degree of hydration at equivalent age, t_e , given after RASTRUP [188] as:

$$\alpha_H(t_e) = \alpha_{Hu} e^{-\left(\frac{\tau}{t_e}\right)^\beta}, \quad (4.17)$$

- τ, β – hydration time and shape parameters which can be calculated acc. to SCHINDLER AND FOLLARD [202] as:

$$\tau = 66.78 p_{C_3A}^{-0.154} p_{C_3S}^{-0.401} Blaine^{-0.804} p_{SO_3}^{-0.758} e^{[2.187 p_{Slag} + 9.50 p_{FA} p_{FA, Cao}]}, \quad (4.18a)$$

$$\beta = 181.4 p_{C_3A}^{0.146} p_{C_3S}^{0.227} Blaine^{-0.535} p_{SO_3}^{0.558} e^{[-0.647 p_{Slag}]}, \quad (4.18b)$$

α_{Hu} – ultimate degree of hydration ($\alpha_{Hu} \leq 1$):

$$\alpha_{Hu} = \frac{1.031w/c}{0.194 + w/c} + 0.50 p_{FA} + 0.30 p_{Slag}. \quad (4.19)$$

RIDING ET AL. [192] proposed more developed method for determination of α_{Hu} , τ and β accounting not only for cement composition but also addition of admixtures.

There are also some direct proposals for definition of the hydration heat development, $Q(t)$, functions. DE SCHUTTER [69] proposed a rational function of the equivalent age:

$$Q(t, T) = Q_{tot} \frac{a t_e}{1 + a t_e}, \quad (4.20)$$

where a is material coefficient, 1/s.

The exponentially-decaying function of time was adopted by many authors [31, 110, 220, 232, 233]. The following formulations for the hydration heat development were proposed:

$$Q(t) = Q_{tot} e^{-at}, \quad (4.21a)$$

$$Q(t) = Q_{tot} (1 - e^{-at}), \quad (4.21b)$$

where a is a hydration rate coefficient dependent on the type of cement; time can be replaced with the equivalent age to express the influence of temperature. A refined exponential function was also adopted by KLEMCZAK AND KNOPPIK-WRÓBEL [145] after RASTRUP:

$$Q(t, T) = Q_{tot} e^{-a_1 t e^{a_2}}, \quad (4.22)$$

where a_1 and a_2 are the coefficients dependent on the type of cement. The above functions fail to depict a typical ‘‘S’’ shape of the hydration heat curve, however, the function in Eq. 4.22 provides a sufficiently accurate hydration heat rate.

4.1.1.3 Activation energy

The activation energy in the Arrhenius formulation defines the temperature sensitivity of the hydration process. It depends on the type and class of cement, water-to-binder ratio, additions and admixtures. JONASSON [114] introduced the following formula for the activation energy:

$$E_K = E_{K,ref} \left(\frac{30}{T + 10} \right)^a, \quad (4.23)$$

where $E_{K,\text{ref}}$ and a are material parameters dependent on the cement. SCHINDLER [201] proposed the formula to calculate the activation energy based on the chemical cement composition:

$$E_K = 22100 f_E p_{C_3A}^{0.30} p_{C_4AF}^{0.25} \text{Blaine}^{0.35}, \quad (4.24)$$

where:

- p_{C_3A}, p_{C_4AF} – weight ratio of C_3A and C_4AF , respectively, with respect to the total cement content;
- Blaine – specific surface area of cement, m^2/kg ;
- f_E – activation energy modification to account for SCMs, defined as:

$$f_E = 1 - 1.05 p_{FA} \left(1 - \frac{p_{FA, \text{CaO}}}{0.40} \right) + 0.40 p_{\text{Slag}}, \quad (4.25)$$

- p_{FA}, p_{Slag} – weight ratio of fly ash and slag, respectively, with respect to the total cementitious material content;
- $p_{FA, \text{CaO}}$ – weight ratio of the CaO content in fly ash.

A similar empirical approach was proposed by POOLE [186] and RIDING ET AL. [191] who additionally took into consideration the effect of admixtures in the concrete mix.

SOFI ET AL. [208] have shown, however, that the value of the activation energy does not significantly affect prediction of temperature-dependent time-development of the material properties of concrete, which is important from the point of view of simplification of calculations. That is why simplified proposals given by standards and recommendations can be used. HANSEN AND PEDERSEN [98] suggest the value of $E_K = 33.5 \text{ kJ/mol}$ while RILEM [196] the value of $E_K = 33.536 \text{ kJ/mol}$ given that the temperature of concrete T is at least 20°C . MODEL CODE 2010 [50] suggests that the value of $E_K = 33 \text{ kJ/mol}$ can be assumed. Nevertheless, it must be emphasised that these values are determined for concrete mixes with predominant Portland cement content; for concrete mixes in which large amounts of pozzolans are used as a replacement of cement, activation energy should be determined experimentally because the proposed values are no longer valid [50].

4.1.1.4 Setting time

An important point in the process of concrete hardening is the setting time, t_s , which defines the moment when fresh concrete sets and starts to gain stiffness and strength. The setting time differs between different concrete mixes and depends on many factors, among the others the type of cement and the temperature of concrete.

The fact that development of mechanical properties of concrete does not begin instantaneously after mixing of cement with water is taken into consideration when modelling early-age concrete. When time-development approach is used, the setting time, t_s , is set as a starting point, so the time-development functions are defined for age of concrete $t \geq t_s$. When degree of hydration is used, the threshold value of the degree of hydration, α_0 , is defined, below which no strength development occurs; time-development is then defined for the degree of hydration $\alpha_H(t) \geq \alpha_0$.

4.1.2 Thermal and shrinkage strain

One of the issues in modelling of early-age concrete is a method of coupling of temperature, moisture and stresses. It is possible to assume full coupling of thermal–moisture–mechanical fields (model of deformable body) and to separate thermal–moisture and mechanical fields (model of undeformable body). The first approach takes into account the influence of the mechanical field changes on the changes of concrete temperature and humidity, such as the increased heat and moisture exchange through crack, increased moisture removal due to loading or changing of boundary conditions as volumetric changes of concrete may cause it to separate from the boundaries [19]. In the second approach the influence of the mechanical field on thermal diffusion processes is neglected. This approach, because of its simplicity, is more popular in applications [19, 27, 57, 62, 79, 99, 134, 153, 159, 232]. In such a model the thermal–moisture fields are determined first. The stress state is determined assuming that the thermal–shrinkage strains are imposed strains.

The thermal strain is caused by temperature change, dT , and is proportional to that change according to the equation:

$$d\varepsilon_T = \alpha_T dT, \quad (4.26)$$

where:

- dT – temperature difference, °C;
- α_T – thermal dilation coefficient, $1/^\circ\text{C}$.

The shrinkage strain is caused by a volume change due to the variations of moisture content. When the humidity change is known, the shrinkage strain can be calculated based on the moisture content by volume, dW , or by mass, dc [28]:

$$d\varepsilon_W = \alpha_W dW, \quad (4.27)$$

$$d\varepsilon_c = \alpha_c dc, \quad (4.28)$$

where:

- dW – difference of moisture content by volume, m^3/m^3 ;
- dc – difference of moisture content by mass, kg/kg ;
- α_W, α_c – moisture dilation coefficient (also called hydrous compressibility factor).

To determine the temperature and moisture content variations thermal and humidity fields must be determined over the period of concrete hardening. It is possible to assume full coupling of thermal and humidity fields, to neglect the influence of humidity changes on temperature changes (partial coupling) or to assume uncoupled equations. Most of the models for early-age concrete account only for thermal volume changes (thermal strains) [57, 62, 69, 78, 232] or thermo–chemical volume changes (thermal strain and autogeneous shrinkage strain) [27, 38, 57, 79, 159, 234]; drying shrinkage strain is usually neglected.

Heat diffusion within concrete is defined by the heat equation based on the Fourier’s law, in which the vector of heat flux is directly proportional to the temperature gradient, combined with

the energy conservation law. Generation of heat in the element due to hydration is described by introduction of the rate of hydration heat generation, $q_v(t, T)$, as a source function:

$$\dot{T} = \text{div}(\alpha_{TT} \text{grad}T) + \frac{q_v(t, T)}{c_b \rho}, \quad (4.29)$$

where:

- T – temperature, K;
- α_{TT} – thermal diffusion coefficient, m^2/s ;
- ρ – density of concrete, kg/m^3 ;
- c_b – specific heat of concrete, $\text{kJ}/(\text{kg K})$.

The source function relates the unit rate of cement hydration, $q(t, T)$ [$\text{J}/(\text{g s})$], and the amount of cement, C_c [kg/m^3]:

$$q_v(t, T) = q(t, T) C_c, \quad (4.30)$$

with unit rate of hydration:

$$q(t, T) = \frac{dQ(t, T)}{dt}. \quad (4.31)$$

Autogenous shrinkage is also driven by the cement hydration process and is also defined in relation to the rate of hydration heat development. Its development is proposed to be defined as a function of the degree of hydration [27, 37, 213]:

$$\varepsilon_{ca} = K_H \bar{\alpha}(t), \quad (4.32)$$

where K_H is a material constant and $\bar{\alpha}(t)$ is a function of the degree of hydration development which can be taken according to Eq. 4.83 by DE SCHUTTER AND TAERWE [66], $\bar{\alpha}(t) = \beta_c(t)$, or as a rate of degree of hydration, $\bar{\alpha}(t) = \dot{\alpha}_H(t)$. Most of the authors state that autogenous shrinkage strain is in a linear dependence on the degree of hydration; however, ZREIKI ET AL. [234] suggest that for some concretes (especially high performance concretes) the autogenous shrinkage and degree of hydration are not in a linear dependence and proposed the exponential function for evolution of the autogenous shrinkage strain:

$$\bar{\alpha}(t) = \frac{\langle \alpha_H(t) - \alpha_0 \rangle_+^\beta}{1 - \alpha_0}, \quad (4.33)$$

with exponent β to be determined experimentally for given concrete. The $\langle x \rangle_+$ is defined as a positive part of x , i.e.

$$\langle x \rangle_+ = \begin{cases} 0 & \text{for } x < 0 \\ x & \text{for } x \geq 0. \end{cases} \quad (4.34)$$

Nevertheless, although drying shrinkage has little effect on stresses arising in massive concrete elements, its influence is more pronounced in medium-thick elements, so some authors advocate considering it in the analysis [19, 132, 153, 233]. To account for the moisture transport due to both self-dessication and surface drying it is convenient to describe moisture diffusion based on the Fick's second law of diffusion, analogical to Fourier's law, in which the vector of moisture flux

is proportional to the moisture concentration gradient [2, 15, 19, 121, 131, 132, 153]. As moisture diffusion in hardening concrete is additionally driven by cement hydration (self-dessication), a mass sink function was introduced which is a function of the rate of hydration heat generation, $q_v(t, T)$:

$$\dot{c} = \text{div}(\alpha_{WW} \text{grad}c) - K_H q_v(t, T). \quad (4.35)$$

where:

c – moisture concentration by mass, kg/kg, which is in the following relation with the moisture content by volume W , m^3/m^3 :

$$c \rho = W \rho_w \quad (4.36)$$

where ρ_w and ρ are volume density of water in concrete and density of concrete, kg/m^3 , respectively.

α_{WW} – moisture diffusion coefficient;

K_H – coefficient to reflect the effect of hydration on the moisture content, m^3/J .

During the progress of hydration the moisture content decreases which is connected with internal drying and bounding of water by cement. Thus, the amount of moisture is directly related to the progress of hydration and expressed in a form of the coefficient of the water–cement proportionality, K_H , which relates the amount of bounded water to the rate of heat. As the overall amount of water decreases this coefficient has always a positive value. The $K_H q_v(t, T)$ component of the equation represents the autogenous shrinkage of concrete.

Most often partial coupling is taken into account in which the influence of the increased or reduced temperature on the rate of moisture diffusion is taken into account. After BAŽANT AND THONGUTHAI [26] the moisture diffusion coefficient is expressed not only as a function of relative pore humidity but also temperature. Although thermal and moisture phenomena appear in different time scales [19], some authors suggest that it is important to take into consideration the effect of moisture diffusion on development of thermal fields – the thermal diffusion coefficient is being defined as a function of humidity, e.g. by ANDREASIK [13]. Another approach to thermal and moisture fields coupling was proposed by KLEMCZAK [134, 135]. Leaving the thermal diffusion coefficient fixed the mutual influence of temperature and moisture gradients (and thus also their migration) has been accounted for by introducing additional coupling coefficients: α_{TW} to represent the influence of the moisture transport on the heat transfer and coefficient α_{WT} to represent the influence of the heat transfer on the moisture transport. The coupled equations have a form:

$$\dot{T} = \text{div}(\alpha_{TT} \text{grad}T + \alpha_{TW} \text{grad}c) + \frac{q_v(t, T)}{c_b \rho}, \quad (4.37a)$$

$$\dot{c} = \text{div}(\alpha_{WW} \text{grad}c + \alpha_{WT} \text{grad}T) - K_H q_v(t, T). \quad (4.37b)$$

The heat transfer through the surface of the element occurs in five forms [220]: solar radiation, convection, thermal radiation, evaporation and condensation. The last two have negligible

influence and are not considered in the heat transfer analysis. The boundary conditions are usually assumed to be of convective type defined with the Newton's cooling law [15, 27, 39, 62, 69, 135, 153, 232, 234]. Analogical boundary conditions are defined for moisture transfer [15, 19, 121, 124, 131, 135, 153]. The heat and moisture flux are expressed as follows:

$$\tilde{q} = \frac{\alpha_p}{c_v} (T_{\text{sur}} - T_a), \quad (4.38a)$$

$$\tilde{\eta} = \beta_p (c_{\text{sur}} - c_a), \quad (4.38b)$$

where:

- α_p – coefficient of heat exchange by convection, $\text{W}/(\text{m}^2\text{K})$;
- β_p – coefficient of moisture exchange, m/s ;
- c_v – heat capacity of concrete, $\text{kJ}/\text{m}^3\text{K}$;
- T_{sur}, T_a – surface and ambient temperature, respectively, K ;
- c_{sur}, c_a – surface and ambient humidity, respectively, kg/kg .

The effect of radiation is usually expressed by the increase of the coefficient of heat exchange by convection. The thermal radiation coefficient is determined with the Stefan–Boltzmann equation and the solar radiation is accounted for by multiplication of the incident solar energy by the solar absorptivity of concrete surface [79]. Models exist which allow to determine the influence of solar radiation based on exposure conditions [35, 105, 193].

4.1.3 Thermo–physical properties of concrete

In thermal analysis the following physical properties of concrete are crucial for proper simulation of heat transfer: thermal conductivity, specific heat and thermal diffusivity, which are in mutual relationship, and heat transfer coefficient, which represents the degree of heat exchange with the environment. Analogically, the moisture diffusion and moisture transfer coefficient are important for proper simulation of moisture transport. Precise determination of their values and variations are essential in the analysis of early-age concrete.

4.1.3.1 Coefficients in thermal analysis

Thermal diffusion coefficient, α_{TT} , is taken as equal in all directions. It is in the following relationship with the other physical properties of concrete:

$$\alpha_{TT} = \frac{\lambda}{c_b \rho} = \frac{\lambda}{c_v}, \quad (4.39)$$

where:

- λ – thermal conductivity coefficient, $\text{W}/(\text{m K})$;
- c_v – heat capacity, $\text{kJ}/(\text{m}^3\text{K})$;
- c_b – specific heat, $\text{kJ}/(\text{kg K})$;
- ρ – density, kg/m^3 .

Thermal conductivity, λ , and specific heat, c_b , of concrete depend on temperature, moisture content, density of concrete and ageing [175]. Numerous authors concluded that the specific heat and thermal diffusivity of hardening concrete decrease linearly with the degree of hydration; REINHARDT ET AL. [189], VAN BREUGEL [214], DE SCHUTTER AND TAERWE [65] and DE BORST [58] proposed the following functions of the degree of hydration:

$$\lambda(t) = \lambda_0 (a_1 - a_2 \alpha_H(t)), \quad (4.40a)$$

$$c_b(t) = c_{b,0} (b_1 - b_2 \alpha_H(t)), \quad (4.40b)$$

where $\lambda(t)$, λ_0 and $c_b(t)$, $c_{b,0}$ represent time-development and final value of thermal conductivity or specific heat and a_1 , a_2 and b_1 , b_2 are constant parameters. However, many authors have obtained good numerical predictions neglecting the change of the values of thermal conductivity and specific heat over time and average values are mostly used [38, 57, 62, 234]. It was shown by BRIFFAUT ET AL. [39] that the assumption of constant values of thermal parameters of concrete gives safe results (expected temperatures are overestimated). These average values of thermal conductivity and specific heat of concrete can be calculated based on its composition when the mass fraction, p_i , of the constituents and their thermal conductivities, λ_i , and heat capacities, $c_{b,i}$, are known [111, 130, 234]:

$$\lambda = \sum p_i \lambda_i, \quad (4.41)$$

$$c_v = \sum p_i \rho_i c_{b,i}. \quad (4.42)$$

Such formulation is valid for specific heat but for thermal conductivity is only an approximation. Expression of a property of a material as a weighted average of the properties of its constituents signifies that the constituents are connected in parallel – it is not true for thermal conductivity of concrete, in which the concrete constituents are in random positions with respect to one another. Thermal properties of concrete mix components are listed in Tab. 4.1. Thermal conductivity and specific heat of concretes with typical aggregates are listed in Tab. 4.2.

component	λ_i [W/(m K)] [130]	$c_{b,i}$ [kJ/(kg K)] [130]	ρ_i [kg/m ³] [185]
water	0.60	4.18	1000
cement	1.28	0.56	3000
sand	3.08	0.74	2650
basalt	1.91	0.77	2650
dolomite	4.32	0.82	2650
granite	2.94	0.74	2650
quartzite	4.60	0.72	2650
rhyolite	1.88	0.78	2650

TABLE 4.1: Thermal properties of concrete components.

Little is known about the coefficients for coupling of thermal–moisture equations, α_{TW} and α_{WT} . They are taken also as equal in all directions and constant. GAWIN [89] proposed the coefficient $\alpha_{TW} = 0.9375 \cdot 10^{-4}$ (m² K)/s. The α_{WT} coefficient is also not well recognised parameter and few authors elaborate on its value. WYRWAL AND SZCZĘSNY [229] proposed the coefficient $\alpha_{WT} = 2.0 \cdot 10^{-11}$ m²/(K s).

aggregate	λ [W/(m K)]	ρ [kg/m ³]	$\alpha_T \cdot 10^{-6}$ [1/°C]
quartzite	3.5 [175], 4.5 [5]	2440	11.7–12.8 [175], 11–13 [5], 13 [130]
dolomite	3.3 [175], 4.2 [5]	2500	11.7–13.1 [175], 7–10 [5], 6.7–8.6 [130]
granite	2.6 [175], 2.6–2.7 [5]	2420	7.7–9.5 [175], 7–9 [5], 8 [130]
basalt	2.0 [175], 1.9–2.2 [5]	2520	6–8 [5], 10 [130]
sandstone	2.9 [175]	2400	8.6–11.7 [175], 11–12 [5]
limestone	3.2 [175], 2.6–3.3 [5]	2450	5.9–7.4 [175], 6 [5], 8–10 [130]
rhyolite	2.2 [5]	N/A	
barite	2.0 [175]	3040	

TABLE 4.2: Thermal properties of concretes with different aggregates.

For exchange of heat with the environment the convection–radiation coefficient, α_{pr} , is used [79]:

$$\alpha_{pr} = \alpha_p + \alpha_r. \quad (4.43)$$

The coefficient of heat exchange by free convection for concrete, α_p , can be assumed as equal to $\alpha_p = 6.0 \text{ W}/(\text{m}^2 \text{ K})$ [35, 130]. The heat exchange coefficient changes with the variations of the wind velocity [39, 153]. To account for forced convection due to wind action the heat exchange coefficient is defined as a function of wind velocity, v [m/s], according to BRANCO ET AL. [35], ANDREASIK [13] and JONASSON [114], respectively:

$$\alpha_{pv} = 3.7 v, \quad (4.44a)$$

$$\alpha_{pv} = 15.12 v^{0.5}, \quad (4.44b)$$

$$\alpha_{pv} = \begin{cases} 5.6 + 3.95 v & v \leq 5 \text{ m/s} \\ 7.6 v^{0.78} & v > 5 \text{ m/s.} \end{cases} \quad (4.44c)$$

For a covered surface the value of the coefficient can be calculated when the conductivity of the covering material is known. The equivalent heat exchange coefficient, $\alpha_{p,\text{eq}}$, is determined based on the assumption that the layers of the covering material are associated in series [79, 110, 159]:

$$\alpha_{p,\text{eq}} = \frac{1}{\frac{1}{\alpha_p} + \sum_i \frac{d_i}{\lambda}}, \quad (4.45)$$

where:

- α_p – heat exchange coefficient between concrete surface and environment, $\text{W}/(\text{m}^2 \text{ K})$;
- d_i – thickness of i -th layer, m;
- λ_i – conduction coefficient for each i -th layer, $\text{W}/(\text{m K})$.

The coefficient of heat exchange by radiation, α_r , can be calculated for a given ambient temperature, $T_a \geq 5^\circ\text{C}$, and the emissivity of concrete, e [35, 79]:

$$\alpha_r = e [4.8 + 0.075 (T_a - 5)]. \quad (4.46)$$

The coefficient of thermal dilation, α_T , varies strongly with concrete mix constituents (particularly aggregate type), moisture content, temperature and time [23, 49]; the time dependence is especially pronounced in the first hours after casting [118]. It was observed that the thermal expansion coefficient increases with the increasing temperature but decreases with the increasing moisture content. Minimum value of α_T is obtained in a wet state which is beneficial because it also allows to largely eliminate autogeneous shrinkage [205]. Nevertheless, many authors assume constant value of the thermal expansion coefficient over time and with temperature [38, 62, 79, 159, 233, 234]. The final, steady value of the thermal expansion coefficient can be determined with thermal coefficients of its constituents [49]; EMANUEL AND HULSEY [75] proposed a formula to account for the moisture content and temperature alterations:

$$\alpha_T = f_T(f_M f_A k_p \alpha_{T,sp} + k_{fa} \alpha_{T,fa} + k_{ca} \alpha_{T,ca}), \quad (4.47)$$

where:

f_T	–	correction factor for temperature alterations;
f_M	–	correction factor for moisture content;
f_A	–	correction factor for age; for concrete age < 6 months no influence of age was accounted ($f_A = 1.0$);
k_p, k_{fa}, k_{ca}	–	proportion by volume of paste, fine and coarse aggregate, respectively;
$\alpha_{T,sp}, \alpha_{T,fa}, \alpha_{T,ca}$	–	thermal expansion coefficient of saturated cement paste ($= 10.8 \cdot 10^{-6}/^{\circ}\text{C}$), fine aggregate and coarse aggregate, respectively.

4.1.3.2 Coefficients in moisture analysis

Moisture diffusion coefficient, α_{WW} , is also taken as equal in all directions. It depends on the humidity of concrete [24, 97, 115, 124]; many authors proposed functions to describe this dependence. HANCOX [97] introduced a quadratic function to define the diffusion coefficient as a function of the volumetric moisture content:

$$\alpha_{WW}(W) = a_2 W_1^2 + a_1 W_1 + a_0, \quad (4.48)$$

where:

W_1	=	$6W + 0.7$, where W – moisture content by volume, m^3/m^3 ;
a_0, a_1, a_2	–	coefficients.

ANDREASIK [13] proposed to simplify $W_1 = W$ and $a_2 = 2 \cdot 10^{-7}$, $a_1 = 0.2$ and $a_0 = 0$.

AYANO AND WITTMANN [16] proposed an exponential function for the moisture diffusion coefficient expressed as a function of the relative humidity of concrete:

$$\alpha_{WW}(c) = a e^{b(1-c)}, \quad (4.49)$$

where a and b are experimentally determined material coefficients. Similar, though more elaborated formulation was proposed by MENSI ET AL. [169].

In MODEL CODE 2010 [50] the moisture diffusion coefficient was defined as a function of the diffusion coefficient in the saturated concrete and relative humidity. The formula was first proposed by BAŽANT AND NAJJAR [24] and refined by ABBASNIA ET AL. [2]:

$$\alpha_{WW}(c) = \alpha_{WW,1} \left[\bar{\alpha}_{WW,0} + \frac{1 - \bar{\alpha}_{WW,0}}{1 + \left[\frac{1 - c}{1 - c_{0.5}} \right]^n} \right], \quad (4.50)$$

where:

$\alpha_{WW,1}$ – diffusion coefficient in saturated concrete (for $c = 1.0$) which can be estimated acc. to MODEL CODE [50] from the equation:

$$\alpha_{WW,1} = \frac{\alpha_{WW,1,o}}{f_{cm} - 8 \text{ MPa}} = \frac{1 \cdot 10^{-8} \left[\frac{\text{m}^2}{\text{s}} \right]}{f_{cm} - 8 \text{ [MPa]}}, \quad (4.51)$$

and according to ABBASNIA ET AL. [2] as a linear function of the w/c ratio:

$$\alpha_{WW,1} = [1.157 + 9.92 (w/c - 0.45)] \cdot 10^{-10}, \quad (4.52)$$

- $\bar{\alpha}_{WW,0}$ – ratio $\frac{\alpha_{WW,0}}{\alpha_{WW,1}}$; $\bar{\alpha}_{WW,0} = 0.05$ can be assumed [2, 50];
- $\alpha_{WW,0}$ – minimum of $\alpha_{WW}(c)$ at $c = 0.0$;
- $c_{0.5}$ – relative humidity at $\alpha_{WW}(c) = 0.5 \alpha_{WW,1}$; $c_{0.5} = 0.80$ [50] or $c_{0.5} = 0.75$ [2];
- n – exponent; MODEL CODE [50] recommends constant value of $n = 15$, while ABBASNIA ET AL. [2] notes that the value of coefficient depends on the w/c ratio and increases as w/c increases.

Another proposal for the moisture diffusion coefficient was given by XI ET AL. [231]:

$$\alpha_{WW}(c) = \alpha_h + \beta_h \left[1 - 2^{-10\gamma_h(c-1)} \right], \quad (4.53)$$

where:

- α_h – coefficient representing the lower bound of diffusivity approached at low humidity level;
- β_h – diffusivity increment from low humidity level to saturation state;
- γ_h – coefficient characterising the humidity level at which the diffusivity begins to increase.

The values of the above coefficients depend strongly on w/c ratio, which was also observed by ABBASNIA ET AL.

The humidity exchange coefficient, β_p , is proposed to be taken as constant [13, 15, 152, 153]. The value of the coefficient varies strongly between the authors but the experimentally-determined value of $\beta_p = 2.78 \cdot 10^{-8} \text{ m/s}$ is most often referred. KWAK ET AL. [153] proposed a function to

determine the moisture exchange coefficient for a given water-to-cement ratio:

$$\beta_p \left[\frac{\text{m}}{\text{s}} \right] = 6.028 \cdot 10^{-7} w/c - 2.378 \cdot 10^{-7}, \quad (4.54)$$

according to which the value of $\beta_p = 2.78 \cdot 10^{-8}$ m/s is obtained for a w/c ratio of 0.44.

In the presence of the covering material the β_p coefficient can be modified acc. ANDREASIK [13] as:

$$\beta_{p,\text{eq}} = \beta_p \frac{D_{WW,i}}{D_{WW,i} + d_i \beta_{p,i}}, \quad (4.55)$$

where:

- $D_{WW,i}$ – moisture diffusion coefficient of the covering material, m^2/s ;
- d_i – thickness of the covering material layer, m;
- $\beta_{p,i}$ – humidity exchange coefficient of the covering material, m/s.

The value of the coefficient of moisture dilation is not well-determined. When moisture content variation is expressed by volume, the value of α_W differs among the authors from 0.001 to even 0.03 [13, 28, 124]. When moisture content is expressed in a form of relative humidity, the value of α_c is proposed to be equal to $\alpha_c = 10^{-5}$ [28].

4.1.4 Creep and ageing

4.1.4.1 Viscous effects – creep

Creep is expressed in a form of a strain which represents the delayed part of the elastic strain, $\varepsilon_{cc} = \phi \varepsilon_e$, where ϕ is a creep coefficient. In the general form, the time-development of strain due to creep can be expressed as a function of stress, σ , with a creep function, J :

$$\varepsilon_\sigma = \sigma(t_0) \cdot J(t, t_0) + \int_{t_0}^t \frac{\partial \sigma(\tau)}{\partial \tau} \cdot J(t, \tau) d\tau, \quad (4.56)$$

where the creep function defines the following relationship:

$$J(t, t_0) = \frac{1}{E_c(t_0)} + C(t, t_0) = \frac{1}{E_c(t_0)} [1 + \phi(t, t_0)], \quad (4.57)$$

where:

- $E_c(t_0)$ – modulus of elasticity of concrete at the time of loading, t_0 ;
- $\phi(t, t_0)$ – creep coefficient, which is the ratio between the delayed deformation, $\varepsilon_{cc}(t, t_0)$, and the elastic part, ε_e ; no indication is given in literature whether to consider the elastic strain at the moment of loading, t_0 , or at the age of concrete $t = 28$ days [49].

A number of rheological models have been developed to simulate the creep strain of concrete. The main basic models are the Kelvin model and the Maxwell model. The most popular model for early-age concrete which accounts for viscous effects in concrete is viscoelastic model

[17, 27, 33, 38, 46, 60, 71, 93, 198, 233, 234]. In the simplest manner the model is composed of an elastic body and a Kelvin unit [46, 60, 234]. For more precise determination of creep evolution a series of Kelvin units can be used [27]. Examples of Maxwell model application can also be referred [15, 57, 69, 217]. Nevertheless, as it was concluded in *fib* BULLETIN 70 [49], viscoelastic material model does not correspond well to the real behaviour of early-age concrete. Thus, attempts are also made to use more advanced models: viscoelasto–plastic [132], elasto–viscoplastic [170] or viscoelasto–viscoplastic [134, 210] models. Different material models of early-age concrete were compared by KLEMCZAK [136]. It was pointed out that viscous effects are crucial during concrete hardening and should be taken into consideration in the analysis of early-age concrete structures; the viscoelasto–viscoplastic material model was recommended.

A great number of creep functions for concrete are proposed in the literature. The currently used creep functions are formulated as the product of the age at loading and the load duration function. It was agreed that the product approach appropriately represents the creep strain development. This type of creep formulation has been adopted in the BP-model [26], MODEL CODE 1990 [47] and MODEL CODE 2010 [50], EUROCODE 2 [183], ACI REPORT 209 [6], JSCE STANDARD SPECIFICATION FOR CONCRETE STRUCTURES [116] and AASHTO model [1]; it is also commonly used in the literature of the subject both with the maturity and degree of hydration approach [112, 159]. It was shown by e.g. GUÉNOT ET AL. [94] and SONG ET AL. [209] that the MODEL CODE approach is the best for representation of early-age creep. In the application of this model superposition rule can be used, which represents well the behaviour of early-age concrete in loading, but in unloading it is advised not to use the superposition rule [50]. Nevertheless, it has to be noted that this recommendation is crucial in case of rapid unloading of a concrete element, while in case of early-age thermal–shrinkage strains both loading and unloading processes are very slow and smooth.

In MODEL CODE 1990 [47] the creep function is given as follows:

$$J(t, t_0) = \frac{1}{E_c(t_0)} + C(t, t_0) = \frac{1}{E_c(t_0)} + \frac{\phi(t, t_0)}{E_{c,28}}, \quad (4.58)$$

and the creep coefficient is defined with the following function:

$$\phi(t, t_0) = \phi_0(t_0) \beta_c(t, t_0) = \phi(RH) \beta(f_{cm}) \beta(t_0) \beta(t, t_0), \quad (4.59)$$

where:

- $\phi(RH)$ – coefficient dependent on the relative humidity of the surrounding air;
- $\beta(f_{cm})$ – coefficient dependent on the class of concrete;
- $\beta(t_0)$ – function of time for the concrete age at loading;
- $\beta(t, t_0)$ – time-development of creep.

The effect of the age of loading was expressed with the function of time for the concrete age at loading, thus $E_{c,28}$ is used in the formulation of the creep function in Eq. 4.58:

$$\beta(t_0) = \frac{1}{0.1 + t_0^{0.2}}. \quad (4.60)$$

The time-development function of creep, $\beta(t, t_0)$, is defined with the rational function:

$$\beta(t, t_0) = \left[\frac{t - t_0}{\beta_H + (t - t_0)} \right]^{\gamma(t)}, \quad (4.61)$$

where the exponent $\gamma(t)$ is constant, $\gamma = 0.3$. Coefficient β_H describes the kinetics of the creep process and depends on the relative humidity of air, RH , and the notional size of the element, h_0 .

MODEL CODE 2010 [50] distinguishes drying creep and basic creep in the total creep of concrete. The creep coefficient is expressed as a sum of basic creep and drying creep, and is given by the function:

$$\phi(t, t_0) = \phi_{bc}(t, t_0) + \phi_{dc}(t, t_0) = \beta_{bc}(f_{cm}) \beta_{bc}(t, t_0) + \beta(RH) \beta_{dc}(f_{cm}) \beta_{dc}(t_0) \beta_{dc}(t, t_0), \quad (4.62)$$

where:

- $\beta(RH)$ – coefficient dependent on the relative humidity of the surrounding air;
- $\beta_{dc}(f_{cm}), \beta_{bc}(f_{cm})$ – coefficient dependent on the class of concrete for drying and basic creep;
- $\beta_{dc}(t_0), \beta_{bc}(t_0)$ – function of time for the concrete age at loading for basic and drying creep;
- $\beta_{dc}(t, t_0), \beta_{bc}(t, t_0)$ – time-development of drying and basic creep.

It was emphasised in the *fib* BULLETIN 70 [49] that the functions of time for the concrete age at loading, $\beta(t_0)$, and the duration of loading, $\beta(t, t_0)$, should be appropriately adjusted to each other. The time-development of drying creep, $\beta_{dc}(t, t_0)$, was expressed with a function according to Eq. 4.61 but with the exponent defined as a function of the age at loading, $\gamma = \gamma(t_0)$, which corresponds to experimental observations. It was observed in high performance concretes that basic and drying creep phenomena differ and should be described with different ageing and time-development functions. The time-development of basic creep was defined with a logarithmic function:

$$\beta_{bc}(t, t_0) = \ln \left[\left(\frac{30}{t_0} + 0.035 \right)^2 (t - t_0) + 1 \right]. \quad (4.63)$$

Separation of creep into basic creep and drying creep is more precise from a physical point of view and important for analysis of creep in high performance concretes but does not provide any greater accuracy when analysing normal strength concretes [49, 172].

The creep of concrete depends on the degree of hydration and is accelerated under elevated temperature. This effect is proposed to be expressed by modification of the actual age of concrete. MODEL CODE 2010 suggests to relate this effect to the type of cement and modify the age of loading, t_0 , in time-development function to $t_{0,adj}$ according to the following equation:

$$t_{0,adj} = t_{0,e} \left[\frac{9}{2 + t_{0,e}^{1.2}} + 1 \right]^s, \quad (4.64)$$

where:

- $t_{0,e}$ – equivalent age of concrete at loading, days;

s – coefficient dependent on the type of cement, which takes value $s = -1$ for 32.5 N; $s = 0$ for 32.5 R, 42.5 N; and $s = 1$ for 42.5 R, 52.5 N, 52.5 R.

However, it appears that if the value of the s exponent is positive, the value of creep decreases with increasing temperature. Another proposal by MODEL CODE 2010 for temperature effects of creep can be used, according to which the effect of the increased temperature on creep can be expressed by modification of β_H as well as ϕ_{bc} and ϕ_{dc} coefficients. The effect of temperature, T [°C], on the rate of creep development is expressed by replacing β_H with β_{HT} :

$$\beta_{HT} = \beta_H \beta_T, \quad (4.65)$$

with:

$$\beta_T = e^{\left[\frac{1500}{T+273} - 5.12\right]}, \quad (4.66)$$

It can be observed that coefficient β_T is a reducing coefficient – when temperature increases, the value of β_T decreases, and consequently the final value of creep increases. To represent the effect of temperature, T [°C], on the magnitude of creep, ϕ_{bc} and ϕ_{dc} coefficients are advised to be replaced with $\phi_{bc,T}$ and $\phi_{dc,T}$, respectively:

$$\phi_T(t, t_0) = \phi_{bc,T}(t, t_0) + \phi_{dc,T}(t, t_0) = \phi_{bc}(t, t_0) \phi_T + \phi_{dc}(t, t_0) \phi_T^{1.2}, \quad (4.67)$$

with:

$$\phi_T = e^{0.015(T-20)}, \quad (4.68)$$

The value of parameter ϕ increases with the increasing temperature.

To remove this shortcoming, some authors propose to express the effect of temperature on creep by relating the creep directly to the degree of hydration. JIANG ET AL. [112] proposed the formulation of the compliance function similar to the expression in Eq. 4.61 but the function of loading depends on the degree of hydration (or degree of reaction). The compliance function has a form:

$$J(t, t_0) = \mu_0(r_{H,0}) \left[\frac{t - t_0}{\mu_1(r_{H,0}) + (t - t_0)} \right]^{0.35}, \quad (4.69)$$

where:

- $\mu_0(r_{H,0})$ – function of time for the concrete age at loading dependent on the degree of reaction and stress level at the moment of loading;
- $\mu_1(r_{H,0})$ – coefficient dependent on the degree of reaction at the moment of loading.

DE SCHUTTER [63] proposed the formula for creep development explicitly dependent on the degree of hydration. The final creep coefficient is in a linear dependence with the degree of hydration at the moment of loading [60] while the time-development of the creep with the development of the degree of hydration is non-linear and can be expressed with a development function proposed by DE SCHUTTER AND TAERWE according to Eq. 4.83 with the exponent dependent on the degree of hydration at the moment of loading [68]:

$$\phi(\alpha_H, \alpha_{H,0}) = c_1(\alpha_{H,0}) \left(\frac{\alpha_H - \alpha_{H,0}}{1 - \alpha_{H,0}} \right)^{c_2(\alpha_{H,0})}, \quad (4.70)$$

where:

- α_H – degree of hydration at the moment of analysis (at time t);
- $\alpha_{H,0}$ – degree of hydration at the moment of loading (at time t_0);
- $c_1(\alpha_{H,0}), c_2(\alpha_{H,0})$ – parameters dependent on the cement type.

Some authors postulate that the creep behaviour of concrete differs in compression and in tension. Total creep capacity is smaller for tensile creep and tensile creep has a more pronounced effect of loading age [158]. As concrete exhibits higher creep in tension [14, 100], the early-age tensile stresses determined under the assumption of symmetrical creep may be overestimated. Tensile creep can be modelled with the models available for compressive creep [10, 14, 158] but the parameters of the models, including the modulus of elasticity (see Sec. 4.1.4.2), must be adjusted to account for different rate and magnitude of tensile creep. Nevertheless, the postulates of asymmetrical creep of concrete are questionable. This is due to the fact that tests on concrete in tension are performed for much lower strains than in compression and the effects of temperature and moisture variations are more pronounced and as such may perturb the results.

4.1.4.2 Ageing

To account for the effect of ageing and the influence of temperature on ageing in early-age concrete the material properties of concrete are expressed as time-dependent and temperature-dependent functions. Time-development of material properties is defined by the function that expresses gain in time with respect to the reference value of a given property. One of the formulations of the time-development functions is with the exponential function which was introduced by REINHARDT ET AL. [189]. The exponential time-development is provided for both compressive and tensile strength and modulus of elasticity by the European standards [47, 50, 183] and used by numerous authors in Europe [57, 69, 115, 122, 123, 155]. MODEL CODES [47, 50] and EUROCODE 2 [183] propose the following function to describe the time-development of the mechanical properties:

$$\beta_c(t) = e^{s \left[1 - \sqrt{\frac{28}{t}} \right]}, \quad (4.71)$$

where s is a coefficient dependent on the type of cement. The time-development is related to the final value which is set at 28 days age. Development of the compressive strength, $f_c(t)$, is defined as follows [50, 183]:

$$f_c(t) = \beta_c(t) f_{c,28}, \quad (4.72)$$

and tensile strength, $f_t(t)$, as follows [183]:

$$f_t(t) = [\beta_c(t)]^n f_{t,28}, \quad (4.73)$$

where for early-age concrete ($t < 28$ days) the tensile strength development is suggested to be of the same rate as the compressive strength development ($n = 1$), although KANSTAD ET AL. [122, 123] – among the others – suggest that $n < 1$ (depending on concrete composition the value of exponent ranges between 0.50 to 0.67).

Alternatively, a rational function is used which was introduced by KEE [125]. The ACI REPORT 209 [6] and JSCE GIUDELINE FOR CONCRETE [116] suggest the following function:

$$\beta_c(t) = \frac{t}{a + bt}, \quad (4.74)$$

where a , b and c are experimental coefficients dependent on the type of cement. To account for the fact that concrete starts to gain strength after it reaches a threshold age, t_s , corresponding to initiation of hardening, the time component in the Eq. 4.74 is replaced by the $\langle t - t_s \rangle_+$ component. Development of the compressive strength, $f_c(t)$, is defined as:

$$f_c(t) = \beta_c(t) f_{c,28}, \quad (4.75)$$

and the tensile strength, $f_t(t)$, by ACI REPORT 209 [6] and JSCE [116], respectively:

$$f_t(t) = 0.0069 \sqrt{\rho f_c(t)} = 0.0069 \sqrt{\beta_c(t)} \sqrt{\rho f_{c,28}}, \quad (4.76)$$

$$f_t(t) = c \sqrt{10 f_c(t)} = c \sqrt{\beta_c(t)} \sqrt{10 f_{c,28}}, \quad (4.77)$$

where ρ is a unit weight of concrete and c is a coefficient dependent on cement. Faster development of tensile strength than compressive strength is emphasised. Definition of time-development of the strength with a rational function has also been used by other authors [232, 233].

Development of the modulus of elasticity is more rapid than development of the compressive strength. There is a relationship between the compressive strength and the modulus of elasticity of concrete which can be expressed with a power function; most often a square-root function is suggested [61]:

$$E_c(t) = k \sqrt{f_c(t)}, \quad (4.78)$$

where k is a material constant. Thus, the time-development of the modulus of elasticity, E_c , was expressed in MODEL CODE 2010 [50] with square root of time-development function according to Eq. 4.71 as:

$$E_c(t) = \sqrt{\beta_c(t)} E_{c,28}, \quad (4.79)$$

and by JSCE STANDARD [116] and ACI REPORT 209 [6] explicitly with square root of the compressive strength function (with square root time-development function according to Eq. 4.74):

$$E_c(t) = 4.7 \cdot 10^3 \cdot \sqrt{f_c(t)} = 4.7 \cdot 10^3 \cdot \sqrt{\beta_c(t)} \sqrt{f_{c,28}}, \quad (4.80)$$

$$E_c(t) = 0.043 \sqrt{\rho f_c(t)} = 0.043 \sqrt{\beta_c(t)} \sqrt{\rho f_{c,28}}. \quad (4.81)$$

EUROCODE 2 [183] proposes the same time-development function for the modulus of elasticity as MODEL CODE 2010 but points out to faster development of the modulus of elasticity:

$$E_c(t) = [\beta_c(t)]^{0.3} E_{c,28}, \quad (4.82)$$

which complies with observations of e.g. KANSTAD ET AL. [122, 123] who show that the value of the exponent of the time-development function for the modulus of elasticity, depending on the concrete mix composition, ranges between 0.30 and 0.43.

Time-development of the modulus of elasticity is often expressed with an exponential function [14, 57, 189, 232] but the rational formulation is also popular [27]. Both approaches prove to give results for development of the strength and stiffness compliant with experimental data but material parameters which are dependent on the type of cement – especially the n exponent – should be adjusted based on the experimental data provided [49, 137, 208].

Some authors emphasise that the modulus of elasticity differs in compression and tension. It is generally stated that the tensile modulus of elasticity is higher than the compressive modulus of elasticity [14, 40]. Thus, it is proposed to relate compressive modulus of elasticity with compressive strength but tensile modulus of elasticity with tensile strength of concrete.

To account for the influence of temperature, the equivalent age is applied instead of time in time-development function. This approach was applied in standards, e.g. MODEL CODE 2010 [50] or EUROCODE 2 [183], and is popular in the literature of the subject [57, 69, 218]. However, some authors believe that it is more fundamental to relate development of the mechanical properties of early-age concrete to the degree of hydration [27, 38, 66, 78, 79, 93, 234]. In that approach development of material properties is related to the final value when the hydration process ends ($\alpha_H = 1$), $f_c, f_{ct}, E_c|_{\alpha_H=1}$. The time-development is expressed with the function of hydration rate, $\bar{\alpha}$, proposed by DE SCHUTTER AND TAERWE [66] after CARINO [45]:

$$\beta_c(t) = \frac{\langle \alpha_H(t) - \alpha_0 \rangle_+}{1 - \alpha_0}, \quad (4.83)$$

where α_0 is a coefficient dependent on the concrete composition, mainly w/c ratio, representing a threshold value of the hydration degree at which hardening begins.

Material properties development was also expressed with the degree of hydration by CERVERA ET AL. [51] who introduced the ageing degree, κ_H , as a function of time-development:

$$\beta_c = \kappa_H, \quad (4.84)$$

such that:

$$\dot{\kappa}_H = g(T) f(\alpha_H) \dot{\alpha}_H, \quad (4.85)$$

where:

- $g(T)$ – function of temperature,
- $f(\alpha_H)$ – function of the degree of hydration development; linear relationship is assumed, i.e. $f(\alpha_H) = A \langle \alpha_H(t) - \alpha_0 \rangle_+ + B$.

Tensile strength develops faster than the compressive strength but not as fast as the modulus of elasticity. This is represented by introduction of the n exponent to the development rate function, β_c , given by Eq. 4.83 and Eq. 4.84 ($n_{f_c} = 1.0 > n_{f_t} > n_E$).

It is problematic to determine material properties of concrete at complete hydration ($\alpha_H = 1$). Thus, it was proposed to replace 1 in Eq. 4.83 with $\alpha_{H,28}$ and use mechanical properties determined at 28 days, $f_{c,28}, f_{ct,28}$ and $E_{c,28}$ [92]. The time-development of the mechanical properties is then defined as:

$$P(t) = [\beta_c]^n P_{28}, \quad (4.86)$$

where:

- β_c – given by Eq. 4.83 or Eq. 4.84;
- $P_{28}, P(t)$ – value at 28 days and at time t of a given mechanical property;
- n – exponent dependent on the property to describe and concrete composition.

4.1.5 Damage analysis

Damage of concrete is connected with formation of discrete cracks. The study of damage in which damage is modelled in a discrete manner is the interest of fracture mechanics. The discrete models account for discontinuity of the material across the crack. Discrete crack models perform well in representation of structural behaviour governed by a few dominant cracks with large crack widths and which location and direction of propagation can be known *a priori*, and as such are suitable for modelling of laboratory tests [103]. Several discrete models for numerical simulation of massive structures at early age are available (see [178]).

More often damage of concrete due to crack formation is represented with smeared models of cracking. Smeared crack models are good for representation of typical, properly designed reinforced concrete structures characterised by many cracks of small widths [103]. They can be implemented in the solutions of spatial problems and are commonly used in damage intensity analysis of early-age concrete structures [19, 27, 58, 99, 106]. The cracked material is treated as continuum and its cracked parts are assigned with modified properties. Usually it is assumed that the cracked element can no longer transfer the load in the direction perpendicular to the crack plane (tensile stresses) but can still transfer the parallel (shear) stresses [103].

The failure of concrete is connected with formation of a crack under certain level of stress. The level of the compressive stresses induced by the early-age effects is relatively small in the discussed structures, thus many authors apply damage criteria based on the elastic–damage models (or more advanced elasto–plastic–damage models) which account for material degradation in tension. For that purpose stress–strain relationship with strain softening in tension is used (such relationships were proposed e.g. by BAŽANT AND OH [25] or GUTSCH AND ROSTÁSY [92]). These models involve tensile strength of concrete, f_t , and fracture energy, G_f . When modelling softening of concrete as damage progresses it must be remembered that the results of numerical analysis are strongly mesh-dependent [19, 27, 111]. It is advised to discretise the analysed structure based on the density of the fracture energy, g_f , and characteristic length, l_c , [102]. An elastic–damage model was proposed e.g. by MAZARS AND BOURNAZEL [165] and modified by BENBOUDJEMA AND TORRENTI [27]. The damage criterion which defines the formation of cracking is defined as:

$$f = \hat{\varepsilon} - \varepsilon_{ctu}(\alpha_H), \quad (4.87)$$

where:

- $\hat{\varepsilon}$ – equivalent tensile strain $\hat{\varepsilon} = \sqrt{\varepsilon_x^2 + \varepsilon_y^2 + \varepsilon_z^2}$;
- $\varepsilon_{ctu}(\alpha_H)$ – tensile strain capacity defined as a ratio between the tensile strength, $f_t(\alpha_H)$, and the modulus of elasticity, $E(\alpha_H)$, at the time of analysis, t , expressed as a function of degree of hydration, $\alpha_H(t)$.

After the threshold strain is exceeded ($\hat{\varepsilon} \leq \varepsilon_{ctu}(\alpha_H)$), cracking appears. It is assumed that part of the element is sound, and part of the element is cracked; only the sound part of the element can transfer the stress, which is the effective stress, $\hat{\sigma}$:

$$\hat{\sigma} = E_c \hat{\varepsilon}. \quad (4.88)$$

The influence of progressing cracking on stress, σ , is expressed with the damage, D , and effective stress, $\hat{\sigma}$:

$$\sigma = (1 - D) \hat{\sigma}. \quad (4.89)$$

The damage, D , describing the softening behaviour of concrete in tension is given by the formula:

$$D = 1 - \frac{\varepsilon_{ctu}}{\hat{\varepsilon}} \left[(1 + A_t) e^{-B_t \hat{\varepsilon}} - A_t e^{-2B_t \hat{\varepsilon}} \right], \quad (4.90)$$

where A_t and B_t are material parameters defining softening branch of σ - ε diagram.

A simple, strength-based criterion was used by e.g. HATTEL AND THORBORG [99], XIANG ET AL. [232], JCI GUIDELINE FOR CONCRETE [110] and LIU ET AL. [159]. According to this criterion, which introduces the cracking index, I_{cr} , the crack is formed when the maximum principal tensile stress, $\sigma_{t,\max}$, reaches tensile strength of concrete, f_t :

$$I_{cr} = \frac{\sigma_{t,\max}(t)}{f_t(t)} = 1. \quad (4.91)$$

Nevertheless, failure of concrete element is a complex phenomenon which should be analysed in a complex, three-axial stress state allowing to determine the character of the occurring crack [133]. The failure is referred to the failure surface, which is a spatial representation of possible states of stresses for a material. The strengths of the material in certain specific stress states, such as uniaxial compression or tension, or biaxial compression, are the points on the surface. The surface is described with three major meridians: tensile meridian, compressive meridian and shear meridian. The failure mode depends on whether the stress state is on the tensile meridian or the compressive meridian. The failure in the tensile meridian is more brittle than on the compressive meridian: the tensile failure is connected with fracture of concrete in a form of a splitting crack; the compressive failure is caused by crushing of concrete and formation of a slip crack [162]. The state of stress may reach the failure surface in any location, not necessarily on the meridian. The resultant failure mode is then complex [49]. Thus, the damage intensity factor, s_l , similar to the simple cracking index, was introduced by MAJEWSKI [162] and applied by KLEMCZAK [133] to represent the damage of concrete element. Damage intensity factor relates the actual stress level, τ_{oct} , with respect to the stress at failure surface, τ_{oct}^f :

$$s_l = \frac{\tau_{\text{oct}}}{\tau_{\text{oct}}^f}. \quad (4.92)$$

The value of the damage intensity factor equal to unity signifies reaching of failure surface and damage, which character depends on the location where the failure surface was reached. In the classical theory of plasticity behaviour of the material after reaching of failure surface is governed by the material constitutive model. The modelling of damage of concrete due to formation of

cracking in tension is realised by definition of a softening law. According to the softening law the effect of stiffness degradation is modelled by introduction of the softening parameter, κ , to represent the development (shrinkage) of the yield surface when cracks appear.

When defining the failure surface for concrete it was observed in the experimental tests [53, 162] that the shape of deviatoric section is close to triangular in the zone of tensile and low-compressive stresses, and similar to circular in the zone of high-compressive stresses. The deviatoric section is smooth and convex but it is not a circle and the surface is not a solid of revolution. The meridians are smooth, convex and curvilinear but for practical ranges can be approximated with straight lines. There have been multiple proposals for the failure surface to represent the behaviour of concrete under the complex stress state. The single- and double-parameter failure criteria used for description of the failure surface for concrete, such as the Rankine, Mohr–Coulomb and Drucker–Prager failure criteria are commonly applied for description of the failure surface of concrete [111, 154], however, each of them fails to represent some major characteristic of the concrete behaviour. Thus, more advanced approaches are used, e.g. three- or five-parameter Willam–Warnke criterion or four-parameter Ottosen criterion. The criteria are expressed either with stress invariants (I_1 , J_2 and θ) or by means of the mean and octahedral stress (σ_m , τ_{oct} and θ).

According to the three-parameter WILLAM–WARNKE criterion [226] (with the parameters being the mean stress, σ_m , octahedral stress, τ_{oct} , and Lode angle, θ) the failure surface is defined with the following equation:

$$\frac{m_{cc} - m_t}{m_{cc} m_t} r_\theta \sigma_m + \tau_{\text{oct}} \sqrt{0.6} - r_\theta f_c = 0, \quad (4.93)$$

with:

$$m_t = \frac{f_t}{f_c}, \quad (4.94a)$$

$$m_{cc} = \frac{f_{cc}}{f_c}, \quad (4.94b)$$

$$r_\theta = \frac{2r_c (r_c^2 - r_t^2) \cos\theta + r_c (2r_t - r_c) \sqrt{4(r_c^2 - r_t^2) \cos^2\theta + 5r_t^2 - 4r_c r_t}}{4(r_c^2 - r_t^2) \cos^2\theta + (r_c - 2r_t)^2} \quad (4.94c)$$

where:

f_c, f_t – uniaxial compressive and tensile strength, MPa;

f_{cc} – bi-axial compressive strength, MPa;

r_c, r_t – compressive and tensile radius of deviatoric section; the ratio between the radii is constant and equal to $\frac{r_t}{r_c} = \frac{3m_{cc}m_t + m_{cc} - m_t}{2m_{cc} + m_t}$.

The three-parameter Willam–Warnke criterion provides good representation of concrete behaviour within the range of mean stresses $-\frac{4}{3}f_c \leq \sigma_m \leq \frac{1}{3}f_t$. However, because of the assumption of linearity of meridians the strength within bi- and three-axial tensile stresses and three-axial compression is overestimated [162]. This shortcoming is removed in Ottosen failure criterion and five-parameter Willam–Warnke criterion where curvilinear meridians are defined. According to the five-parameter Willam–Warnke criterion deviatoric section is still defined with a triple

elliptical shape but the ratio of the meridians radii, r_t/r_c , is not constant but depends on the level of mean stresses, σ_m . Meridians are defined with curved lines (second-order parabolas) which requires introduction of two additional parameters. Both presented failure surfaces are “open” in the direction of compressive stresses on the mean stresses axis. To remove the shortcomings of the presented criteria and limit the complexity of the model, MAJEWSKI proposed a modified 3-parameter Willam–Warnke failure criterion [162, 163]. In his approach meridians are straight lines but instead of defining meridians in such a way that meridian crosses the points representing the values of appropriate strengths of concrete, the best straight-line approximation was derived. Moreover, to limit the stresses in high-compressive stresses range, a closing cap was defined (tension cut-off). Under the same assumptions the modified Willam–Warnke criterion was adapted by KLEMCZAK [133] for early-age concrete.

4.2 Subsoil

In the literature there are few analyses of early-age concrete structures on subsoil considering both thermo–physical and mechanical cooperation. They are limited to heat exchange between the subsoil and the concrete element and simple stress analysis. Thermal–moisture transport in soil is, indeed, analysed as a separate issue but different approaches are used then in the analysis of concrete. In these analyses it is the ambient environment which is a driving force for heat and moisture diffusion and most often multi-phase models are used in which the constitutive equations are formulated for solid soil particles, pore water and water vapour in pores separately [34, 181]. However, since detailed soil data are usually unavailable, especially at the design phase, simplified phenomenological models are also being proposed [166]. There are also numerous analyses of structure–subsoil interaction where stress and damage analysis is performed, but in which the external load is a cause of the induced stresses (imposed loads in buildings, uneven settlement, etc.). Therefore, definition of the material model for soil, both thermo–physical and mechanical, consistent with the model for early-age concrete is required for the analysis of this multi-material wall-on-subsoil system.

4.2.1 Heat and moisture transport

When heat and mass transfer is analysed in soil as a separate medium, the soil is treated as a half-space where the surface is a contact between the soil block and the ambient environment. Heat and mass transport are driven by a difference in temperature and moisture concentration at that interface. Thus, the gradients are formed only at the depth and the analysis is performed for one-dimensional flux. The heat equation for one-dimensional case has a form:

$$\dot{T} = \frac{\partial}{\partial z} \left(\alpha_{TT} \frac{\partial T}{\partial z} \right), \quad (4.95)$$

where:

- T – temperature, K;
- α_{TT} – thermal diffusion coefficient, m^2/s , given by Eq. 4.39.

For structure–subsoil interaction problem a three-dimensional gradients are due to form so the problem must be analysed in space. For simplicity the thermal diffusion coefficient can be assumed as equal in all directions and the Eq. 4.95 can be expressed as:

$$\dot{T} = \text{div}(\alpha_{TT} \text{grad}T). \quad (4.96)$$

The heat transport in soil is driven not only by heat conduction in soil particles but also liquid water flux and water vapour flux [181]. In phenomenological models this influence can be accounted implicitly. To account for effect of the water vapour in pores the thermal conductivity of soil, λ , is modified [101]:

$$\bar{\lambda} = \lambda + D_v L_v, \quad (4.97)$$

where:

- $\bar{\lambda}$ – instantaneous thermal conductivity, W/(m K);
- D_v – thermal vapour diffusivity, m²/(K s);
- L_v – latent heat of vaporisation, J/m³.

The instantaneous thermal conductivity is determined based on the soil constituents; the weighted average was proposed by DE VRIES [70]:

$$\lambda = \frac{\sum_i w_i k_i \lambda_i}{\sum_i w_i k_i}, \quad (4.98)$$

where:

- k_i – volume fraction of i^{th} soil constituent (minerals, water, organic matter, air);
- λ_i – thermal conductivity of i^{th} constituent per unit mass, W/(m K);
- w_i – weight for the i^{th} soil constituent.

The weights of the subsequent soil components are given by the equation:

$$w_i = \frac{1}{1 + \frac{1}{3} \left(\frac{\lambda_i}{\lambda_c} - 1 \right)}, \quad (4.99)$$

where λ_c is thermal conductivity of the continuous phase which can be formed by air and ice [43]. In case of the soil which is not frozen $\lambda_i = \lambda_{\text{air}}$.

Thermal conductivity of unsaturated soil depends strongly on its moisture content. To account for that fact JOHANSEN [113] proposed to determine thermal conductivity of unsaturated soil as a combination of dry, λ_{dry} , and saturated, λ_{sat} , thermal conductivity weighted by a normalised thermal conductivity called the Kersten number, K_e :

$$\lambda(W) = K_e (\lambda_{\text{sat}} - \lambda_{\text{dry}}) + \lambda_{\text{dry}}. \quad (4.100)$$

Kersten number was defined as a function of the degree of saturation by KERSTEN [126].

The presented methods of calculation of thermal properties of soil require knowledge of multiple thermo-physical parameters of soil while such an accuracy is not needed in the discussed problem. Thus, a simplified approach proposed by ENDRIZZI ET AL. [76] which takes into consideration only thermal conductivities of the soil constituents is sufficient:

$$\lambda = \left(\sum_i k_i \lambda_i \right)^2. \quad (4.101)$$

The heat capacity is determined as a sum of heat capacities of the soil components [80, 101]:

$$c_v = \sum_i k_i c_{b,i} \rho_i, \quad (4.102)$$

where:

- k_i – volume fraction of i^{th} soil constituent (minerals, water, organic matter, air);
- $c_{b,i}$ – specific heat of i^{th} constituent per unit mass, kJ/(kg K);
- ρ_i – density of i^{th} constituent, kg/m³.

To account for the influence of the moisture content on the heat capacity the following formula was proposed [80]:

$$c_v(W) = \frac{\rho_{s,\text{dry}}}{\rho_w} \left(0.18 + 0.5 \frac{W}{100} \right) c_{v,w}, \quad (4.103)$$

where:

- $\rho_{s,\text{dry}}$ – dry unit weight of soil, kg/m³;
- ρ_w – unit weight of water, kg/m³;
- W – water content, m³/m³;
- $c_{v,w}$ – heat capacity per unit volume of water.

Thermal properties of soil constituents are enlisted in Tab. 4.3.

	ρ_i [kg/m ³]	$c_{b,i}$ [kJ/(kg K)]	λ_i , [W/(m K)]
air	1.2	1.005	0.026
quartz	2650	0.73	8.4
organic matter	1300	1.93	0.25
minerals	2650	0.73	2.9
water	1000	4.18	0.60

TABLE 4.3: Thermal properties of soil components [80].

For initial conditions the initial temperature should be assigned. The temperature is not uniform but a temperature gradient is formed at the depth induced by the changes of temperature at the surface. Changing ambient temperature has an effect on the soil temperature to some depth, called damping depth, below which the temperature stabilises. The damping depth can be

determined from the following formula [101]:

$$d_{\text{damp}} = \sqrt{\frac{P\alpha_{TT}}{\pi}}, \quad (4.104)$$

where P is a period of the surface temperature oscillation. For diurnal changes this period can be taken as 24 hours and for annual changes as 365 days.

Liquid water transport is most often expressed with the Richard's equation [34, 179, 221], which is a generalisations of Darcy's law for unsaturated soils. It is analogical to the Fick's equation but the moisture content is represented as moisture content by volume, W [m^3/m^3], instead of the relative humidity, c [kg/kg]. Partial coupling is taken into consideration; in the simplest form and for one-dimensional flux the equation can be expressed as [179, 181]:

$$\dot{W} = \frac{\partial}{\partial z} \left(D_{WW} \frac{\partial W}{\partial z} + D_{WT} \frac{\partial T}{\partial z} \right), \quad (4.105)$$

where:

- W – volumetric water content, m^3/m^3 ;
- T – temperature, K;
- D_{WW} – moisture diffusion coefficient (isothermal liquid diffusivity), m^2/s ;
- D_{WT} – moisture diffusion coefficient induced by temperature (thermal liquid diffusivity), $\text{m}^2/(\text{s K})$.

The isothermal and thermal liquid diffusivity are given by the relationships as follows:

$$D_{WW} = K_h \frac{\partial \psi}{\partial W}, \quad (4.106a)$$

$$D_{WT} = K_h \gamma_T \psi, \quad (4.106b)$$

where:

- K_h – hydraulic conductivity, m/s ;
- ψ – matric potential, m ;
- γ_T – relative change of surface tension with respect to temperature; constant value of $\gamma_T = 2.09 \cdot 10^{-3}/^\circ\text{C}$ given by PHILIP AND DE VRIES [182] can be assumed.

Both hydraulic conductivity and matric potential are functions of the moisture content. The functions defining these parameters relate their values in saturated state and the actual moisture content of the soil [41, 55, 216]. BROOKS AND COREY [41] and VAN GENUCHTEN [216] proposed the functions of the effective saturation, S_e , for hydraulic conductivity, K , and matric potential, ψ . The effective saturation is given by the formula:

$$S_e = \frac{W - W_r}{n - W_r}, \quad (4.107)$$

where:

- W – actual volumetric moisture content in soil, m^3/m^3 ;
- W_r – residual moisture content (irreducible moisture content), m^3/m^3 ;
- n – porosity, m^3/m^3 .

The hydraulic conductivity and metric potential as a function of the moisture content was given by BROOKS AND COREY [41]:

$$K_h(S_e) = K_{h,\text{sat}} S_e^c, \quad (4.108a)$$

$$\psi(S_e) = \psi_a S_e^{-b}. \quad (4.108b)$$

and by VAN GENUCHTEN [216]:

$$K_h(S_e) = K_{h,\text{sat}} S_e^{1/2} \left[1 - \left(1 - S_e^{1/m} \right)^m \right]^2, \quad (4.109a)$$

$$\psi(S_e) = \frac{1}{\alpha} \left(S_e^{-1/m} - 1 \right)^{1-m}. \quad (4.109b)$$

CLAPP AND HORNBERGER [55] proposed simplification of the BROOKS AND COREY formulation and defined the functions for the hydraulic conductivity and metric potential dependent on the degree of saturation, $S = W/n$:

$$K_h = K_{h,\text{sat}} S^c, \quad (4.110a)$$

$$\psi = \psi_a S^{-b}. \quad (4.110b)$$

In the presented equations:

- $K_{h,\text{sat}}$ – saturated hydraulic conductivity, m/s ;
- ψ_a – air-entry tension, m ;
- b, c, α, m – fitting parameters; $c = 2b + 3$ acc. to BURDINE [42] but was more recently proposed by MUALEM [173] to be $c = 2b + 2.5$.

The coefficients required for determination of the hydraulic conductivity and matric potential according to CLAPP AND HORNBERGER are presented in Tab. 4.4.

The liquid diffusivities with parameters defined by CLAPP AND HORNBERGER and with c exponent taken after MUALEM can be calculated as [166]:

$$D_{WW} = \frac{b K_{h,\text{sat}} \psi_a}{W} \left(\frac{W}{n} \right)^{b+2.5}, \quad (4.111a)$$

$$D_{WT} = K_{h,\text{sat}} \psi_a \gamma_T \left(\frac{W}{n} \right)^{b+2.5}. \quad (4.111b)$$

soil type	porosity n	$K_{h,\text{sat}}$ [m/s]	ψ_a [m]	b
sand	0.395	$1.76 \cdot 10^{-4}$	0.121	4.05
loamy sand	0.410	$1.56 \cdot 10^{-4}$	0.090	4.38
sandy loam	0.435	$3.47 \cdot 10^{-5}$	0.218	4.90
silty loam	0.485	$7.19 \cdot 10^{-6}$	0.786	5.30
loam	0.451	$6.94 \cdot 10^{-6}$	0.478	5.39
sandy clay loam	0.420	$6.31 \cdot 10^{-6}$	0.299	7.12
silty clay loam	0.477	$1.70 \cdot 10^{-6}$	0.356	7.75
clay loam	0.476	$2.45 \cdot 10^{-6}$	0.630	8.52
sandy clay	0.426	$2.17 \cdot 10^{-6}$	0.153	10.4
silty clay	0.492	$1.03 \cdot 10^{-6}$	0.490	10.4
clay	0.482	$1.28 \cdot 10^{-6}$	0.405	11.4

TABLE 4.4: Parameters for liquid diffusivity of soils acc. to CLAPP AND HORNBERGER [55].

To perform spatial analysis of the moisture flow in soil it is convenient to assume that the diffusivities of soil are equal in all directions. The spatial moisture flux would be then expressed with the following equation:

$$\dot{W} = \text{div} (D_{WW} \text{grad}W + D_{WT} \text{grad}T). \quad (4.112)$$

It was concluded by KHALILI ET AL. [127] that the overall thermal dilation coefficient of a porous medium in saturated state is equal to the thermal dilation coefficient of the solid constituent and that the size of the pores and porosity have no influence on its value. It is practical to assume that the soil is in saturated state; under such an assumption thermal dilation coefficient can be easily defined for each soil type. The dilation coefficient for soils ranges between $8 \cdot 10^{-6}$ and $10 \cdot 10^{-6}/^\circ\text{C}$ but it is allowed to take in general $\alpha_T = 10 \cdot 10^{-6}/^\circ\text{C}$ [110]. There are no proposals for moisture dilation coefficient, α_W , of soil.

4.2.2 Material model and failure criterion

The most popular material model for soil is the elasto–plastic model. The formulation of the material model for contact problems is usually phenomenological in which soil is treated as continuum [161]. It is also necessary to define a failure criterion. In contact problems when cooperation between the structure and the subsoil is analysed it is convenient to apply a similar approach for both modelling the structural and soil material. Thus, as for the early-age concrete it was chosen to define a spatial boundary surface, the same approach is presented for the soil. The most popular failure criterion for subsoil is the Drucker–Prager failure criterion. The yield surface can be defined with a general formula:

$$f = f_1(\sigma_m, \kappa) + f_2(\bar{\sigma}), \quad (4.113)$$

where:

- κ – hardening/softening parameter;
- σ_m – mean stress, MPa;
- $\bar{\sigma}$ – stress intensity, which is a function of the second deviatoric stress invariant.

Development of the yield surface is defined by the isotropic softening law given by a softening function, $Y(\kappa)$. In the currently developed models based on the Drucker–Prager criterion additional closing caps are introduced. A proposal of a cap model for soil in the soil–concrete interaction problems was presented in detail by MAJEWSKI [161].

In the contact problems it is also crucial to properly represent the behaviour of the system at the contact. One of the popular approaches is to introduce contact elements [161]. The contact surface between the concrete structure and the subsoil is a location of extreme shear stresses which may lead to the slip in the contact plane. Moreover, on the joint plane there should be a possibility of loss of contact between the structure and the soil without transmission of normal tensile stresses. Such a behaviour is realised by modification of some of the characteristics of material model for soil in the contact elements: the material should have no tensile strength and limited possibility to transfer shear stresses.

4.3 Reinforcement

4.3.1 Modelling of reinforcement

There are three main approaches to modelling of reinforcement [103, 162]:

1. distributed (smeared) model in which a substitute material model is introduced composed of concrete and reinforcement, and located in the direction of reinforcement. Such a material has strong anisotropic properties which complicates formulation of failure criteria and constitutive equations. Perfect bonding is assumed in this model.
2. discrete model in which reinforcement is represented with its real location and material properties. Reinforcement is modelled with linear bar elements hinge-connected with the nodes of the concrete elements. The bars are joint with the concrete mesh so deformation of the bars is actually deformation of the block elements adjacent to the bars.
3. embedded model in which reinforcement is superimposed on the concrete elements and bars pass through concrete elements in an arbitrary manner. Perfect bonding is assumed.

Cooperation between steel and concrete can be taken into account by modelling of the bond–slip behaviour and the tension-stiffening effect. In a discrete model this can be realised implicitly by modification of the constitutive relations of steel or concrete, or in detail by introduction of the interface layer between concrete and steel. In the embedded model a perfect bond between steel and concrete is formed so only implicit formulation is possible. Usually the cooperation between steel and concrete is realised by modification of the concrete model [19, 152]. The influence of the tension-stiffening effect can be accounted with the use of the MODEL CODE 2010 method [50] by correction of the stress–strain relationship in tension as proposed by FENESTRA AND DE BORST [81]. However, MAJEWSKI [162] concluded that modelling of reinforcement with the use of simplified discrete models not accounting for slip of reinforcement or tension-stiffening effect in reinforced concrete is sufficient when smeared image of cracking is applied in the model.

4.3.2 Heat transport

The effect of reinforcement in early-age walls is usually limited to the mechanical analysis where it is responsible for the increase of the degree of restraint. In thermal–shrinkage analysis thermal strain of reinforcement was accounted by KLEMCZAK [134] and KLEMCZAK AND KNOPPIK-WRÓBEL [141]. The thermal strain of reinforcement was determined from the temperature difference according to Eq. 3.2. The temperature difference, ΔT , was taken as the averaged temperature difference between the prismatic concrete elements neighbouring the reinforcing bar element. The thermal expansion coefficient was taken as equal to $\alpha_T = 10^{-5}/^{\circ}\text{C}$ [110].

4.3.3 Material model and failure criterion

Reinforcing steel is modelled as either elasto–perfectly plastic [19] or elasto–plastic with isotropic hardening [161], expressed with the hardening function, $Y(\kappa)$. The failure surface is usually defined with the Huber–von Mises–Hencky failure criterion given by the equation:

$$f = \sqrt{3} \bar{\sigma} - Y(\kappa). \quad (4.114)$$

A detailed material model and definition of the failure surface for reinforcing steel was presented by MAJEWSKI [161].

4.4 Summary

Previous chapters presented in detail the phenomena occurring in early-age concrete structures with possible approaches to model these phenomena. Not only is the number of the phenomena great but also they are interrelated. Moreover, there is no single optimum path but several parallel paths that can be chosen when modelling the behaviour of early-age concrete structures. Fig. 4.2 and Fig. 4.3 present schematically a summary of the possible paths for modelling of early-age reinforced concrete walls.

Each path has its advantages and drawbacks so the choice of the optimum path should be made individually for each task. The choice should be based on the desired accuracy of the phenomena description, importance of the individual phenomena, allowable computational complexity and calculation time as well as expected accuracy of the results. Depending on the desired computational complexity either analytic or numerical approach can be chosen. Analytic approaches allow for manual or semi-manual calculations but at the cost of great simplification of the model. Usually thermal and shrinkage strains are determined at one point in time (extreme values) and assumed as uniform throughout the volume of the analysed element. More precise analysis of the temperature and shrinkage development and distribution requires at least minimum computer aid (e.g. the use of a spreadsheet). Based on such determined strains the stress at the total restraint is calculated with the use of the simplified viscoelastic material model and the total stress is calculated with the use of the restraint factor calculated with simple formulas or taken from the experimentally-determined diagrams. Such an approach allows for very quick

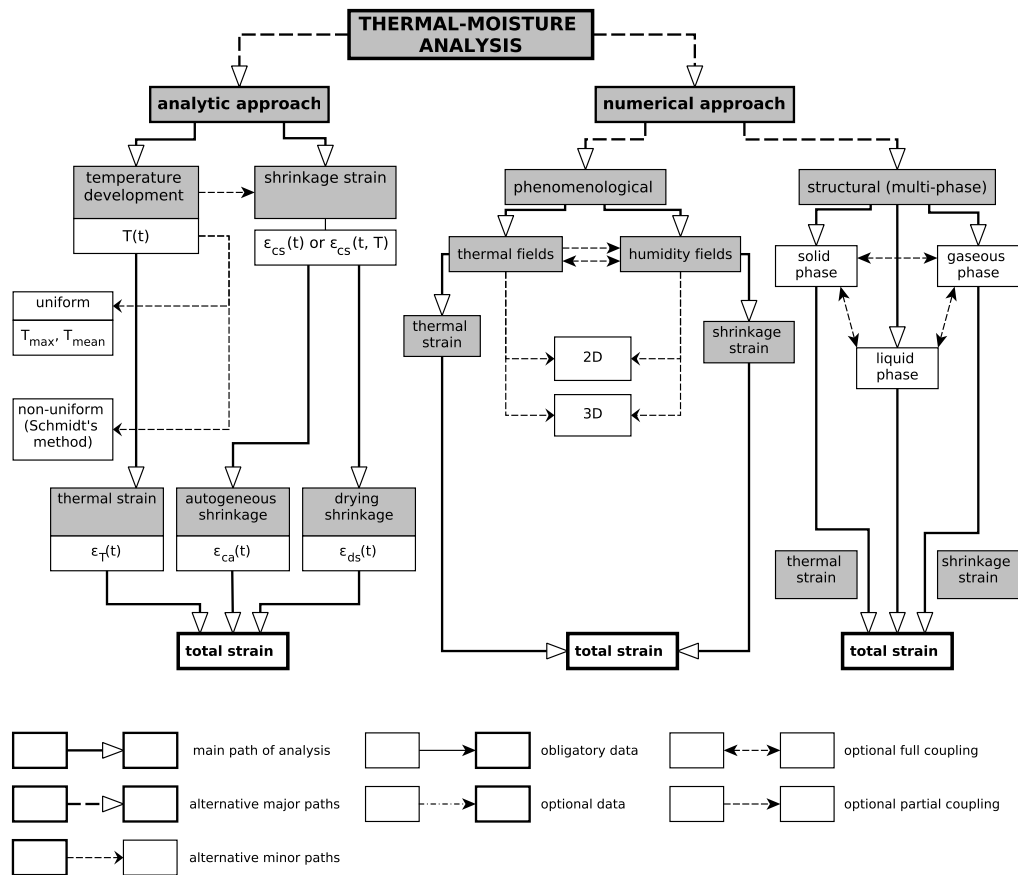


FIGURE 4.2: Thermal-moisture analysis: modelling paths.

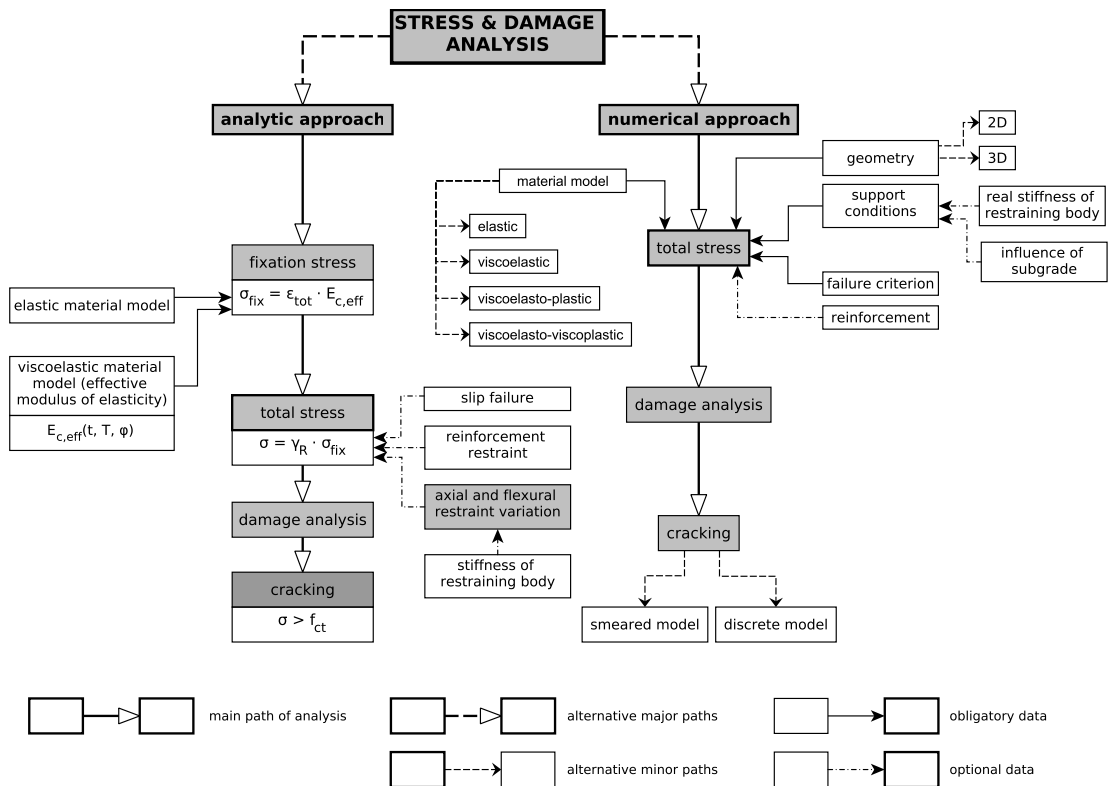


FIGURE 4.3: Stress and damage analysis: modelling paths.

estimation of stresses in concrete walls and is often used both at the design phase and for analysis of the existing engineering structures.

When more detailed analysis of a concrete structure is required, e.g. for analysis of responsible structures, the applied models include a complete description of all the important phenomena and full computer aid is required for their solution. For that purpose numerical models are formulated which allow to translate an analytic formulation into a computer implementation; most often FEM formulation is applied. The models which are currently used for simulation of the early-age concrete structures behaviour are either phenomenological or multi-phase, with the former ones more practical in modelling of whole structural systems. In thermo-physical analysis coupled or uncoupled thermal and moisture fields are derived. The resulting volume changes allow to calculate the expected strains, which are assumed to be imposed strains, based on which the stress analysis can be performed. For that purpose a material model of choice is used. The choice of the material model is also a compromise between the accuracy and complexity. Because viscous effects are highly pronounced in early-age concrete, the choice of the creep model is crucial. It is also advised to account for the elasto-plastic behaviour of concrete and for creep effects both in the elastic and plastic phase. Finally, damage analysis can be performed based on the chosen failure criterion. For evaluation of cracking risk in early-age concrete element simple damage criteria and smeared cracking image is sufficient. For detailed analysis of crack propagation as well as determination of crack width more elaborate damage criteria have to be used.

Chapter 5

Analysis of early-age stresses in reinforced concrete walls

The analysis of the character and distribution of stresses in early-age reinforced concrete walls during early phases of concrete hardening was performed, considering the influence of various parameters, mainly dimensions and restraint conditions of the walls including the influence of the founding subsoil. Behaviour of the walls was analysed with the use of the computer implementation of the model presented in Sec. 5.1.1. The results of the numerical analysis were compared with the results obtained with the use of the analytic model described in Sec. 5.1.2.

5.1 Models for analysis of early-age reinforced concrete walls

5.1.1 Numerical model

The model used in this thesis was developed based on the proposals of KLEMCZAK [134, 135] for thermal–moisture analysis and MAJEWSKI [161, 162, 163] and KLEMCZAK [133, 134] for stress and damage analysis. Formulation of the model was based on the overview in Chap. 4 and is schematically presented in Fig. 5.1. The applied model is a phenomenological model. The analysis of a structure consists of two main steps. The first step is related to determination of non-linear and non-stationary thermal and moisture fields and resulting thermal and shrinkage strains. In the second step stresses are calculated and damage intensity of the structure is determined.

5.1.1.1 Thermal and moisture analysis

Thermal and moisture fields. Early-age concrete and soil are both porous media and similar constitutive equations can be formulated for their thermo–physical behaviour. The temperature and moisture fields in early-age concrete were defined with the coupled equations proposed by KLEMCZAK [134, 135] after Eq. 4.37:

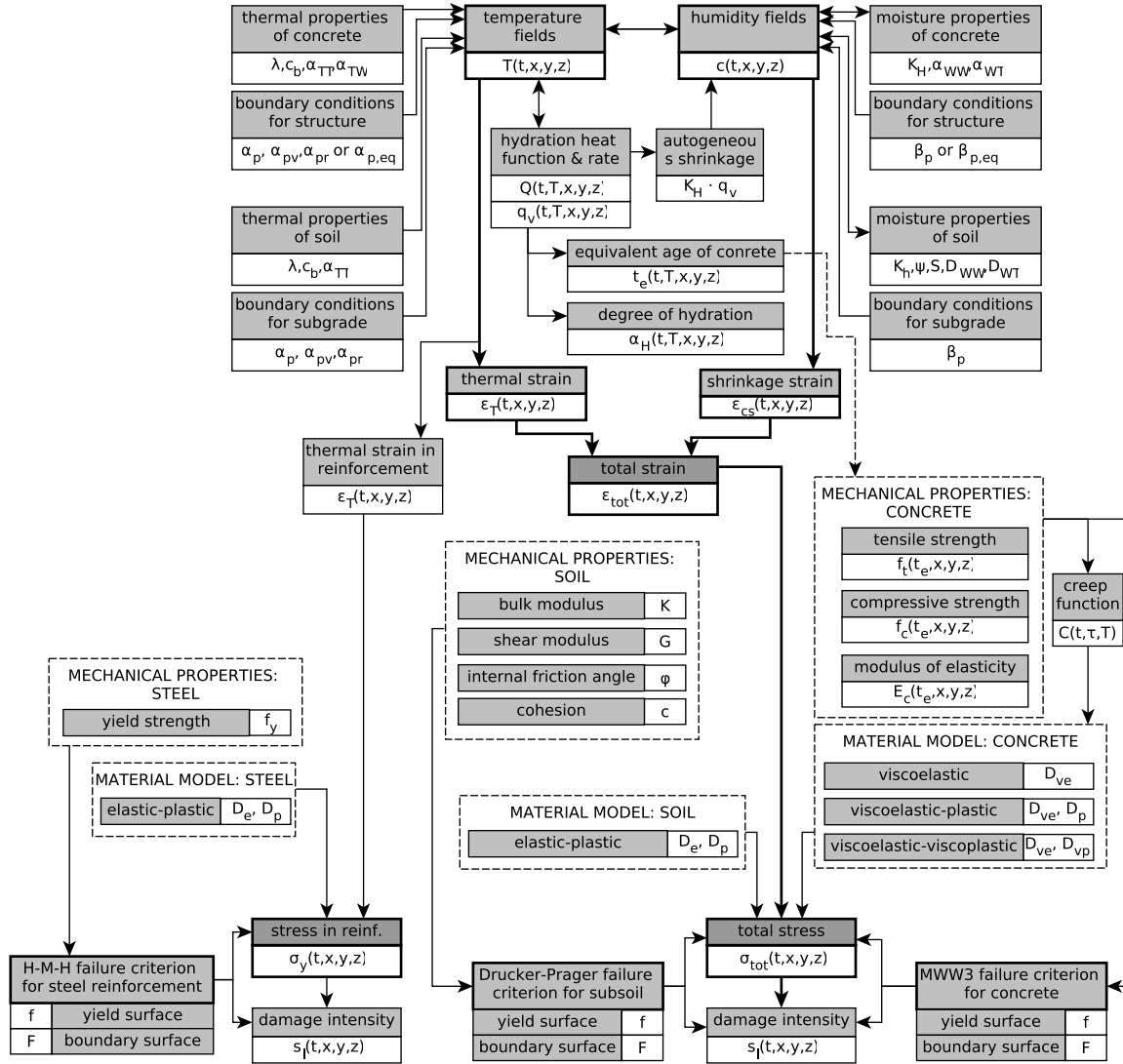


FIGURE 5.1: Model for analysis of early-age walls with the use of the numerical approach.

$$\dot{T} = \text{div}(\alpha_{TT} \text{grad}T + \alpha_{TW} \text{grad}c) + \frac{q_v(t, T)}{c_b \rho},$$

$$\dot{c} = \text{div}(\alpha_{WW} \text{grad}c + \alpha_{WT} \text{grad}T) - K_H q_v(t, T).$$

Analogical equations were defined for soil. The temperature change was defined according to Eq. 4.96 while the humidity change according to Eq. 4.112:

$$\dot{T} = \text{div}(\alpha_{TT} \text{grad}T),$$

$$\dot{c} = \text{div}(\alpha_{WW} \text{grad}c + \alpha_{WT} \text{grad}T),$$

where:

T – temperature, K;

- c – moisture concentration by mass (relative humidity), kg/kg;
 α_{TT} – coefficient of thermal diffusion, m^2/s ;
 α_{WW} – coefficient of moisture diffusion, m^2/s ;
 α_{TW} – coefficient representing the influence of the moisture transport on the heat transfer, $(\text{m}^2 \text{K})/\text{s}$;
 α_{WT} – coefficient representing the influence of the heat transfer on the moisture transport, $\text{m}^2/(\text{sK})$;
 c_b – specific heat, $\text{kJ}/(\text{kgK})$;
 ρ – density of concrete, kg/m^3 ;
 K_H – coefficient of water–cement proportionality, which describes amount of water bounded by cement during hydration process with the rate of heat generated per unit volume of concrete, m^3/J ;
 $q_v(t, T)$ – rate of heat generated per unit volume of concrete, W/m^3 .

The coefficients of thermal diffusion, α_{TT} , both for soil and concrete were calculated acc. to Eq. 4.39 with the values of thermal conductivity, λ , and heat capacity, c_v , constant over time:

$$\alpha_{TT} = \frac{\lambda}{c_v}.$$

The values of λ and c_v were calculated based on the composition of soil and concrete mix, respectively. Thermal conductivity of concrete was calculated acc. to Eq. 4.41:

$$\lambda = \sum p_i \lambda_i,$$

and of soil acc. to Eq. 4.101:

$$\lambda = \left(\sum k_i \lambda_i \right)^2.$$

Heat capacity of concrete was calculated acc. to Eq. 4.42:

$$c_v = \sum p_i \rho_i c_{b,i},$$

and of soil acc. to Eq. 4.102:

$$c_v = \sum k_i \rho_i c_{b,i}.$$

In the equations p_i is a mass fraction and k_i is a volume fraction of the i^{th} component: cement, water and aggregate for concrete and soil particles and water for soil. The properties of concrete components were taken from Tab. 4.1 and for soil from Tab. 4.3.

The coefficient of moisture diffusion, α_{WW} , for concrete was calculated after HANCOX [97] based on the moisture content by volume acc. to Eq. 4.48:

$$D_{WW}(W) = \left[4.6389 \cdot (0.7 + 6W)^2 - 1.0556 \cdot (0.7 + 6W) + 0.3055 \right] \cdot 10^{-10}.$$

The relationship between moisture content by volume and by mass was applied after Eq. 4.36:

$$\alpha_{WW} = D_{WW} \frac{\rho_w}{\rho}. \quad (5.1)$$

The coefficients of the mutual influence of temperature on moisture fields and vice-versa for concrete were taken as constant and equal to $\alpha_{TW} = 0.9375 \cdot 10^{-4} (\text{m}^2 \text{K})/\text{s}$ and $\alpha_{WT} = 2.0 \cdot 10^{-11} \text{m}^2/(\text{K s})$. The coefficient of the water–cement proportionality was taken as equal to $K_H = 0.3 \cdot 10^{-8} \text{m}^3/\text{J}$.

Coefficients in moisture analysis, α_{WW} and α_{WT} , for soil were calculated based on the isothermal and thermal liquid diffusivities according to the relationship given by Eq. 5.1, with the diffusivities calculated after CLAPP AND HORNBERGER [55] acc. to Eq. 4.111. Because of relatively small changes in moisture content of soil the values of the diffusivities were assumed as constant and determined under the assumption of full saturation ($S = 1.0$):

$$D_{WW} = \frac{b K_{h,\text{sat}} \psi_a}{n}, \quad (5.2a)$$

$$D_{WT} = K_{h,\text{sat}} \psi_a \gamma_T. \quad (5.2b)$$

The hydraulic properties of soil after Tab. 4.4 are given in Tab. 5.1.

SOIL TYPE	$D_{WW} [\text{m}^2/\text{s}] \cdot 10^{-6}$	$D_{WT} [\text{m}^2/(\text{s K})] \cdot 10^{-10}$
sand	218.35	445.09
loamy sand	150.00	293.44
sandy loam	85.20	158.07
silty loam	61.80	118.19
loam	39.67	69.38
sandy clay loam	31.96	39.40
silty clay loam	9.83	12.65
clay loam	27.63	32.26
sandy clay	8.10	6.94
silty clay	10.67	10.55
clay	12.27	10.84

TABLE 5.1: Liquid diffusivities of fully-saturated soils after CLAPP AND HORNBERGER [55].

It should be noted that in early-age concrete moisture diffusion also depends on the degree of saturation, not solely moisture content [28]. Moisture diffusion coefficient should be thus also expressed as a function of the degree of saturation and the same model could be used for concrete and soil. Nevertheless, at this moment the hydraulic parameters (K_h , ψ and n) for early-age concrete are not fully recognised and only some proposals of their values for specific concrete mixes can be found in the literature.

Initial and boundary conditions. For the initial conditions the initial temperature and humidity of concrete mix and soil were taken:

$$T(x_i, t = 0) = T_i(x_i), \quad (5.3a)$$

$$c(x_i, t = 0) = c_i(x_i), \quad (5.3b)$$

where $x_i \in (V \cup \partial V)$, $i = x, y, z$ and T_i , c_i are the initial distribution of temperature and the initial concentration of moisture in concrete and soil, respectively.

Boundary conditions were assumed to be 3rd type boundary conditions of convective type:

$$\mathbf{n}^T(\alpha_{TT} \text{grad}T + \alpha_{TW} \text{grad}c) + \tilde{q} = 0, \quad (5.4a)$$

$$\mathbf{n}^T(\alpha_{WW} \text{grad}c + \alpha_{WT} \text{grad}T) + \tilde{\eta} = 0, \quad (5.4b)$$

where $\mathbf{n} = [n_x, n_y, n_z]^T$ is a vector normal to the boundary surface, ∂V . The heat flux, \tilde{q} , depends on the temperature of the boundary surface, $T_{\text{sur}}(x_i, t)$, and the ambient temperature, $T_a(t)$. Similarly, the moisture flux, $\tilde{\eta}$, depends on the moisture concentration at the boundary surface, $c_{\text{sur}}(x_i, t)$, and on the moisture concentration in the surrounding air, $c_a(t)$. Hence:

$$\tilde{q} = \frac{\alpha_p}{c_v} [T_{\text{sur}}(x_i, t) - T_a(t)], \quad (5.5a)$$

$$\tilde{\eta} = \beta_p [c_{\text{sur}}(x_i, t) - c_a(t)], \quad (5.5b)$$

where:

- α_p – heat exchange coefficient, W/(m²K);
- β_p – moisture exchange coefficient, m/s.

The coefficients of the heat and moisture exchange were calculated taking into account the physical properties of materials and covering material (if applies). The ambient humidity, c_a , was calculated based on the known relative humidity of air, RH , using the relationship in Eq. 4.36:

$$c_a = W_a \frac{\rho_w}{\rho}, \quad (5.6)$$

with the moisture content in air, W_a [m³/m³], calculated with the relative air humidity, RH [%]:

$$W_a = 0.0005RH. \quad (5.7)$$

Hydration function. The rate of heat generated per unit volume of concrete was calculated based on a unit heat rate, $q(t)$ [W/g], and the amount of cement, C_c [kg/m³]:

$$q_v(t, T) = C_c q(t, T) = C_c \frac{\partial Q(t, T)}{\partial t}. \quad (5.8)$$

Two methods for definition of the hydration function were implemented. The first method can be used when data from calorimetric tests are available. The hydration heat time-development was described with the approximation function of equivalent age acc. to Eq. 4.22:

$$Q(t, T) = Q_{\text{tot}} e^{[-a_1 t e^{a_2}]},$$

where Q_{tot} is a total heat of hydration [J/g], a_1 and a_2 are coefficients dependent on the type of cement, and t_e [s] is the equivalent age of concrete according to Eq. 4.5. The degree of hydration was calculated as:

$$\alpha_H(t_e) = \alpha_{Hu} \frac{Q(t_e)}{Q_{\text{tot}}}. \quad (5.9)$$

In the second approach the degree of hydration was given by Eq. 4.17:

$$\alpha_H(t_e) = \alpha_{Hu} e^{-\left(\frac{\tau}{t_e}\right)^\beta}.$$

The hydration heat development in time was defined with a degree of hydration:

$$Q(t, T) = Q_{\text{tot}} \alpha_H(t_e), \quad (5.10)$$

and the unit rate of hydration heat development, $q(t, T)$, according to Eq. 4.16:

$$q(t, T) = Q_{\text{tot}} \left(\frac{\tau}{t_e}\right)^\beta \left(\frac{\beta}{t_e}\right) \alpha_H(t_e) e^{\frac{E_K}{R} \left(\frac{1}{T_{\text{ref}}} - \frac{1}{T}\right)}.$$

The total hydration heat, Q_{tot} , was calculated based on the known composition of cement according to the approach proposed by SCHINDLER AND FOLLARD [202] according to Eq. 4.10:

$$Q_{\text{tot}} = 500 p_{C_3S} + 260 p_{C_2S} + 866 p_{C_3A} + 420 p_{C_4AF} + 642 p_{SO_3} + 1186 p_{\text{FreeCao}} \\ + 850 p_{MgO} + 1800 p_{FA, CaO} + 461 p_{\text{Slag}}.$$

The ultimate degree of hydration, α_{Hu} , was calculated with Eq. 4.19:

$$\alpha_{Hu} = \frac{1.031w/c}{0.194 + w/c} + 0.50 p_{FA} + 0.30 p_{\text{Slag}}.$$

Thermal and shrinkage strains. The imposed thermal–shrinkage strains, ε_n , were treated as volumetric strains:

$$d\varepsilon_n = \begin{bmatrix} d\varepsilon_{n,x} & d\varepsilon_{n,y} & d\varepsilon_{n,z} & 0 & 0 & 0 \end{bmatrix}, \quad (5.11)$$

and calculated with the predetermined temperature, T [°C], and moisture content, W [m³/m³]:

$$d\varepsilon_{n,x} = d\varepsilon_{n,y} = d\varepsilon_{n,z} = \alpha_T dT + \alpha_W dW, \quad (5.12)$$

where α_T is the coefficient of thermal dilation and α_W is the coefficient of moisture dilation. For concrete the coefficient of thermal dilation was taken from Tab. 4.2 based on the aggregate used in the mix. The moisture dilation coefficient was taken as equal to $\alpha_W = 0.002$. For soil, the thermal dilation coefficient was taken as equal to $\alpha_T = 10^{-5}/^\circ\text{C}$ and the moisture dilation coefficient was taken as equal to $\alpha_W = 0.001$.

5.1.1.2 Stress and damage analysis

Early-age concrete. For the stress analysis in early-age concrete three material models were proposed: the viscoelastic, viscoelasto–plastic and viscoelasto–viscoplastic model. The applied constitutive formulations were given by KLEMCZAK [136].

In the viscoelastic model the stress–strain relationship has a form:

$$d\sigma = D_{ve} [d\varepsilon - d\varepsilon_n - d\varepsilon_c], \quad (5.13)$$

where \mathbf{D}_{ve} is a viscoelasticity matrix.

The yield surface evolves in the stress space depending on the hardening parameter, $\kappa = \kappa(\boldsymbol{\varepsilon}_p)$, and on the concrete age, t :

$$f(\boldsymbol{\sigma}, \kappa, t) = 0. \quad (5.14)$$

The failure surface was defined with a consistence condition:

$$F(\boldsymbol{\sigma}, t) = 0, \quad (5.15a)$$

$$dF(\boldsymbol{\sigma}, t) = 0. \quad (5.15b)$$

In the viscoelasto–viscoplastic model the viscous effects were taken into consideration both for elastic and plastic strains. The viscoelastic and viscoelasto–viscoplastic areas were distinguished. The following constitutive equations were defined in the viscoelastic area and viscoelasto–viscoplastic area, respectively, expressed with stress and strain rates:

$$\dot{\boldsymbol{\sigma}} = \mathbf{D}_{ve} [\dot{\boldsymbol{\varepsilon}} - \dot{\boldsymbol{\varepsilon}}_n - \dot{\boldsymbol{\varepsilon}}_c], \quad (5.16a)$$

$$\dot{\boldsymbol{\sigma}} = \mathbf{D}_{ve} [\dot{\boldsymbol{\varepsilon}} - \dot{\boldsymbol{\varepsilon}}_n - \dot{\boldsymbol{\varepsilon}}_c - \dot{\boldsymbol{\varepsilon}}_{vp}], \quad (5.16b)$$

with the rate of the viscoplastic strain:

$$\dot{\boldsymbol{\varepsilon}}_{vp} = \dot{\lambda} \frac{\partial f}{\partial \boldsymbol{\sigma}}, \quad (5.17)$$

where $\dot{\lambda}$ is a positive scalar called a consistent parameter. In the consistent concept of the viscoplastic strains description both the yield surface, f , and the boundary surface, F , are rate-dependent and were expressed as functions of the hardening parameter, κ , and its rate, $\dot{\kappa}$:

$$f(\boldsymbol{\sigma}, \kappa, \dot{\kappa}) = 0, \quad (5.18a)$$

$$F(\boldsymbol{\sigma}, \kappa, \dot{\kappa}) = 0. \quad (5.18b)$$

The viscoelastic and viscoelasto–viscoplastic areas were separated by the initial location of the yield surface, defined as the boundary surface multiplied by the viscoelasticity limit, $e_{\text{lim}} < 1$. The value of this coefficient depends on the concrete strength in uniaxial compression, as in the equation:

$$e_{\text{lim}} = 1 - e^{-0.02f_c(t_e)}. \quad (5.19)$$

Viscoelasticity matrix $\mathbf{D}_{ve}(t_{i+1})$ was given by the formula:

$$\mathbf{D}_{ve}(t_{i+1}) = \frac{\mathbf{D}_e(t_{i+1})}{1 + 0.5E(t_{i+1}) \left[\frac{1}{E(t_i)} - \frac{1}{E(t_{i+1})} + \int_{t_i}^{t_{i+1}} -\frac{\partial C(t_{i+1}, \tau)}{\partial \tau} d\tau \right]}, \quad (5.20)$$

and the additional denotation $\Delta\varepsilon_c(t_{i+1})$ was given by the formula:

$$\Delta\varepsilon_c(t_{i+1}) = \mathbf{D}^{-1} \left[\int_0^{t_i} -\frac{\partial C(t_{i+1}, \tau)}{\partial \tau} \boldsymbol{\sigma}(\tau) d\tau + \boldsymbol{\sigma}(t_i) \int_0^{t_{i+1}} -\frac{\partial C(t_{i+1}, \tau)}{\partial \tau} d\tau - \int_0^{t_i} -\frac{\partial C(t_i, \tau)}{\partial \tau} \boldsymbol{\sigma}(\tau) d\tau \right], \quad (5.21)$$

where \mathbf{D} is a matrix of the Poisson's ratio, ν (assumed as constant):

$$\mathbf{D}^{-1} = \begin{bmatrix} 1 & -\nu & -\nu & 0 & 0 & 0 \\ -\nu & 1 & -\nu & 0 & 0 & 0 \\ -\nu & -\nu & 1 & 0 & 0 & 0 \\ 0 & 0 & 0 & 2(1+\nu) & 0 & 0 \\ 0 & 0 & 0 & 0 & 2(1+\nu) & 0 \\ 0 & 0 & 0 & 0 & 0 & 2(1+\nu) \end{bmatrix}. \quad (5.22)$$

The creep function, $C(t, \tau)$, was assumed according to MODEL CODE 1990 [47] after GUÉNOT ET AL. [94]:

$$C(t, \tau) = \left(\frac{1}{E_c(t)} \right) \left(\frac{16.8}{(f_{c,28})^{0.5}} \right) \left(\frac{1}{0.1 + \tau^{0.2}} \right) \left(\frac{t - \tau}{1500 + t - \tau} \right)^{0.3}. \quad (5.23)$$

Because of the questionable effect of temperature in the formulation given by the standard no influence of temperature was taken into account. To compute the creep strain stresses were taken as linear over each time step and material properties were constant within each step. It was assumed that creep is symmetrical in compression and tension.

The following mechanical properties of concrete are needed to define the failure surface: uniaxial compressive strength, f_c , uniaxial tensile strength, f_t , and biaxial compressive strength, f_{cc} . If the values of these mechanical properties are not known and only the class of concrete is provided, the compressive strength can be assumed based on the class ($f_{c,28} = f_{cm,28}$) and the remaining parameters can be calculated. MODEL CODE 2010 suggests the following formulas to determine final values of the tensile strength and the modulus of elasticity:

$$f_{ctm,28} [\text{MPa}] = 0.3 (f_{cm,28} - 8)^{2/3}, \quad (5.24)$$

$$E_{cim,28} [\text{GPa}] = 21.5 \alpha_E \left(\frac{f_{cm,28}}{10} \right)^{1/3}, \quad (5.25)$$

where the coefficient α_E depends on the type of aggregate and ranges between 0.7 and 1.2. The biaxial compressive strength can be calculated as follows [49]:

$$f_{cc}(t) = \left[1.2 - \frac{f_c(t)}{1000} \right] f_c(t). \quad (5.26)$$

The modified 3-parameter Willam–Warnke failure criterion, MWW3, was used [133, 162]. The boundary surface for early-age concrete was assumed as a fixed surface in the proposed coordinate

system. The meridians are straight lines and in the low-compression and tension regime the caps defined by the second-order parabolas were introduced (Fig. 5.2a). In the deviatoric plane the boundary surface has a noncircular cross-section, defined according to the Willam–Warnke conception as parts of the elliptic curves (Fig. 5.2b). The same criterion was used to describe both the yield surface and the failure surface.

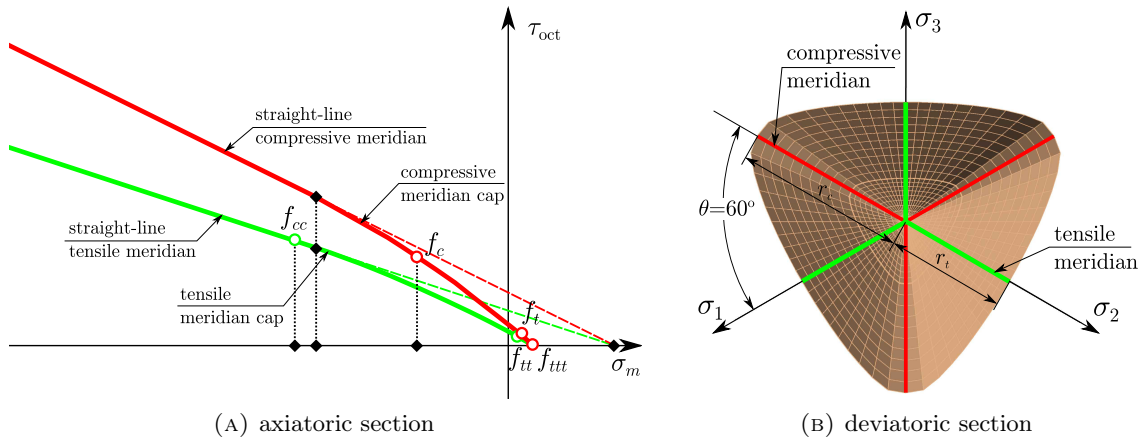


FIGURE 5.2: Boundary surface acc. to the modified 3-parameter Willam–Warnke (MWW3) failure criterion.

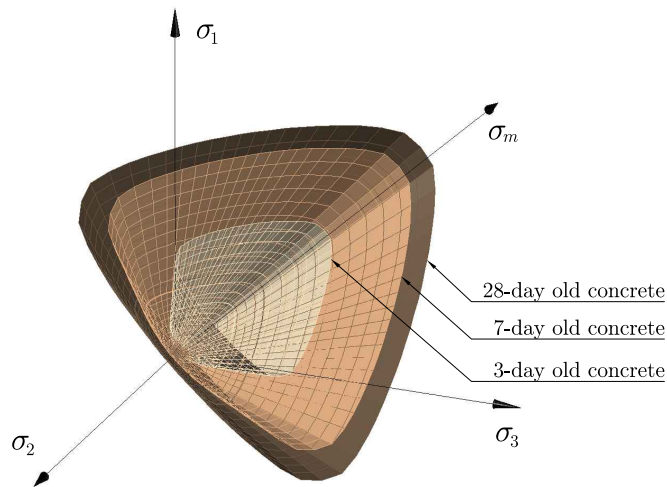


FIGURE 5.3: Development of the boundary surface in time with the maturing process.

Development of the surfaces in time with progressing maturity of concrete was defined by the time-development of the material properties, $P(t, T)$, (Fig. 5.3); ageing of concrete was defined as a function of the equivalent age of concrete:

$$P(t, T) = [\beta_c]^n P_{28},$$

where:

- $P(t, T), P_{28}$ – material property (compressive or tensile strength, modulus of elasticity) in time t and at the actual maturity level, and at the age of 28 days, respectively;
- β_c – time development function given by Eq. 4.71:

$$\beta_c(t, T) = e^s \left[1 - \sqrt{\frac{28}{t_e}} \right]; \quad (5.27)$$

n – exponent dependent on the property to describe and concrete composition.

Subsoil. For soil the elasto–perfectly-plastic material model with a modified Drucker–Prager failure criterion was used. The constitutive equations were given by MAJEWSKI [161, 162]. In the elastic phase the constitutive equation has a form:

$$d\boldsymbol{\sigma} = \mathbf{D}_e d\boldsymbol{\varepsilon}, \quad (5.28)$$

where \mathbf{D}_e is the elasticity matrix. Beyond the elastic phase the constitutive equation was defined:

$$d\boldsymbol{\sigma} = \mathbf{D}_{ep} (d\boldsymbol{\varepsilon}_e + d\boldsymbol{\varepsilon}_p), \quad (5.29)$$

where the magnitude of the plastic strain was determined by the law of plastic flow and:

$$\mathbf{D}_{ep} = \mathbf{D}_e - \mathbf{D}_p. \quad (5.30)$$

The plasticity matrix, \mathbf{D}_p , was given by the equation:

$$\mathbf{D}_p = \mathbf{D}_e \left(\frac{\partial F}{\partial \boldsymbol{\sigma}} \right) \left(\frac{\partial F}{\partial \boldsymbol{\sigma}} \right)^T \mathbf{D}_e \left[\frac{\partial F}{\partial \kappa} \boldsymbol{\sigma}^T \frac{\partial F}{\partial \boldsymbol{\sigma}} + \left(\frac{\partial F}{\partial \boldsymbol{\sigma}} \right)^T \mathbf{D}_e \left(\frac{\partial F}{\partial \boldsymbol{\sigma}} \right) \right]^{-1}. \quad (5.31)$$

The yield surface, f , has a form:

$$f = f_1(\sigma_m, \kappa) + f_2(\bar{\sigma}) = 0, \quad (5.32)$$

where:

- κ – hardening parameter;
- σ_m – mean stress;
- $\bar{\sigma}$ – stress intensity.

The following mechanical properties of soil are required: bulk modulus, K , shear modulus, G , cohesion, c_s , and internal friction angle, φ . The values of the bulk and shear modulus were assumed in a manner similar to DUNCAN AND CHANG model [74] after MAJEWSKI [161]. The bulk modulus, K , and the initial value of the shear modulus, G_1 , were given by the following expressions:

$$K = K_o p_a \left(\frac{\sigma_m}{p_a} \right)^{0.5}, \quad (5.33a)$$

$$G_1 = G_o p_a \left(\frac{\sigma_m}{p_a} \right)^{0.5}, \quad (5.33b)$$

where K_o and G_o are material constants, σ_m is a mean stress and p_a is the atmospheric pressure. For a given value of stress, $\bar{\sigma}$, the value of the shear modulus was calculated as:

$$G = G_1 \left(1 - \frac{\bar{\sigma}}{\sigma_f} r_f \right)^2, \quad (5.34)$$

where r_f is a material parameter and σ_f is a limit value of stress $\bar{\sigma}$ for a given mean stress, σ_m .

If no test data for the soil are available, the values of the cohesion and internal friction angle are taken as average values according to the literature data.

Contact elements. Contact elements between concrete and soil were assigned with the material properties of the modified soil. This material has no tensile strength and limited ability to transfer shear stresses.

Moisture diffusion coefficient for this contact material was additionally reduced to the value of $\alpha_{WW} = 10^{-10}$ to imitate the sliding layer of tarboard introduced between concrete foundation and soil.

Reinforcement. Reinforcement was modelled as bar elements connected with concrete elements in the nodes. Full bonding between reinforcement and adjoining concrete was considered, so the assumed model is simplified. Elasto-plastic material model with Huber-von Mises-Hencky failure criterion was assumed. The yield strength of steel, f_y , required for calculations was assumed based on the class of the reinforcing steel.

Damage intensity. A smeared cracking image was applied in the model. The possibility of the crack occurrence was defined based on the damage intensity factor, s_l , given by the Eq. 4.92:

$$0 \leq s_l = \frac{\tau_{\text{oct}}}{\tau_{\text{oct}}^f} \leq 1.$$

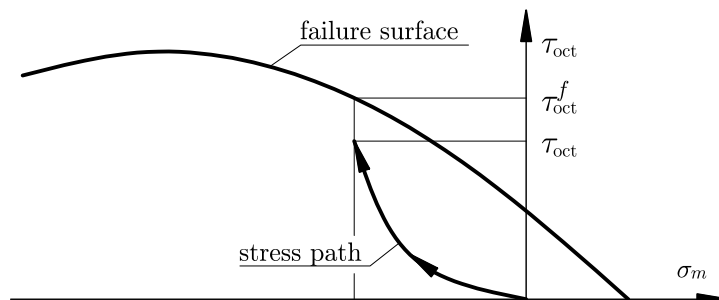


FIGURE 5.4: Graphical interpretation of the damage intensity factor.

Fig. 5.4 shows graphical interpretation of the damage intensity factor. The damage intensity factor equal to unity is equivalent to the stress reaching the failure surface and signifies failure of the element. The character of this failure depends on the position where the failure surface was reached [162]. In the analysed cases reaching of the failure surface in a concrete structure always occurred in within the range of the hydrostatic tensile stresses which was equivalent to formation of the splitting crack in the plane perpendicular to the direction of the maximum principal stress.

5.1.1.3 Implementation

The implementation of the model has a modular architecture, which is schematically presented in Fig. 5.5. The mesh is defined with use of the MAFEM3D module created by WANDZIK [219]. The same mesh is used in thermal–moisture and stress analysis. The data for the project are defined in a sequence of modules which allow to define e.g. the hydration function, thermo–physical and mechanical properties of the materials and parameters of the project.

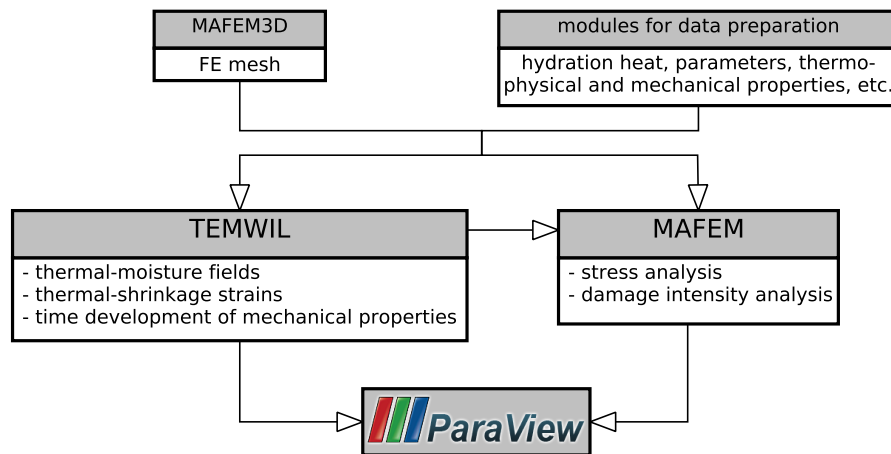


FIGURE 5.5: Scheme of the software architecture.

The main calculations are performed with the use of two computational modules. The first module, TEMWIL, is used for the thermal–moisture analysis. This module implements the thermal–moisture part of the numerical model (Sec. 5.1.1.1). The second module, MAFEM, is used for the stress and damage analysis; it implements the stress part of the model (Sec. 5.1.1.2). Implementation of the model is based on the proposal of KLEMCZAK [134] for thermal–moisture analysis and of MAJEWSKI [161, 162] for stress analysis. The implementation is written in FORTRAN 90. The software is cross-platform – it has been successfully developed and used on Windows and Linux.

The results of the analyses are presented with open-source software PARAVIEW [228].

5.1.2 Analytic model

Possible approaches to description of the individual phenomena and methods of analysis of early-age walls with analytic approaches were presented and discussed in Chap. 3. The graph in Fig. 5.6 presents the proposal of a complete analytic model for early-age walls.

5.1.2.1 Thermal and shrinkage analysis

Due to the fact that the main aim of this research was the analysis of stresses, simplifications in the thermal–shrinkage analysis were made. For the purpose of the research temperature development was calculated with the use of the numerical model. The linear thermal strain

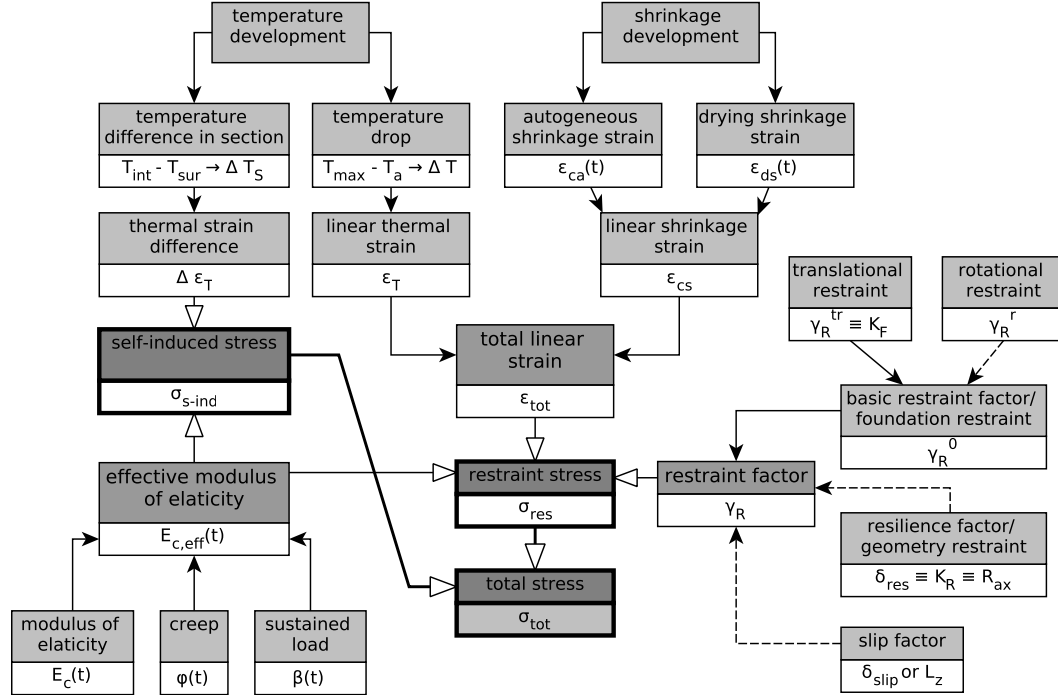


FIGURE 5.6: Model for analysis of early-age walls with the use of the analytic approach.

resulting from temperature drop during cooling was calculated acc. to Eq. 3.2 taking into account the correction given in Eq. 3.15:

$$\varepsilon_T = \alpha_T \Delta T.$$

Shrinkage strain, ε_W , was calculated acc. to Eq. 3.16 given in MODEL CODE 2010 (see Sec. 3.1.2):

$$\varepsilon_W(t) = \varepsilon_{ca}(t) + \varepsilon_{cd}(t),$$

however, for the purpose of this analysis only autogenous shrinkage was taken into account ($\varepsilon_W(t) = \varepsilon_{ca}(t)$) and it was assumed that the shrinkage was uniform in the wall.

5.1.2.2 Stress analysis

Stress analysis was performed assuming elastic behaviour of the walls (uncracked sections). Restraint stresses, σ_{res} , were calculated with the use of the restraint factor which was calculated according to different proposals presented in Sec. 3.2.1. For long walls the restraint factor was assumed to be equal to the basic restraint factor considering only translational restraint ($\gamma_R = \gamma_R^t$ by NILSSON [177], $\gamma_R = K_F$ by ACI 207.2 [5]):

$$\gamma_R(y) = \frac{1}{1 + \frac{A_c E_c}{A_F E_F}}.$$

The effect of the rotational restraint was shown with the use of the formula for the restraint factor given by NILSSON [177] acc. to Eq. 3.41:

$$\gamma_R(y) = 1 - \gamma_R^0 = 1 - (\gamma_R^t(y) + \gamma_R^{ry}(y) + \gamma_R^{rx}(y)).$$

To evaluate the descriptions of the effect of geometry (L/H ratio) resilience factors were introduced into calculation of the restraint factor:

- K_R factor given by ACI 207.2 either in Fig. 3.9 or by Eq. 3.36;
- δ_{res} factor given by NILSSON in Fig. 3.10a.

In short walls the effect of slip on reduction of the degree of restraint was analysed by introduction of the slip factor (δ_{slip} in Fig. 3.10b) after NILSSON.

Sustained (effective, reduced) modulus of elasticity, $E_{c,\text{eff}}$, was applied acc. to Eq. 3.52 to account for the effect of creep and sustained loading:

$$E_{c,\text{eff}}(t) = E_{c,\text{eff}}(t_e) = \frac{E_c(t)}{1 + \beta(t, t_0)\phi(t, t_0)}.$$

The restraint stress was then calculated as:

$$\sigma_{\text{res}}(t) = \gamma_R \varepsilon_{\text{tot}} E_{c,\text{eff}}(t). \quad (5.35)$$

5.2 Character of early-age stresses in reinforced concrete walls

The early-age behaviour of walls was presented on the example of two real walls: a wall in a nuclear power plant and a tunnel wall. The first example presents the development of the thermal–moisture fields and stresses with focus put on the influence of creep, share of self-induced and restraint stresses and the effect of the construction of the wall in lifts. The second example focuses on the effect of the construction sequence on the character of the restraint stresses.

5.2.1 Nuclear containment wall

The analysed wall was a benchmark nuclear containment wall tested during the French National Project CEOS.fr in 2008 related to safety analysis of a nuclear power plant near Civaux, France. The data for the analysis were provided courtesy of F. Benboudjema.

During the construction of the Civaux nuclear power plant two reinforced concrete walls were built in order to evaluate the risk of cracking of the real containment at early age, using two different concrete mixes: ordinary concrete (OC) and high performance concrete (HPC). The walls were equipped with thermocouples in order to follow the evolution of the temperature in different locations. The walls were both 1.2 m wide, 2.8 m high (in total) and 20 m long, supported on a 0.4 m-thick raft foundation. The main reinforcement of the walls were $\varnothing 20$ bars

spaced vertically and horizontally every 20 cm (steel strength $f_y = 400$ MPa). Fig. 5.7 presents the geometry of the walls. Breaks between the execution of the following segments were 2 weeks.

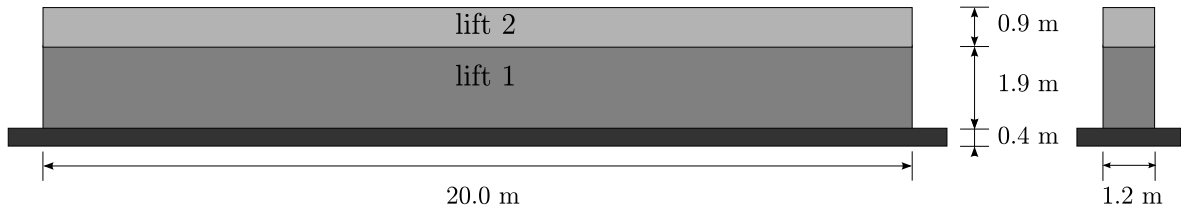


FIGURE 5.7: Geometry of the CEOS.fr benchmark wall.

In this study analysis of the wall made of ordinary concrete was performed. The initial temperature of concrete of the wall was 17°C . The temperature of the foundation, which had already been hardened and pre-cooled at the moment when the wall was cast, was 7°C . The wall was kept in formwork for the whole time. The following concrete mix was used: cement CPA 55 (\sim CEM I 52.5) 350 kg/m^3 , water 195 kg/m^3 and rounded aggregate 1841 kg/m^3 . The measured mechanical properties were as follows: $E_{c,28} = 33.7\text{ GPa}$, $E_{c,365} = 36.4\text{ GPa}$, $\nu = 0.25$, $f_{c,28} = 40.2\text{ MPa}$ and $f_{t,90} = 3.7\text{ MPa}$. Fig. 5.8 shows the locations of thermocouples with the measured temperature development in these locations and variation of the ambient temperature.

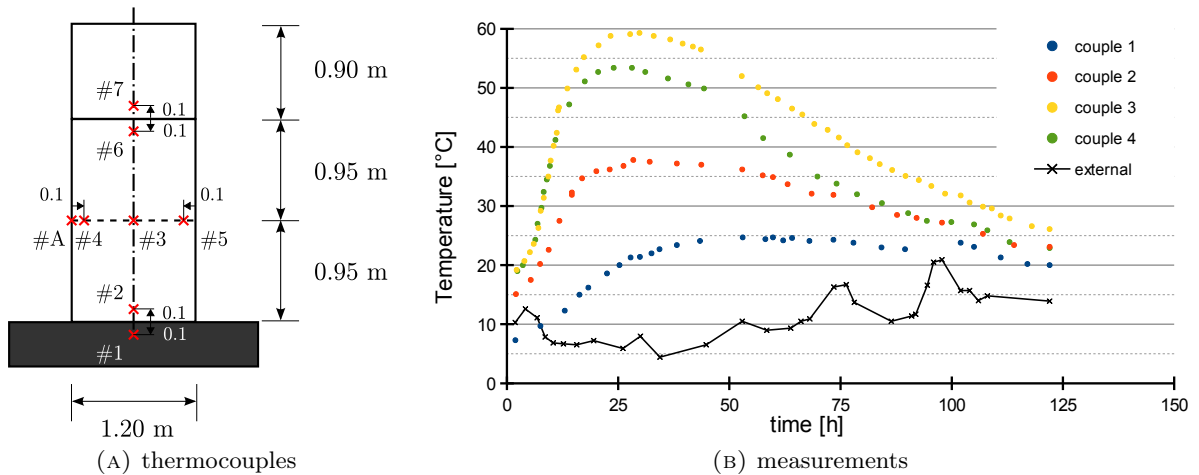


FIGURE 5.8: Temperature development in the CEOS.fr benchmark wall.

The numerical analysis was performed on a quarter of the wall. Fig. 5.9 presents the model and the finite element mesh; the subsequent lifts were marked with different colours. Tab. 5.2 presents the time discretisation. Definition of the mesh and time discretisation were based on the recommendations given by JCI GUIDELINE [110]. Total restraint of vertical deformation of the foundation base was assumed to simulate the fact that the foundation was a large slab. The same material was assumed for both the wall and the foundation. Constant ambient temperature of 10°C was assumed.

The analysis was limited to the first lift because only for that lift the data were available (measurements from the couples 1–6 and cracking pattern).

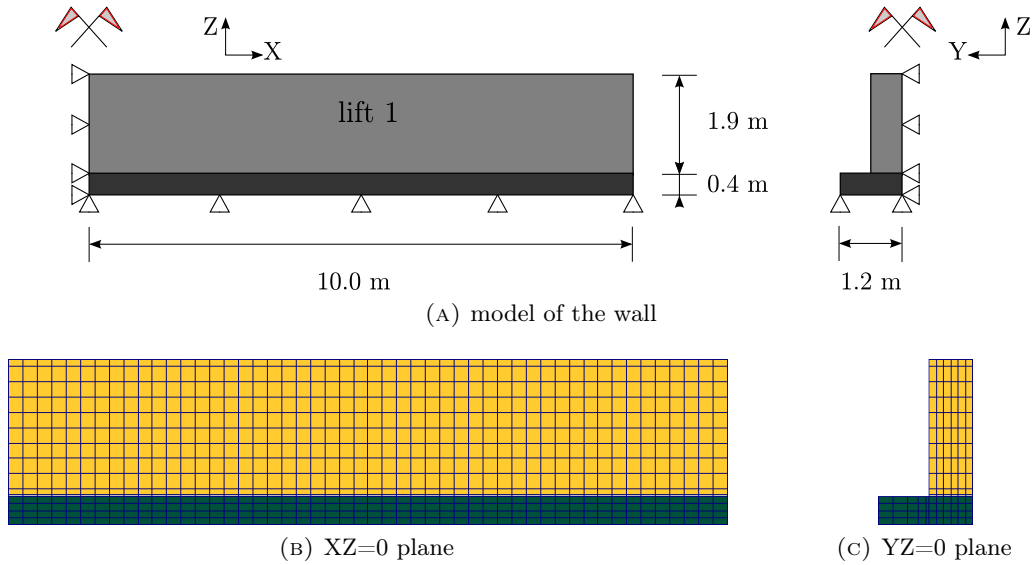


FIGURE 5.9: Model and FE mesh of the CEOS.fr benchmark wall.

TIME, h		TIME INTERVAL, h
age of foundation	age of wall lift 1	
0 – 6		1
6 – 24		2
24 – 72		3
72 – 168		6
168 – 336		12
336 – 342	0 – 6	1
342 – 360	6 – 24	2
360 – 408	24 – 72	3
408 – 504	72 – 168	6
504 – 672	168 – 336	12

TABLE 5.2: Time discretisation used in the analysis of the CEOS.fr benchmark wall.

5.2.1.1 Thermal analysis

Detailed thermo-physical parameters used in the analysis are shown in Tab. 5.3. The hydration heat development was described with the approximation function ($Q_{\text{tot}} = 510 \text{ J/g}$).

PARAMETER	UNIT	VALUE
thermal conductivity, λ	W/(m K)	3.0
specific heat, c_b	kJ/(kg K)	1.0
density, ρ	kg/m ³	2260
coefficient of heat exchange with environment, α_p	W/(m ² K)	3.0
coefficient of moisture exchange with environment, β_p	m/s	$0.18 \cdot 10^{-8}$
thermal dilation coefficient, α_T	1/°C	0.00001
moisture dilation coefficient, α_W	–	0.002

TABLE 5.3: Thermo-physical parameters used in the analysis of the CEOS.fr benchmark wall.

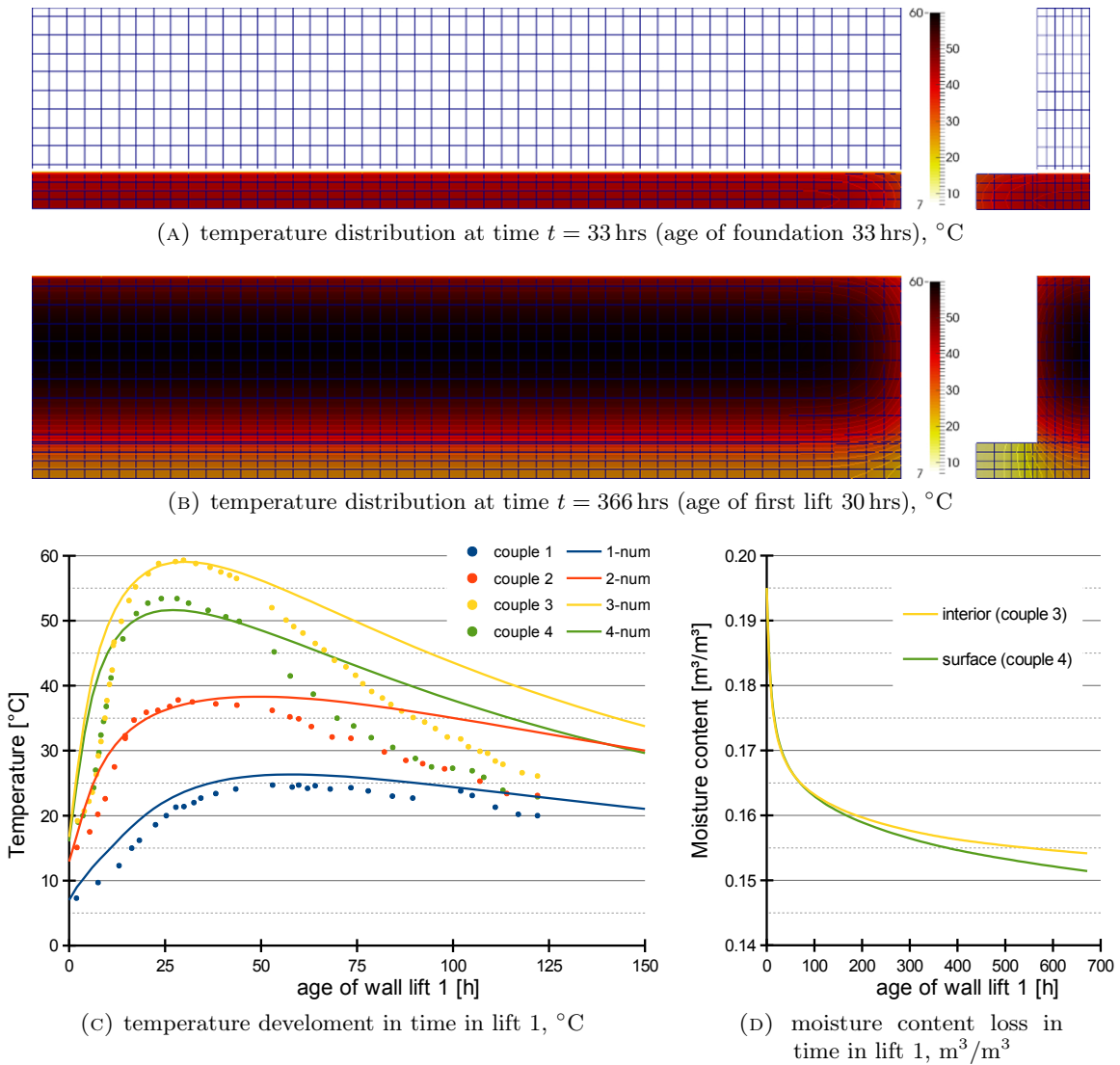


FIGURE 5.10: Results of thermal analysis of the CEOS.fr benchmark wall.

Fig. 5.10 presents the results of the thermal analysis. Fig. 5.10a shows the maps of the temperature distribution at the moment when the maximum core temperature was reached in the foundation. Fig. 5.10b presents analogical maps for the first lift. It can be noticed that the thermal field in any segment is not symmetrical with respect to the neutral axis of the segment. In case of the foundation cooling is more rapid at the top than at the base, where the heat is transmitted to the ground. In case of the first lift the heat is intensively transmitted to the pre-cooled foundation and the highest temperature concentrates above the mid-height of the lift. Relatively large gradients form at the thickness of the wall which exceed $10^{\circ}C$.

The comparison between the measured and calculated temperatures in the first lift of the wall is shown in Fig. 5.10c. The temperature development in the wall was well simulated with the numerical model in the heating phase. The value and the moment of the occurrence of the maximum temperature in each point was well reproduced. The heating rate was a little bit too high because the hydration heat development was represented with the exponential function (high initial rate), while in reality the hydration heat development curve has an “S” shape. The cooling of the real wall was more rapid than obtained in the numerical simulation. This also results from

the character of the hydration heat development function: it is not possible to properly describe the hydration heat development with a single function. Nevertheless, although the results of the numerical analysis do not perfectly comply with the observations, it must be emphasised that the relative rate of the temperature decrease in the numerical analysis and reality do comply, i.e. the descending curves of the temperature diagram go with respect to one another in the same manner in reality and in the numerical simulations. This is a very important observation because the early-age stresses depend on the rate of strain.

Variation of the moisture content in the interior and on the surface of the first lift is shown in the diagram in Fig. 5.10d. The reduction of the moisture content was connected mainly with autogenous shrinkage; drying was limited by keeping the wall in the formwork. There were no significant gradients of moisture content within the wall: moisture content decreased to $0.154 \text{ m}^3/\text{m}^3$ in the interior in comparison to $0.151 \text{ m}^3/\text{m}^3$ near the surface where drying appeared; hence, the maps of the moisture concentration were not shown.

5.2.1.2 Analysis of stresses and cracking

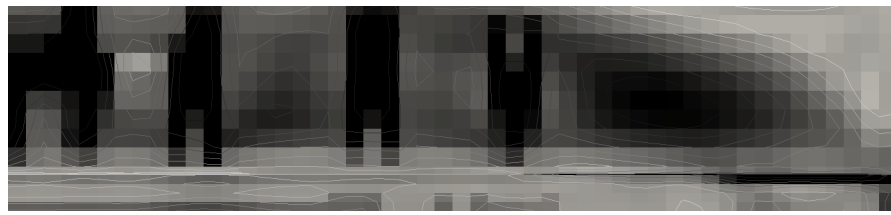
Detailed mechanical data used in the analysis are presented in Tab. 5.4. The stress and damage intensity analysis was performed with the use of the viscoelasto–viscoplastic model.

PARAMETER	UNIT	VALUE
compressive strength, f_c	MPa	40.2
tensile strength, f_t	MPa	3.2
modulus of elasticity, E_c	GPa	33.7
shape coefficient, s	–	0.20
time coefficient for tensile strength, n_f	–	1.0
time coefficient for modulus of elasticity, n_E	–	0.5
yield strength of steel reinforcement, f_y	MPa	400
yield strength of steel reinforcement, f_u	MPa	600
modulus of elasticity of steel reinforcement, f_u	GPa	210

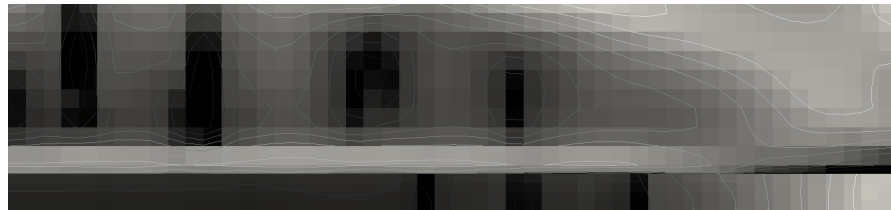
TABLE 5.4: Mechanical parameters used in the analysis of the CEOS.fr benchmark wall.

Fig. 5.11 shows the maps of the damage intensity observed in the first lift right before execution of the second lift. Black areas depict probable locations of cracks. Fig. 5.12 presents the actual cracking pattern observed in the real wall. The cracks in the wall were vertical and ranged the whole height of the lift. It can be noticed that application of the viscoelasto–viscoplastic model allowed to obtain proper cracking pattern. Because the wall was kept in the formwork, the cracks started to develop in the interior and internal cracking was more intensive. Surface cracks followed, though, and all the cracks were through cracks. The cracks concentrated a bit above the mid-height of the lift where the highest temperature was observed.

This character of cracking pattern can be explained by thorough stress and damage intensity analysis. The maps of stresses in the first lift are shown in Fig. 5.13 in the heating phase and Fig. 5.14 in the cooling phase just before initiation of the first crack. Development of stresses and damage intensity factor in time in the location of the first crack formation (marked in pink) is presented in Fig. 5.15. The wall exhibited the following behaviour of the stress development in



(A) damage intensity in the interior



(B) damage intensity on the surface (internal view)

(c)

FIGURE 5.11: Damage intensity in lift 1 of the CEOS.fr benchmark wall at $t = 672$ hrs (age of lift 336 hrs).

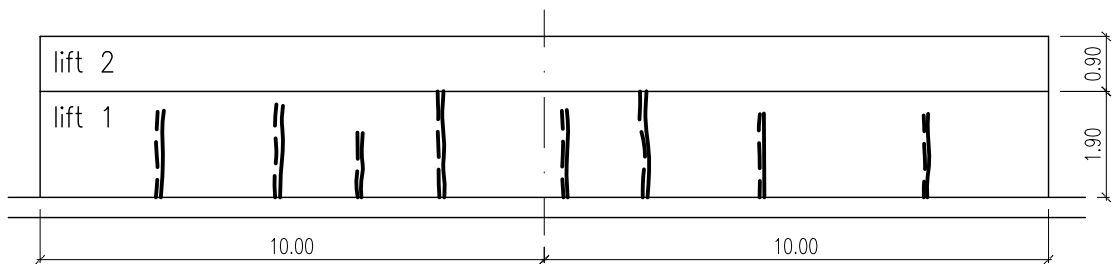
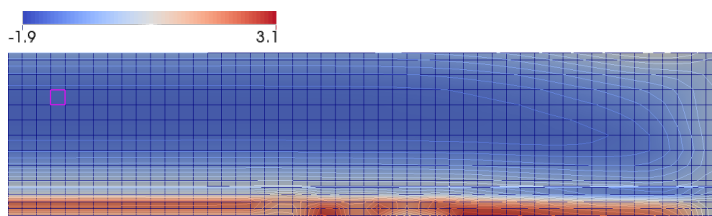
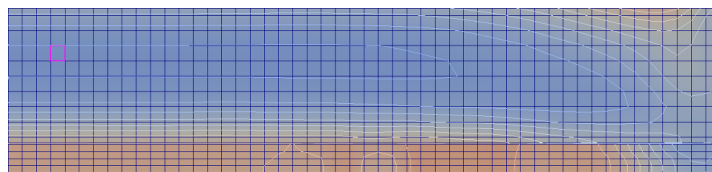


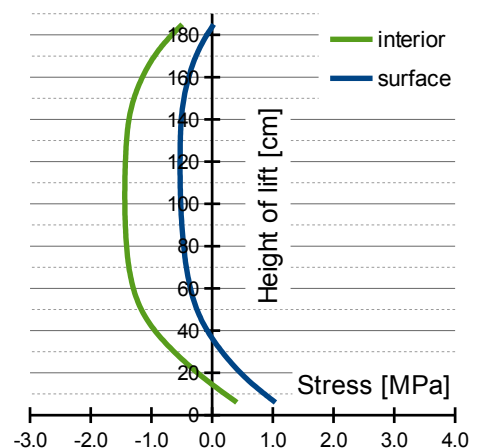
FIGURE 5.12: Cracking pattern in lift 1 of the CEOS.fr benchmark wall.



(A) interior



(B) surface (internal view)



(c) distribution along centreline

FIGURE 5.13: Distribution of σ_{xx} stresses in lift 1 of the CEOS.fr benchmark wall: heating phase, $t = 348$ hrs (age of lift 12 hrs), MPa.

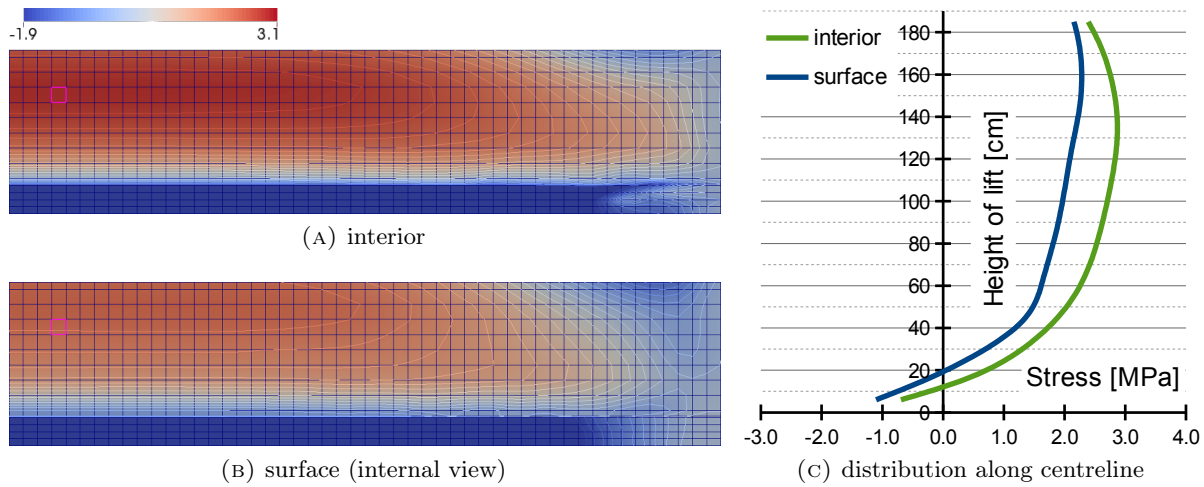


FIGURE 5.14: Distribution of σ_{xx} stresses in lift 1 of the CEOS.fr benchmark wall: cooling phase before initiation of cracking, $t = 516$ hrs (age of lift 180 hrs), MPa.

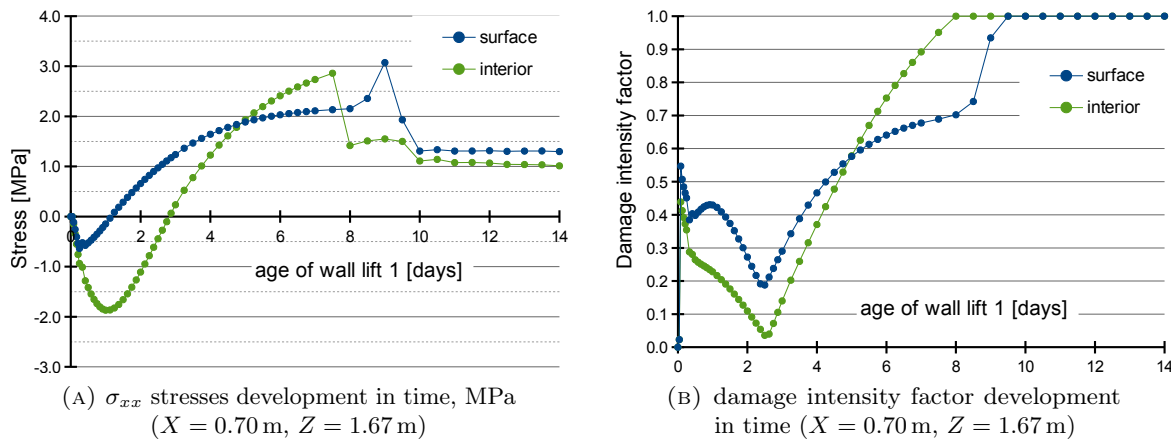


FIGURE 5.15: Time-development of stresses and damage intensity in lift 1 of the CEOS.fr benchmark wall.

time: compressive stresses were formed in the heating phase and tensile stresses developed in the cooling phase. After execution of the first lift compressive stresses appeared in the restraining foundation. Considerable massivity also influenced the character of stresses – their distribution in the cross-section resembled distribution of the self-induced stresses in lift 1 where the external restraint was weak due to relatively flexible foundation ($A_F/A_c = 0.2$). Moreover, significantly higher stresses developed in the interior of the wall due to the fact that the formwork was kept during the whole hardening process. Combination of these three facts explains the character of the observed cracking: the cracks were vertical due to the base-restraint but despite a weak foundation reached the whole height of the lift due to the considerable influence of the self-induced stresses; the first crack appeared in the interior of the wall (8 days after casting) but surface cracks followed (9.5 days after casting). The image of cracking observed in lift 1 complied with the cracking pattern observed in the real wall.

5.2.2 Tunnel wall

The wall analysed in this study was an internal wall of a tunnel presented in Sec. 2.4.4, which geometry is shown in Fig. 2.24 and cracking pattern in chosen segments in Fig. 5.21. The data for the analysis were provided courtesy of A. Hösthagen.

The analysed wall was cast in stages: either the segments were cast one after another, or even and odd segments were cast alternately. In consequence, three types of restraint conditions were formed: (1) segment restrained along the base only – C06 type, (2) segment restrained along the base and one side – C07 type – and (3) segment restrained along the base and both sides – C08 type. Firstly, all the foundations were placed and then the walls were cast.

The concrete of the segments was of class C35/45, made with 430 kg/m^3 low-heat cement ($Q_{\text{tot}} = 325 \text{ J/g}$) and $w/c = 0.40$ (170 kg/m^3 of water). The initial temperature of concrete 15°C and the ambient temperature was taken as constant and equal to 0°C . The relative humidity of air was taken as 60%. It was assumed that each element was cast one month after the previous one and that the formwork was removed 14 days after casting of the segment.

Fig. 5.16 presents the finite element mesh for all the three models with different restraint conditions. The whole foundation was cast before the walls. In the analysis half of the restrained wall and quarter of the restraining wall were modelled. Fig. 5.16d shows a complete mesh for the model in Fig. 5.16c; for the remaining models the mesh was analogical. Tab. 5.5 presents the time discretisation. Definition of the mesh and time discretisation were based on the recommendations given by JCI GUIDELINE [110]. Total restraint of vertical deformation of the foundation base was assumed because the foundation was formed into a continuous strip foundation at the moment of the wall execution and rotation of its ends did not have an influence on the behaviour of the analysed segment. The same material was assumed for all the wall segments and the foundation.

age of lift	TIME INTERVAL, h
0 – 12	2
12 – 24	3
24 – 48	4
48 – 72	6
72 – 120	8
120 – 336	12
336 – 348	2
348 – 360	3
360 – 384	4
384 – 408	6
408 – 456	8
456 – 504	12
504 – 672	24

x3

TABLE 5.5: Time discretisation used in the analysis of the tunnel benchmark wall.

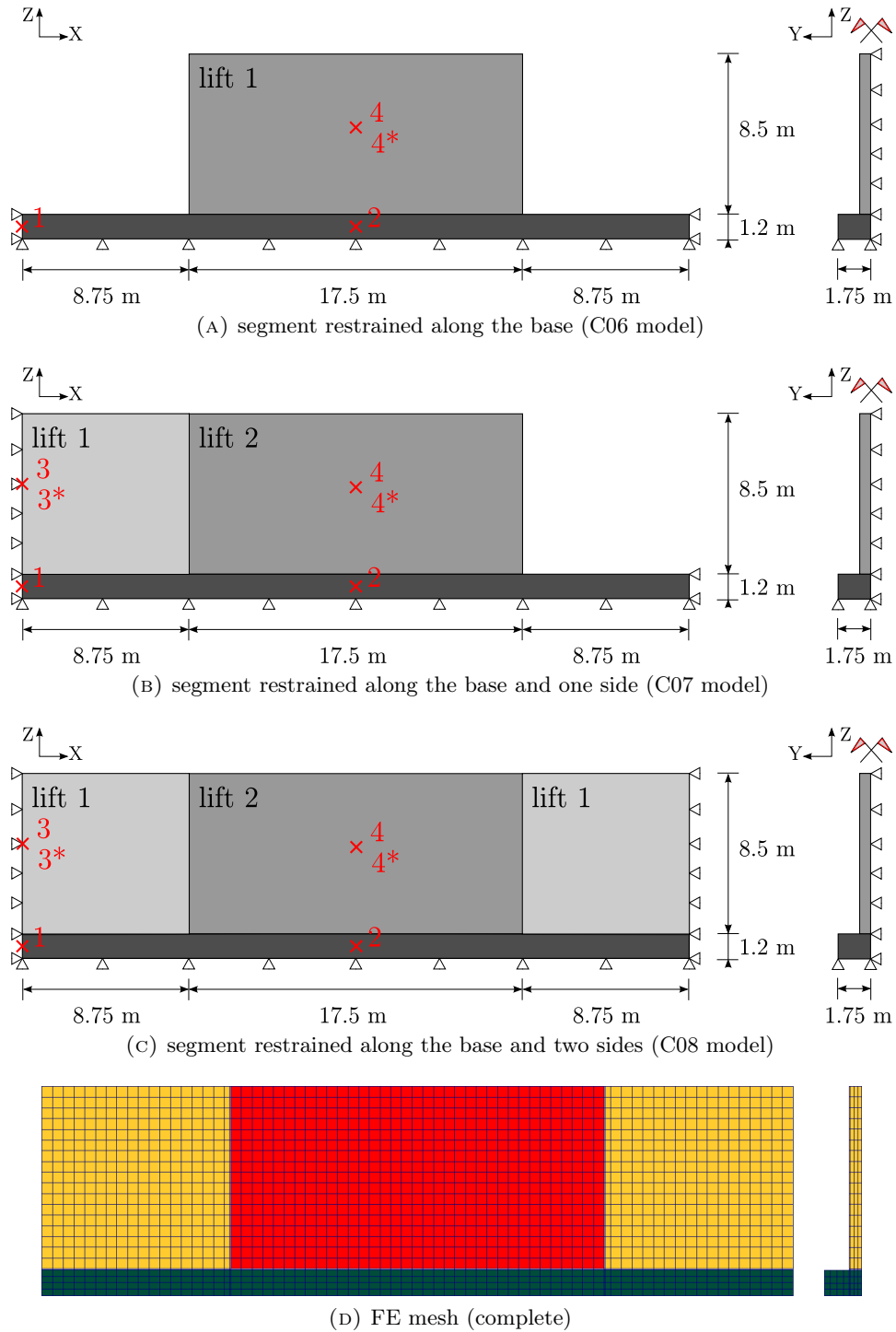


FIGURE 5.16: Models and FE mesh of the tunnel benchmark wall.

5.2.2.1 Thermo–physical analysis

Detailed thermo–physical parameters used in the analysis are shown in Tab. 5.6. The hydration heat development was described with the approximation function.

PARAMETER	UNIT	VALUE
thermal conductivity, λ	W/(m K)	2.2
specific heat, c_b	kJ/(kg K)	1.0
density, ρ	kg/m ³	2350
coefficient of heat exchange with environment, α_p	W/(m ² K)	3.0 covered 6.0 free
coefficient of moisture exchange with environment, β_p	m/s	$0.18 \cdot 10^{-8}$ covered $2.78 \cdot 10^{-8}$ free
thermal dilation coefficient, α_T	1/°C	0.00001
moisture dilation coefficient, α_W	–	0.002

TABLE 5.6: Thermo–physical parameters used in the analysis of the tunnel benchmark wall.

The temperature development and moisture loss in the central part of the analysed walls was practically identical irrespectively of the restraint conditions. Fig. 5.17 shows development of the temperature and loss of the moisture in the locations marked in Fig. 5.16 (points labelled with a star were located on the surface). The maximum core temperature was equal to 47.3°C in the side-restrained walls (lift 2 point 4 in C07 and C08) and 46.8°C in the base-restrained wall (lift 1 point 4 in C06) and restraining walls (lift 1 point 3 in C07 and C08). Lower temperature in lift 1 resulted probably from larger area of the heat exchange. The maximum surface temperatures were also equal in lift 2 – the side-restrained walls, 34.6°C (in point 4* in C07 and C08), as well as lift 1 – base-restrained wall (point 4* in C06) and restraining walls in other cases (point 3* in C07 and C08), 34.0°C. Moisture loss was also almost identical in all cases; after 28 days the moisture content decreased from 0.17 to 0.13 m³/m³ in the interior and as much as 0.09 m³/m³ on the surface. The moment of the formwork removal could be easily noticed both in the temperature decrease and moisture loss: a sudden drop and accelerated rate in both diagrams is visible.

The following figures present the maps of the temperature distribution. Fig. 5.18a shows the map of the temperature distribution in the C06 model at the moment of reaching of the maximum core temperature. Fig. 5.18c and Fig. 5.18e, respectively, present the moment when the maximum core temperature was reached in the restraining segments while Fig. 5.18d and Fig. 5.18f that moment in the restrained wall (C07 and C08 models). Temperature development was similar in all the elements and thermal field is practically uniform and symmetrical in all cases: it can be observed that the neighbouring elements had been always cooled down when the adjacent segments were cast. Analogical diagram for the moisture concentration in the restrained walls at the end of the analysis (age of wall 28 days) is presented in Fig. 5.18b on the example of the C06 model. It can be observed that the increased drying after the formwork removal was visible mostly near the surface.

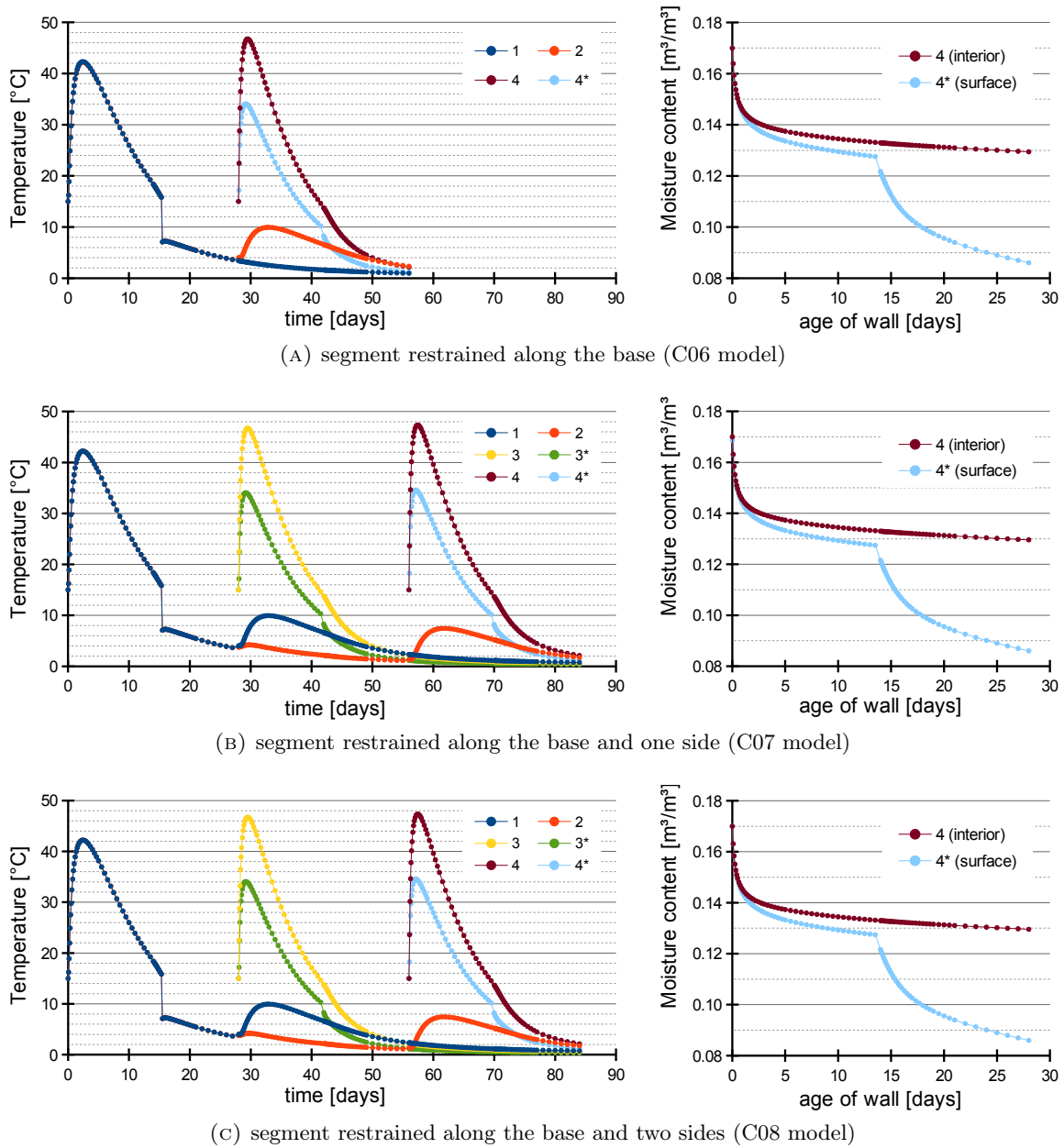


FIGURE 5.17: Temperature development and moisture loss in time in the tunnel benchmark wall.

5.2.2.2 Analysis of stresses and cracking

Detailed mechanical data used in the stress analysis are presented in Tab. 5.7. Viscoelasto-viscoplastic material model was used to determine stress development and damage intensity of the wall.

The maps of damage intensity for models C07 and C08 are shown in Fig. 5.19 and Fig. 5.20, respectively. Possible locations of cracks were marked in black. On the left side of the figure the damage intensity map in the first lift is shown at the moment right before execution of the second lift. In both cases similar pattern of damage was observed: a single, dominating through crack was formed which extended to approx. half of the wall's height. However, there are no maps of

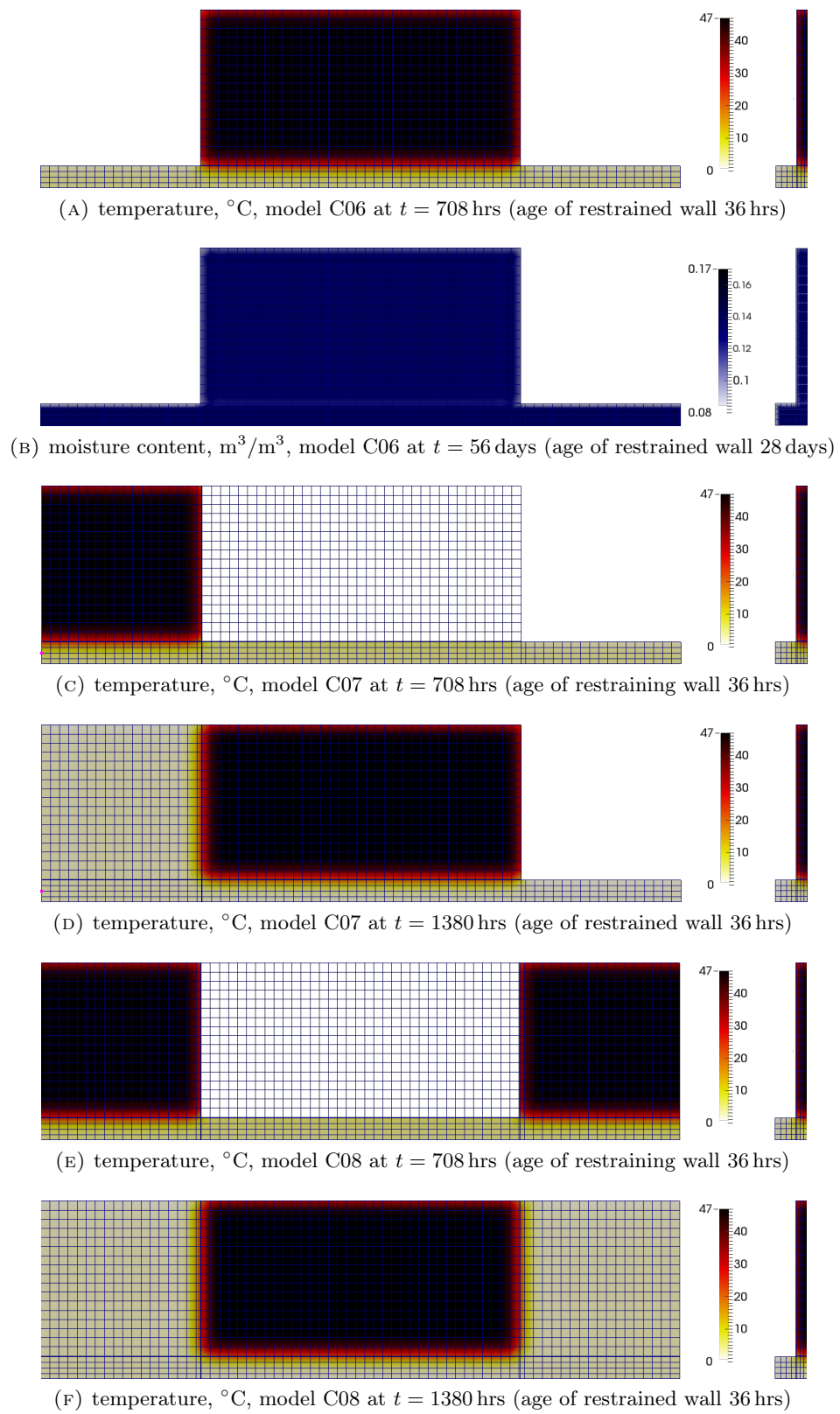


FIGURE 5.18: Temperature distribution and moisture concentration in the tunnel benchmark wall.

PARAMETER	UNIT	VALUE
compressive strength, f_c	MPa	53
tensile strength, f_t	MPa	3.7
modulus of elasticity, E_c	GPa	35
shape coefficient, s	–	0.25
time coefficient for tensile strength, n_f	–	1.0
time coefficient for modulus of elasticity, n_E	–	0.5

TABLE 5.7: Mechanical parameters used in the analysis of the tunnel benchmark wall.

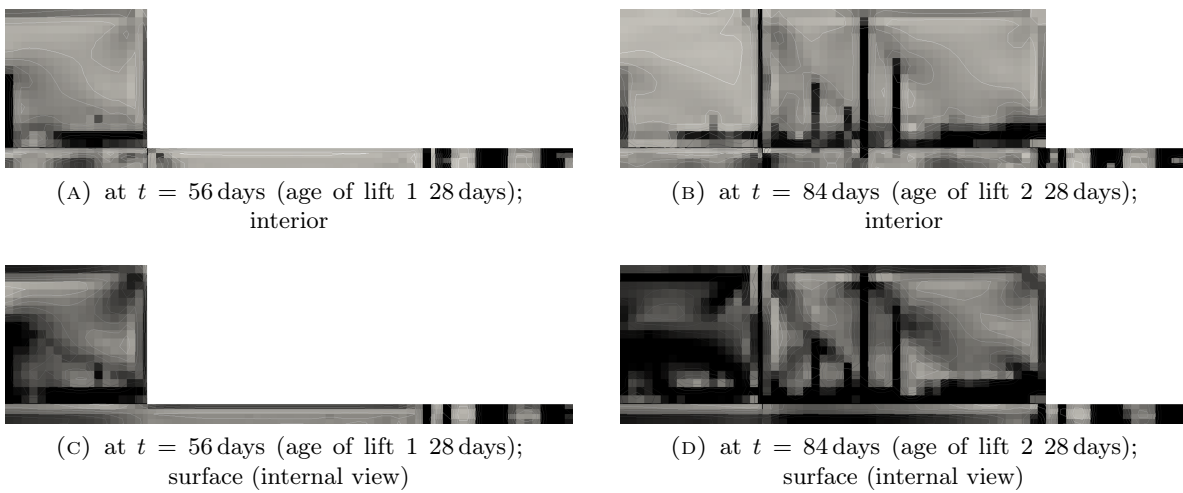


FIGURE 5.19: Damage intensity in the C07 model of the tunnel benchmark wall.

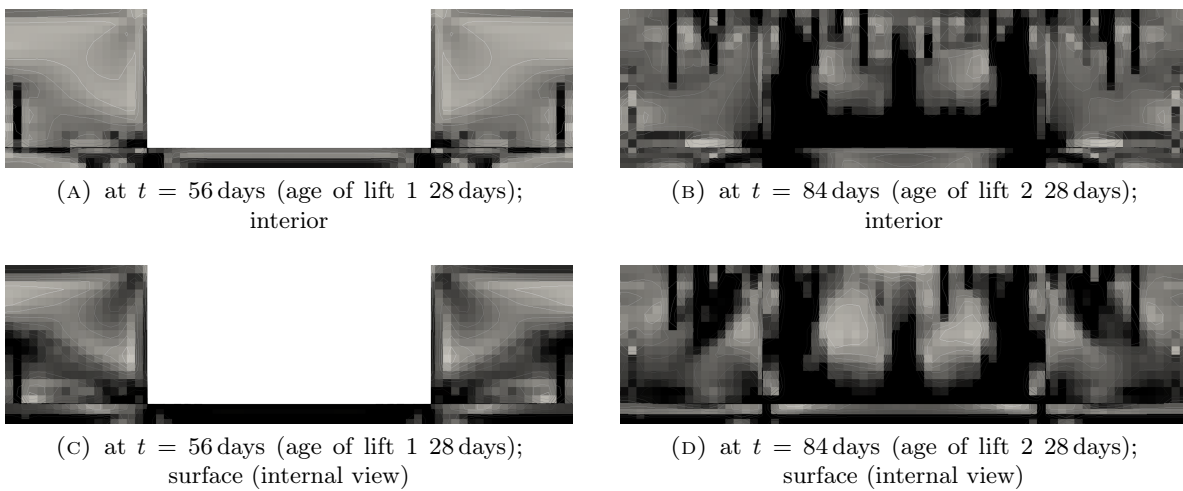


FIGURE 5.20: Damage intensity in the C08 model of the tunnel benchmark wall.

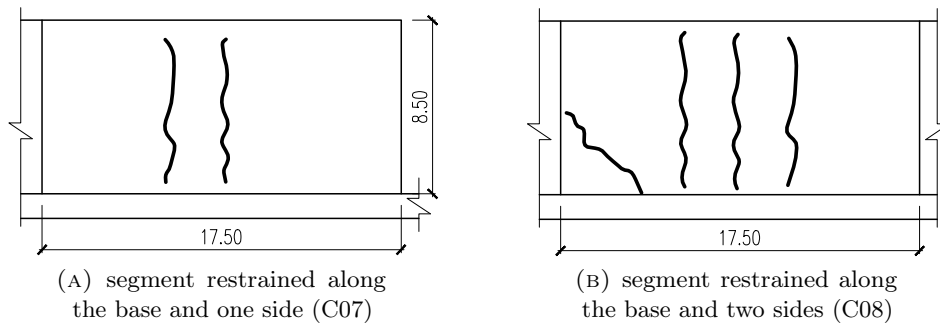


FIGURE 5.21: Cracking pattern in segments of the tunnel benchmark wall.

the actual cracking in such types of segments available so comparison cannot be made. As far as the segments of the second lift are concerned, in both cases (C07 and C08) through cracking appeared. In case of the C07 wall, restrained along the base and one side, two dominating cracks developed in the central part of the segment, starting slightly above the base joint and reaching almost whole height of the wall. This complied with the cracking image observed in the real segment (see Fig. 5.21a). In case of the C08 wall, due to the stiff end restraint, intensive cracking was observed. Vertical cracking developed in the central part of the wall reaching almost whole height of the wall. Moreover, cracks splayed towards the vertical joints were additionally formed. This also complied with the actual observations (see Fig. 5.21b).

These cracking patterns resulted from the character of stresses. Development of stresses in time is shown in Fig. 5.22 while Fig. 5.23 and Fig. 5.24 present distribution of stresses in the walls; the locations in which the time-development was presented are marked in pink. Presentation of the stresses in the walls was limited to the interior because the character of these stresses on the surface was similar. Irrespectively of the restraint conditions each wall exhibited a two-phase behaviour: compressive stresses occurred in the heating phase and tensile stresses in the cooling phase. In case of the segments restrained only along the base (lift 1 in C07 and C08) typical stress distribution was observed in both phases: the maximum value of the stress occurred above the joint (approx. 1.5 m); the crack started to develop at this location. At the moment of execution of the second lift the neighbouring restraining walls had already been cracked which can be observed in the stress map (reduction of stress in the cracked locations). Distribution of stresses in the segments of the second lift depended strongly on the restraint conditions. In the segment of the second lift in the C07 model (base- and side-restrained wall) the stress distribution was asymmetric. That is why asymmetric cracking was formed with cracks concentrating in the vicinity of the vertical joint and some cracks reaching almost whole height of the wall (not only half of that height as in case of the base-restrained wall). Symmetric stress distribution was observed in the segment of the second lift in the C08 model (base- and end-restrained wall). Due to additional end restraint stresses reached higher values. Stress intensity concentrated in the vicinity of joints – base joint and side joints – which, apart from intensive vertical cracking in the central part of the wall, led also to formation of cracks splayed towards the vertical joints.

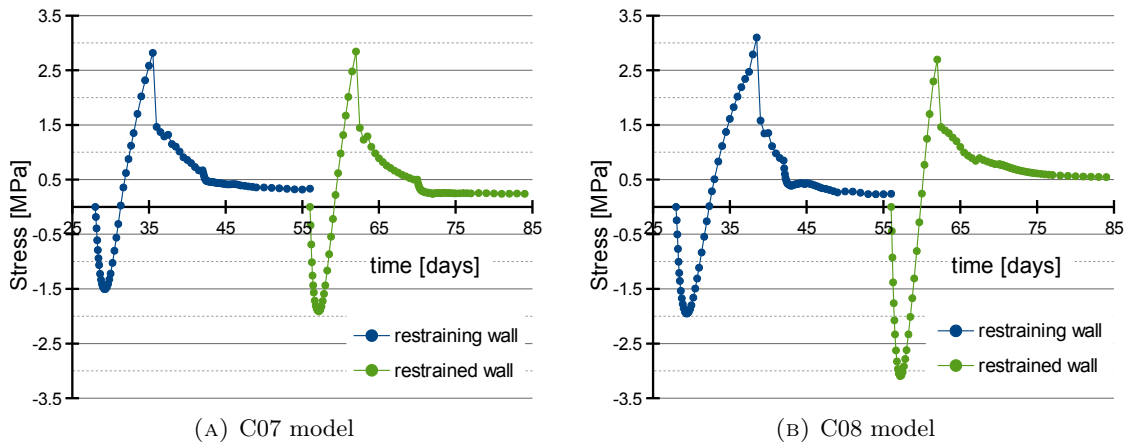


FIGURE 5.22: σ_{xx} stress development in time in the tunnel benchmark wall.

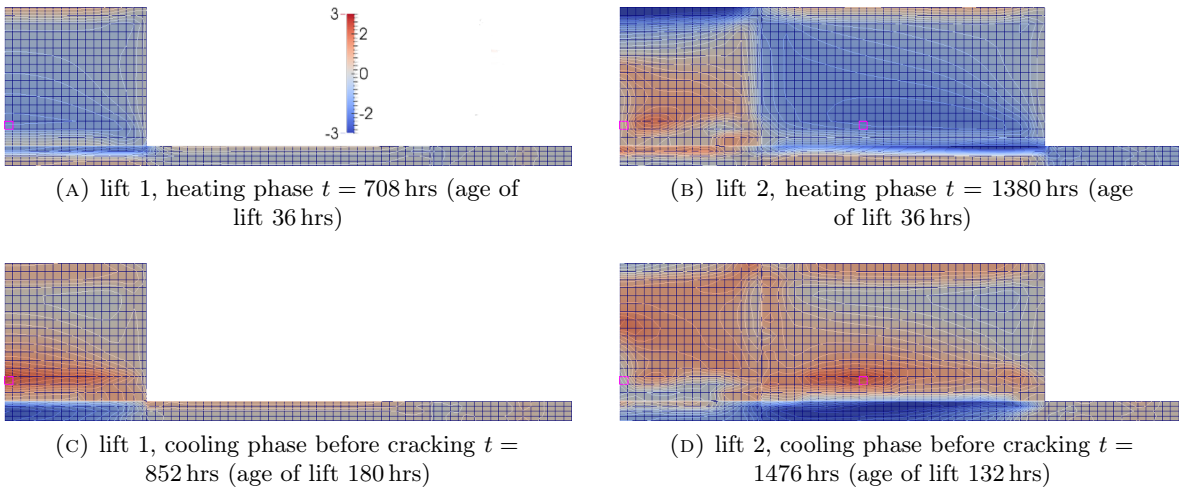


FIGURE 5.23: σ_{xx} stress distribution in the C07 model of the tunnel benchmark wall, MPa.

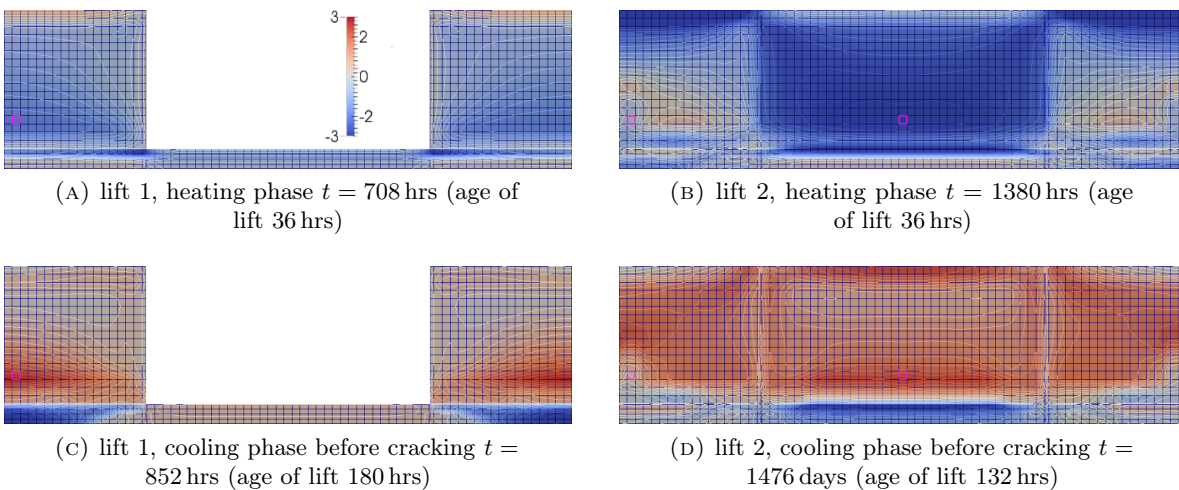


FIGURE 5.24: σ_{xx} stress distribution in the C08 model of the tunnel benchmark wall, MPa.

5.3 Influence of geometry and restraint conditions on early-age stresses in walls

Reinforced concrete walls are predominantly externally restrained and restraint stresses are induced in these elements. Their character and magnitude depend on the degree of restraint of the wall by the restraining body. The degree of restraint depends on the linear restraint exerted by the restraining body, L/H , and the ratio of the stiffness of the wall and the restraining body:

$$\gamma_R = \gamma_R \left(\frac{L}{H}, \frac{A_c E_c}{A_F E_F} \right). \quad (5.36)$$

Internal restraint is connected with the massivity of the element which relates the volume of the element, V [m³], and the total area of surfaces through which heat can be released to the environment, S [m²] [5]:

$$M_c = \frac{V}{S}. \quad (5.37)$$

Nevertheless, it was proven by DE SCHUTTER AND TAERWE [67] that there is no unique relationship between the massivity and the temperature development in the element (maximum temperature and temperature gradient). Thus, equivalent thickness was proposed as a measure of the internal restraint. The equivalent thickness represents the transport path of the heat from the element into the ambient environment. For an element with simple geometry such as a wall in which one-dimensional heat flow prevails the equivalent thickness is equal to half of the wall's thickness ($d_{eq} = 0.5 B_c$). However, for more complex geometries it was proposed to modify the massivity concept by introduction of the correction factor, γ_a , which represents the heat flow pattern in a spatial object. The equivalent thickness can be expressed as:

$$d_{eq} = \gamma_a M_c, \quad (5.38)$$

where the correction factor, γ_a , is a measure of the distance of the most inner point of the element volume to the exposed surface, relative to the distance of the centre of gravity of the heat flow area to the exposed surface.

5.3.1 Dimensions of the wall

Geometry and dimensions of the wall have major effect on the character and magnitude of the early-age stresses [140, 144, 145]. This influence was investigated in detail. The analysis was performed on 12 walls which geometrical characteristics are listed in Tab. 5.8. The concepts of the restraint factor as a measure of external restraint and the equivalent thickness as a measure of the internal restraint were used in the evaluation of stresses in the walls.

The same material was assumed in all the analysed cases and both for the wall and its foundation. The ambient temperature was set at $T_a = 20^\circ\text{C}$ and the initial temperature of concrete at $T_i = T_a + 5^\circ\text{C} = 25^\circ\text{C}$ (temperature increase due to mixing [110]). Relative humidity of air was set at 55%. The wall was assumed to be executed 2 weeks after the foundation. It was assumed that both elements were kept in formwork during the whole process of curing (to reduce the effect of drying). When the elements were in formwork, the top surface was covered with PE foil.

NO.	WALL				FOUNDATION			CHARACTERISTICS	
	L , m	H_c , m	B_c , m	A_c , m ²	H_F , m	B_F , m	A_F , m ²	L/H , [-]	A_F/A_c , [-]
01	15	1.50	0.7	1.05	0.70	1.50	1.05	10	1.0
02	15	2.14	0.7	1.50	0.70	2.14	1.50	7	1.0
03	15	3.00	0.7	2.10	0.70	3.00	2.10	5	1.0
04	10	1.42	0.7	0.99	0.70	1.42	0.99	7	1.0
05	10	2.00	0.7	1.40	0.70	2.00	1.40	5	1.0
06	10	3.33	0.7	2.33	0.70	3.33	2.33	3	1.0
07	7	1.40	0.7	0.98	0.70	1.40	0.98	5	1.0
08	7	2.33	0.7	1.63	0.70	2.33	1.63	3	1.0
09	7	3.50	0.7	2.45	0.70	3.50	2.45	2	1.0
10	5	1.67	0.7	1.17	0.70	1.67	1.17	3	1.0
11	5	2.50	0.7	1.75	0.70	2.50	1.75	2	1.0
12	5	3.57	0.7	2.50	0.70	3.57	2.50	1.4	1.0

TABLE 5.8: Geometrical data for the analysed walls.

The composition of the assumed concrete was as follows: cement CEM I 42.5N 365 kg/m³, water 160 l/m³ ($w/c = 0.44$), aggregate – sand 641 kg/m³ and granite 1289 kg/m³. The design class of concrete was C30/37. Composition of cement is shown in Tab. 5.9. The parameters used in the analysis are presented in Tab. 5.10 and Tab. 5.11.

COMPONENT	C ₃ S	C ₂ S	C ₃ A	C ₄ AF	SO ₃	CaO	MgO	$Blaine$, m ² /kg
AMOUNT [%]	64.0	15.0	10.0	8.0	3.3	0.8	0.6	367

TABLE 5.9: Mineral composition of cement used in the parametric study.

PARAMETER	UNIT	VALUE
thermal conductivity, λ	W/(m K)	2.5
specific heat, c_b	kJ/(kg K)	0.95
density, ρ	kg/m ³	2455
coefficient of heat exchange, α_p	w/(m ² K)	5.8 – PE foil
		3.6 – 1.8 cm plywood
		0.8 – soil
coefficient of moisture exchange, β_p	m/s	$0.10 \cdot 10^{-8}$ – PE foil
		$0.18 \cdot 10^{-8}$ – 1.8 cm plywood
		$0.01 \cdot 10^{-8}$ – soil
thermal dilation coefficient, α_T	1/°C	$10 \cdot 10^{-6}$
moisture dilation coefficient, α_W	–	0.002

TABLE 5.10: Thermo–physical parameters used in the parametric study.

The meshing of the wall and time discretisation of the analysis were made according to the recommendations of JCI GUIDELINE [110]. The scheme of the assumed model of an exemplary wall (09) with its finite element mesh is presented in Fig. 5.25. The time discretisation is shown in Tab. 5.12. In numerical analysis the coupled thermal and moisture fields were determined and then the stress and damage intensity development was analysed (viscoelasto–viscoplastic

PARAMETER	UNIT	VALUE
compressive strength, f_{cm}	MPa	38
tensile strength, f_{ctm}	MPa	2.9
modulus of elasticity, E_{ci}	GPa	33.0
coefficient s	—	0.25
coefficient n for tensile strength	—	0.67
coefficient n for modulus of elasticity	—	0.50

TABLE 5.11: Mechanical parameters used in the parametric study.

material model of concrete was applied). Simultaneously, stress distribution in the centre section was determined with the use of the analytic approach. The results were compared.

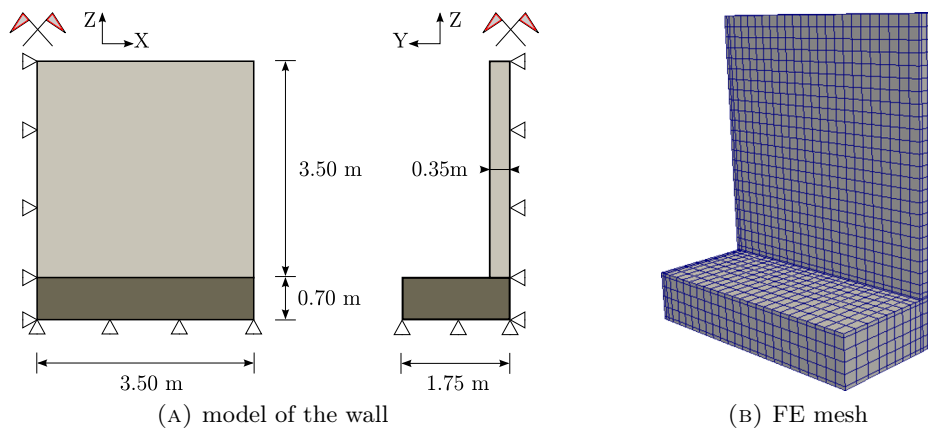


FIGURE 5.25: Model and FE mesh of an exemplary wall used in the parametric study.

TIME, h		TIME
age of foundation	age of wall	INTERVAL, h
0 – 6		1
6 – 24		2
24 – 72		3
72 – 168		6
168 – 336		12
336 – 342	0 – 6	1
342 – 360	6 – 24	2
360 – 408	24 – 72	3
408 – 504	72 – 168	6
504 – 1008	168 – 672	12

TABLE 5.12: Time discretisation used in the parametric study.

The maximum temperature and temperature difference in walls with simple geometry depend on the thickness of the wall [144]. Thus, all the walls were assigned with the same thickness which would assure almost equal self-induced part of the stress. The maximum temperature in the core of the wall varied between 47.0°C for the longest and highest wall (03) and 46.7°C for the shortest and lowest one (10). The shrinkage strain varied between 4.80 and $5.00 \cdot 10^{-5}$ analogically; the value of the shrinkage strain calculated acc. to MODEL CODE was equal to $4.51 \cdot 10^{-5}$. Fig. 5.26a presents development of the temperature in the interior of the wall 03

while Fig. 5.26b presents development of the shrinkage strain in the interior of that wall (due to limited drying this shrinkage can be correlated with autogenous shrinkage).

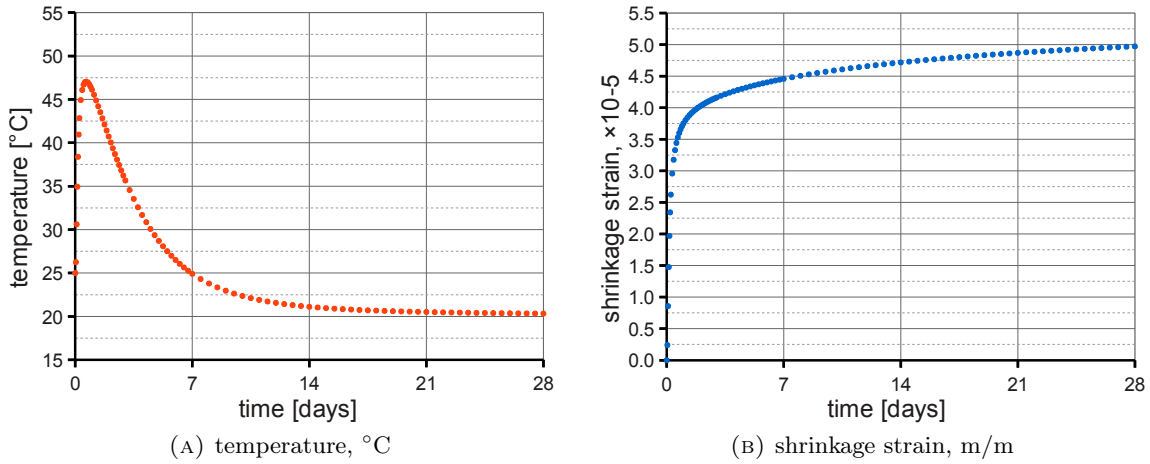


FIGURE 5.26: Temperature and shrinkage development in time in an exemplary wall.

Fig. 5.27a presents development of the temperature in the core of the wall with respect to the temperature development in the supporting foundation. The temperature increase in the wall led to heating up of the foundation, which at the moment of execution of the wall had already cooled down to the temperature of the surrounding air ($T_f \simeq T_a$). The ratio between the thermal strain during cooling of the wall and the foundation heated by the wall at the depth of the foundation was calculated as:

$$\gamma = \frac{\varepsilon_{T,\text{wall}} - \varepsilon_{T,d}}{\varepsilon_{T,\text{wall}}} \quad (5.39)$$

and it is shown in Fig. 5.27a. The thermal strain of the wall was determined as:

$$\varepsilon_{T,\text{wall}} = (T_{\text{max,wall}} - T_f) \alpha_T, \quad (5.40)$$

and analogically the strain at depth d of the foundation as:

$$\varepsilon_{T,d} = (T_{\text{max,d}} - T_f) \alpha_T. \quad (5.41)$$

The mean value of $\gamma = 0.7$ can be assumed for this particular case.

The final value of the ratio between the stiffness of the wall and the foundation was equal to 0.98 in all the cases; it was expressed by the ratio of the average moduli of elasticity, E_c/E_F . Development of the moduli of elasticity of the foundation and the wall as well as development of the stiffness ratio is presented in Fig. 5.28. It can be observed that the ratio of the stiffness increases rapidly in the first hours and at the moment when the maximum temperature is reached in the wall and cooling begins the stiffness of the wall is already 75% of the stiffness of the foundation.

For stress analysis it was assumed that the temperature and moisture content are uniform within the wall – this allows to eliminate the influence of the self-induced stresses and clarifies analysis. The temperature and shrinkage strain in each time step were assumed as equal to the temperature and shrinkage strain in the core of the element, as shown in Fig. 5.26a and Fig. 5.26b, respectively.

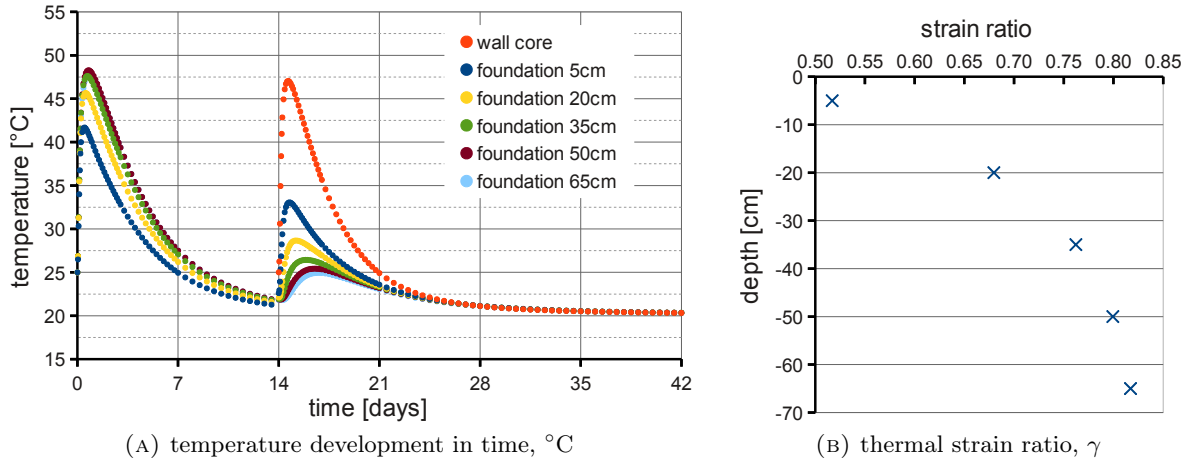


FIGURE 5.27: Relative thermal strain in an exemplary wall.

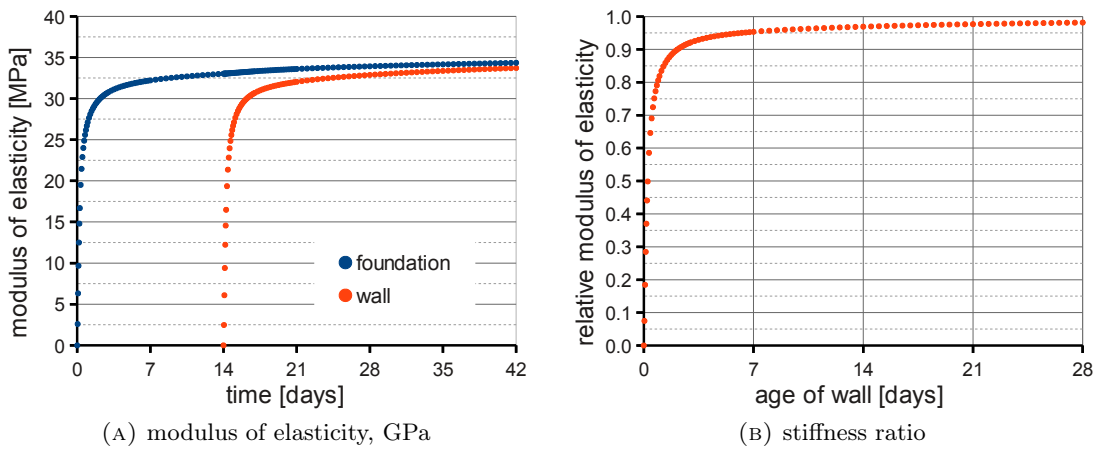


FIGURE 5.28: Relative stiffness development in time in an exemplary wall.

The influence of the linear restraint, expressed with the L/H ratio, was analysed. Distribution of the total stress differs between the walls with different L/H , nevertheless, it was also investigated if the effect of the restraint is the same in the walls with equal L/H but different dimensions. Dimensions of the walls were chosen in a way that wide range of L/H (from 1.4 to 10) was covered but with different walls representing the same L/H ratios.

Fig. 5.29 presents the results of the stress analysis. The results of the analysis are shown for the time $t = 16.5$ days (age of wall $t = 2.5$ days). The diagram in Fig. 5.29a presents distribution of the degree of restraint determined as a ratio between the actual stress, σ , and the stress caused by the same strain but under total restraint, $\sigma_{\text{fix}} = 1.5$ MPa, i.e. $\gamma_R = \sigma/\sigma_{\text{fix}}$. For comparison the degree of restraint determined with the analytic approach is shown in Fig. 5.29b and Fig. 5.29c. The degree of restraint acc. to ACI was calculated as a product of $K_F K_R$, with K_R factor taken from the diagrams (except for the $L/H = 1.4$ for which the K_R factor was calculated). The degree of restraint acc. to LULEÅ method was calculated taking into account the resilience and possibility of slip failure; the coefficients of the polynomial functions used for definition of the resilience factors, δ_{res} , are listed in Tab. 5.13 while the assumed values of the slip factors, δ_{slip} , are

listed in Tab. 5.14. No rotation was taken into account because total base restraint was assumed. The ratio between the moduli of elasticity was taken as $E_F/E_c = 1.10$ ($E_c/E_F = 0.91$).

L/H_c	a_0	a_1	a_2	a_3	a_4
7	1	-0.185	0.222	-0.253	0.127
5	1	-0.387	0.036	0.132	-0.031
3	1	-0.912	-0.041	0.189	0.054
2	1	-1.238	-0.541	1.158	-0.441
1.4	1	-2.362	0.931	1.581	-1.224

TABLE 5.13: Polynomial coefficients for calculation of δ_{res} acc. to LULEÅ method used in the parametric study.

wall no.	01	02	03	04	05	06	07	08	09	10	11	12
δ_{slip}	1	1	1	1	1	0.83	0.84	0.77	0.73	0.74	0.68	0.60

TABLE 5.14: Slip factor δ_{slip} acc. to LULEÅ method used in the parametric study.

Comparing the results obtained with different calculation methods it can be observed that the values of the restraint factor calculated acc. to the LULEÅ method comply better with the results of the numerical analysis than these calculated with the use of the ACI method – the latter one underestimated the value of the degree of restraint. Moreover, the LULEÅ approach reproduced a phenomenon observed by the author [142] that although in the walls with lower L/H the degree of restraint is generally lower, the influence of the restraining body is more pronounced in the close vicinity of the joint. Nevertheless, when analysing the degree of restraint obtained with the numerical analysis it is easily noticed that it is not equal in the walls with the same L/H , as suggested by the analytic approach. Therefore, the influence of length, L , and height, H , of the wall on the degree of restraint was further investigated.

Firstly, the diagrams of the degree of restraint distribution for the walls with the same length were compared to analyse the influence of the height of the wall. This comparison is shown in Fig. 5.30. The diagrams on the left show the actual restraint factor distribution while the diagrams on the right the “normalised” restraint factor. The normalised restraint factor, $\gamma_{R,1}$, was proposed by the author to be calculated by introduction of the modification factor, M_1 :

$$\gamma_{R,1} = \frac{\gamma_R}{M_1}. \quad (5.42)$$

It was observed that there is a direct relationship between the value of the modification factor, M_1 , and the ratio of the heights of the walls. The wall height ratio, ζ_H , was calculated for each length, L , in such a way the shortest wall was set a basic wall with the height H_{bas} and the heights of the other walls, H_i , were taken as the relative heights, i.e. the wall height ratio for the i^{th} wall was calculated as:

$$\zeta_H = \frac{H_{\text{bas}}}{H_i}, \quad (5.43)$$

with $H_{\text{bas}} < H_i$. Comparing the M_1 and ζ_H it was observed that with the increasing height of the wall the magnitude of the restraint decreases. This relationship becomes more pronounced as the length of the wall increases. It was graphically presented in Fig. 5.32.

Secondly, analogical analysis was performed on the walls with the same L/H ratios but different dimensions. This comparison is shown in Fig. 5.31. The diagrams on the left show the actual

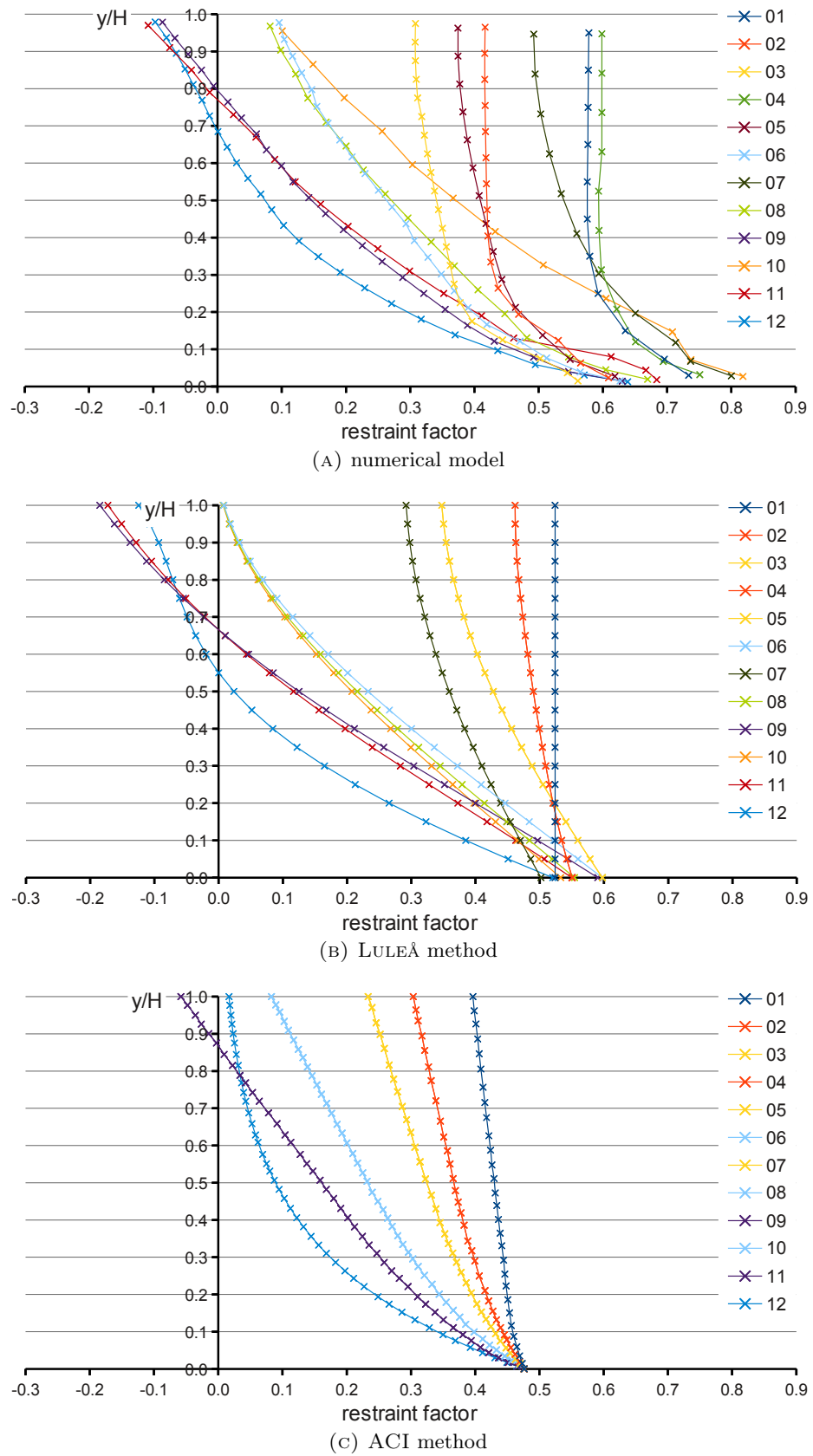


FIGURE 5.29: Degree of restraint distribution along the centreline of the walls.

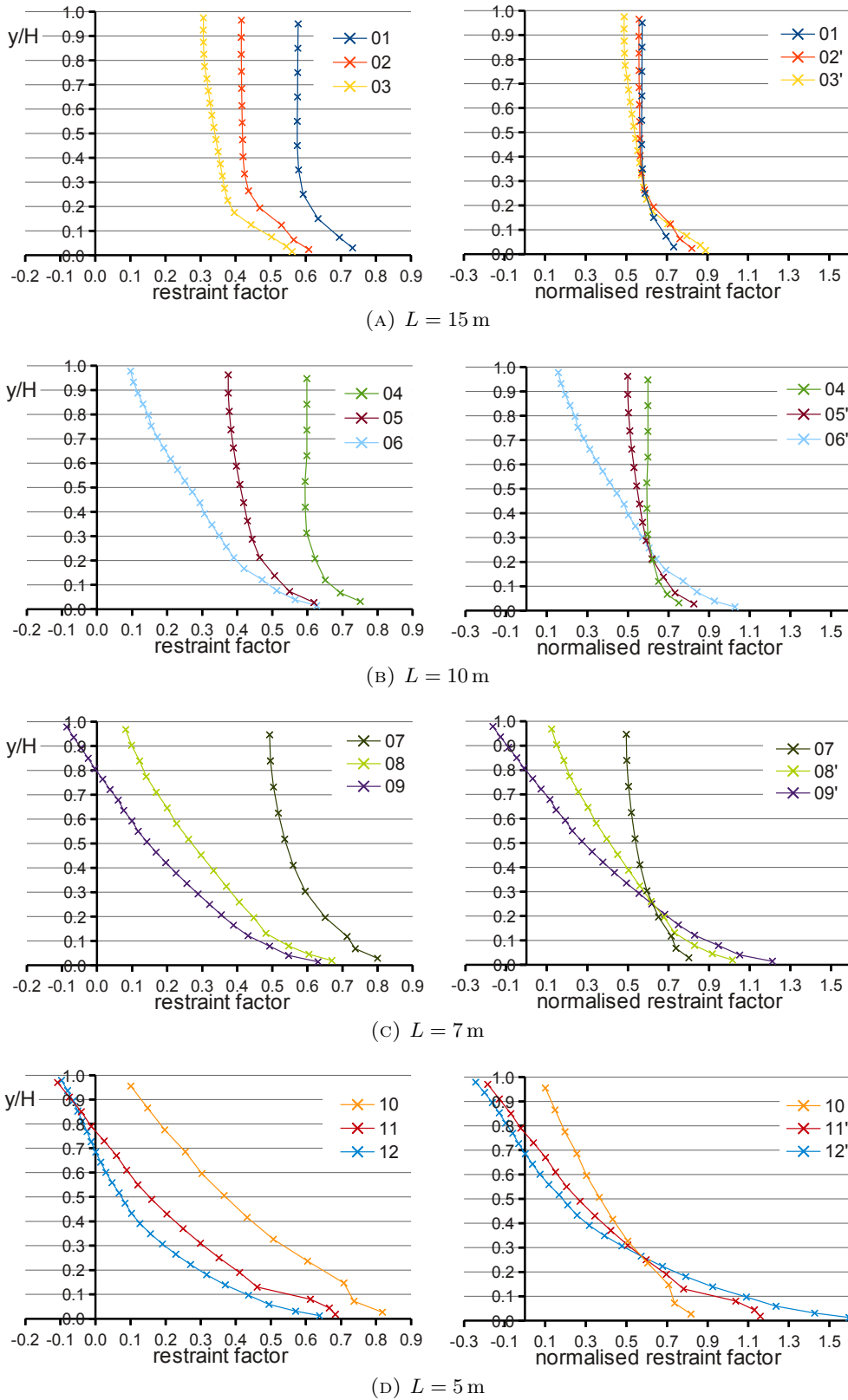


FIGURE 5.30: Degree of restraint for the walls with equal lengths and different L/H ratios.

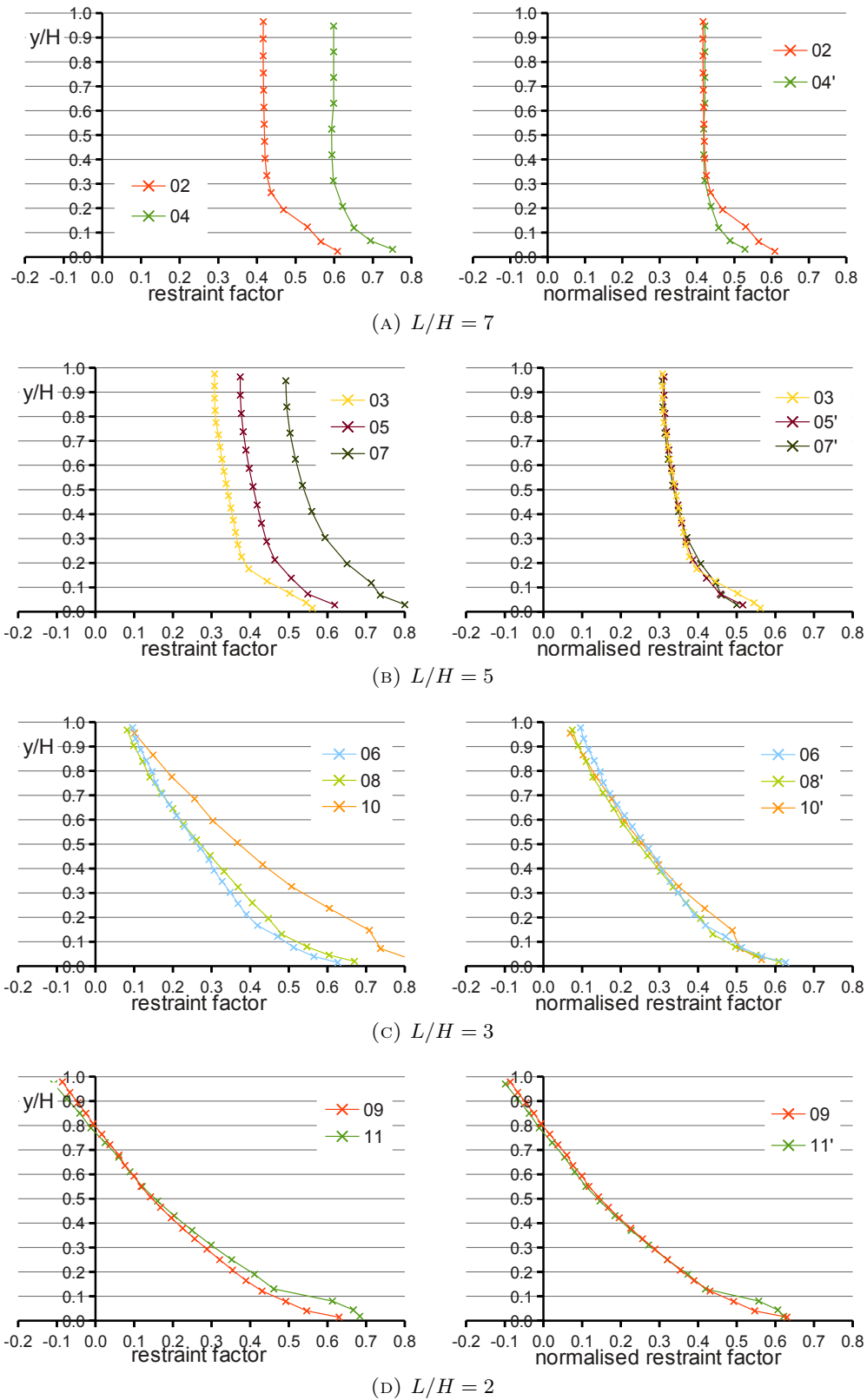


FIGURE 5.31: Degree of restraint for the walls with equal L/H ratios and different lengths.

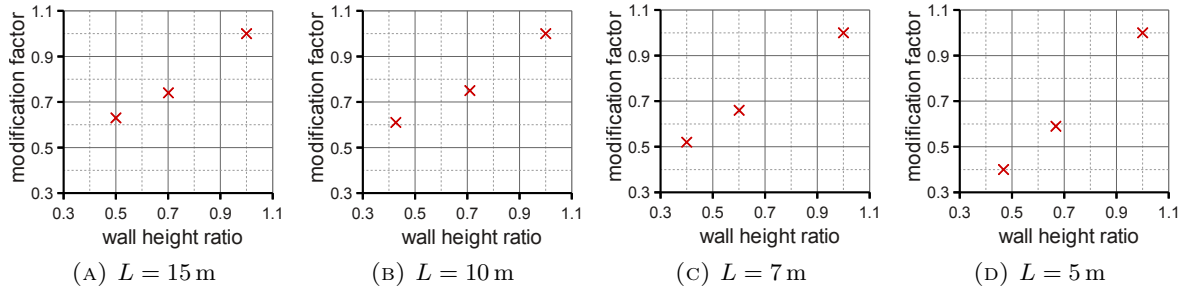


FIGURE 5.32: Modification factor M_1 for the walls with equal lengths and different L/H ratios.

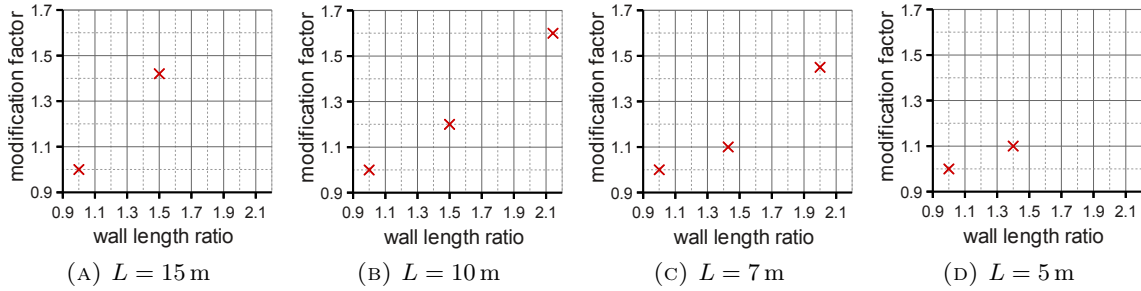


FIGURE 5.33: Modification factor M_2 for the walls with equal L/H ratios and different lengths.

restraint factor distribution while the diagrams on the right the “normalised” restraint factor. The normalised restraint factor, $\gamma_{R,2}$, was proposed by the author to be calculated by introduction of the modification factor, M_2 :

$$\gamma_{R,2} = \frac{\gamma_R}{M_2}. \quad (5.44)$$

It was also observed that there is a direct relationship between the value of the modification factor, M_2 , and dimensions of the wall; in this case it was the ratio between the lengths of the walls. The wall length ratio, ζ_L , was calculated for each L/H ratio in such a way that the longest wall was set as a basic wall with the length L_{bas} and the lengths of the other walls were taken as the relative lengths, i.e. the wall length ratio for i^{th} wall was calculated as:

$$\zeta_L = \frac{L_{\text{bas}}}{L_i}, \quad (5.45)$$

with $L_{\text{bas}} > L_i$. Comparing the M_2 and ζ_L it was observed that with the increasing length of the wall the magnitude of the restraint decreases. The influence of the wall length increases with the increasing L/H ratio. This relationship is shown in Fig. 5.33.

5.3.2 Support conditions

The character and magnitude of stresses in early-age walls depend not only on their geometry, but also on the support conditions. In the previous analyses it was assumed that the walls are fully base-restrained and that supporting foundation has no possibility to rotate. Thus, the influence of the subsoil with actual mechanical properties on the degree of restraint was analysed. Two walls with distinctly different geometries were chosen – a short wall (12, $L/H = 1.4$) and a long wall (02, $L/H = 7$). Two types of subsoil were also investigated: one which can be characterised

as soft soil and the other as a stiff one; mechanical parameters of these soils were taken after [161]. Models of the walls are presented in Fig. 5.34; Fig. 5.34c shows a finite element mesh on the example of the long wall. Thermo-physical and mechanical properties of the soils are listed in Tab. 5.15 and Tab. 5.16. The same thermo-physical parameters were assumed to clarify the comparison of stresses.

PARAMETER	UNIT	HARD SOIL & SOFT SOIL
thermal conductivity, λ	W/(m K)	1.5
specific heat, c_b	kJ/(kg K)	1.0
density, ρ	kg/m ³	2600
liquid diffusivity, D_{WW}	m ² /s	10 ⁻⁵
liquid diffusivity, D_{WT}	m ² /(s K)	10 ⁻⁹
coefficient of heat exchange, α_p	W/(m ² K)	1.5
coefficient of moisture exchange, β_p	m/s	0.01 · 10 ⁻⁸
thermal dilation coefficient, α_T	1/°C	10 · 10 ⁻⁶
moisture dilation coefficient, α_W	—	0.001

TABLE 5.15: Thermo-physical parameters of soil used in parametric study.

PARAMETER	UNIT	HARD SOIL	SOFT SOIL
coefficient for bulk modulus, K_o	-	900	100
coefficient for shear modulus, G_o	-	405	45
cohesion, c	MPa	0.02	0.05
internal friction angle, φ	°	40	25

TABLE 5.16: Mechanical parameters of soil used in parametric study.

Diagrams in Fig. 5.35 present distribution of the degree of restraint in walls with different support conditions and calculated with different methods. The results obtained with the numerical approach and the analytic approach (LULEÅ approach) were compared. In the numerical calculations the comparison was made for the degree of restraint calculated assuming total base restraint (full translational and rotational restraint) as well as taking into account the real stiffness of the founding soil. Analogical comparison was made for analytic calculations, however, in case when rotation of the wall was allowed the founding soil was infinitely stiff.

It can be observed that both numerical and analytic model present the same character of the behaviour of the walls: the influence of the possibility of rotation of the wall on the restraint factor is observed and it is more pronounced in the long wall (there is almost no influence of rotation in a short wall; according to the analytic approach the difference is not visible). The difference in results between the numerical and analytic model is caused by the fact that the actual length of the wall is not taken into account in analytic calculations (which was discussed in the previous section). It can also be observed that the stiffness of the soil influences the distribution of the restraint factor: when the soil is softer, larger rotation occurs. Also in the long wall, in which the effect of the real soil stiffness is more visible, it can be observed that in general the magnitude of the restraint is smaller when the wall is founded on the softer soil. Similar character of stresses accounting for the possibility of rotation can be also obtained with the approach postulated by FLAGA [83, 84].

Deformation of both walls on different soils is shown in Fig. 5.36. In the walls with the total restraint, the foundation has only a possibility of elongation/contraction; when real founding

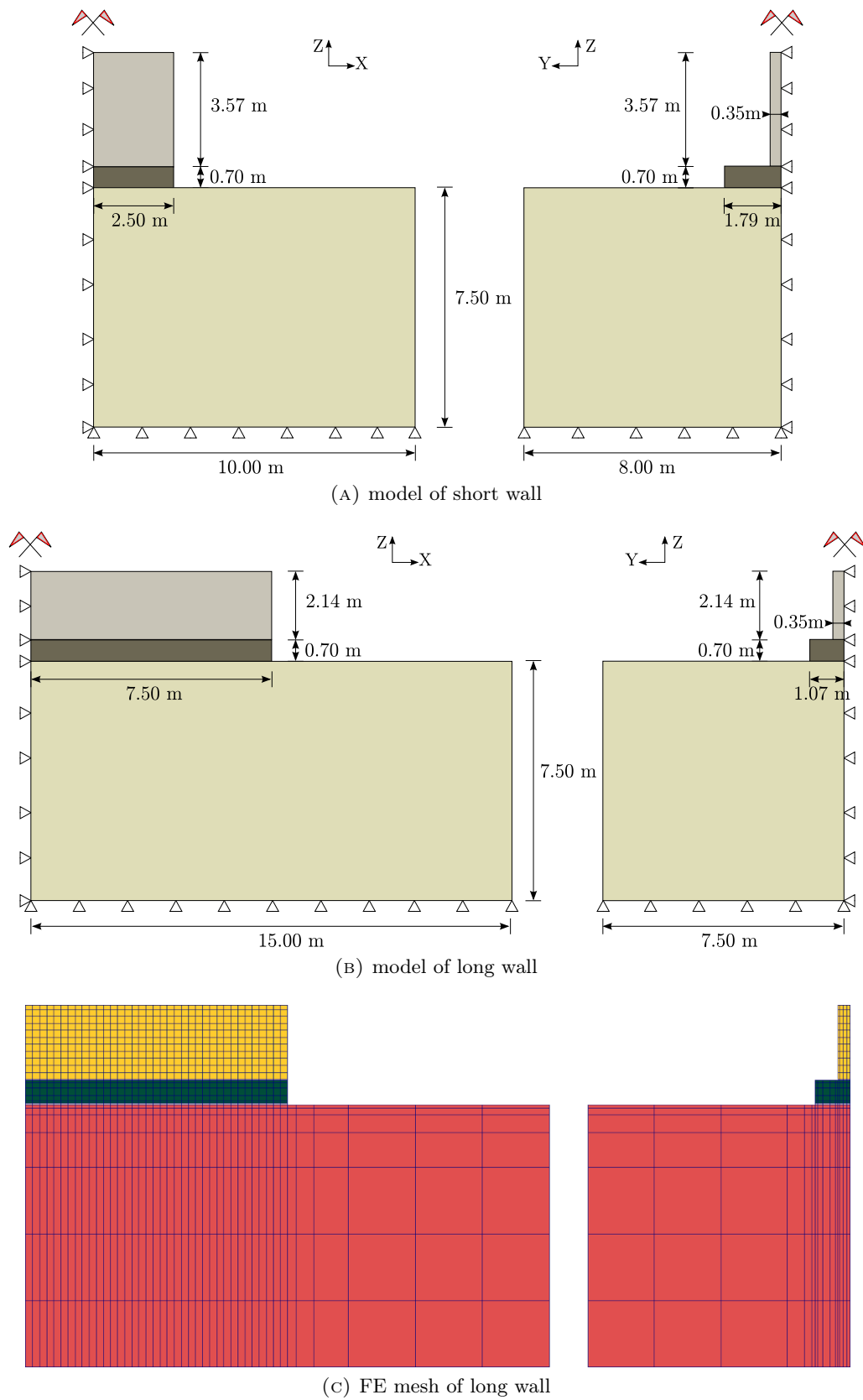


FIGURE 5.34: Models and FE mesh of the walls with real support conditions (founding soil).

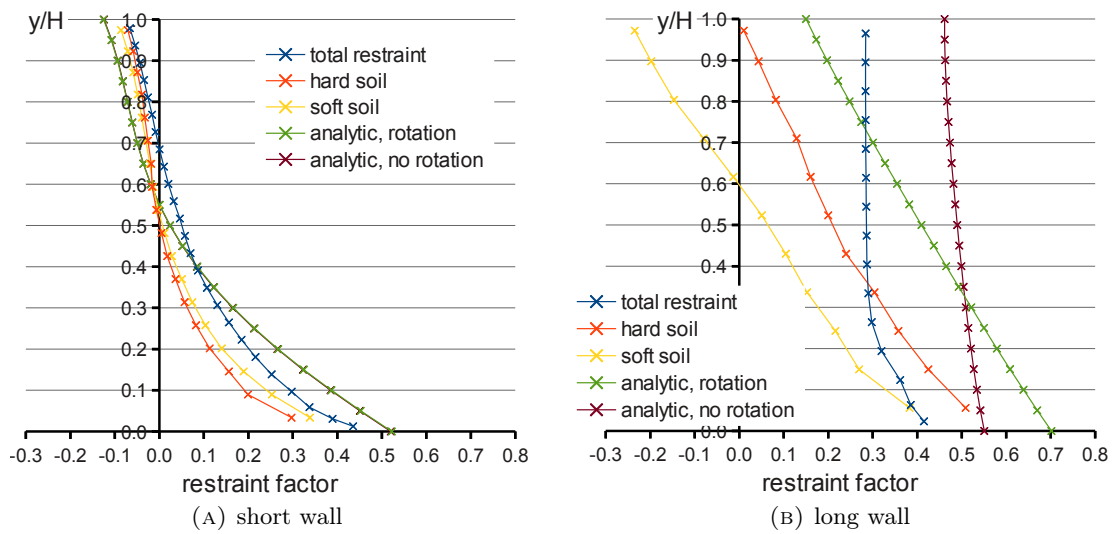


FIGURE 5.35: Degree of restraint in the walls with different support conditions.

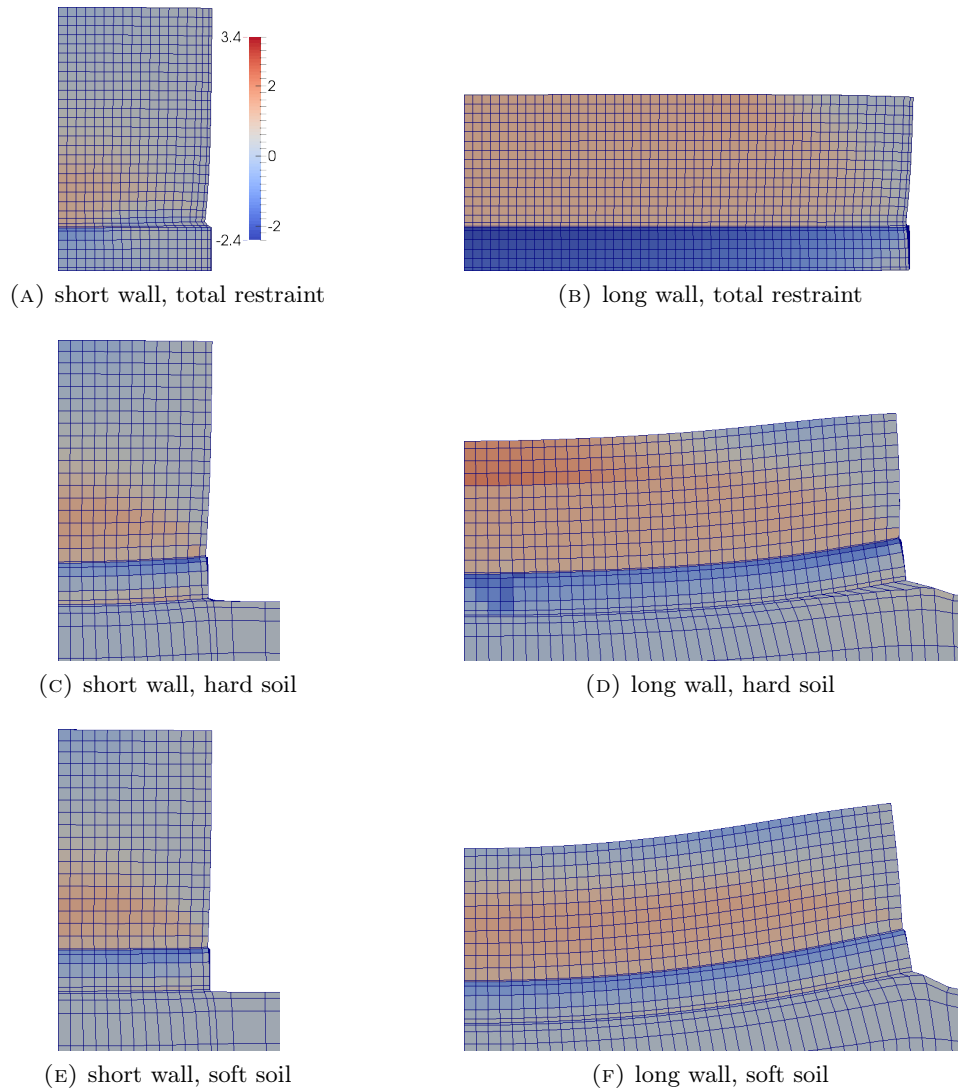


FIGURE 5.36: Deformation (scale 500:1) and σ_{xx} stresses, MPa, in the walls with different support conditions .

subsoil is taken into account, the rotation of the foundation occurs. The effect of the rotation is also visible in the maps of stresses, and is more pronounced on softer soil and in a longer wall. As it can be deduced from the diagram of the degree of restraint, by allowing the possibility of rotation the value of the tensile stress near the joint increases. Due to that fact in the long wall founded on hard soil cracking reaching approx. 60% of the wall's height occurred; concentration of stresses in the upper part of the wall results from the consequent redistribution of stresses in the cracked wall. In the wall supported on the softer soil the magnitude of the restraint was generally reduced. As a result the value of the stress decreased significantly (with respect to the wall founded on hard soil) and only a part of the wall (60%) was subjected to tensile stresses (with respect to 100% in the wall without the possibility of rotation). Nevertheless, the values of these stresses were lower than in the wall on hard soil and did not lead to cracking.

5.4 Influence of other factors on early-age stresses in walls

The most important factor when analysing early-age stresses is the temperature development in a concrete element. There are two main concerns: the maximum temperature rise, which influences the cracking risk due to the external restraint, and the maximum temperature difference, which influences the risk of cracking due to the internal restraint. Specifications typically limit the maximum temperature to 65 to 70°C and the maximum temperature difference to 15 to 20°C [3, 175, 190]. This simple criterion based on the engineering experience suggests that concrete can withstand the volume changes associated with such temperature differences. However, it is important to point out that this criterion has limitations. The limitations are related to externally-restrained structures in which lower temperature differences can induce cracks. CIRIA C660 [21] proposed the equation to calculate the maximum allowable temperature drop during cooling, ΔT_{allow} , and the maximum temperature difference in cross-section, $\Delta T'_{\text{allow}}$, in restrained elements:

$$\Delta T_{\text{allow}} = \frac{\varepsilon_{ctu}}{K_1 \alpha_T R_N}, \quad (5.46a)$$

$$\Delta T'_{\text{allow}} = \frac{\varepsilon_{ctu}}{K_1 \alpha_T R_i}, \quad (5.46b)$$

where:

- ε_{ctu} – tensile strain capacity of concrete;
- K_1 – modification factor for sustained loading and creep; it can be taken as $K_1 = 0.65$;
- α_T – coefficient of thermal expansion, $1/^\circ\text{C}$;
- R_N – translational restraint factor;
- R_i – internal restraint factor.

Since early-age effects are caused by a mutual action of thermal and moisture volume changes, the temperature change should include both the actual temperature change, ΔT , and moisture-induced shrinkage expressed as the equivalent temperature change, ΔT_W .

The magnitude of the early-age stresses and the resulting risk of cracking depend on many factors. Apart from the geometry, dimensions and support conditions, the variables that affect the rate of the temperature increase, the maximum temperature and the temperature difference as well as the autogenous shrinkage and the rate of the moisture loss due to drying are [138]:

- thermo-physical properties of early-age concrete;
- conditions during casting and curing of concrete;
- technology of concreting;
- environmental conditions.

The methods used currently to minimise the cracking risk of concrete structures relate to the factors enlisted above. The methods of the temperature control include optimal concrete mix design, concrete cooling before or after placement, the use of smaller lifts and insulation. Early-age cracking sensitivity is also associated with moisture evaporation through the exposed surfaces of a concrete element. This loss of water while the concrete is still in plastic stage results in plastic shrinkage and later in drying shrinkage. Both plastic and drying shrinkage are highly dependent on the environmental conditions. Additionally, significant autogenous shrinkage can develop, especially in concrete with low w/c ratio. The plastic and drying shrinkage are usually limited by application of proper curing conditions such as providing water to the exposed surfaces of concrete or sealing the surfaces to prevent evaporation. Autogenous deformations are reduced by internal curing of concrete. Finally, it must be remembered that mechanical properties of concrete, including tensile strength, modulus of elasticity and creep are functions of the maturity of concrete; they are not only time- but also temperature-dependent. The following sections discuss further the factors that have an influence on the early-age stresses in walls.

5.4.1 Concrete mix composition

Composition of concrete mix determines – to the great extent – physical and mechanical properties of the hardening and hardened concrete. Ones of particular importance are thermal properties of early-age concrete, such as the rate of heat development, q , and the total amount of heat, Q_{tot} , specific heat, c_b , thermal conductivity, λ , and coefficient of thermal expansion, α_T . It has also influence on other physical properties, such as autogenous shrinkage, ε_{ca} . Mechanical properties of concrete and the rate of their time-development also depend strongly on the amount and properties of concrete components, especially the amount and type of cement. The following factors connected with the concrete mix design have an influence on the early-age concrete behaviour:

- type, amount and fineness of cement, including type and amount of supplementary cementitious materials,
- water content and water-to-binder ratio,
- type and composition of aggregate,

- type, composition and amount of fibre reinforcement.

Design of the optimum concrete mix is considered as the easiest way to minimise negative effects in early-age concrete. The optimal concrete mix design usually relates to application low-heat cement, minimisation of the total amount of cement per unit volume of concrete or partial replacement with SCMs and use of cement with low fineness [110]. The cement-to-binder ratio is also crucial - structures with denser cement paste matrix (lower w/c) are more prone to cracking [29].

The use of lower-heat Portland cement and blended cement, especially with fly ash and slag addition, is recommended mostly because the reduction of the total hydration heat results in smaller thermal strains. Moreover, higher rate of creep is observed in blended cement which reduces early-age stresses [194]. In general, autogenous shrinkage is also decreased in blended cements [174, 180] and it is lower when more than one SCM component is used [7]. However, it is reported that addition of some SCMs may increase the hydration rate and the total amount of hydration heat, and consequently autogenous shrinkage and thermal strain (mainly silica fume is referred [119, 180]) and that drying shrinkage is higher in blended cements [7]. Furthermore, blended cements exhibit slower development of mechanical parameters (tensile strength, modulus of elasticity) [149, 174] with the rate of development decreasing with the increasing SCMs content [7]. Concrete mixes made of coarser cements and with higher w/c ratio also exhibit such characteristics [29]. Consequently, in elements made of these concrete mixes, despite smaller strains, cracking may occur almost as early and be as intensive as in OPC concrete elements [7, 29, 148].

Early-age properties and behaviour of concrete elements is also governed by the characteristics of aggregate. It was presented in previous sections that the aggregates used for production of concrete vary in thermal properties (see Sec. 4.1.3.1) and thus highly influence the magnitude of thermal strains in a concrete element [143, 195]. The type of aggregate influences also the strength of concrete – generally concrete made of crushed aggregate (basalt, granite) presents higher strength than this made of rounded aggregate. The level of water saturation influences the magnitude of autogenous shrinkage of concrete: saturated aggregates are used to minimise autogenous shrinkage, however, there is no direct correlation between the degree of saturation of the aggregate and the magnitude of autogeneous shrinkage [56].

The influence of concrete mix composition was analysed by the author [148]. The analysis focused on the type and amount of cement. In each case a mix was designed under the assumption that the final values of mechanical parameters of the mature concrete were the same. Considered mixes are shown in Tab. 5.17. Fig. 5.37a shows the damage intensity factor development in time for concrete mixes with different types of cements while Fig. 5.37b presents the comparison of the cracking risk depending on the type and amount of cement. For concrete mixes with the same type of cement there was a direct correlation: greater amounts of cement generated more heat and exerted greater stresses on the structure thus posing higher risk of cracking. Every 50 kg of cement increased the cracking risk by about 7%. When different types of cements were used, there were two factors of importance: the total amount of heat together with its development rate and the rate of mechanical parameters development. Cements with lower hydration heat generate lower hardening temperatures, however, they have slower rate of the mechanical parameters development. Therefore, until the concrete hardens, the value of the elasticity modulus of the

element is lower comparing to the elements made of cements with fast strength development. It is a serious issue in restrained concrete structures where stresses arise mainly as a result of an external restraint such as a stiffer foundation. Moreover, the tensile strength development is slower. Thus, it was observed that in the wall made of CEM III the damage risk was the same as in the wall made of CEM I.

	Mix 1	Mix 2	Mix 3	Mix 4	Mix 5	Mix 6
cement type	CEM I 42.5R			CEM II B-S 42.5R	CEM III/A 42.5N	CEM V/A 32.5R
cement amount, kg/m ³	325	375	425	375	375	375
Q_{tot} , kJ/kg		508		466	469	396
water, kg/m ³	147	170	193	170	170	151
aggregate, kg/m ³	1973	1868	1762	1868	1868	1918
λ , W/(m K)	2.54	2.52	2.57	2.52	2.52	2.53
c_b , kJ/(kg K)	0.99	0.95	0.92	0.95	0.95	0.92
s parameter	0.20	0.20	0.20	0.20	0.25	0.25

TABLE 5.17: Concrete mix compositions used in the parametric study of the influence of the concrete mix composition of the cracking risk of walls [148].

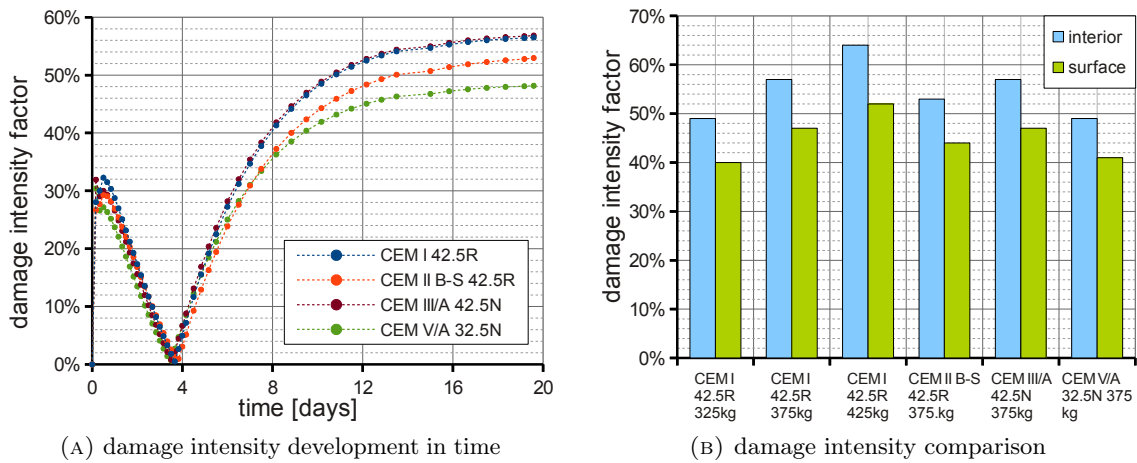


FIGURE 5.37: Damage intensity in the walls made of concretes with different cements [148].

To mitigate cracking induced by the thermal–shrinkage strains fibres are added into the concrete mix. Their primary aim is to increase the tensile strength and arrest crack propagation in order to limit the crack width. Among the vast assortment of fibres the metallic fibres serve best to increase the tensile strength of concrete, however, a relatively high dosage ($> 2\%$) of fibres is required to achieve a visible effect [203, 207]. Addition of polypropylene (PP) fibres, on the other hand, improves the ductility of concrete [12, 203]. It is advised to blend different types of fibres to achieve the best results [12]. A change in the process of crack formation is observed in the fibre-reinforced early-age concrete with respect to the plain concrete: although primary cracks are formed in a similar manner as in the plain concrete (stress development before cracking is similar irrespectively of the fibres dosage), the moment of their formation is delayed and numerous secondary cracks are formed thanks to which the width of the cracks can be reduced [207].

5.4.2 Environmental conditions

Environmental conditions during the period of concrete hardening have an influence on the rate of the heat and humidity exchange between the structure and the ambient environment. As such,

the environmental conditions determine the values of the temperature and humidity, the rate of their development and gradients. The following environmental factors have an influence on the early-age stresses:

- ambient temperature and relative humidity of the air – their magnitudes as well as diurnal and seasonal variations;
- magnitude and variations of the wind velocity and wind direction;
- sun exposure and sun radiation;
- temperature, humidity and physical properties of the subsoil.

The most important role in the cracking risk of walls is played by the initial temperature of the concrete mix, the ambient temperature and their relationship [160]. Heat exchange is driven by the difference between these two temperatures and the heat flux increases as this difference increases. Generally, favourable conditions for concreting of a massive structure are considered as low but positive ambient temperature. It was observed that concrete curing should be performed under moderate environmental conditions (ambient temperature of 15°C) with initial cooling of the concrete mix additionally applied [140]. It is advised to commence concreting at night, especially in summer, both due to the lowest diurnal temperature and sun action [110, 143, 195, 227]. Analogically, the moisture flux is driven by the difference between the relative humidity of concrete and air, and is greater in dry climates than in wet ones.

The rates of the heat exchange and drying are also influenced by the wind velocity: Eq. 4.44 express the observed fact that the heat flux increases with an increasing wind velocity due to the increased convection. It is also pointed out that higher wind velocity increases the rate of drying of the concrete surface and contributes to drying shrinkage [5].

Finally, the properties of the subsoil influence the development of thermal and moisture fields and stresses in a concrete element. The temperature and humidity of soil determine the heat and moisture exchange rate between the structure and the subsoil via the contact surface at the base. This temperature and humidity difference is a driving force for the heat and moisture migration. Mechanical properties of the subsoil, especially its friction and cohesion properties and stiffness, are also of great importance [177]. Friction and cohesion properties of soil determine the level of the translational restraint exerted by the subsoil on the structure: low-friction/cohesion soil exerts almost no restraint to translation and the restraint increases with the increasing friction/cohesion. Stiffness of the subsoil, on the other hand, determines the level of the rotational restraint – it defines the extent to which the structure can bend into the ground. Stiffer soils exert greater rotational restraint.

5.4.3 Technological conditions

The character, magnitude and rate of development of the early-age stresses depend on the conditions during casting and curing of the structure. These conditions can be modified and controlled with an appropriate technology. From the structural point of view the cracking of

walls can be mitigated by the construction sequence which determines the restraint conditions exerted to the wall. There are the following possibilities to realise the wall:

1. by continuous casting: when the wall and the foundation are cast in a single lift by continuous pouring of concrete;
2. by sequential casting in which the wall is cast in segments; this can be realised in a following manner:
 - the foundation is cast in the first step and then the wall is cast in the second step; the wall is restrained along the base only;
 - the foundation is cast in the first step and the wall is cast in vertical/horizontal segments; the segments of the wall can be restrained along one, two or three edges and the restraint conditions change in time.

The restraint conditions determine the character of stresses developing in the early-age wall while the length of the breaks between the subsequent lifts influences their values (see Sec. 5.2.2.2).

Another important factor is the initial temperature of a concrete mix. Typically, the initial temperature of a concrete mix is more or less equal to the ambient temperature. Due to the temperature increase during hydration the difference between the temperature of the concrete element and the ambient temperature increases. That is why it is advised to cool the concrete mix before placement in order to reduce the future temperature difference [130, 139]. The choice of the method for mix pre-cooling depends on the local conditions as well as the willingness and experience of the concrete supplier. The least costly way is to use the chilled water which pre-cools the concrete by up to 3°C [4, 117]. The initial temperature of concrete mix can be then estimated as follows [110]:

$$T_i = \frac{0.2 (T_{ag} W_{ag} + T_c W_c) + T_w W_w}{0.2 (W_{ag} + W_c) + W_w}, \quad (5.47)$$

where:

- $T_{i(i=ag,c,w)}$ – temperature of i^{th} component of concrete mix, °C;
 $W_{i(i=ag,c,w)}$ – mass of i^{th} component of concrete mix related to 1 m³ of concrete mix, kg/m³;
 ag, c, w – index related to aggregate, cement and water, respectively.

However, it should be remembered that the actual initial temperature of the concrete mix will be a little bit higher because of the mechanical work made during the process of the concrete mix preparation. Shaved or chipped ice can substitute up to about 75% of the mix water to reduce the concrete temperature by up to 20°C [4, 175]. In extreme pre-cooling liquid nitrogen is used to pre-cool the concrete mix and in this method the initial temperature can be reduced by about 35°C [4, 117]. However, the liquid nitrogen cooling requires highly specialised equipment and as a result it is the most expensive method.

The influence of the initial temperature and difference between the initial temperature of concrete and the ambient temperature was investigated by the author [139, 148]. The following cases

were taken into consideration: the external temperature of 15, 20 and 25°C, without pre-cooling of the concrete mix, and additionally in each case lowering of the mix initial temperature by 5 and 10°C. Diagrams in Fig. 5.38 present the expected temperature and the resultant damage intensity in walls with different initial and ambient temperature. It was observed that concrete curing should be performed under moderate environmental conditions (ambient temperature of 15°C) with initial cooling of concrete mix additionally applied. In such case pre-cooling has the greatest efficiency: it allows for limitation of the self-heating temperatures and moisture removal, reduction of the compressive stresses, delaying inversion and consequently reduction of the tensile stresses and cracking.

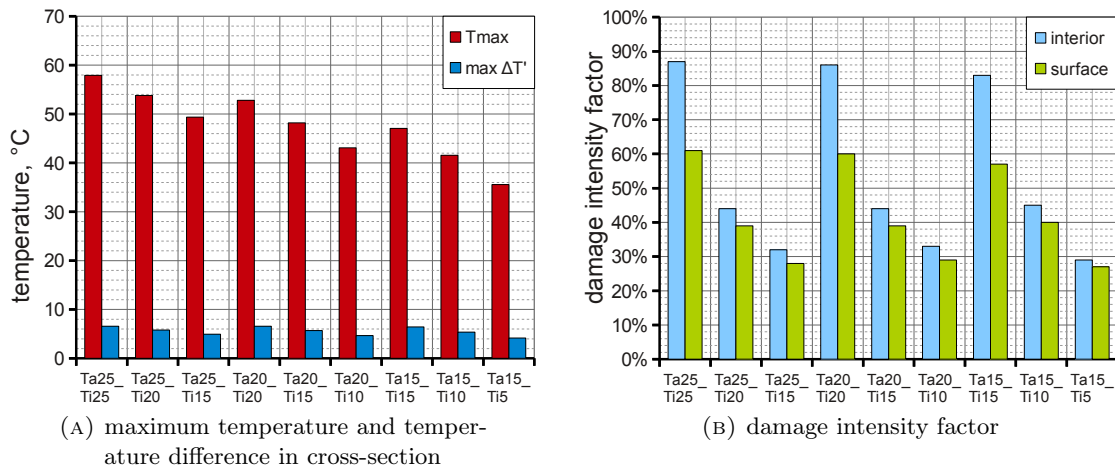


FIGURE 5.38: Influence of the initial and ambient temperature on the cracking risk of walls [139].

The conditions in which concrete of the element is cured have also influence on the developing stresses. The following means have an effect on the early-age behaviour of concrete walls:

- type of formwork and time of its removal;
- application of thermal and water-proof insulation;
- surface cooling;
- internal curing by introduction of pipe-cooling in the early-age element and/or pipe-heating in the restraining element.

Commonly applied methods to control the temperature differences within the maturing concrete elements include application of insulation in addition to classical formwork and delayed formwork removal [107, 139, 156]. For insulation, in most cases concrete insulating blankets are used, however, any insulating material is usually acceptable; cracking risk decreases with lowering the value of thermal conductivity of the covering material [159]. The important issue is that insulation should be kept in place until the hottest portion of concrete cools to the ambient temperature [139]. The effectiveness of the insulation on the reduction of the temperature difference and thermal stresses depends on the thickness of the insulation layer but also on the size of the insulated element: it was observed that the effectiveness of the increase of the insulation thickness is greater in thicker elements [156].

Formwork is usually removed very early, in 1 to 3 days after concrete casting. Such early removal leads to a thermal shock in the element, especially near surface, and increased drying thus cracks develop on the surface of the element. It is advised to delay the moment of the formwork removal [139, 160]. The attained tensile strength of concrete should be controlled before the formwork is removed to ensure that the stresses that result from the sudden cooling and drying of the concrete surface are sufficiently lower, thereby reducing the likelihood of cracking [156]. However, when the element is detained in the formwork stresses develop towards the interior of the wall [237] and so internal cracking may develop, which is extremely difficult to control.

The effect of insulation and formwork was also analysed by the author [139, 148]. Under the assumption of the external temperature being 25°C and without initial cooling of the concrete mix three cases were compared: the first in which the wall was detained in the formwork for the whole analysed time, the second in which additional insulation was applied and the last in which the formwork was removed after 3 days. Comparison of the temperature is presented in Fig. 5.39a and of the cracking risk in Fig. 5.39b. Early formwork removal resulted in accelerated heat and moisture removal out of the structure and led to significant increase in stresses, especially in near-surface areas. That is why damage intensity factor increase was observed. Although not so considerable in the interior, the risk of cracking almost doubled on the surface of the wall. Additional thermal insulation has generally positive influence on reduction of the cracking risk in walls but its application must be thoroughly considered. On one hand, stress inversion in the insulated walls occurs later and the resulting tensile stresses do not pose the risk of cracking of the wall. On the other hand, though, the originating temperatures reach significant values which leads to formation of high compressive stresses in the early phases of concrete curing.

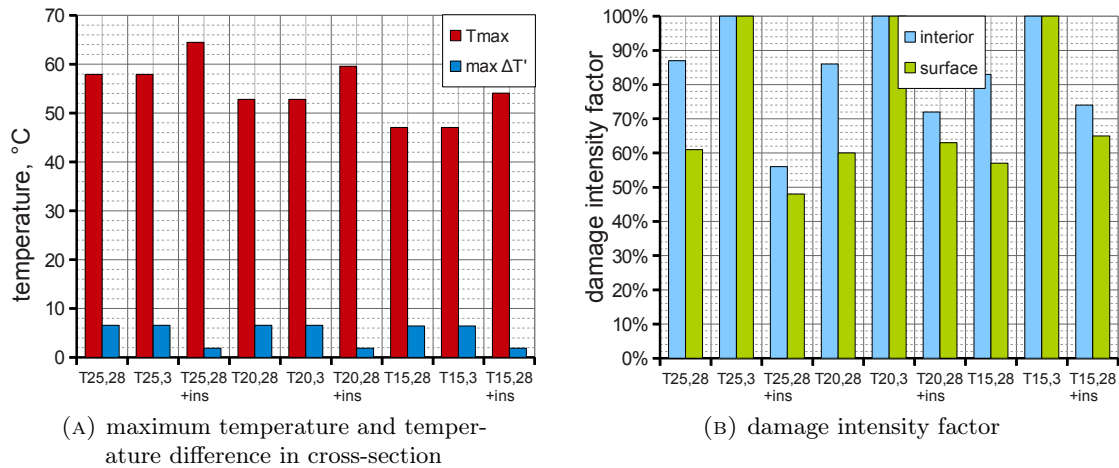


FIGURE 5.39: Influence of formwork conditions during curing on the cracking risk of walls [139].

It is also advised to apply cooling after placement. Surface cooling by spraying concrete element's surface allows to reduce the temperature increase and moisture loss due to drying [4, 44, 107, 227], however, it was observed that longer moist-curing periods result in the increased drying shrinkage after concrete is finally exposed to air drying [11]. Cooling pipes installed prior to concrete placement can be also used to remove the heat from the interior of the concrete [4, 196]. Cooling pipes typically consist of a uniformly distributed array of plastic pipes embedded in the concrete. Water is most often used as a coolant but also ventilated air has been proposed as an alternative [18]. It is important to limit the use of pipe-cooling only to the phase of the concrete temperature

increase; otherwise it may have an adverse effect to accelerate the temperature drop [110]. Heating can be also applied to the restraining material to balance the temperature and hence equilibrate strains of the self-heating element and its restraint. Undoubtedly, these methods increase the cost of construction, but limit the maximum temperature and greatly reduce the temperature differences in massive concrete.

Chapter 6

Summary and conclusions

6.1 Final conclusions

The following conclusions can be drawn from the research presented in this thesis:

1. General conclusions concerning **the character of the early-age stresses** and cracking in reinforced concrete walls:
 - Formation of cracks is observed in medium-thick concrete elements like reinforced concrete walls which if not restrained would not exhibit such a behaviour. These cracks are caused by limitation of free deformation of the wall along the restraint joint caused by contraction during cooling.
 - The total early-age stresses are induced by restrained volume changes caused by the temperature and moisture variations with a predominant role of the restraint stresses which decide about the character of the total early-age stresses. The share of the self-induced stresses increases with the increasing thickness of the wall, but even in relatively thin elements it has an influence on the total stresses distribution in the wall due to the existing thermal and humidity gradients.
2. Conclusions concerning **modelling of early-age behaviour** of reinforced concrete walls:
 - Engineering analytic models describe the thermal fields and the moisture fields in a simplified way. In these models calculation of the temperature relates only to determination of the peak temperature due to development of the hydration heat. The non-uniform distribution of the temperature and moisture content inside a given structural element is usually neglected. The time evolution of the before-mentioned fields is also omitted and only the cooling phase is considered in the analytic models. Nevertheless, the analytic models can be helpful in the preliminary risk assessment to answer the question whether the thermal and shrinkage effects are important in the actual structure and can lead to its cracking. The structural analysis is performed with the use of the degree of restraint concept. The restraint factor is used as representation of the degree of restraint. In the most complete form the restraint factor takes into

account the geometry of the early-age element and the restraining body, the relative stiffness of the restraining body and the influence of cracking on the change of restraint. The restraint factor is a very good concept for representation of the character of stresses in early-age walls.

- A phenomenological numerical model with implementation was proposed in the thesis for simulation of the early-age behaviour of walls. The main goal of the model was to estimate the thermal–shrinkage stresses in early-age concrete elements without the necessity to perform a series of experimental tests in order to determine the values of the subsequent parameters. This aim was successfully achieved.
- The model was used for analyses of stresses in early-age concrete walls. Three-dimensional numerical analysis allowed to explain the important phenomena observed in early-age elements. The numerical approach allowed to describe the time evolution of the various phenomena as concrete maturity developed. What is more, the different technological conditions like casting sequence, variable environmental conditions, different initial temperature of the concrete lifts or different time of the formwork removal for the lifts could be simulated. The share of the self-induced stresses could be also evaluated.
- The results of the analyses confirmed a typical two-phase, compressive–tensile character of stresses in the wall. The greatest value of the thermal–shrinkage stress occurred above the restraint joint. This fact resulted from the non-uniform distribution of temperature and moisture within the element which concentrated in its central parts. Consequently, formation of the first crack could have been consistently observed at some level above the restraint joint. The location of this point depended on the L/H ratio of the wall and relative stiffness of the restraining body – it was located closer to the joint as the L/H and $E_F A_F/E_c A_c$ increased. The spatial analysis showed the influence of the self-induced stresses which are responsible for the variation of the total stresses in the cross-section of the wall.
- Taking into account the construction sequence of the wall (« excavation in soil → foundation → wall » or « lift 1 → lift 2 → ... → lift n ») the real temperature distribution in the concrete element was obtained; this included the effect of the heat exchange between the foundation and the soil and resulting heating up of the soil as well as secondary heating of the foundation/adjacent segment by the hardening wall. Such an approach allowed to determine the actual difference in strain between the early-age element and the restraining body; this differential strain is the cause of the arising stresses. Moreover, taking into account the real stiffness of the restraining bodies (founding soil, concrete foundation or adjacent concrete segment) provided the real values of the degree of restraint for determination of the stresses in the wall.

3. Detailed conclusions concerning **the influence of the restraint conditions on the early-age stresses** in reinforced concrete walls:

- The early-age stresses in reinforced concrete walls are caused by a coupled action of the self-induced and restraint stresses. The self-induced stresses are caused by the internal restraint related to the massivity of the element; in walls with simple geometry the influence of the self-induced stresses depends directly on the thickness

of the wall. The restraint stresses are caused by the external restraint of the wall by the restraining body, which can be expressed with the restraint factor.

- The value of the restraint factor varies throughout the volume of the wall and is the greatest at the joint between the wall and the restraining body decreasing towards the free edges. The value of the restraint factor depends on the degree of translational restraint (length and height of the wall and their ratio and relative stiffness of the restraining body), rotational restraint, possibility of slip at the joint as well as the properties of the founding soil (friction, cohesion and stiffness).
- The degree of restraint increases with an increasing L/H ratio but also decreases with an increasing height and increasing length of the wall for a given L/H ratio.
- It is crucial to provide real support conditions of the early-age wall, especially concerning founding soil; rotation of the wall needs to be allowed. The influence of the rotation of the wall on the degree of restraint increases with an increasing length of the wall (it is almost unnoticed in short walls). There is also an influence of the soil stiffness on the value of the restraint factor: when soil is softer, larger rotation occurs.

4. Detailed conclusions concerning **the influence of the chosen parameters on the early-age stresses** in reinforced concrete walls:

- The factors which influence the early-age stresses relate to the concrete composition, environmental and technological conditions during casting and curing of the element.
- The most common way of mitigation of the early-age effects is the optimum concrete mix design, which includes reduction of the amount of cement or use of the low-heat cement, partial replacement of cement with mineral additions or reduction of cement fineness, application of aggregate with high strength but reduced temperature-induced deformability and saturated aggregates as well as addition of fibres. Nevertheless, in externally-restrained elements there are two crucial issues: (1) when aiming to decrease the hydration heat by application of low-heat cement or reduced amount of cement the mechanical properties development rate cannot be substantially decelerated and (2) when aiming to decrease the concrete temperature rise by adjusting the type of aggregate the aggregate cannot undergo large thermal dilation.
- Development of the early-age stresses is highly dependent on the environmental conditions during curing of concrete. The most disadvantageous are very high and very low ambient temperature and its variations, low humidity of the surrounding air, solar radiation which leads to the rapid increase of the surface temperature of the element and strong wind which causes rapid cooling and drying of the surface. It is advised to realise concreting in moderate ambient temperature with additional pre-cooling of the concrete mix.
- The early-age stresses are also strongly influenced by the technology of casting and curing of the concrete element. The casting technology defines transient restraint conditions. Curing technology relates mostly to the surface protection and includes formwork technology, insulation and cooling. Appropriate curing technology can be applied when curing is realised in unfavourable conditions. To mitigate early-age cracking in walls insulation should be applied and the moment of formwork removal should be delayed – it must prevent from thermal shock and assure that the tensile strength of the concrete element is able to withstand the cooling tensile stresses.

6.2 Future work

There are the following directions for future development of the presented research:

1. **Development of the numerical model.** The presented numerical model requires further development. Development of the model requires improvement of the hydration function and creep function description. Parameters of the model need to be well described. Moreover, at this moment the numerical model is implemented only for orthonormal finite elements – it should be extended to isoparametric elements.
2. **Improvement of the model for other concrete mixes.** The presented research was dedicated to elements made of normal-weight concrete with Portland cement. Nevertheless, some of the early-age phenomena have different character and importance in concrete mixes with different composition, technology of production and casting, such as high-strength and high-performance concretes, concretes made of cements with high amounts of mineral additions, self-compacting concretes or roller-compacted concretes.
3. **Probabilistic sensitivity analysis.** For safe use of the models it is needed to perform the sensitivity analysis in which the variability of the material, environmental and technological parameters would be taken into account. The results of such an analysis would show what is the range of influence of the foreseeable variability of subsequent parameters on the stresses and resulting cracking risk in early-age concrete structures.
4. **Crack width analysis and design of reinforcement.** In structures in which the appearance of the cracks is allowed but their width should be controlled the cracking pattern can be modified by appropriate design of reinforcement. The expected width of crack can be calculated acc. to e.g. MODEL CODE 2010 based on the numerically determined strains of concrete and steel. For proper determination of this strain difference it is required to model the interface zone between steel and concrete (steel-to-concrete bond).
5. **Development of the simplified engineering model.** Simplified engineering models have potential to properly describe the behaviour of early-age concrete structures, however, this requires appropriate definition of the following parameters and phenomena:
 - temperature and shrinkage development and distribution;
 - creep function;
 - degree of restraint which should take into account geometrical characteristics of the analysed element and restraint conditions, including the character of the restraint, the effect of reinforcement and the influence of the subsoil.

The future work should focus on development of the robust methods for definition of the above. The simplified engineering models should allow for analysis of the cracking risk, including determination of the expected crack width and design of proper reinforcement.

Bibliography

- [1] AASHTO. LRFD Bridge Design Specification, 1994.
- [2] ABBASNIA R., SHEKARCHI M. AND AHMADI J. Evaluation of concrete drying shrinkage related to moisture loss. *ACI Materials Journal*, 110(3):269–277, 2013.
- [3] ACI COMMITTEE 207. ACI 207.1R-05: Guide to mass concrete, 2005.
- [4] ACI COMMITTEE 207. ACI 207.4R-05: Cooling and insulating systems for mass concrete, 2005.
- [5] ACI COMMITTEE 207. ACI 207.2R-07: Report on thermal and volume change effects on cracking of mass concrete, 2007.
- [6] ACI COMMITTEE 209. ACI 209R-92: Prediction of creep, shrinkage, and temperature effects in concrete structures, 1992 (Reapproved 1997).
- [7] AKKAYA Y., OUYANG C. AND SHAH S. P. Effect of supplementary cementitious materials on shrinkage and crack development in concrete. *Cement & Concrete Composites*, 29:117–123, 2007.
- [8] AL-GBURI M., JONASSON J.-E., NILSSON M., HEDLUND H. AND HÖSTHAGEN A. Simplified methods for crack risk analyses of early age concrete. Part 1: Development of Equivalent Restraint Method. *Nordic Concrete Research*, 46:17–38, 2012.
- [9] AL RAWI R. S. AND KHEDER G. F. Control of cracking due to volume change in base-restrained concrete members. *ACI Structural Journal*, 87(4):397–405, 1990.
- [10] ALTOUBAT S. A. AND LANGE D. A. Tensile basic creep: Measurements and behaviour at early age. *ACI Materials Journal*, 98(5):386–392, 2001.
- [11] ALY T. AND SANJAYAN J. G. Mechanism of early age shrinkage of concretes. *Materials and Structures*, 42:461–468, 2009.
- [12] ALY T. AND SANJAYAN J. G. Shrinkage-cracking behavior of OPC-fiber concrete at early-age. *Materials and Structures*, 43:755–764, 2010.
- [13] ANDREASIK M. *Naprężenia termiczno-skurczowe w masywach betonowych*. PhD thesis, Cracow University of Technology, Cracow, Poland, 1982.
- [14] ATRUSHI D. S. *Tensile and compressive creep of early age concrete: Testing and modelling*. PhD thesis, Norwegian University of Science and Technology, Trondheim, Norway, 2003.
- [15] AURICH M., FILHO A. C., BITTENCOURT T. N. AND SHAH S. P. Finite element modeling of concrete behaviour at early age. *Revista IBRACON de Estruturas e Materiais*, 2(1):37–58, 2009.
- [16] AYANO T. AND WITTMANN F. H. Drying, moisture distribution, and shrinkage of cement-based materials. *Materials and Structures*, 35:134–140, 2002.
- [17] AYOTT E., MASSICOTTE B., HOUDE J. AND GOCEVSKI V. Modeling the thermal stresses at early ages in a concrete monolith. *ACI Materials Journal*, 94(6):577–587, 1997.
- [18] AZENHA M., LAMEIRAS R., DE SOUSA C. AND BARROS J. Application of air cooled pipes for reduction of early age cracking risk in a massive RC wall. *Engineering Structures*, 62–63:148–163, 2014.

-
- [19] AZENHA M., SOUSA C., FARIA R. AND NEVES A. Thermo-hygro-mechanical modelling of self-induced stresses during the service life of RC structures. *Engineering Structures*, 33:3442–3453, 2011.
- [20] BALLIM Y. AND GRAHAM P. C. A maturity approach to the rate of heat evolution in concrete. *Magazine of Concrete Research*, 55(3):249–256, 2003.
- [21] BAMFORTH P. B. CIRIA C660: Early-age thermal crack control in concrete. CIRIA, London, UK, 2007.
- [22] BAMFORTH P. B. AND PRICE W. F. *Concreting deep lifts and large volume pours*. Construction Industry Research and Information Association, London, UK, 1995.
- [23] BANGASH M. Y. H. *Manual of numerical methods in concrete*. Thomas Telford Ltd., London, UK, 2001.
- [24] BAŽANT Z. P. AND NAJJAR L. J. Nonlinear water diffusion in nonsaturated concrete. *Materials and Structures*, 5(25):3–20, 1972.
- [25] BAŽANT Z. P. AND OH B. H. Crack band theory for fracture of concrete. *Materials and Structures*, 16:155–177, 1983.
- [26] BAŽANT Z. P. AND THONGUTHAI W. Pore pressure and drying of concrete at high temperature. *ASCE Journal of Engineering Mechanics*, 104(EM5):1059–1079, 1978.
- [27] BENBOUDJEMA F. AND TORRENTI J.-M. Early-age behaviour of concrete nuclear containments. *Nuclear Engineering and Design*, 238:2495–2506, 2008.
- [28] BENBOUDJEMA F. AND TORRENTI J.-M. Modelling desiccation shrinkage of large structures. *EPJ Web of Conferences*, 56, 2013.
- [29] BENTZ D. P. AND PELTZ M. A. Reducing thermal and autogenous shrinkage contributions to early-age cracking. *ACI Materials Journal*, 105(4):414–420, 2008.
- [30] BILISZCZUK J. AND RAJSKI O. Zastosowanie betonów wysokich klas w mostownictwie. In *Proceedings of “Dni Betonu”*, Wisła, Poland, 2002.
- [31] BOFANG Z. *Thermal stresses and temperature control of mass concrete*. China Electric Power Press, Beijing, People’s Republic of China, 2003.
- [32] BOGUE J. H. *The chemistry of Portland cement*. Reinhold Publishing Corporation, New York, USA, 1947.
- [33] BORUCKA-LIPSKA J., FREIDENBERG P. AND KIERNOŻYCKI W. Oddziaływania pośrednie zachodzące w masywnych elementach betonowych o zróżnicowanym składzie. *Przegląd Budowlany*, 3:26–30, 2006.
- [34] BOTTELLI M., VENTURA F., CAMPBELL G. S., SNYDER R. L., GALLEGATI F. AND PISA P. R. Coupling of heat, water vapour, and liquid water fluxes to compute evaporation in bare soil. *Journal of Hydrology*, 362:191–205, 2008.
- [35] BRANCO F. A., MENDES P. A. AND MIRAMBELL E. Heat of hydration effects in concrete structures. *ACI Materials Journal*, 89(2):139–145, 1992.
- [36] BRANDT A. M. Concrete as a shielding material in nuclear energy constructions. *Cement Wapno Beton*, 2:115–136, 2013.
- [37] BRIFFAUT M., BENBOUDJEMA F., TORRENTI J.-M. AND NAHAS G. Numerical analysis of the thermal active restrained shrinkage ring test to study the early age behavior of massive concrete structures. *Engineering Structures*, 33:1390–1401, 2011.
- [38] BRIFFAUT M., BENBOUDJEMA F., TORRENTI J.-M. AND NAHAS G. Concrete early age basic creep: Experiments and test of rheological modelling approaches. *Construction and Building Materials*, 36:373–380, 2012.
- [39] BRIFFAUT M., BENBOUDJEMA F., TORRENTI J.-M. AND NAHAS G. Effects of the early age

- thermal behaviour on long term damage risk in massive concrete structures. *European Journal of Environmental and Civil Engineering*, 16(5):598–605, 2012.
- [40] BROOKS J. J. AND NEVILLE A. M. A comparison of creep, elasticity and strength of concrete in tension and in compression. *Magazine of Concrete Research*, 29(100):131–141, 1977.
- [41] BROOKS R. H. AND COREY A. T. Properties of porous media affecting fluid flow. *ASCE Journal of the Irrigation and Drainage Division*, 92(IR2):61–88, 1966.
- [42] BURDINE N. T. Relative permeability calculations from pore size distribution data. *Petroleum Transactions AIME*, 198:71–78, 1953.
- [43] CAMPBELL G. S. AND NORMAN J. M. *An introduction to environmental biophysics*. Springer, New York, USA, 2nd edition, 1998.
- [44] CANO-BARRITA P. F. J., BALCOM B. J., BREMNER T. W., MACMILLAN M. B. AND LANGLEY W. S. Moisture distribution in drying ordinary and high performance concrete cured in a simulated hot dry climate. *Materials and Structures*, 37:522–531, 2004.
- [45] CARINO N. J. Maturity functions for concrete. In *Proceedings of the RILEM International Conference on Concrete at Early Ages*, pages 111–115, Paris, France, 1982.
- [46] CAROL I. AND BAŽANT Z. P. Viscoelasticity with aging caused by solidification of nonaging constituent. *ASCE Journal of Engineering Mechanics*, 119(11):2252–2269, 1993.
- [47] CEB-FIP *fib*. Model Code 1990, 1991.
- [48] CEB-FIP *fib*. Bulletin 15. State-of-the-art report: Nuclear containments. 2001.
- [49] CEB-FIP *fib*. Bulletin 70. State-of-the-art report: Code-type models for concrete behaviour. Background of MC2010. 2013.
- [50] CEB-FIP *fib*. Model Code 2010, 2013.
- [51] CERVERA M., FARIA R., OLIVER J. AND PRATO T. Numerical modelling of concrete curing, regarding hydration and temperature phenomena. *Computers and Structures*, 80:1511–1521, 2002.
- [52] CERVERA M., OLIVER J. AND PRATO T. Thermo-chemical—mechanical model for concrete. Part I: Hydration aging. *ASCE Journal of Engineering Mechanics*, 125(9):1018–1027, 1999.
- [53] CHEN W.-F. *Plasticity in reinforced concrete*. McGraw-Hill, New York, USA, 1982.
- [54] CHENGJU G. Maturity of concrete: Method for predicting early-age strength. *ACI Materials Journal*, 86(4):341–353, 1989.
- [55] CLAPP R. B. AND HORNBERGER G. M. Empirical equations for some soil hydraulic properties. *Water Resources Research*, 14(4):601–604, 1978.
- [56] CORTAS R., ROZIÈRE E., STAQUET S., HAMAMI A., LOUKILI A. AND DELPLANCKE-OGLETREE M.-P. Effect of the water saturation of aggregates on the shrinkage induced cracking risk of concrete at early age. *Cement & Concrete Composites*, 50:1–9, 2014.
- [57] CRAEYE B., DE SCHUTTER G., HUMBEECK H. V. AND COTTHEM A. V. Early age behaviour of concrete supercontainers for radioactive waste disposal. *Nuclear Engineering and Design*, 239:23–35, 2009.
- [58] DE BORST R. AND VAN DEN BOOGAARD A. H. Finite-element modeling of deformation and cracking in early-age concrete. *ASCE Journal of Engineering Mechanics*, 120(12):2519–2534, 1994.
- [59] DE LARRARD T., COLLIAT J. B., BENBOUDJEMA F., TORRENTI J.-M. AND NAHAS G. Effect of the young modulus variability on the mechanical behaviour of a nuclear containment vessel. *Nuclear Engineering and Design*, 240:4051–4060, 2010.
- [60] DE SCHUTTER G. Degree of hydration based Kelvin model for the basic creep of early age concrete. *Materials and Structures*, 32:260–265, 1999.
- [61] DE SCHUTTER G. Extension towards early age concrete of CEB-FIP Model Code 1990 stress-strain

- relation for short-term compressive load. *ACI Materials Journal*, 96(1):95–100, 1999.
- [62] DE SCHUTTER G. Finite element simulation of thermal cracking in massive hardening concrete elements using degree of hydration based material laws. *Computers and Structures*, 80:2035–2042, 2002.
- [63] DE SCHUTTER G. Fundamental study of early age concrete behaviour as a basis for durable concrete structures. *Materials and Structures*, 35:15–21, 2002.
- [64] DE SCHUTTER G. AND TAERWE L. General hydration model for portland cement and blast furnace slag cement. *Cement and Concrete Research*, 25(3):593–604, 1995.
- [65] DE SCHUTTER G. AND TAERWE L. Specific heat and thermal diffusivity of hardening concrete. *Magazine of Concrete Research*, 47(172):203–208, 1995.
- [66] DE SCHUTTER G. AND TAERWE L. Degree of hydration-based description of mechanical properties of early age concrete. *Materials and Structures*, 29:335–344, 1996.
- [67] DE SCHUTTER G. AND TAERWE L. Estimation of early-age thermal cracking tendency of massive concrete elements by means of equivalent thickness. *ACI Materials Journal*, 93(5):403–408, 1996.
- [68] DE SCHUTTER G. AND TAERWE L. Fictitious degree of hydration method for the basic creep of early age concrete. *Materials and Structures*, 33:370–380, 2000.
- [69] DE SCHUTTER G. AND VUYLSTEKE M. Minimisation of early age thermal cracking in a J-shaped non-reinforced massive concrete quay wall. *Engineering Structures*, 26:801–808, 2004.
- [70] DE VRIES D. A. *Physics of Plants Environment*, chapter Thermal properties of soils, pages 210–235. North-Holland Publishing Co., Amsterdam, Netherlands, 1963.
- [71] DI LUZIO G. AND CEDOLIN L. Numerical model for time-dependent fracturing of concrete structures and its application. In *Proceedings of the International Conference on New Trends in Fracture Mechanics of Concrete*, pages 175–180, Catania, Italy, 2007.
- [72] DI LUZIO G. AND CUSATIS G. Hygro–thermo–chemical modeling of high performance concrete. Part I: Theory. *Cement & Concrete Composites*, 31:301–308, 2009.
- [73] DI LUZIO G. AND CUSATIS G. Hygro–thermo–chemical modeling of high-performance concrete. Part II: Numerical implementation, calibration, and validation. *Cement & Concrete Composites*, 31:309–324, 2009.
- [74] DUNCAN J. M. AND CHANG C. Y. Nonlinear analysis of stress and strain in soil. *ASCE Journal of the Soil Mechanics and Foundations Division*, 96(SM5):1629–1653, 1970.
- [75] EMANUEL J. H. AND HULSEY J. L. Prediction of the thermal coefficient of expansion of concrete. *ACI Materials Journal*, 74:149–155, 1977.
- [76] ENDRIZZI S., QUINTON W. L. AND MARSH P. Modelling of spatial pattern of ground thaw in a small basin in the arctic tundra. *The Cryosphere Discussions*, 5:367–400, 2011.
- [77] ESEN Y. AND YILMAZER B. Investigation of some physical and mechanical properties of concrete produced with barite aggregate. *Scientific Research and Essays*, 5(24):3826–3833, 2010.
- [78] ESTRADA C. F., GODOY L. A. AND PRATO T. Thermo–mechanical behaviour of a thin concrete shell during its early age. *Thin-Walled Structures*, 44:483–495, 2006.
- [79] FARIA R., ANZENHA M. AND FIGUEIRAS J. A. Modelling of concrete at early ages: Application to an externally restrained slab. *Cement & Concrete Composites*, 28:572–585, 2006.
- [80] FAROUKI O. T. *Thermal properties of soils*. Monograph 81-1. U.S. Army Cold Regions Research and Engineering Laboratory, Hanover, USA, 1981.
- [81] FENESTRA P. AND DE BORST R. Aspect of robust computational modelling for plain and reinforced concrete. *Heron*, 38:5–76, 1993.
- [82] FLAGA K. *Napężenia własne termiczne typu “makro” w elementach i konstrukcjach z betonu*.

- Monograph 106. Wydawnictwo Politechniki Krakowskiej, Cracow, Poland, 1990.
- [83] FLAGA K. *Naprężenia skurczowe i zbrojenie przypowierzchniowe w konstrukcjach betonowych*. Monograph 391. Wydawnictwo Politechniki Krakowskiej, Cracow, Poland, 2nd edition, 2011.
- [84] FLAGA K., KLEMCZAK B. AND KNOPPIK-WRÓBEL A. Early-age thermal–shrinkage crack formation in bridge abutments – experiences and modelling. In *Proceedings of the fib Symposium*, pages 435–438, Tel-Aviv, Israel, 2013.
- [85] FLAGA K. *Opinia naukowo–techniczna w sprawie zarysowań obiektów mostowych budowanej autostrady A1 węzeł Sośnica–Bełk oraz w sprawie mieszanki betonowej wbudowanej w konstrukcje tych obiektów*. Department of Bridges and Tunnels, Cracow University of Technology, Cracow, Poland, 2008.
- [86] FLAGA K. Zarysowania termiczne ścian przyczółków i ścian oporowych obiektów mostowych w pobliżu styku z fundamentami. *Inżynieria i Budownictwo*, 1:15–20, 2009.
- [87] FLAGA K. *Opinia naukowa na temat przyczyn powstania zarysowań w ramowych obiektach mostowych przy realizacji inwestycji pod nazwą: Budowa autostrady A4 Tarnów–Rzeszów, na odcinku od węzła Dębica Pustynia do węzła Rzeszów Zachodni km około 573+550 do około 570+300 wraz z podaniem środków zaradczych i sposobu naprawy*. Department of Bridges and Tunnels, Cracow University of Technology, Cracow, Poland, 2011.
- [88] FLAGA K. AND FURTAK K. Problem of thermal and shrinkage cracking in tanks vertical walls and retaining walls near their contact with solid foundation slabs. *Architecture–Civil Engineering–Environment*, 2(2):23–30, 2009.
- [89] GAWIN D. Numerical solution of coupled heat and moisture transfer problems with phase changes in porous building materials. *Archives of Civil Engineering*, 34(4):393–412, 1993.
- [90] GAWIN D., PESAVENTO F. AND SCHREFLER B. A. Hygro–thermo–chemo–mechanical modelling of concrete at early ages and beyond. Part I: Hydration and hygro–thermal phenomena. *International Journal for Numerical Methods in Engineering*, 67:299–331, 2006.
- [91] GAWIN D., PESAVENTO F. AND SCHREFLER B. A. Hygro–thermo–chemo–mechanical modelling of concrete at early ages and beyond. Part II: Shrinkage and creep of concrete. *International Journal for Numerical Methods in Engineering*, 67:332–363, 2006.
- [92] GUTSCH A. AND ROSTÁSY F. S. Young concrete under high tensile stresses – creep, relaxation and cracking. In *Proceedings of the International RILEM Conference on Thermal cracking in concrete at early ages*, pages 111–118, London, UK, 1994.
- [93] GUTSCH A.-W. Properties of early age concrete – Experiments and modelling. *Materials and Structures*, 35:76–79, 2002.
- [94] GUÉNOT I., TORRENTI J.-M. AND LAPLANTE P. Stresses in early age concrete: Comparison of different creep models. *ACI Materials Journal*, 93(3):254–258, 1996.
- [95] HALICKA A. AND FRAN CZAK D. *Projektowanie zbiorników żelbetowych. Tom 2: Zbiorniki na ciecz*. Wydawnictwo Naukowe PWN, Warsaw, Poland, 2013.
- [96] HALICKA A., FRAN CZAK D. AND FRONCZYK J. Analiza przyczyn zarysowań cylindrycznego zbiornika żelbetowego ujawnionych podczas próby szczelności. *Przegląd Budowlany*, 4:35–41, 2012.
- [97] HANCOX N. L. *The diffusion of water in concrete*. UKAEA, Winfrith, UK, 1966.
- [98] HANSEN P. F. AND PEDERSEN J. Maturity computer for controlled curing and hardening of concrete. *Nordisk Betong*, 21:19–34, 1977.
- [99] HATTEL J. H. AND THOTBORG J. A numerical model for predicting the thermomechanical conditions during hydration of early-age concrete. *Applied Mathematical Modelling*, 27:1–26, 2003.
- [100] HILAIRE A., BENBOUDJEMA F., DARQUENNES A., BERTHAUD Y. AND NAHAS G. Modeling basic creep in concrete at early-age under compressive and tensile loading. *Nuclear Engineering and*

- Design*, 269:222–230, 2014.
- [101] HILLEL D. *Fundamentals of soil physics*. Academic Press, San Diego, USA, 1st edition, 1998.
- [102] HILLERBORG A., MODEER M. AND PETERSSON P. Analysis of crack formation and crack growth in concrete by means of fracture mechanics and finite elements. *Cement and Concrete Research*, 6:773–82, 1976.
- [103] HOFSTETTER G. AND MANG H. A. *Computational mechanics of reinforced concrete structures*. Vieweg, Wiesbaden, Germany, 1995.
- [104] HOLT E. Very early age autogenous shrinkage: governed by chemical shrinkage or self-desiccation? In *Proceedings of the Third International Research Seminar on Self-desiccation and its importance in concrete technology*, pages 1–25, Lund, Sweden, 2002.
- [105] HONORIO T., BARY B. AND BENBOUDJEMA F. Evaluation of the contribution of boundary and initial conditions in the chemo-thermal analysis of a massive concrete structure. *Engineering Structures*, 80:173–188, 2014.
- [106] HUANG C.-X. The three dimensional modelling of thermal cracks in concrete structure. *Materials and Structures*, 32:673–678, 1999.
- [107] HUO X. S. AND WONG L. U. Experimental study of early-age behavior of high performance concrete deck slabs under different curing methods. *Construction and Building Materials*, 20:1049–1056, 2006.
- [108] HÖSTHAGEN A., JONASSON J.-E., EMBORG M., HEDLUND H., WALLIN K. AND STELMARCZYK M. Thermal crack risk estimations of concrete tunnel segments - Equivalent Restraint Method correlated to empirical observations. *Nordic Concrete Research*, 49:127–143, 2014.
- [109] INTERNATIONAL ATOMIC ENERGY AGENCY. Power Reactor Information System (<http://www.iaea.org/pris>), Jan 2015.
- [110] JAPANESE CONCRETE INSTITUTE. Guidelines for Control of Cracking of Mass Concrete, 2008.
- [111] JENDELE L., ŠMILAUER V. AND ČERVENKA J. Multiscale hydro-thermo-mechanical model for early-age and mature concrete structures. *Advances in Engineering Software*, 72:134–146, 2014.
- [112] JIANG W., DE SCHUTTER G. AND YUAN Y. Degree of hydration based prediction of early age basic creep and creep recovery of blended cements. *Cement & Concrete Composites*, 48:83–90, 2014.
- [113] JOHANSEN O. Thermal conductivity of soils and rocks. In *Proceedings of the 6th International Congress of the Foundation Francaise d'Etudes Nordiques*, volume 2, Le Havre, France, 1975.
- [114] JONASSON J.-E. *Modelling of temperature, moisture and stress in young concrete*. PhD thesis, Luleå University of Technology, Luleå, Sweden, 1994.
- [115] JONASSON J.-E., GROTH P. AND HEDLUND N. Modelling of temperature and moisture field in concrete to study early age movements as a basis for stress analysis. In *Proceedings of the International RILEM Conference on Thermal cracking in concrete at early ages*, pages 45–52, London, UK, 1994.
- [116] JSCE. Guidelines for Concrete. No. 15: Standard Specifications for Concrete Structures. Design, 2011.
- [117] JUENGER M. C. G., SOLT S. M. AND HEMA J. Effects of liquid nitrogen cooling on fresh concrete properties. *ACI Materials Journal*, 107(2):123–131, 2010.
- [118] KADA H., LACHEMI M., PETROV N., BONNEAU O. AND AITCIN P.-C. Determination of the coefficient of thermal expansion of high performance concrete from initial setting. *Material and Structures*, 35:35–41, 2002.
- [119] KADRI E.-H., DUVAL R., AGGOUN S. AND KENAI S. Silica fume effect on hydration heat and compressive strength of high-performance concrete. *ACI Materials Journal*, 106(2):107–113, 2009.
- [120] KAMEN A., DENARIE E., SADOUKI H. AND BRUHWILER E. Thermo-mechanical response of

- UHPFRC at early age – Experimental study and numerical simulation. *Cement and Concrete Research*, 38:822–831, 2008.
- [121] KANG S.-T., KIM J.-S., LEE Y., PARK Y.-D. AND KIM J.-K. Moisture diffusivity of early age concrete considering temperature and porosity. *KSCE Journal of Civil Engineering*, 16(1):179–188, 2011.
- [122] KANSTAD T., HAMMER T. A., BJØNTEGAARD Ø. AND SELLEVOLD E. J. Mechanical properties of young concrete. Part I: Experimental results related to test methods and temperature effects. *Materials and Structures*, 36:218–225, 2003.
- [123] KANSTAD T., HAMMER T. A., BJØNTEGAARD Ø. AND SELLEVOLD E. J. Mechanical properties of young concrete. Part II: Determination of model parameters and test program proposals. *Materials and Structures*, 36:226–230, 2003.
- [124] KASPERKIEWICZ J. Some aspects of water diffusion process in concrete. *Materials and Structures*, 5(28):209–214, 1972.
- [125] KEE C. F. Relation between strength and maturity of concrete. *ACI Journal Proceedings*, 68(3):196–203, 1971.
- [126] KERSTEN M. S. Bulletin 28: Thermal properties of soils. University of Minnesota, Minneapolis, USA, 1949.
- [127] KHALILI N., UCHAIPICHAT A. AND JAVADI A. A. Skeletal thermal expansion coefficient and thermo-hydro-mechanical constitutive relations for saturated homogeneous porous media. *Mechanics of Materials*, 42(6):593–598, 2010.
- [128] KHEDER G. F. A new look at the control of volume change cracking of base-restrained concrete walls. *ACI Structural Journal*, 94(3):262–270, 1997.
- [129] KHEDER G. F., AL RAWI R. S. AND AL DHALI J. K. Study of the behaviour of volume change cracking in base-restraint concrete walls. *ACI Structural Journal*, 91(2):150–157, 1994.
- [130] KIERNOŻYCKI W. *Betonowe konstrukcje masywne*. Polski Cement, Cracow, Poland, 2003.
- [131] KIM J.-H. AND LEE C.-S. Moisture diffusion of concrete considering self-desiccation at early ages. *Cement and Concrete Research*, 29:1921–1927, 1999.
- [132] KLEMCZAK B. *Lepko-sprężysto-plastyczny model materiałowy do numerycznej symulacji zjawisk zachodzących we wczesnym okresie dojrzewania betonu*. PhD thesis, Silesian University of Technology, Gliwice, Poland, 1999.
- [133] KLEMCZAK B. Adapting of the Willam–Warnke failure criteria for young concrete. *Archives of Civil Engineering*, 53(2):323–339, 2007.
- [134] KLEMCZAK B. *Modelowanie efektów termiczno-wilgotnościowych i mechanicznych w betonowych konstrukcjach masywnych*. Monograph 183. Silesian University of Technology, Gliwice, Poland, 2008.
- [135] KLEMCZAK B. Prediction of coupled heat and moisture transfer in early-age massive concrete structures. *Numerical Heat Transfer, Part A: Applications*, 60(3):212–233, 2011.
- [136] KLEMCZAK B. Modeling thermal-shrinkage stresses in early age massive concrete structures – Comparative study of basic models. *Archives of Civil and Mechanical Engineering*, 14(4):721–733, 2014.
- [137] KLEMCZAK B. AND BATOG M. Validation of analytical models for compressive strength development of concretes with blended cements. In *Proceedings of the 8th International Conference on Analytical Models and New Concepts in Concrete and Masonry Structures*, pages 237–247, Wrocław, Poland, 2014.
- [138] KLEMCZAK B. AND KNOPPIK-WRÓBEL A. Early-age thermal and shrinkage cracks in concrete structures – description of the problem. *Architecture–Civil Engineering–Environment*, 4(2):35–48,

- 2011.
- [139] KLEMCZAK B. AND KNOPPIK-WRÓBEL A. Early-age thermal and shrinkage cracks in concrete structures – influence of curing conditions. *Architecture–Civil Engineering–Environment*, 4(4):47–58, 2011.
- [140] KLEMCZAK B. AND KNOPPIK-WRÓBEL A. Early-age thermal and shrinkage cracks in concrete structures – influence of geometry and dimensions of a structure. *Architecture–Civil Engineering–Environment*, 4(3):55–70, 2011.
- [141] KLEMCZAK B. AND KNOPPIK-WRÓBEL A. Numerical analysis of early-age thermal and moisture effects in RC wall. In *Proceedings of the 7th International Conference on Analytical Models and New Concepts in Concrete and Masonry Structures*, pages 223–224, Cracow, Poland, 2011.
- [142] KLEMCZAK B. AND KNOPPIK-WRÓBEL A. Comparative study of methods for analysis of early-age thermal–shrinkage stresses in externally restrained concrete structures. In *Proceedings of the 10th International Conference on New Trends in Statics and Dynamics of Buildings*, pages 41–44, Bratislava, Slovakia, 2012.
- [143] KLEMCZAK B. AND KNOPPIK-WRÓBEL A. Wpływ wybranych czynników materiałowo-technologicznych na temperatury twardnienia betonu w masywnej płycie fundamentowej. In *Proceedings of “Dni Betonu”*, pages 291–301, Wisła, Poland, 2012.
- [144] KLEMCZAK B. AND KNOPPIK-WRÓBEL A. Comparison of analytical methods for estimation of early-age thermal–shrinkage stresses in RC walls. *Archives of Civil Engineering*, 59:97–117, 2013.
- [145] KLEMCZAK B. AND KNOPPIK-WRÓBEL A. Analysis of early-age thermal and shrinkage stresses in reinforced concrete walls. *ACI Structural Journal*, 111(2):313–322, 2014.
- [146] KLEMCZAK B. AND KNOPPIK-WRÓBEL A. Reinforced concrete tank walls and bridge abutments: early-age behaviour, analytic approaches and numerical models. *Engineering Structures*, 84:233–251, 2015.
- [147] KMITA A., MUSIAŁ M. AND STYŚ D. Problemy związane z zarysowaniem zbiorników na wodę w oczyszczalni ścieków. *Przegląd Budowlany*, 4:31–34, 2012.
- [148] KNOPPIK-WRÓBEL A. Cracking risk in early-age RC walls. In *Proceedings of the 9th fib International PhD Symposium in Civil Engineering*, pages 129–135, Karlsruhe, Germany, 2012.
- [149] KNOPPIK-WRÓBEL A. The influence of self-induced and restraint stresses on crack development in reinforced concrete wall subjected to early-age thermal–shrinkage effects. In *Proceedings of the 14th International Conference of Postgraduate Students Juniorstav*, page 162, Brno, Czech Republic, 2012.
- [150] KNOPPIK-WRÓBEL A. Cracking due to restraint stresses in early-age radiation shielding wall. *Architecture–Civil Engineering–Environment*, 7(3):49–61, 2014.
- [151] KOSMATKA S. H., KERKHOFF B. AND PANARESE W. C. Design and control of concrete mixtures. Portland Cement Association, Skokie, USA, 2003.
- [152] KWAK H.-G. AND HA S.-J. Non-structural cracking in RC walls. Part II: Quantitative prediction model. *Cement and Concrete Research*, 36:761–775, 2006.
- [153] KWAK H.-G., HA S.-J. AND KIM J.-K. Non-structural cracking in RC walls. Part I: Finite element formulation. *Cement and Concrete Research*, 36:749–760, 2006.
- [154] LACKNER R. AND MANG H. A. Chemoplastic material model for the simulation of early-age cracking: From the constitutive law to numerical analyses of massive concrete structures. *Cement & Concrete Composites*, 26:551–562, 2004.
- [155] LARSON M. *Thermal crack estimation in early age concrete. Models and methods for practical application*. PhD thesis, Luleå University of Technology, Luleå, Sweden, 2003.
- [156] LAWRENCE A. M., TIA M. AND BERGIN M. Considerations for handling of mass concrete: Control

- of internal restraint. *ACI Materials Journal*, 111(1):3–12, 2014.
- [157] LEE S. Y., DAUGHERTY A. M. AND BROTON D. J. Assessing aggregates for radiation-shielding concrete. *Concrete International*, 35(5):31–38, 2013.
- [158] LI K., JU Y., HAN J. AND ZHOU C. Early-age stress analysis of a concrete diaphragm wall through tensile creep modeling. *Materials and Structures*, 42:923–935, 2009.
- [159] LIU X., JIANG W., DE SCHUTTER G., YUAN Y. AND SU Q. Early-age behaviour of precast concrete immersed tunnel based on degree of hydration concept. *Structural Concrete*, 15(1):66–80, 2014.
- [160] LIU X., YUAN Y. AND SU Q. Sensitivity analysis of the early-age cracking risk in an immersed tunnel. *Structural Concrete*, 15(2):179–190, 2014.
- [161] MAJEWSKI S. *Sprężysto–plastyczny model współpracującego układu budynek–podłoże poddanego wpływowi górniczych deformacji terenu*. Silesian University of Technology, Gliwice, Poland, 1995.
- [162] MAJEWSKI S. *Mechanika betonu konstrukcyjnego w ujęciu sprężysto–plastycznym*. Monograph 45. Silesian University of Technology, Gliwice, Poland, 2003.
- [163] MAJEWSKI S. MWW3 — Elasto–plastic model for concrete. *Archives of Civil Engineering*, 50(1):11–43, 2004.
- [164] MASLEHUDDIN M., NAQVI A. A., IBRAHIM M. AND KALAKADA Z. Radiation shielding properties of concrete with electric arc furnace slag aggregates and steel shots. *Annals of Nuclear Energy*, 53:192–196, 2013.
- [165] MAZARS J. AND BOURNAZEL J. P. Modelling of damage processes due to volumic variations for maturing and matured concrete. In *Proceedings of the International RILEM Conference on Concrete: from Material to Structure*, pages 43–54, Arles, France, 1996.
- [166] MCCUMBER M. C. AND PIELKE R. A. Simulation of the effects of surface fluxes of heat and moisture in a mesoscale numerical model. *Journal of Geophysical Research*, 86(C10):9929–9938, 1981.
- [167] MEISWINKEL R., MEYER J. AND SCHNELL J. *Design and Construction of Nuclear Power Plants*. Ernst & Sohn, Berlin, Germany, 2013.
- [168] MELERSKI E. S. Numerical analysis for environmental effects in circular tanks. *Thin-walled structures*, 40:703–727, 2002.
- [169] MENSİ R., ACKER P. AND ATTOLOU A. Séchage du béton: analyse et modélisation. *Material and Structures*, 21:3–12, 1988.
- [170] MESCHKE G. Consideration of aging of shotcrete in the context of 3-D viscoplastic material model. *International Journal for Numerical Methods in Engineering*, 39:3123–3143, 1996.
- [171] MIHASHI H. AND LEITE J. P. State-of-the-art report on control cracking in early age concrete. *Journal of Advanced Concrete Technology*, 2(2):141–154, 2004.
- [172] MOLA F. AND PELLEGRINI L. M. The new model for creep of concrete in FIP Model Code 2010. In *Proceedings of the 37th Conference: Our World in Concrete & Structures*, pages 53–66, Singapore, 2012.
- [173] MUALEM Y. A new model for predicting the hydraulic conductivity of unsaturated porous media. *Water Resources Research*, 12(3):513–522, 1976.
- [174] NAGY A. Parameter study of thermal cracking in HPC and NPC structures. *Nordic Concrete Research*, 26:1–13, 2001.
- [175] NEVILLE A. M. *Properties of concrete*. Prentice Hall, San Francisco, USA, 5th edition, 2012.
- [176] NILSSON M. *Restraint factors and partial coefficients for crack risk analyses of early age concrete structures*. PhD thesis, Luleå University of Technology, Luleå, Sweden, 2003.

-
- [177] NILSSON M. Thermal cracking of young concrete. Partial coefficients, restraint effects and influence of casting joints. Master's thesis, Luleå University of Technology, Luleå, Sweden, 2007.
- [178] ØSTERGAARD L. *Early-age fracture mechanics and cracking of concrete. Experiments and modelling.* PhD thesis, Technical University of Denmark, Copenhagen, Denmark, 2003.
- [179] PACHEPSKY Y., TIMLIN D. AND RAWLS W. Generalized Richards' equation to simulate water transport in unsaturated soils. *Journal of Hydrology*, 272:3–13, 2003.
- [180] PANE I. AND HANSEN W. Early age creep and stress relaxation of concrete containing blended cements. *Materials and Structures*, 35:92–96, 2002.
- [181] PARLANGE M. B., CAHILL A. T., NIELSEN D. R., HOPMANS J. W. AND WENDROTH O. Review of heat and water movements in field soils. *Soil & Tillage Research*, 47:5–10, 1998.
- [182] PHILIP J. R. AND DE VRIES D. A. Moisture movement in porous materials under temperature gradients. *Transactions – American Geophysics Union*, 38:222–232, 1957.
- [183] PN-EN 1992-1-1. Eurocode 2 – Design of concrete structures. Part 1-1: General rules and rules for buildings, 2008.
- [184] PN-EN 1992-3. Eurocode 2 – Design of concrete structures. Part 3: Liquid retaining and containment structures, 2008.
- [185] PN-EN 206-1. Concrete – Part 1: Specification, performance, production and conformity, 2003.
- [186] POOLE J. L. *Modeling temperature sensitivity and heat evolution of concrete.* PhD thesis, University of Texas at Austin, Austin, USA, 2007.
- [187] PROCHACZEK M. Technical issues of the design of shielding bunker for 235 MeV cyclotron. In *Proceedings of the 9th Central European Congress on Concrete Engineering*, Wrocław, Poland, 2013.
- [188] RASTRUP E. Heat of hydration in concrete. *Magazine of Concrete Research*, 6(17):1–14, 1954.
- [189] REINHARDT H., BLAAUWENDRAAD J. AND JONGEDIJK J. Temperature development in concrete structures taking account of state dependent properties. In *Proceedings of RILEM International Conference on Concrete at Early Ages*, pages 211–218, Paris, France, 1982.
- [190] RIDING K. A., POOLE J. L., SCHINDLER A. K., JUENGER M. G. AND FOLLIARD K. J. Evaluation of temperature prediction methods for mass concrete members. *ACI Materials Journal*, 103(5):357–365, 2006.
- [191] RIDING K. A., POOLE J. L., FOLLIARD K. J., JUENGER M. C. G. AND SCHINDLER A. K. New method for estimating apparent activation energy of cementitious systems. *ACI Materials Journal*, 108(5):550–557, 2011.
- [192] RIDING K. A., POOLE J. L., FOLLIARD K. J., JUENGER M. C. G. AND SCHINDLER A. K. Modeling hydration of cementitious systems. *ACI Materials Journal*, 109(2):225–234, 2012.
- [193] RIDING K. A., POOLE J. L., SCHINDLER A. K., JUENGER M. C. G. AND FOLLIARD K. J. Temperature boundary condition models for concrete bridge members. *ACI Materials Journal*, 104(4):379–387, 2007.
- [194] RIDING K. A., POOLE J. L., SCHINDLER A. K., JUENGER M. C. G. AND FOLLIARD K. J. Quantification of effects of fly ash type on concrete early-age cracking. *ACI Materials Journal*, 105(2):149–155, 2008.
- [195] RIDING K. A., POOLE J. L., SCHINDLER A. K., JUENGER M. C. G. AND FOLLIARD K. J. Effects of construction time and coarse aggregate on bridge deck cracking. *ACI Materials Journal*, 106(5):448–454, 2009.
- [196] RILEM TC 119-TCE. Avoidance of thermal cracking in concrete at early ages. *Materials and Structures*, 30:451–464, 1997.
- [197] RILEM TC 181-EAS. Early age cracking in cementitious systems – Report of RILEM Technical Committee TC 181-EAS. 2002.

- [198] SANTURJIAN O. AND KOLAROW L. A spatial FEM model of thermal stress state of concrete blocks with creep consideration. *Computers and Structures*, 58(3):563–574, 1996.
- [199] SAUL A. G. A. Principles under the steam curing of concrete at atmospheric pressure. *Magazine of Concrete Research*, 2(6):127–140, 1951.
- [200] SCHINDLER A. K. *Concrete hydration, temperature development, and setting at early ages*. PhD thesis, University of Texas at Austin, Austin, USA, 2002.
- [201] SCHINDLER A. K. Effect of temperature on hydration of cementitious materials. *ACI Materials Journal*, 101(1):72–81, 2004.
- [202] SCHINDLER A. K. AND FOLLIARD K. J. Heat of hydration models for cementitious materials. *ACI Materials Journal*, 102(1):24–33, 2005.
- [203] SCHWARTZENTRUBER A., PHILIPPE M. AND MARCHESE G. Effect of PVA, glass and metallic fibers, and of an expansive admixture on the cracking tendency of ultrahigh strength mortar. *Cement & Concrete Composites*, 26:573–580, 2004.
- [204] SCIUMÉ G. *Modèle thermo-hydro-chemo-mécanique du béton au jeune âge et son adaptation pour l'analyse numérique de la croissance des tumeurs cancéreuses*. PhD thesis, École normale supérieure de Cachan/Université de Padoue, Padua, Italy, 2013.
- [205] SELLEVOLD E. J. AND BJØNTEGAARD Ø. Coefficient of thermal expansion of cement paste and concrete: Mechanisms of moisture interaction. *Materials and Structures*, 39:809–815, 2006.
- [206] SERUGA A., SZYDŁOWSKI R. AND ZYCH M. The evaluation of sequential process of cracking of wall segments in monolithic cylindrical reinforced concrete tanks. *Czasopismo Techniczne*, 1-B:135–163, 2008.
- [207] SHAH H. R. AND WEISS J. Quantifying shrinkage cracking in fiber reinforced concrete using the ring test. *Materials and Structures*, 39:887–899, 2006.
- [208] SOFI M., MENDIS P. A. AND BAWEJA D. Estimation of early-age in situ strength development of concrete slabs. *Construction and Building Materials*, 29:659–666, 2012.
- [209] SONG H.-W., KIM S.-H., BYUN K.-J. AND SONG Y.-C. Creep prediction of concrete for reactor containment structures. *Nuclear Engineering and Design*, 217:225–236, 2002.
- [210] TANABE T., ISHIKAWA Y. AND ANDO N. Visco-elastic and visco-plastic modeling of transient concrete. In *Proceedings of EURO-C 1998 International Conference on Computational Modelling of Concrete Structures*, pages 441–453, Bad Gastein, Austria, 1998.
- [211] TOPÇU I. B. Properties of heavyweight concrete produced with barite. *Cement and Concrete Research*, 33:815–822, 2003.
- [212] ULM F. J. AND COUSSY O. Strength growth as chemo-plastic hardening in early age concrete. *ASCE Journal of Engineering Mechanics*, 122(12):1123–1132, 1996.
- [213] ULM F. J. AND COUSSY O. Couplings in early-age concrete: From material modelling to structural design. *International Journal of Solids Structures*, 35(31/32):4295–4311, 1998.
- [214] VAN BREUGEL K. *Simulation of hydration and formation of structure in hardening cement based materials*. PhD thesis, Delft University of Technology, Delft, Netherlands, 1991.
- [215] VAN BREUGEL K. Numerical modelling of volume change at early-age – Potential, pitfalls and challenges. *Material and Structures*, 34:293–301, 2001.
- [216] VAN GENUCHTEN M. T. A closed form of the equation for predicting the hydraulic conductivity of unsaturated soils. *Soil Science Society of America Journal*, 44:892–898, 1980.
- [217] VAN ZIJL G. P. A. G., DE BORST R. AND ROTS J. G. Time-dependent fracture of cementitious materials. *Heron*, 45(4):255–273, 2001.
- [218] WALLER V., D'ALOÏA L., CUSSIGH F. AND LECRUX S. Using the maturity method in concrete cracking control at early ages. *Cement & Concrete Composites*, 26:589–599, 2004.

- [219] WANDZIK G. *Numeryczna symulacja przebiecia w płycie żelbetowej*. PhD thesis, Silesian University of Technology, Gliwice, Poland, 1999.
- [220] WANG C. AND DILGER W. H. Prediction of temperature distribution in hardening concrete. In *Proceedings of the International RILEM Conference on Thermal cracking in concrete at early ages*, pages 21–28, London, UK, 1994.
- [221] WANG Q.-J., ZHANG J.-H. AND FAN J. An analytical method for relationship between hydraulic diffusivity and soil sorptivity. *Pedosphere*, 16(4):444–450, 2006.
- [222] WEAVER J. AND SADGROVE B. M. Report no. 36: Striking times for formwork – tables of curing periods to achieve given strength. CIRIA, London, UK, 1971.
- [223] WESELI J., RADZIECKI A. AND ŁAZIŃSKI P. Ekspertyza: Określenie przyczyn powstania rys na przyczółkach i ścianach oporowych obiektów mostowych węzła Sońnica na skrzyżowaniu autostrady A1 i A4. Department of Bridges, Silesian University of Technology, Gliwice, Poland, 2009.
- [224] WESELI J., RADZIECKI A. AND ŁAZIŃSKI P. Ekspertyza: Określenie przyczyn powstania rys na przyczółkach mostu nr MS9 budowanej drogi ekspresowej S-7 odcinek Skrażysko Kamienna–Występa. Department of Bridges, Silesian University of Technology, Gliwice, Poland, 2010.
- [225] WESELI J., RADZIECKI A. AND ŁAZIŃSKI P. Ekspertyza: Określenie przyczyn powstania rys na przyczółkach wiaduktu nr WS8 budowanej drogi ekspresowej S-7 odcinek Skrażysko Kamienna–Występa. Department of Bridges, Silesian University of Technology, Gliwice, Poland, 2010.
- [226] WILLAM K. J. AND WARNKE E. P. Constitutive models for the triaxial behaviour of concrete. *International Association of Bridge Structure Engineering*, 19:1–30, 1975.
- [227] WITAKOWSKI P. Technologia budowy konstrukcji masywnych z betonu. In *Proceedings of the 13th Scientific Conference on Computer Methods in Design and Analysis of Hydrotechnic Structures*, Korbielew, Poland, 2001.
- [228] WWW.PARAVIEW.ORG.
- [229] WYRWAŁ J. AND SZCZĘSNY J. Migracja wilgoci wywołana gradientami temperatury w płytach betonowych poddanych obróbce termicznej. *Archives of Civil Engineering*, 32(1):421–432, 1986.
- [230] WYRZYKOWSKI M. *Modelowanie sprzężonych procesów cieplno-wilgotnościowych zachodzących w dojrzewającym betonie poddanym pielęgnacji wewnętrznej i zewnętrznej*. PhD thesis, Technical University of Łódź, Łódź, Poland, 2010.
- [231] XI Y., BAŽANT Z. P., MOLINA L. AND JENNINGS H. M. Moisture diffusion in cementitious materials. Moisture capacity and diffusion. *Advanced Cement Based Materials*, 1(6):258–266, 1994.
- [232] XIANG Y., ZHANG Z., HE S. AND DONG G. Thermal–mechanical analysis of a newly cast concrete wall of a subway structure. *Tunnelling and Underground Space Technology*, 20:442–451, 2005.
- [233] YUAN Y. AND WAN Z. L. Prediction of cracking within early-age concrete due to thermal, drying and creep behavior. *Cement and Concrete Research*, 32:1053–1059, 2002.
- [234] ZREIKI J., BOUCHELAGHEMA F. AND CHAOUCHA M. Early-age behaviour of concrete in massive structures – Experimentation and modelling. *Nuclear Engineering and Design*, 240:2643–2654, 2010.
- [235] ZYCH M. Thermal stresses in the wall of the RC tank. *Czasopismo Techniczne*, 1-Ś:191–208, 2007.
- [236] ZYCH M. Numerical analysis of cracking in hardening concrete of RC tank’s wall. *Czasopismo Techniczne*, 3-Ś:227–249, 2008.
- [237] ZYCH M. *Analiza pracy ścian zbiorników żelbetowych we wczesnym okresie dojrzewania betonu w aspekcie ich wodoszczelności*. PhD thesis, Cracow University of Technology, Cracow, Poland, 2011.